FUNCTIONAL SYNTHETIC ARCHITECTURES DERIVED FROM PHLOROGLUCINOL

March 29, 2010

By

YAN LI

A DISSERTATION PRESENTED TO THE GRADUATE SCHOOL
OF THE UNIVERSITY OF FLORIDA IN PARTIAL FULFILLMENT
OF THE REQUIREMENTS FOR THE DEGREE OF
DOCTOR OF PHILOSOPHY

UNIVERSITY OF FLORIDA

2010

To my parents Fangchao Li and Shengying Lu
To my wife Ling Meng
To my beloved daughter Connie M. Li

ACKNOWLEDGMENTS

I would like to thank my advisor, Prof. Ronald K. Castellano, for offering me the opportunity to study and perform research in his laboratory. I have truly appreciated his patience, guidance, and encouragement. I feel honored to have been one of his students; what I have learned from him not only in science but also in character is priceless and will influence me for the rest of my lifetime. I would also like to thank my lab mates in the Castellano group, especially Dr. Andy Lampkins, Dr. Ling Yuan, Pamela Cohn, Matt Baker, and Michelle Robinette for sharing their interesting AAT and lactone chemistry with me. I thank Dr. Alisha Martin, Dr. Roslyn Butler, Alexandre Al Abbas, Ben Schulze, for scientific discussions and their friendship. Special thanks go to Matt Baker and Pamela Cohn for proofreading my dissertation.

I also would like to thank our collaborators: Dr. Bobby Sumpter (Computer Science and Mathematics Division at Oak Ridge National Laboratory (ORNL)), Drs. Khalil Abboud, Ion Ghiviriga (Department of Chemistry at the University of Florida), and Dr. Valentin Craciun (Major Analytical Instrumentation Center (MAIC) at the University of Florida) for their help and scientific discussions throughout my studies.

I would like to thank my committee members: Prof. William Dolbier, Prof. Kirk Schanze, Prof. Adam Veige, and Prof. Anthony Brennan for serving on my committee and for their scientific advice.

Finally, the foremost and special thanks go to my family. I would like to thank my parents, Fangchao Li and Shengying Lu, for their unconditional love and support. I thank my wife, Ling Meng, for her love and encouragement. I want to especially thank my adorable daughter, Connie M. Li, for bringing so much happiness into my life.

TABLE OF CONTENTS

page

LIST OF TABLES

LIST OF FIGURES

LIST OF ABBREVIATIONS

AAT	1-Aza-admantanetrione
ACN	Acetonitrile
BTF	Benzotrifuranone
DCM	Dichloromethane
DMF	Dimethylformamide
DSC	Differential scanning calorimetry
EWG	Electron withdrawing group
HMPA	Hexamethylphosphorictriamide
HMTA	Hexamethylenetetramine
IR	Infrared spectroscopy
NLO	Nonlinear optics
POM	Polarized optical microscopy
Red-Al	Sodium bis(2-methoxyethoxy)aluminumhydride
SEM	Scanning electron microscopy
TBI	Through-bond interaction
TFA	Trifluoroacetic acid
TGA	Thermal gravimetric analysis
TMBTF	Trimethylbenzotrifuranone
XRD	X-ray diffraction

Abstract of Dissertation Presented to the Graduate School
of the University of Florida in Partial Fulfillment of the
Requirements for the Degree of Doctor of Philosophy

FUNCTIONAL SYNTHETIC ARCHITECTURES DERIVED FROM PHLOROGLUCINOL

By

Yan Li

May 2010

Chair: Ronald. K. Castellano
Major: Chemistry

Phloroglucinol-derived benzotrifuranone (BTF) is introduced herein as a key intermediate for the rapid synthesis of diverse phloroglucinol scaffolds. IR spectra of BTF show unusually high energy stretching for its C=O bonds (1821 cm^{-1}) relative to simple benzofuranone (1807 cm^{-1}), a property likely linked to its reactivity. BTF forms a non-centrosymmetric single crystal which occupies the orthorhombic space group *aba2* and its helical packing pattern is particularly unique. The packing structure is dominated by C=O···C=O multipolar interactions and $O_{lactone}$···C=O interactions. Two diastereomers of α,α',α''-trimethyl-substituted BTF (*syn* and *anti*) have also been prepared as models of functionalized derivatives. The stereoisomers have been studied by X-ray crystallography and investigated in solution, in terms of their interconversion, by NMR. Exhaustive *O*-acylation of the BTFs via their respective enolates with various acyl chlorides has afforded new C_{3h}-symmetric polyhetero-aromatic systems in moderate to good yields (60-85%). These discotic molecules self-assemble by π-π interactions, as identified in their respective X-ray crystal structures, and have potential uses in materials science. Another family of phloroglucinol derived molecules — 1-aza-adamantanetriones (AATs) has also been studied. The multiple donor-σ-acceptor through-bond interactions (TBI) within the AAT core define its inherent dipole and present a partial driving force for the self-

assembly of the molecules. X-ray structural analysis of AAT reveals bond lengths and angle variations consistent with TBI (e.g., a shortening of the C–N bond, elongation of the central C–C bond (to ~1.6 Å), and a significant pyramidalization of the carbonyl carbon within the donor-σ-acceptor pathway). UV/Vis spectra of the AATs reveal a new absorption maximum (λ_{max} = 260–275), the so-called "σ-coupled transition"; this band reversibly disappears upon addition of acid. IR and ^{13}C NMR spectroscopic data show trends consistent with through-bond donation to the carbonyl acceptor groups and commensurate weakening of the carbonyl π bond. A final family of C_3-symmetric phloroglucinol derivatives, containing H-bond acceptors on the side chains, could also be accessed readily from BTF. These molecules feature seven-membered-ring intramolecular H-bonding between phenolic hydroxyl groups and H-bond acceptors (heterocycles, carbonyls) which are capable of preorganizing the conformation of the molecules in solution and the solid state as shown by X-ray crystallography and NMR chemical shift analysis, respectively.

CHAPTER 1
INTRODUCTION

Motivation

One of ultimate goals of science is to look for the smallest building blocks of the universe. For centuries, scientists have been devoted to dividing matter further and further to discover smaller and smaller units such as molecules, atoms, protons, electrons, neutrons, etc. However, unlike physicists infinitely exploring the smallest particles of the universe, chemists stop at the atomic level and utilize a "bottom-up" approach to assemble atoms into molecules via covalent bonds and chemical reactions. Different atoms, functional groups, and substructures impart equally unique chemical, physical, and biological properties to synthesized molecules, and numerous new organic and inorganic compounds have been prepared by this approach for medical and materials applications. In the last few decades, chemists have extended their investigations beyond atomic and molecular chemistry into the area of supramolecular chemistry.

Generally speaking, supramolecular chemistry is the study of interactions between, rather than within, molecules. It has been defined by Jean-Marie Lehn, a pioneer in the area, as the "chemistry of molecular assemblies and of the intermolecular bond".[1] Weak intermolecular non-covalent interactions, such as hydrogen bonding, polar attractions, van der Waals forces, hydrophobic interactions, etc., are utilized as driving forces to assemble functional molecules into superstructures to achieve unique properties. The research targets of supramolecular chemistry are generally on a larger scale (1−100 nm) than traditional small-molecule chemistry (1−100 Å) and their construction underlies current developments in nanotechnology and materials science.[2]

Useful molecular platform candidates for supramolecular applications are generally straightforward to prepare and rich in their electronic, optical, and/or molecular recognition

properties. Among the many small molecule building blocks used in supramolecular chemistry and materials science, persubstituted benzene rings have been a mainstay. Representative molecules are shown in Figure 1-1 whose applications span nonlinear optics,[3] organic electronics,[4] receptors for sensing,[5,6] and liquid-crystalline materials.[7]

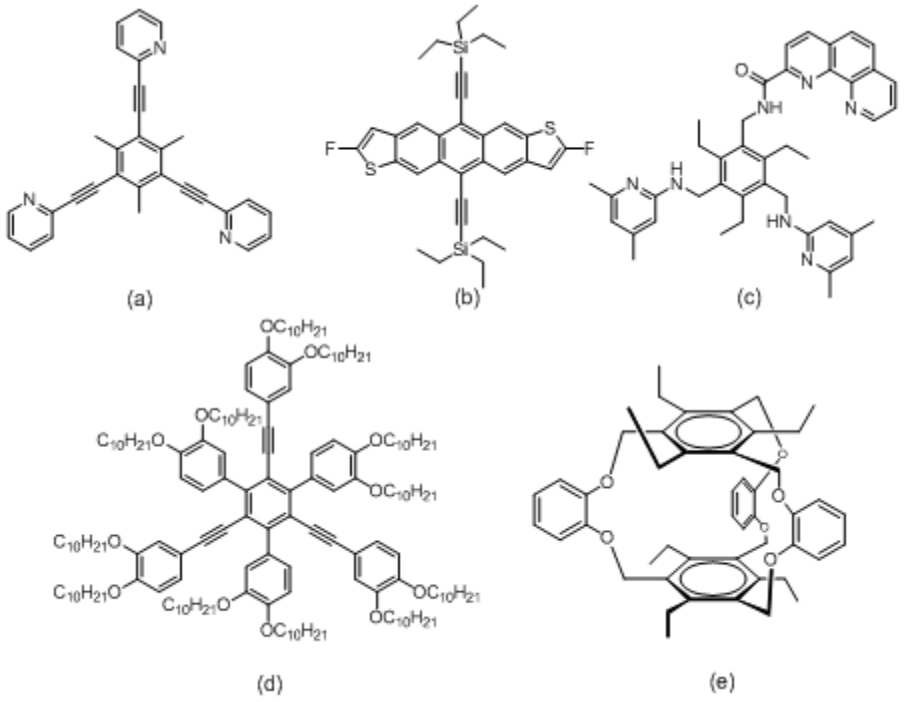

Figure 1-1. Representative persubstituted benzenes used as building blocks for supramolecular chemistry and functional materials: (a) a nonlinear optical chromophore; (b) an organic semiconductor; (c) a carbohydrate receptor; (d) a liquid crystal mesogen; (e) a cage molecule for cation recognition.

This dissertation focuses specifically on the synthesis and characterization of new persubstituted aromatics derived from phloroglucinol (1,3,5-trihydroxybenzene). This unique aromatic molecule is ubiquitous in biology and has recently found widespread applications as a building block for new liquid crystals, low molecular weight gelators, and sensors. This chapter will highlight the structural features that continue to make the molecule attractive for exploration in materials and supramolecular chemistry.

Phloroglucinol: Structure and Availability

Phloroglucinol (1,3,5-trihydroxybenzene, **1-1**), a colorless and odorless solid compound, was first isolated as a hydrolysis product of glucoside phloretin obtained from the bark of fruit trees. The well known industrial synthesis of phloroglucinol begins from 1,3,5-trinitrobenzene (TNT); reduction to 1,3,5-triaminobenzene and subsequent hydrolysis gives phloroglucinol in around 80% yield.[8] Easy industrial preparation makes the price of phloroglucinol ($0.06/g) much lower than some well-known aromatic supramolecular synthons, such as 1,3,5-triethylbenzene (~ $5/g). Frost and coworkers recently reported the biosynthesis of phloroglucinol from *Pseudomonoas fluorescens*, an enzyme that catalyzes the conversion of three malonyl coenzyme A units to the target aromatic.[9] This safer and "greener" method allows the preparation of phloroglucinol from glucose in fermentors in yields of up to 10 g/L, and demonstrates that the molecule can potentially be made in a sustainable way from renewable resources.

C_3-symmetry is aesthetically pleasing in both natural and synthetic contexts, but it also is important for applications that include metal-ligand binding, chiral recognition, and catalysis. Phloroglucinol is a C_3-symmetric molecule that has three hydroxyl groups alternately located on a central benzene ring. The phenolic hydroxyl groups represent phloroglucinol's acidic sites (pK_{a1} = 8.0, pK_{a2} = 9.2, pK_{a3} = 14.5);[8] they also increase the electron density of the central benzene ring which makes it easy to introduce functional groups via electrophilic aromatic substitution reactions. The hydroxyl groups on phloroglucinol are also good donors for H-bonding, one of the most important and useful weak non-covalent interactions for supramolecular applications and the conformational control of synthetic templates. Particularly, intramolecular H-bonds play important roles in nature and synthetic chemistry, having potential applications in biological systems and materials science that will be discussed in a later chapter.

Lastly, the hydroxyl groups represent useful synthetic handles as they can be functionalized through simple reactions, such as etherification and esterification.

Phloroglucinol cannot be categorized as a simple phenol because it has partial 1,3,5-cyclohexatrione (**1-2**, Figure 1-2) properties that arise from enol-keto tautomerism. As early as 1886, Baeyer[10] discovered that phloroglucinol forms the corresponding trioxime (**1-3**, Figure 1-2) upon reaction with hydroxylamine, a product that must arise from ketone-containing tautomers (Figure 1-2). Although a computational study (all-electron ab initio Hartree-Fock calculation)[11] has shown that the gas-phase stability of 1,3,5-benzenetriol is higher than 1,3,5-cyclohexatrione by 146 kJ/mol, the energy difference of keto and enol forms of the phloroglucinol system is 25% lower than a simple phenol. Solvation effects notwithstanding, the results speak to phloroglucinol's ability to participate in chemical reactions via its keto form. In other relevant studies, Sonntag and Knoche[12,13] have used ^{13}C NMR and UV spectroscopies to investigate the pH-dependence of the phloroglucinol tautomerism. Experiments found that when the pH = 12~13, the C_{2v}-symmetric keto form is the dominant species of the phloroglucinol dianion (^{13}C NMR δ 46, 101,188, 197 ppm). This structure is consistent with the UV absorption spectrum that shows a maximum at 348 nm in the same pH range (Figure 1-2). Overall, these findings illustrate that phloroglucinol is an unusual aromatic molecule with ambivalent chemical behavior.

The properties described above define phloroglucinol as a unique C_3-symmetric synthetic building block for the construction of functional molecules. Some applications, including metal binding, catalysis, dendrimer construction, liquid crystal formation, and host-guest chemistry will be discussed in the following sections.

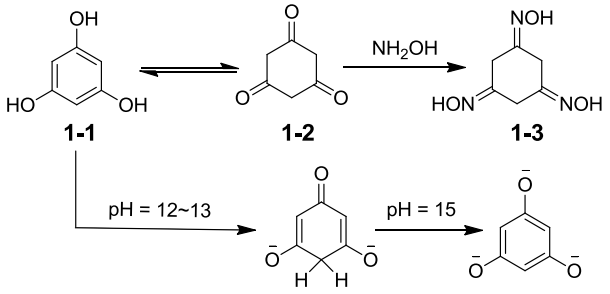

Figure 1-2. The enol-keto tautomerism of phloroglucinol and its reaction with hydroxylamine. The dominant keto species of the phloroglucinol dianion (pH = 12~13) is also shown.[12,13]

Phloroglucinol as a Scaffold in Biology

Phloroglucinol occurs in many natural products in the form of derivatives such as flavones, catechins, coumarins, anthocyanidins, xanthins, and glucosides.[8] Some of these natural products have very interesting bioactivities and potential medical applications. Among the recent examples, lysidicins A–C (lysidicin A is shown in Figure 1-3),[14] isolated from *Lysidice rhodostegia*, could be the active ingredients for treatment of ache, fractures, and hemorrhage in Chinese medicines. Natural products dichamanetin (Figure 1-3) and 2'''-hydroxy-5''-benzylisouvarinol-B,[15] isolated from *U. chamae* and *X. afticana* respectively, are potent inhibitors of the GTPase activity of FtsZ, a highly conserved protein that is essential for bacterial cytokinesis. Myristinin A–C (myristinin A is shown in Figure 1-3), flavonoids isolated from *Myristica cinnamomea*, were found to be potent polymerase β inhibitors and DNA damaging agents.[16,17] Prenylated flavanones (±)-bonannione A (Figure 1-3) and (±)-sophoraflavanone A were isolated and artificially synthesized since they have a wide range of interesting physiological properties (i.e., antifungal, antibacterial, and antitumor).[18] In all, these natural products showcase the rich structures accessible to the phloroglucinol core. Along these lines, intramolecular H-bonds can be identified in each (Figure 1-3), where the phloroglucinol

hydroxyl group acts as an H-bond donor. In corresponding ^{1}H NMR spectra, the H-bonded –OH signals are shifted downfield to 12~14 ppm (corresponding to $\Delta\delta$ values of 3–4 ppm versus non-H-bonded OH groups).

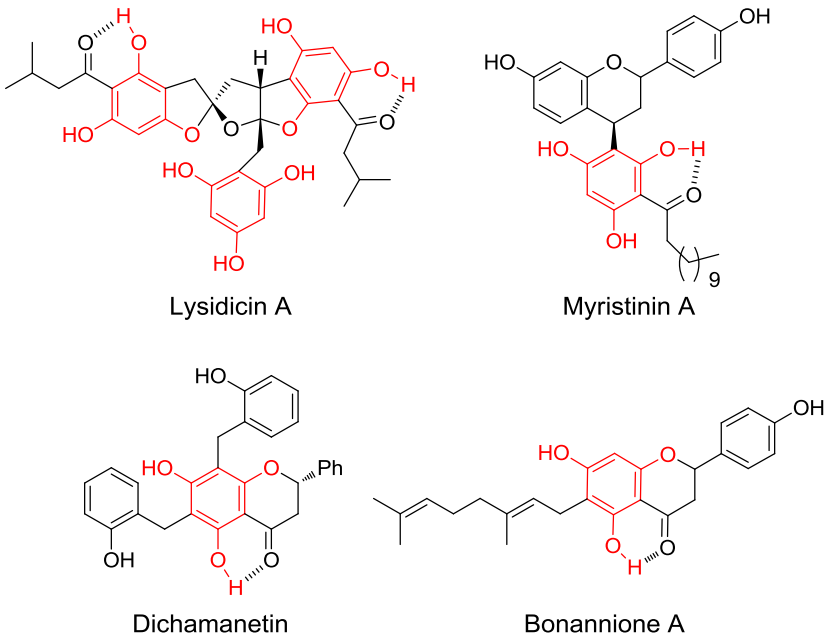

Figure 1-3. Some biologically active natural products containing the phloroglucinol moiety[14-18] (highlighted in red color); intramolecular H-bonding is indicated with dash lines.

For medical applications, coumarins, a family of natural products containing the phloroglucinol substructure that include the calanolides and inophyllums, have been established as specific inhibitors of human immunodeficiency virus (HIV) reverse transcriptase. These compounds could therefore potentially be useful for AIDS treatment (anti-HIV half maximal effective concentration (EC_{50}) of (+)-calanolide-A is as low as 0.2 μM) (Figure 1-4a).[19,20] The natural product xanthohumol from hops (*Humulus lupulus L.*), and its analogues (Figure 1-4b), have shown high bioactivities for inhibiting the proliferation of human breast cancer (MCF-7), colon cancer (HT-29), ovarian cancer (A2780), and prostate cancer (DU145) cell lines in vitro.[21] Many natural and synthetic phloroglucinol derivatives have shown very strong anti-bacterial activities (Figure 1-4c); [22-24] in this context it is worth noting that the keto derivatives of

phloroglucinol that can be obtained by disubstitution at the α position show good activities against antibiotic-resistant bacteria (Figure 1-4d).[25] Lastly, the natural compounds that bear extended conjugated systems and differentially functionalized aromatic rings, such as Catanolide-A and Xanthohumol, remind us of the possible materials-relevant derivatives of phloroglucinol that might be synthetically accessible.

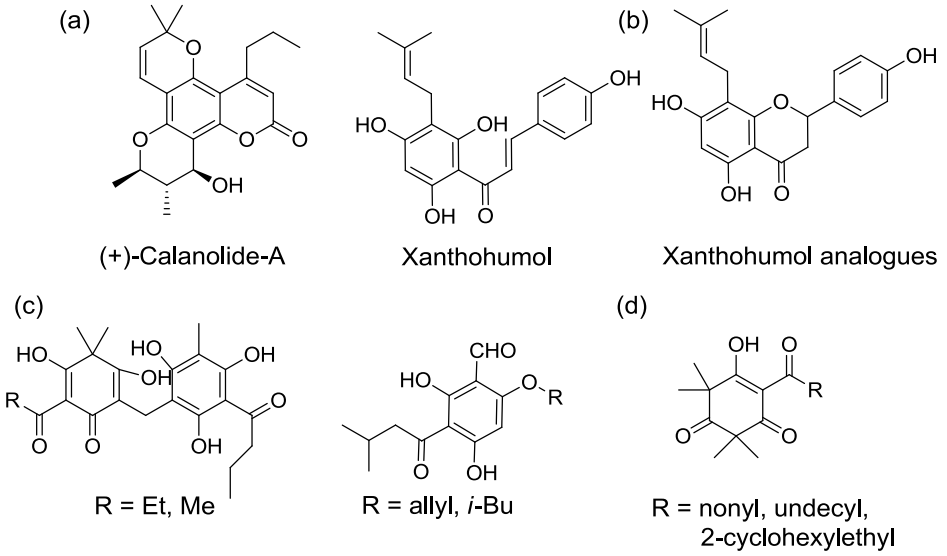

Figure 1-4. Phloroglucinol derivatives for medicinal applications: (a) anti-HIV reagents; [19,20] (b) anti-tumor reagents; [21] (c) anti-microbial reagents[22-24] and (d) anti-microbial reagents containing the diketo form of phloroglucinol.[25]

Phloroglucinol in Supramolecular Chemistry and Materials Science

Besides their broad biological applications, phloroglucinol derivatives are also widely used as building blocks in supramolecular chemistry and materials science. With some unique structural and electronic characteristics, phloroglucinol derivatives are very good building blocks for supramolecular chemistry applications. For example, the hydroxyl groups on the phloroglucinol core are potential H-bond donors and can form inter- and intramolecular H-bonds for conformational control and self-assembly. A more electron-rich aromatic core and access to keto tautomers are among the properties that distinguish phloroglucinol derivatives from other aromatics and are important to their synthesis and functional properties.

Phloroglucinol in Liquid-Crystalline Materials

A liquid crystal is a phase of matter in which molecules are more ordered than in a liquid but less ordered than in a crystal. The history of liquid crystals dates back over one century and the materials have steadily increased in both their scientific and technological importance, driven, for example, by exciting applications in display technologies.[26]

Many disk-shaped molecules have been found to display liquid-crystalline behavior, and those derived from the phloroglucinol platform are no exception. Among the most recent work in this area is from Yalammagad and coworkers[27-29] who tactfully introduced three imine groups to the vacant phloroglucinol positions to form planar tris(*N*-salicylideneanilines) (Figure 1-5a). This modification interestingly locks the tri-keto form of phloroglucinol by exclusively forming the keto-enamine tautomer. Within these compounds, the oxygen atoms of the phloroglucinol core serve as intramolecular H-bond donors, and two different symmetries of the keto-enamine tautomers, C_{3h} and C_s, are formed given by the configuration (*E* or *Z*) of one enamine double bond (Figure 1-5a). Upon the addition of appropriate functional groups to the periphery of this type of discotic molecule, interesting columnar liquid crystalline and optical properties (such as luminescence emission) can be imparted. This work nicely demonstrates the unique characteristics and importance of phloroglucinol's keto tautomers in a supramolecular setting.

Lehmann and coworkers have installed oligobenzoate units on the phloroglucinol hydroxy groups as spacers which are end-capped with substituted phenyl or naphthalene groups. The resulted C_3-symmetric or non-C_3-symmetric (different terminal groups or length of spacers) star-shaped molecules are new types of flexible mesogens. These molecules are not traditional disk-shaped mesogens but they have a rich mesomorphism that includes columnar hexagonal, columnar rectangular, lamellar, to cubic phases, depending on the nature of the oligobenzoate arms (Figure 1-5b).[30-33] Some of the molecules may have potential semiconducting properties.[34]

That different liquid-crystalline properties arise from different symmetries of the molecules reveals the importance of symmetry control in the design and synthesis of functional phloroglucinol derivatives (vide infra).

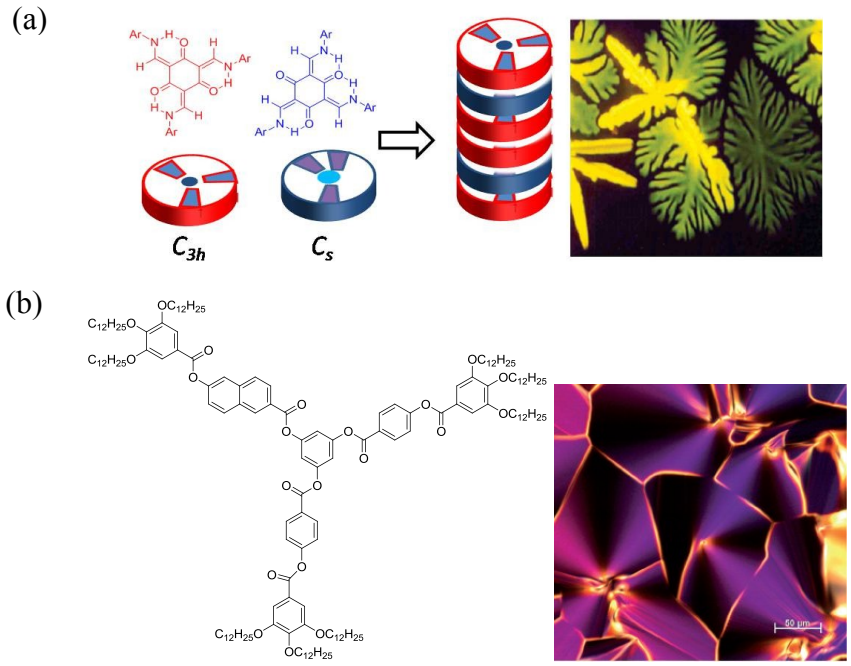

Figure 1-5. Examples[27-33] of phloroglucinol derived liquid crystalline molecules and images of their liquid-crystalline phases as viewed by polarized optical microscopy (between crossed polarizers). Figure 1-5a–Reproduced (in part) with permission from Ref 28. Copyright 2007 American Chemical Society. Figure 1-5b–Reproduced by permission of The Royal Society of Chemistry.

As alkylated alkoxyphenyl groups are well-known moieties for imparting liquid crystallinity to small molecules, phloroglucinol derivatives have been widely used as mesogens either as the core or side chains.[35-38] Included here are the phloroglucinol derived 1,3,5-trialkoxy-2,4,6-triamidobenzene compounds which self-assemble through a combination of π-π stacking interactions and head-to-tail amide H-bonds.[39] Chiral substituents are easily introduced on the side chains of these types of molecules to induce self-organization into helical columns which further stack to create superhelical arrangements in concentrated solutions.[40]

Phloroglucinol-derived Gels

Similar to liquid crystals, organogels arise as a consequence of the self-assembly of organic molecules via weak interactions and therefore fall within the realm of supramolecular chemistry. Gels form when organic solvents are immobilized by a three-dimensional network composed of aggregated gelators.[41] Applications of gels formed from low molecular weight gelators (LMWG) include material separations, sensing, drug delivery, cosmetics, etc.[42] Their attractiveness generally stems from convenient (bio)degradation properties, ready tuning of physical properties and sol-gel phase transition by monomer chemical modification, and amenability to rational design that includes response to specific external stimuli (such as temperature and pH).

Recently, Yamanaka and coworkers reported tris-urea phloroglucinol derivatives as a novel class of LMWG for chloroalkane solvents such as 1,1,2-trichloroethane and dichloromethane (Figure 1-6a,b). Scanning electron microscopy (SEM) images show the fiber structures in the xerogel (Figure 1-6c). The π-π interactions between phloroglucinol cores and intermolecular H-bonds between urea groups of neighboring gelators contribute to the formation of 1-D fibers. When $CuBr_2$ was added to the system a different gelation mechanism was indentified that resulted in spherical nano-structures (Figure 1-6d).[43,44] Hardie and coworkers synthesized an alternative "metallo-gel" based on phloroglucinol by installing quinolinylmethyl groups on the hydroxyl groups to define the tripodal ligand. Coordination of copper(II) ion led to the gelation of nitromethane and dichloromethane, a process partially driven by π-π interactions as suggested by the X-ray crystal structure of a phloroglucinol-copper complex similar to that of the gelator (distance between two phloroglucinol planes = 3.55Å).[45]

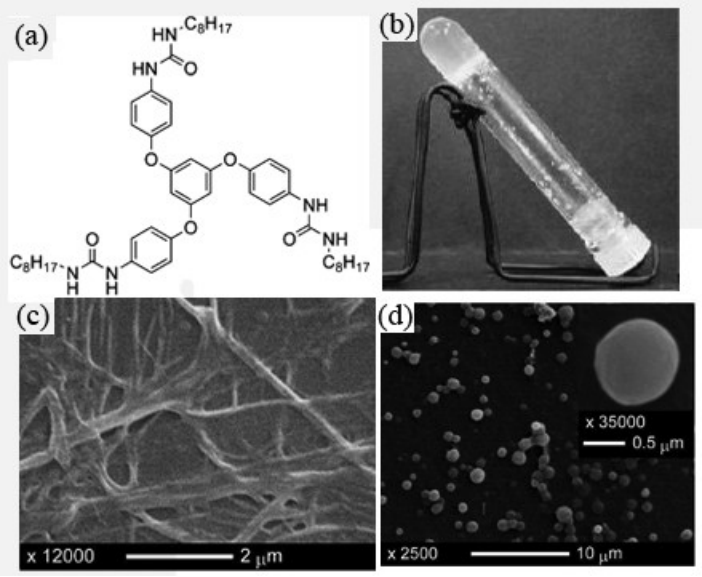

Figure 1-6. An example[43,44] of a phloroglucinol-derived LMWG: (a) structure of the gelator; (b) gel formation in 1,1,2-trichloroethane; (c) SEM image of the 1,1,2-trichloroethane gel; (d) SEM image of the 1,1,2-trichloroethane gel of the gelator with added $CuBr_2$. Figure reproduced (adapted) with permission from Ref 43. Copyright 2007 American Chemical Society.

Phloroglucinol-derived Non-linear Optical Materials

The functionality of phloroglucinol-derived organic compounds has also found application in non-linear optical (NLO) materials. Second order NLO materials, in particular, can be used for processes such as frequency doubling, frequency mixing, parametric oscillation, and electrooptical modulation.[1] Traditional organic molecules considered as good candidates for NLO-active materials include the push-pull polyenes that contain electron-donating and -accepting groups on opposite ends of a conjugated linker.[46] However, the large ground-state dipole moment of these one-dimensional (1-D) molecules generally leads to centrosymmetric arrangements in the solid state; practical NLO materials require noncentrosymmetric ordering. There now lies significant interest in designing NLO-active molecules that lack a ground-state dipole,[47,48] and phloroglucinol provides a good platform for study due to its inherent C_3-symmetry.

Cho[49] and Hennrich[50-52] have prepared donor-acceptor NLO chromophores by using alkoxy groups as the electron donors and electron deficient alkenyl and alkynyl groups as electron acceptors (Figure 1-7). These two-dimensional (2-D) molecules feature three charge-transfer pathways with no net dipole and each system has been shown to display high NLO activity. For the compounds made by Hennrich, long alkoxy groups also make the molecules liquid crystalline (Figure 1-7b). Other researchers[53,54] have prepared hyperbranched dendrimers and polymers from the phloroglucinol scaffold that have also shown decent nonlinearity.

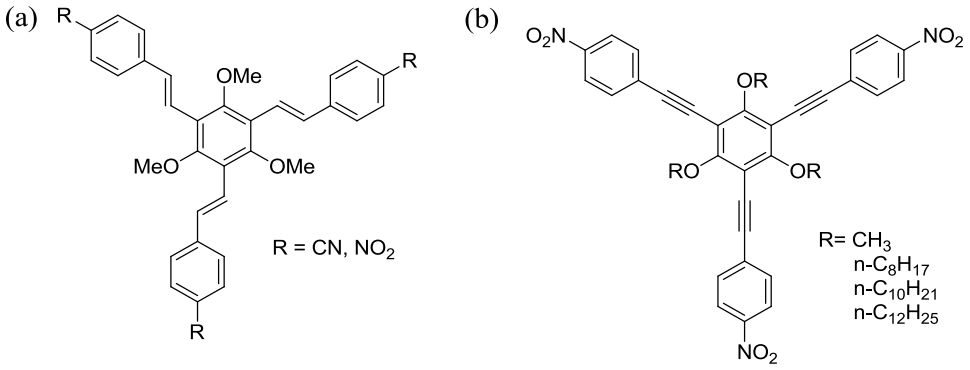

Figure 1-7. Examples of C_3-symmetric phloroglucinol derivatives as NLO materials. [49-52]

Phloroglucinol-based Receptors, Ligands and Hosts

One challenge in supramolecular chemistry is to construct a molecule which will adopt a specific conformation, such as bowl shape for molecular recognition or a helix for biomimicry. Along these lines, Still and coworkers[55] have employed cyclic polypetides as side walls and phloroglucinol as the base to create bowl-shaped receptor molecules that selectively recognize small peptides with high binding affinity. Likewise, Kim and coworkers[56] have made a bowl-shaped molecule from the one-pot condensation of ninhydrin and phloroglucinol, and X-ray crystallography has confirmed the desired conformation.

Glaser and coworkers have managed to make triple-salen hybrid ligands (**1-5**) based on the phloroglucinol structure (Figure 1-8a).[57,58] After complexation with metal ions (Cu^{II}, Ni^{II}), the

ligands symmetrically fold to form bowl-shaped structures that have been identified by X-ray crystallography (Figure 1-8b). A supramolecular host-guest structure was also found that features two host complexes and two dichloromethane molecules like "two pearls in an oyster" (Figure 1-8c). It is worth noting that the phloroglucinol hydroxyls serve as the metal coordination sites, and appropriate side chains on the 2,4,6 positions of the central benzene ring enhance this coordination.

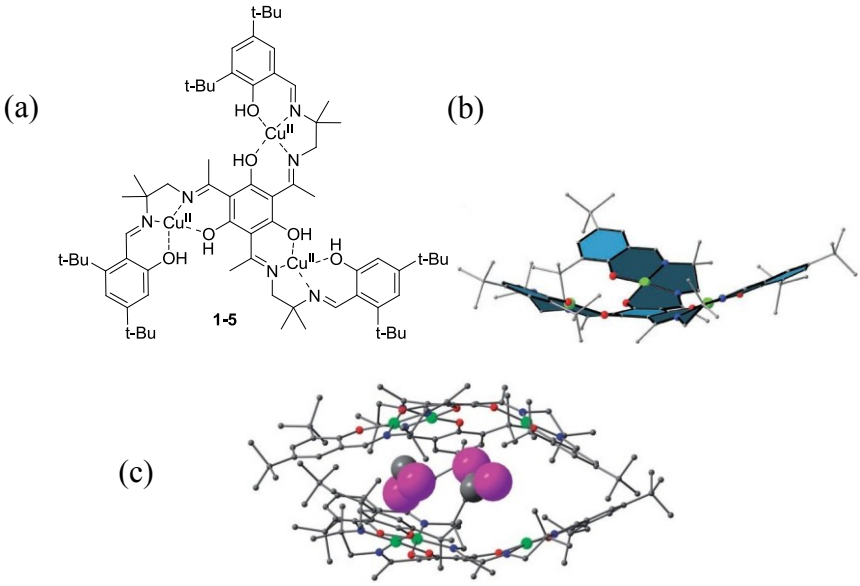

Figure 1-8. Bowl-shaped triple-salen complex: [57,58] (a) chemical structure of the metal-ligand complex with three Cu(II) ions; (b) crystal structure of the complex; (c) supramolecular arrangement of two complexes and two dichloromethane molecules. Color code: Cu green, O red, N blue, Cl violet. Copyright Wiley-VCH Verlag GmbH & Co. KGaA. Figure reproduced with permission.

When substituted with rigid side chains, as in the many examples mentioned above, phloroglucinol derivatives may adopt a planar conformation. However, when relatively flexible side chains are introduced to the phloroglucinol core, the molecules can adopt an all *syn*, bowl-shaped conformation in which the side chains point to the same side of the central benzene plane. Then, via either covalent or noncovalent bonds, two molecules can be brought together to form

dimeric molecular cages or capsules for applications that include storage,[59] molecular recognition,[60] delivery,[61] or catalysis.[62]

Covalent phloroglucinol derived molecular cages have been constructed via three triazole linkers (Figure 1-9a) using "click chemistry",[63] in this case the 1,3-dipolar cycloaddition reaction of azido groups and terminal alkynes with Cu(I) catalysis. Molecular modeling shows that the cage molecule is stabilized by a toluene guest molecule via π-π interactions.[64] Ahn and coworkers[65] have reported heterodimeric cage molecules (**1-6**) formed from trimethyl- or triethyl-substituted phloroglucinol derivatives. These cages are composed of five benzene rings and feature a π-rich cavity that selectively binds NH_4^+ and K^+ ions (Figure 1-9b) through well-positioned cation- π interactions.

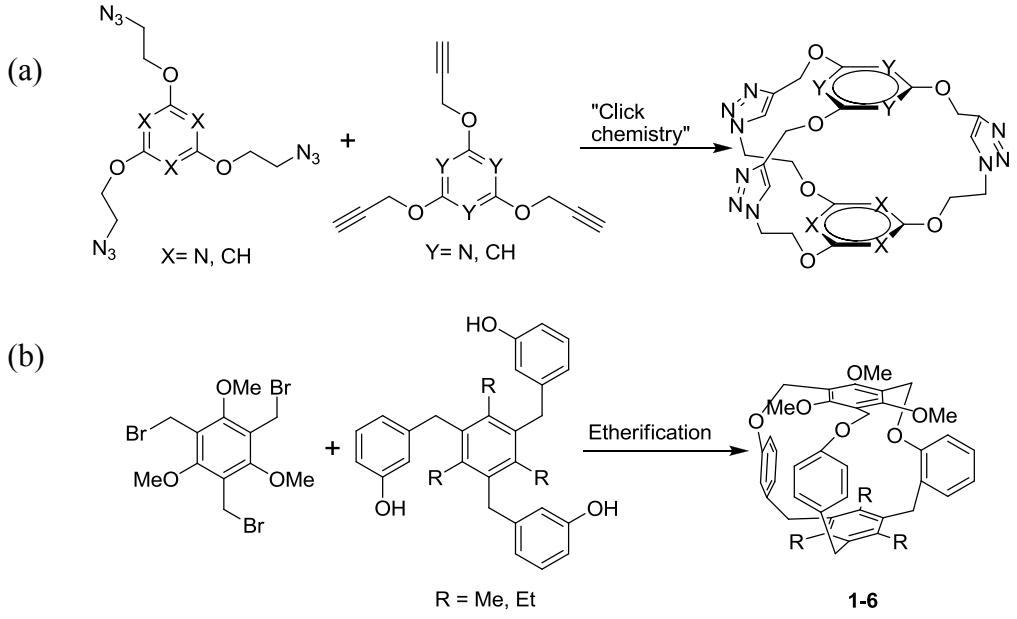

Figure 1-9. Dimeric cage molecules formed through covalent bonds via three-fold "click chemistry" [64] (a) and etherification[65] (b) reactions.

Dimeric trimethoxybenzene cages have also been prepared using three rigid isoxazolopyridines as linkers. Ferrini and coworkers[66] found that the nitrogen atoms of the three pyridine groups all point to the center of the cage, suitable for chelating Ag(I) and Ni(II) as

revealed by mass spectrometry. In the area of noncovalent capsule formation, MacLachlan and coworkers[67] have found that two tris(*N*-salicylideneaniline)s (see Figure 1-4a) can be linked by weak noncovalent interactions such as H-bonds and π-π interactions to form capsule-like dimeric units in the solid state.

Molecular recognition is a major area of supramolecular chemistry that encompasses cation, anion, and neutral molecule binding via weak noncovalent interactions. The phloroglucinol platform is particularly well suited for these applications. Wang and coworkers[68] have synthesized a novel host (1-7, Figure 1-10) by installing three carboxydecyl groups on the phloroglucinol core. This molecule can self-assemble on surfaces to form 2-D hexagonal networks through intermolecular H-bonding of the terminal carboxyl groups, and the tetragonal cavities that arise from the network can then be used for hosting appropriately sized guest molecules, such as Cu(II) phthalocyanine. The host-guest arrays are conveniently amenable to study by scanning tunneling microscopy (STM) (Figure 1-10).

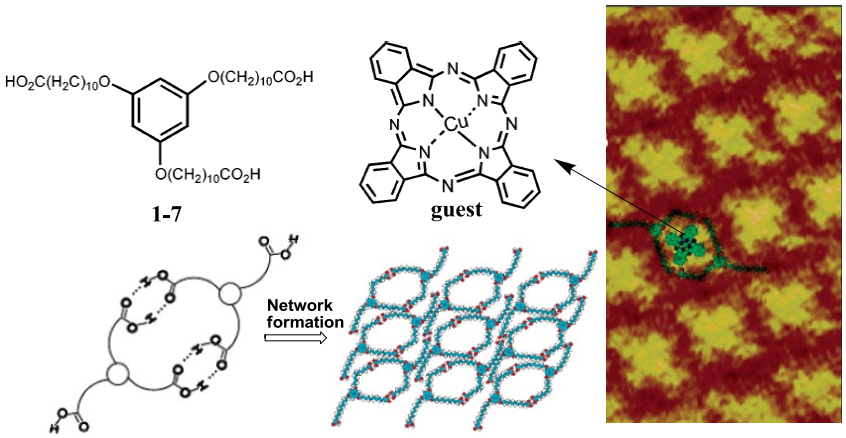

Figure 1-10. Compound **1-7** self-assembles to form a 2-D network on surfaces.[68] Scanning tunneling microscopy (STM) images show the formation of host-guest architectures upon adding phthalocyanine guest molecules. Figure reprinted (adapted) with permission from Ref 68. Copyright 2004 American Chemical Society.

Huang and coworkers[69] have used the phloroglucinol scaffold equipped with polyethyleneglycol units to create a cryptand cage molecule that incorporates three (*m*-

phenylene)-32-crown-10 ethers (**1-8**). The host specifically recognizes pyridinium salts as guests to form a host-guest threaded structure. When a linear bispyridinium salt (**1-9**) was used as the guest, a pseudorotaxane was formed; the structure as confirmed by X-ray crystallography is shown in Figure 1-11. A number of other phloroglucinol derived host systems have also been used for cation,[66] anion,[70] and neutral molecule[71] recognition.

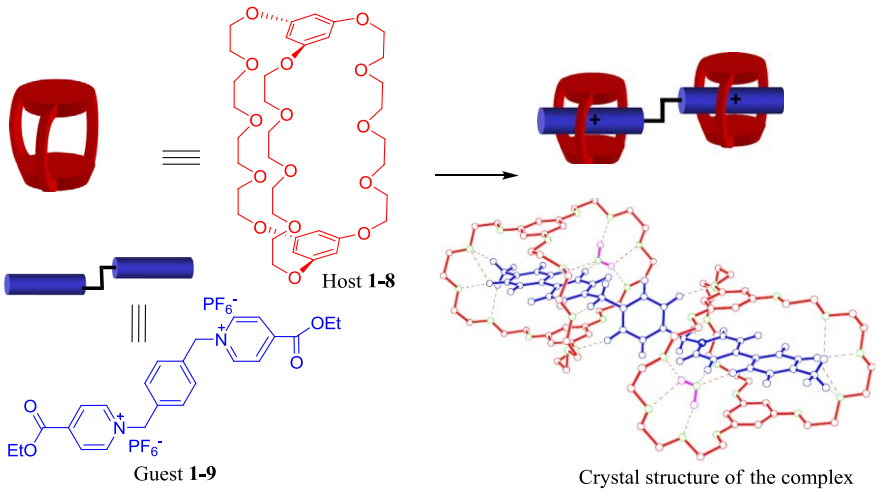

Figure 1-11. A phloroglucinol-derived pseudorotaxane.[69] Figure reprinted from Ref 69, Copyright (2007), with permission from Elsevier.

Dendrimers with Phloroglucinol Building Blocks

In the last three decades, dendrimer chemistry has become a hot area in supramolecular chemistry. Dendrimers are repeatedly branched molecules which are spheroid or globular nanostructures that can be precisely engineered to carry molecules within their interior voids or attached to their surfaces. The size, shape, and reactivity of dendrimers can be controlled by the shells and chemical composition of the core, interior branching, and surface functionalities.[72]

Phloroglucinol has emerged as a good candidate for dendrimer construction due to its symmetry and functionality; some systems, with particularly interesting applications, are highlighted here. Vögtle and coworkers[73] have introduced an unconventional rotaxane system with phloroglucinol-based dendrimers as "stoppers" to study deslipping behavior. Ghaddar[74] has

incorporated polypyridyl ruthenium(II) complexes on the surfaces of first and second generation phloroglucinol-centered dendrimers (Figure 1-12a) and studied their efficiency as dye sensitized solar cells. Armaroli and coworkers[75] have studied the formation of host-guest complexes between C_{60} and polybenzylether dendrimers with different central cores. They found that the interior of the dendrimers with a phloroglucinol core (Figure 1-12b) provides the correctly sized space for encapsulation of fullerene based on UV-Vis and ^{13}C NMR spectroscopy.

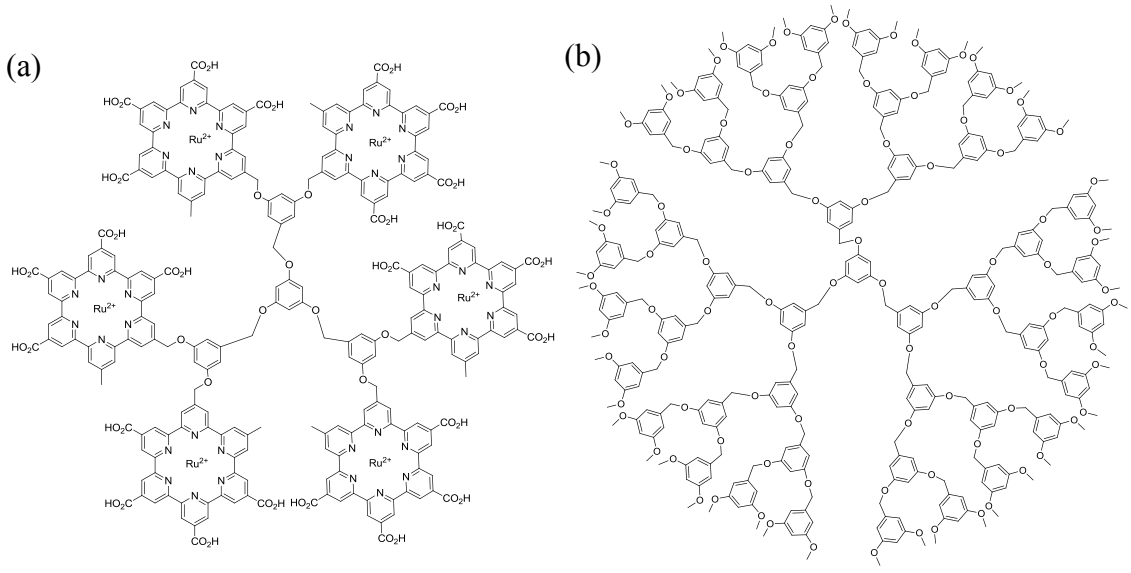

Figure 1-12. Examples of phloroglucinol-cored dendrimers for different applications such as (a) dye-sensitized solar cells and (b) fullerene encapsulation.

Phloroglucinol has also been used to construct the side chains of dendrimers. Das[36] and coworkers, for example, have reported dendritic architectures with alkyl-linked phloroglucinol units and substituted azobenzenes on their surfaces. Likewise, Yokoyama[76] successfully attached phloroglucinol-based dendrons on a photochromic core. The thick wall of the dendron at the outmost edge of the molecule helps to maintain core fluidity and high photochromic conversion ratios in polymer matrices. A number of other reported examples also use phloroglucinol-based side chains for novel dendrimer synthesis to explore new properties.[77-79]

Symmetry Control in the Synthesis of Phloroglucinol Derivatives

Most syntheses of functional phloroglucinol-derived molecules, including dendrimers, cage molecules, and hosts for molecular recognition, take advantage of the parent aromatic's C_3-symmetry. However, access to less symmetrical compounds, which means introduction of different functional groups around the periphery of the aromatic core, can dramatically change materials properties and allow access to new applications. While nature does this adeptly, only a few research groups have reported the synthesis and applications of non-C_3-symmetric phloroglucinol derivatives. Lehmann and coworkers[80] protected the phloroglucinol OHs as benzyl ethers (OBn) first, replaced one benzyl with a silyl protecting group through a monodeprotection-protection strategy, and then deprotected one benzyl group again to form an ABC building block (**1-10**) for differential-armed-star molecule synthesis (Figure 1-13). In later work, the differentially *O*-substituted star molecules were used as the mesogens of liquid crystals that showed properties unique from those constructed from C_3-symmetric components.[30,33] Addition of a naphthalene chromophore to one arm of the star molecules imparts semiconducting properties to the liquid crystals.[34]

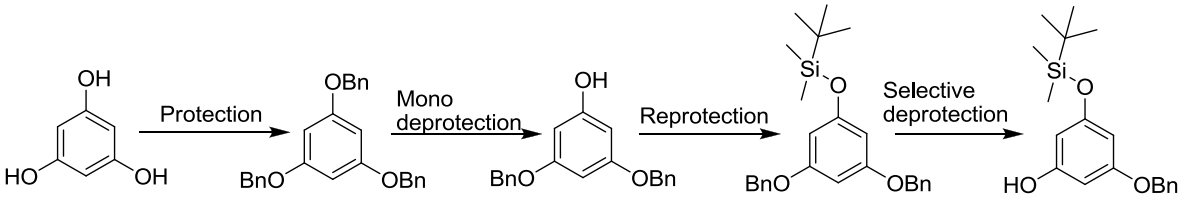

1-10

Figure 1-13. Strategy for the synthesis of ABC-type building blocks for differential-armed-star molecules.[80]

Although the overall yield for this synthetic route is moderate, the repeating protection and deprotection makes it redundant. Most reported examples of non-C_3-symmetric phloroglucinol derivatives have been prepared by introducing different substituents on the phenolic hydroxyls; hardly any rational protocols are known for installing different functional groups on the carbon

(2,4,6-) positions of the ring. Chapter 2 of this dissertation will discuss this type of functionalization.

Scope and Organization of Dissertation

The author of this dissertation was deeply attracted to the broad chemistry and applications of phloroglucinol and its derivatives, especially as they relate to supramolecular chemistry. Chapter 2 describes the preparation of the first benzotrifuranones (BTFs), phloroglucinol-derived lactones with a number of possible applications in synthesis and technology. Reported are their detailed syntheses, crystal structures, reactivity profiles, and spectroscopic properties. Derived from BTF molecules in one synthetic step, new *O*-acylated benzotrifurans have been made and studied as the topic of Chapter 3. These disk-shaped heterocycles tend to stack via π-π interactions and this behavior has been studied experimentally by X-ray crystallography and theoretically by DFT methods. Chapter 4 will discuss the synthesis, optical properties, and crystal structures of 1-aza-adamantanetriones (AATs), phloroglucinol-derived donor-σ-acceptor molecules. These systems have been shown to have unusual self-assembly and electronic properties; the studies reported here focus on a fundamental understanding of the AAT molecular structure. Utilizing phloroglucinol's phenolic hydroxyl groups as H-bond donors, a seven-membered-ring (SMR) intramolecular H-bonding strategy has been introduced for the shape and conformational control of phloroglucinol derivatives. Variable-concentration and -temperature ^{1}H NMR experiments and X-ray crystallographic studies on SMR H-bonds will be discussed in Chapter 5.

CHAPTER 2
SYNTHESIS AND PROPERTIES OF BENZOTRIFURANONES

Introduction

Benzofuran-2-ones **2-1'**, derived from substituted phenols, boast a diverse chemical profile, summarized in Figure 2-1, underlying an equally rich suite of applications for the molecules. Shown are typical transformations for the lactone core including ring opening, enolization, and anion formation, among others, leading to wide applications of the molecule in synthetic chemistry, materials science, and supramolecular chemistry (vide infra).

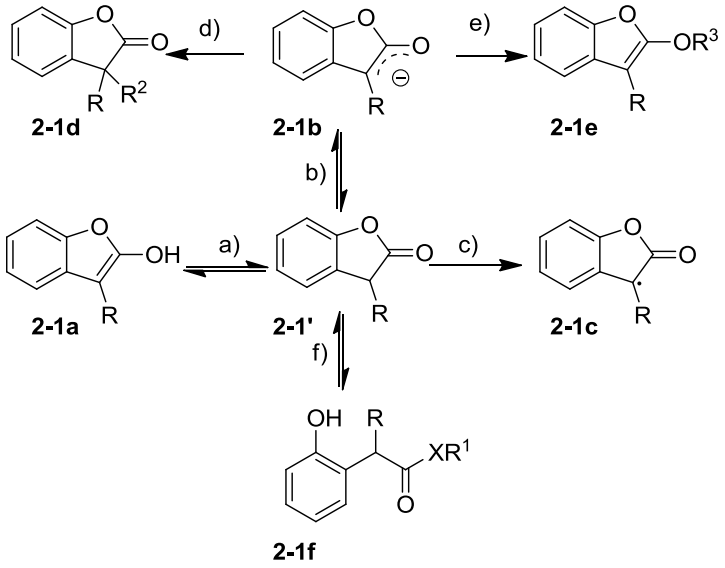

Figure 2-1. Chemistry of benzofuran-2-ones **2-1'**: a) Keto-enol tautomerization; b) enolate formation; c) radical generation; d) C-alkylation; e) O-alkylation or acylation; f) nucleophilic ring opening.

It is surprising that this chemistry has yet to be extended to systems with multiple lactone rings around a central arene scaffold. Notably, phloroglucinol, as a triphenol species, is a suitable precursor for building up three lactone rings to form a benzotrifuranone species (Figure 2-2). Besides the rich chemical profile inherited from benzofuran-2-ones, benzotrifuranones would also feature C_{3h}-symmetry and possible access to polycyclic heteroaromatics that can display useful self-assembly and electronic properties. The following sections will briefly

review the physical and chemical properties of benzofuran-2-ones and discuss their relationship to the potential properties and applications of novel benzotrifuranones.

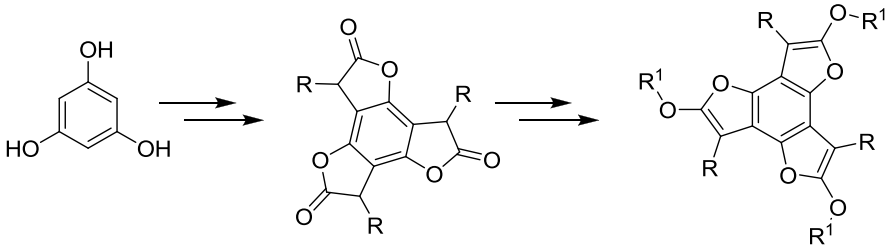

Figure 2-2. Designed C_3-symmetric benzotrifuranones and polycyclic heteroaromatic systems from phloroglucinol.

Chemical Properties of Benzofuran-2-ones

Benzofuran-2-one (**2-1**) is a common substructure of natural products, such as garvin C (anti-tumor reagent),[81] fumimycin (anti-bacterial reagent),[82] and natural yellow pigment isoaurone (Figure 2-3).[83] Benzofuran-2-one derivatives are also used as building blocks for the total synthesis of some natural products such as aplysin.[84]

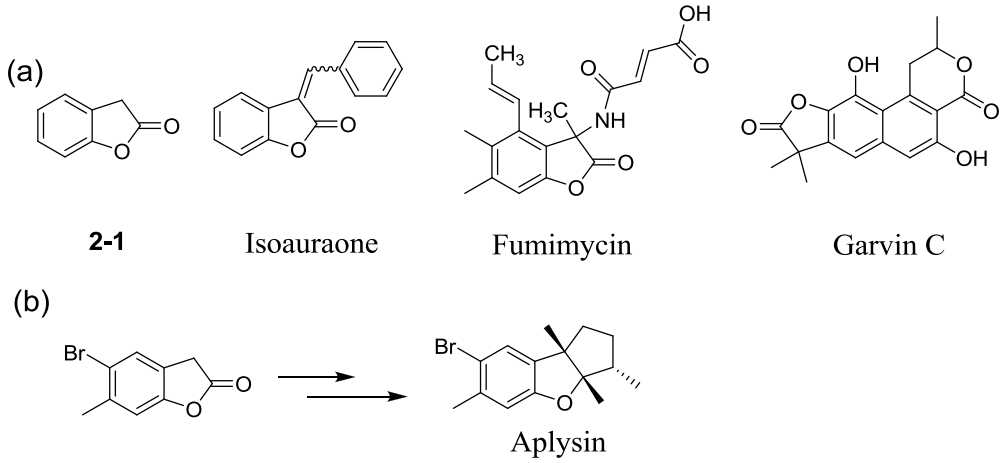

Figure 2-3. Examples of benzofuran-2-one (**2-1**) as a (a) substructure in different natural products and (b) building block for natural product total synthesis.

Carboxylic acid esters, including lactones, are capable of enol tautomerization and their enolate anions are important intermediates in many chemical and biological reactions; however, the enols and enolate anions of simple esters are quite unstable kinetically and

thermodynamically.[85] Different from simple acyclic esters, benzofuran-2-ones feature a cyclic system adjacent to an aryl ring and enolization accesses a substituted benzofuran, favorably extending π-conjugation and aromaticity (Figure 2-1a). The enolate anion is well stabilized by the benzene ring due to resonance delocalization (the pKa of the α-proton of benzofuran-2-one is 13.5[86] vs. a pKa ~ 22.7 for acyclic ethyl phenylacetate in DMSO) (Figure 2-1b). Although characterization of the enol form of benzofuran-2-one can be difficult,[87,88] the enolation chemistry is still attractive for its synthetic and physical organic chemistry potential.[86,89,90]

As a five-membered cyclic system, benzofuran-2-one , like other butyrolactones,[91] possesses a certain amount of ring strain[92] that can enhance ring opening reactivity.[93] Consequently, the benzofuran-2-one ring opens readily upon nucleophilic attack, such as by amines, alcohols, and hydroxide, forming the corresponding phenol derived amides, esters, and carboxylic acids (Figure 2-1f).

Delocalization through the aryl ring renders radicals of benzofuran-2-ones relatively stable, enhancing possibilities for potential applications (Figure 2-1c). Magus and coworkers[94] have shown that generation and dimerization of α-substituted benzofuran-2-one radicals at high temperature allows synthesis of an important building block of diazoamide A. Another well known application of a substituted benzofuran-2-one radical is its use as a chain-breaking antioxidant. Oxidative processes which involve a radical chain reaction lead to degradation of many materials; each radical initiation can damage numerous molecules in the system. Small molecule chain-breaking antioxidants, including Ciba's Irganox® HP-136 (Figure 2-4), are reactive through α-hydrogen abstraction; the resulting radicals trap harmful chain-propagating radicals and prevent degradation of organic materials.[95]

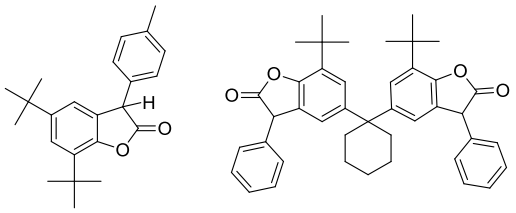

Irganox HP-136 GB 2257140A

Figure 2-4. Structures of commercial antioxidant HP-136 and patented polymer stabilizer GB2257140A.[96]

Benzotrifuranone (BTF) and its Potential Applications

Extension of the benzofuran-2-one chemical profile to phloroglucinol-derived lactones could expose new applications for such systems in supramolecular and materials chemistry. Toward this goal, a new small molecule, benzotrifuranone (BTF, **2-2**), was rationally designed. The target features pleasant C_{3h}-symmetry and three butyrolactone moieties around the central arene core.

It follows from the above discussion that BTF could serve as an important synthetic precursor for functionalized phloroglucinol derivatives. For example, the lactone rings could be opened by a variety of nucleophiles to introduce functional groups on the periphery of the phloroglucinol core (Figure 2-5a). Depending on the groups introduced, the resulting C_3-symmetric molecules may have potential applications in molecular recognition, molecular cage or capsule formation, and as LMWG.

More interestingly, it is reasonable to assume that the first lactone ring opening (that partially releases ring strain and changes the electronic nature of the arene core) will affect the reactivities of the remaining two lactone rings. Conceivable then is that two or more nucleophiles could open the three lactone rings sequentially in order to access differentially substituted phloroglucinol targets and a rational approach to controlling the symmetry of phloroglucinol derivatives (Figure 2-5b); the importance of the non-symmetric modification of persubstituted aromatics has been discussed in Chapter 1.

Extension of enolization reactions to BTF introduces opportunities to efficiently form *O*-substituted benzotrifurans (Figure 2-5c), [97] which are fully conjugated planar molecules. Although the benzotrifuran core was made over one century ago,[98] it has not been extensively studied due to a high-temperature and low-yielding traditional preparation. Such disk-shaped aromatic molecules have potential applications as liquid crystals[99] and gelators, and in charge transfer complexes and molecular electronics. The synthesis and properties of phloroglucinol-derived benzotrifurans will be discussed in Chapter 3.

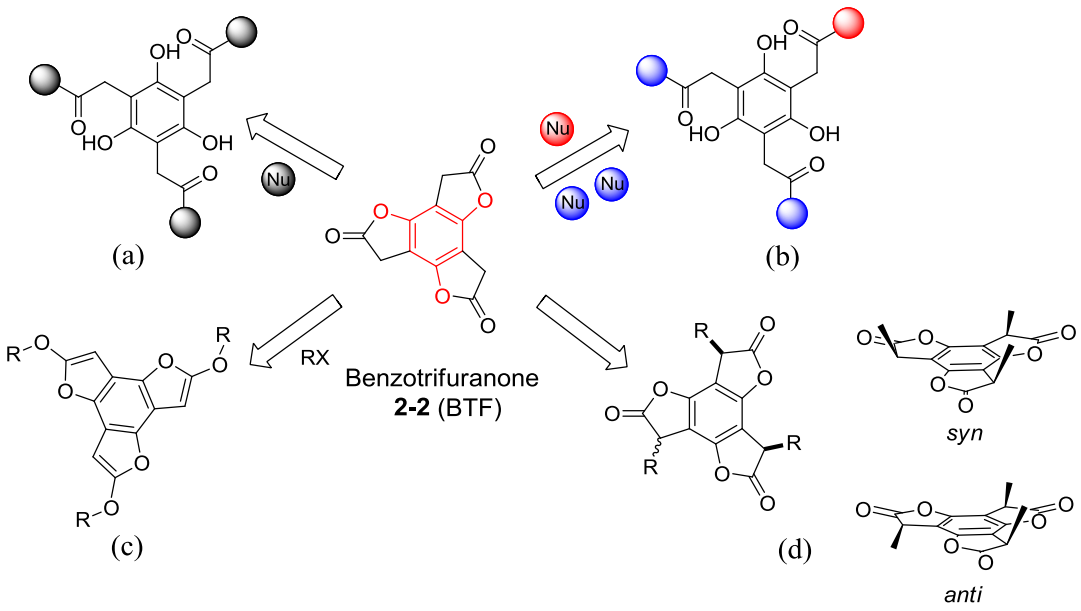

Figure 2-5. Potential applications of benzotrifuranone **2-2** (BTF): (a) C_3-symmetric phloroglucinol scaffold molecules; (b) differentially-functionalized persubstituted aromatics; (c) formation of benzotrifurans, disk-shaped aromatic molecules; (d) α-alkylated-BTF scaffolds.

Opportunities also exist for modification at the α-positions to the carbonyl groups of BTF. When functional groups are introduced to two or more α-positions, *syn* and *anti* diastereomers can be formed; shown are those arising from single substitution at each of the three sites (Figure 2-5d). The *syn* diastereomer bears C_3-symmetry, and having three functional groups point to the same side of the central benzene plane is potentially very useful for molecular recognition

studies, the formation of molecular cages, and catalyst design. This scaffold is reminiscent of the well studied "sterically-geared" 1,3,5-triethylbenzene platforms,[100] that have found numerous applications in these areas. Unlike the trialkylbenzene scaffolds, BTF features a larger and more electron rich aromatic ring component. Another point of distinction is that the *anti* diastereomer (Figure 2-5d), with two of three arms on the same side of the aryl plane, may be converted to the *syn* form through acid- or base-catalyzed keto-enol tautomerization. Additionally, through some external induction, such as crystallization, chelation, or chemical reaction, preferential consumption of one diastereomer can lead to interconversion to the other; these dynamics will be a topic of later discussion.

Synthesis

The construction of lactone rings involves fairly routine chemistry and many high-yielding methods have been reported specifically for benzofuran-2-one formation.[101-103] In one approach, cyclization occurs through reaction of the phenolic hydroxyl group with carboxylic acid derivatives at the *ortho* position, forming a benzolactone through a dehydration or transesterification reaction (Figure 2-6a).

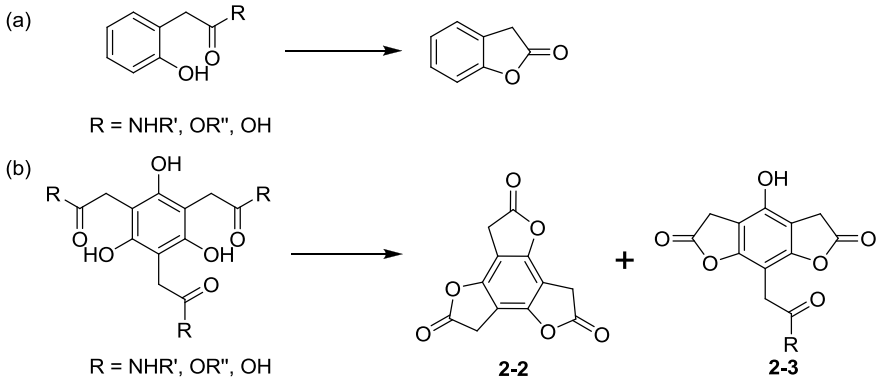

Figure 2-6. (a) A classical approach to the benzofuran-2-one; (b) possible synthesis of BTF (**2-2**) and its major dilactone by-product (**2-3**).

The same synthetic method can be applied to appropriately substituted phloroglucinol derivatives to form BTF, however, several partially-cyclized intermediates, including C_2-symmetric dilactone species **2-3**, can be obtained (Figure 2-6b). Even so, the initial synthetic plan was to introduce pendant esters to the 2,4,6-positions of phloroglucinol to form BTF **2-2** via transesterification chemistry under acidic conditions.

As previously reported,[104,105] trimethoxytriisopropylester **2-5** could be accessed from commercially available 1,3,5-trimethoxybenzene (via trinitrile intermediate **2-4**) in four steps. Demethylation of **2-5** using a strong Lewis acid, BBr_3, already yielded some of the monolactone species **2-7** as a by-product along with the desired product **2-6**; the yield of **2-7** increased up to 20% with higher temperature (Figure 2-7a). Utilizing **2-6** as the starting material, a variety of acid-catalyzed lactonization reaction conditions were then explored (Figure 2-7b). The desired **2-2** was formed in only trace quantities under most conditions, and irreproducibly up to 15% using a TFA/*o*-xylene mixture. Two possible dilactone intermediates, C_2-symmetric **2-8** and C_s-symmetric **2-9**, were generally isolated as the major products in the reactions.

Advanced dilactone intermediate **2-9** was used for complementary lactonization studies. When **2-9** was heated to reflux in toluene with catalytic HCl, the hydrolyzed dilactone species **2-10** formed and precipitated, indicating that the interconversion between the two dilactone species could occur under these conditions. Switching to trifluoroacetic acid (TFA) allowed formation of the desired product **2-2** in reasonable yield along with **2-8** and starting material **2-9** (Figure 2-7c). Again, the results speak to the reversibility of the acid-catalyzed lactonization reaction, but also the difficulty to exclusively form target product **2-2** under the reaction conditions. Additionally, the chromatographic separation of **2-8** and **2-9** from **2-2** turned out to be tedious, made worse by the sensitivity of **2-2** to silica gel. Overall, while target **2-2** could be prepared

from **2-9**, this route did not appear useful for the larger-scale production of the compound for further study.

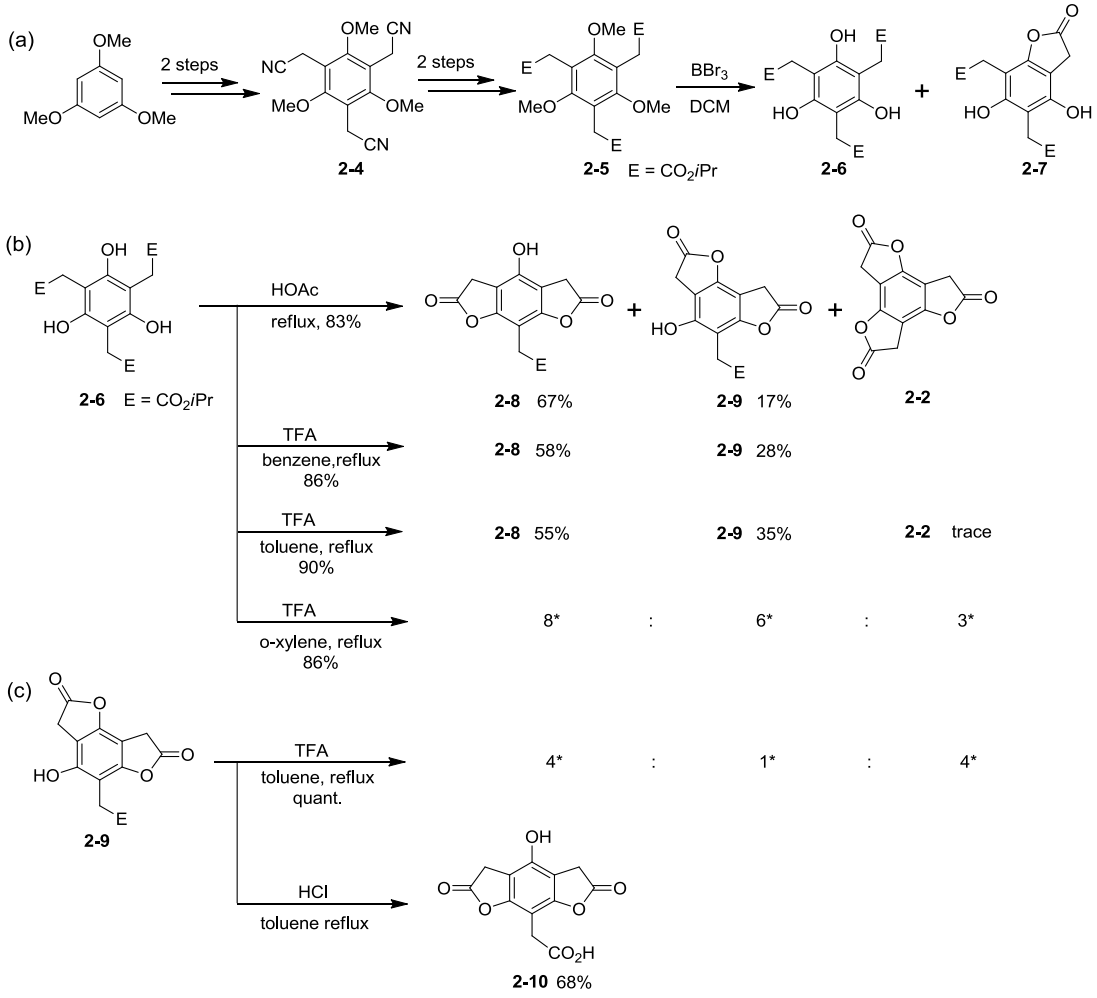

Figure 2-7. Attempts to prepare BTF from ester-functionalized phloroglucinol derivatives and advanced lactone intermediates: (a) synthesis of triester precursor **2-6**; (b) from **2-6** using protic acids; (c) from C_s-symmetric dilactone **2-9** using protic acids. Asterisk (*) indicates that the ratio of different products indentified by ^{1}H NMR.

In order to prepare BTF in higher yield, an alternative route was envisioned that would form **2-2** irreversibly via simple dehydration of intermediate triacid **2-11**, available from saponification of triester **2-6** (Figure 2-8). Among the different dehydrating conditions screened (Table 2-1), heating in polyphosphoric acid (PPA) was the highest yielding and most reproducible. The success of the reaction is due in part to the easy separation of BTF from **2-10**,

the major by-product, given a large solubility difference between the compounds in dichloromethane (DCM). DCM is first used to extract most of the BTF from the reaction mixture; the small amount of **2-10** transferred to the organic phase is removed by washing with aqueous base ($NaHCO_3$).

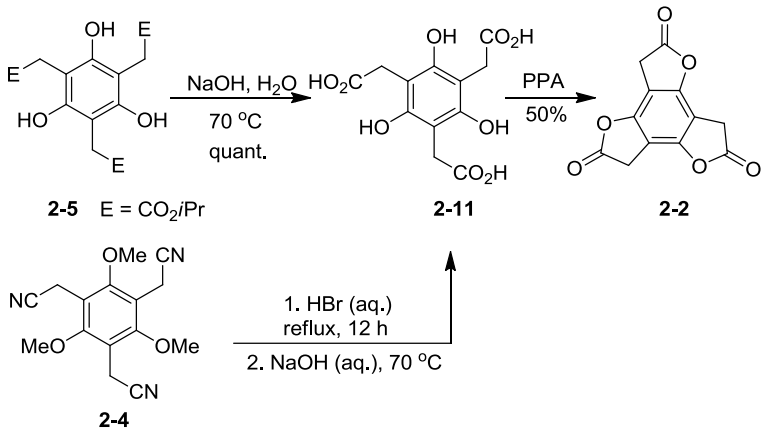

Figure 2-8. Optimized synthesis of BTF **2-2**.

An alternative and shortened synthesis of **2-2** was later found which directly converted **2-4** to **2-11** by overnight heating (of **2-4**, to reflux) in concentrated hydrobromic acid[106] followed by a basic work-up. The same dehydration conditions as described above gave **2-2** in 50% yield. Although the overall yield of the optimized syntheses of **2-2** are modest, the routes are reproducible and can supply BTF **2-2** on a multi-gram scale (Figure 2-8).

Table 2-1. Results of dehydration reaction (**2-11** → **2-2**) condition screening.

Dehydrating conditions	Reaction condition	Yield of **2-2**
$POCl_3$	Reflux 1 hour	< 10%
$POCl_3$	Reflux 4 hours	< 10%
PPA	110 °C, 4 hours	20%
PPA	130 °C, overnight	40%
PPA	110 °C, overnight	50%
None	TFA, toluene, reflux overnight	No product (**2-8** obtained)
4 Å molecular sieves	120 °C	trace

Characterization of BTF 2-2

NMR Spectra of 2-2

BTF **2-2** was obtained as an off-white powder that has modest solubility in many common organic solvents including DMSO, THF, CH_3CN, DCM and $CHCl_3$. The identity of the highly symmetric compound is quickly confirmed by NMR analysis (DMSO-d_6) where it shows a single peak in the ^{1}H NMR spectrum at $\delta = 4.01$ ppm for the six chemically equivalent methylene protons and just four peaks by ^{13}C NMR analysis (δ) 30.1 (CH_2), 101.9 (O−C=<u>C</u>), 148.8 (O−<u>C</u>=C), and 173.4 (C=O) ppm. Comparison of the NMR data with the corresponding signals of reference benzofuran-2-one **2-1** (^{1}H NMR: $\delta = 3.90$ (CH_2) ppm; ^{13}C NMR: $\delta = 32.6$ (CH_2), 110.1 (O−C=<u>C</u>), 154.1 (O−<u>C</u>=C), and 174.4 (C=O) ppm) shows most notably that the α-methylene protons of **2-2** are somewhat deshielded while its C−O lactone bond is also perturbed. Although the enol tautomer of BTF possesses a more extended π-conjugation system, it is not detectable in solution and no benzofuran aromatic or enol hydroxyl protons were found by ^{1}H NMR in various solvents ($CDCl_3$, DMSO-d_6, and CD_3CN).

Crystallographic Analysis of BTF 2-2

A single crystal of **2-2** was obtained by slow diffusion of pentane into its concentrated chloroform solution; the X-ray crystal structure is shown in Figure 2-9. Most surprisingly, the crystal is *noncentrosymmetric* and occupies the orthorhombic space group *aba2* (point group *mm2*); the result defines a relatively rare example of polar crystal formation from an achiral, C_{3h}-symmetric species. A Cambridge Structural Database (version 5.30) search reveals that **2-2** is the first reported example of a C_{3h}-symmetric molecule in the *aba2* space group. Two slightly different molecules comprise the crystal unit cell. In one, **A**, the central benzene ring and three fused lactone rings are essentially planar; the most that any non-hydrogen ring-containing atom deviates from the C3–C4–C7 plane is 0.05 Å. The second molecule, **B**, is slightly distorted with

respect to its central six-membered and peripheral five membered rings; here the most that any non-hydrogen ring containing atom is removed from the C3–C4–C7 plane is 0.18 Å (for C9B). Although these small deviations are not reproduced in electronic structure calculations that predict a planar **2-2**, the calculated and experimental bond lengths and angles agree within 0.02 Å and 1.5°. Worth noting, the experimentally determined parameters for **2-2** are also similar to those reported for simple 5-hydroxy-2(3*H*)benzofuranone (CSD code: BIZCIW[107]) and calculated for **2-1**.

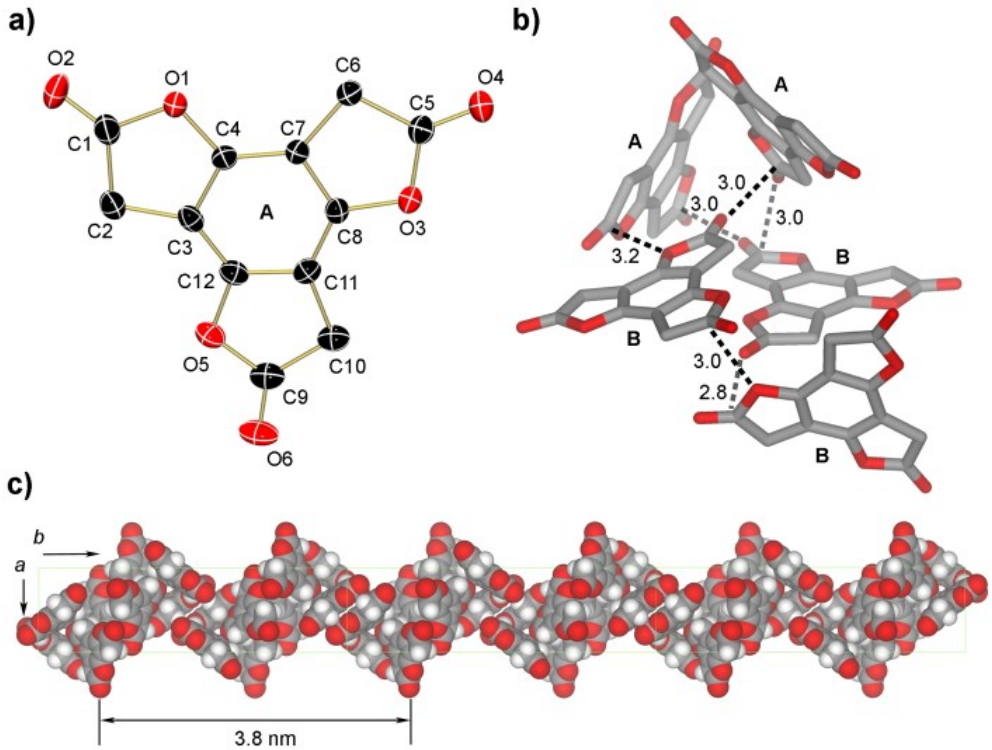

Figure 2-9. X-ray crystal structure of **2-2**: (a) ORTEP plot of molecule A (thermal ellipsoids shown at the 50% probability level and hydrogen atoms have been removed for clarity); (b) O···C=O interactions between molecules A and B that define the molecular packing (distances in Å); (c) helical arrangement of **2-2** along the *b* axis.

The packing structure of **2-2** (Figure 2-9b) is surprisingly devoid of stacking arrangements and is instead dominated by O···C=O dipolar interactions[108] and C−H···O contacts.[109] The former come in two forms: C=O···C=O defined by an O···C distance of 2.8–3.0 Å and an

O···C=O angle of 97–107° (approaching the Bürgi-Dunitz angle[110]), and (O=C)O···C=O interactions, also defined by short distances (3.0–3.2 Å) and an O···C=O angle of 76–98°. Most striking is the consequence of these primarily electrostatic interactions on the packing structure, where a helical arrangement develops with a repeat distance defined by the *b* unit cell dimension (37.939 Å) (Figure 2-9c). Helices are relatively rarely presented by planar, achiral molecules in the context of acentric crystals,[111] although the architectures are relevant to the design of nonlinear optics (NLO, importance and applications have been discussed in Chapter 1), ferroelectrics, and electrooptics.[112]

Optical Properties of BTF 2-2

The UV-Vis spectra of all prepared phloroglucinol-derived lactones were recorded for evidence of enol tautomers. Since the enol tautomers of BTF and related lactones feature more extended π-conjugation, the major absorption of the enol species should be red-shifted relative to the corresponding carbonyl forms. The UV-Vis spectrum of **2-2** in CH_3CN shows a strong absorption at λ_{max} = 215 nm (ε = 22 400 M^{-1} cm^{-1}), a shoulder at intermediate energy, and a very weak absorption at lower energy (λ_{max} = 270 nm; ε = 710 M^{-1} cm^{-1}). However, the UV absorption at 270 nm is not unique to **2-2**; it is found in the UV spectra of dilactone species **2-8** and **2-9**, and benzofuran-2-one **2-1**. In fact, all of the lactones share the same absorption pattern and intensity (Figure 2-10, Table 2-2).

The weak UV absorption at ~ 270 nm is easily ruled out as an evidence of enol tautomers because the known compound 2-keto-3,3-dimethyl-2,3-dihydrobenzofuran[113] and new compound **2-24** (vide infra) (Figure 2-11), both lacking lactone α-protons, have similar UV absorption spectra. The origin of this UV absorption is possibly from a π→π* transition of the central arene ring (known as the B band[114]).

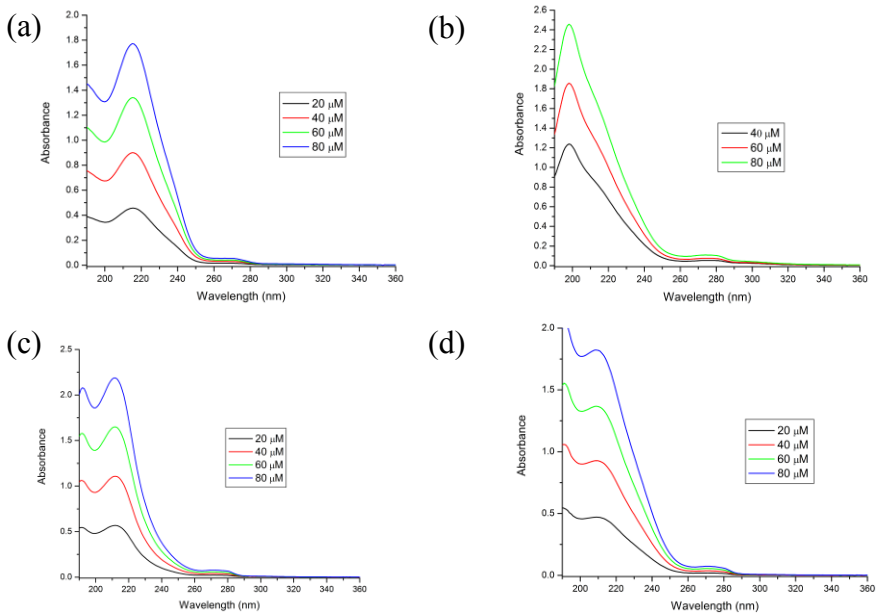

Figure 2-10. UV spectra of (a) **2-2**; (b) **2-1**; (c) **2-8**; and (d) **2-9**.

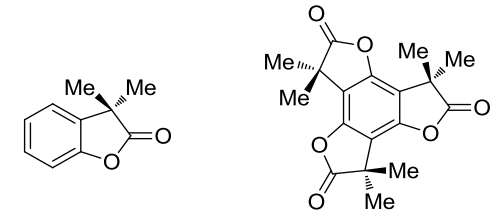

2-keto-3,3-dimethyl-2,3-dihydrobenzofuran

2-24

Figure 2-11. Structures of two benzofuranone species lacking α-hydrogens.

Table 2-2. UV absorption bands and intensities of BTF **2-2,** dilactones **2-8** and **2-9**, and benzofuran-2-one **2-1** in CH_3CN.

Compound	λ_{max} (nm)	ε (M^{-1} cm^{-1})
2-2	215	22400
	270	710
2-1	199	31000
	275	1328
2-8	212	27000
	271	976
2-9	209	23000
	271	929
2-24	218	22459
	270	1092
2-Keto-3,3-dimethyl-2,3-dihydrobenzofuran (in ethanol)	270	1225

IR spectroscopic studies have been performed to further explore the unique structure of **2-2**. In the IR spectrum of **2-2** (KBr pellet), no sp^2 C–H stretching absorptions indicative of enol tautomers were found. It is worth noting that the single C=O stretch (1822 cm^{-1}) of **2-2** is higher in energy than **2-1** (1807 cm^{-1}) (Figure 2-12) and comparable to four-membered ring *β*-butyrolactone (1825 cm^{-1}; neat[115]); these trends are also reproduced in DFT vibrational frequency calculations (calculated (DFT-RB3LYP/6-311+G*) C=O vibrational frequencies (unscaled): **2-1** (1877 cm^{-1}); **2-2** (1891 cm^{-1}); *β*-butyrolactone (1909 cm^{-1})). The explanation for the C=O IR shift for **2-2** (relative to **2-1**) is that increased ring strain uses more *p* orbital character in the C−C(=O) bond causing a reduction of *p* orbital character and increase of *s* orbital with respect to the C=O σ bond. The implied strengthening of the C=O bond of **2-2** versus **2-1** is reflected in its stretching frequency[116,117] and appears consistent with the ^1H and ^{13}C NMR data. To conclude, the NMR, UV, IR, and X-ray data for **2-2** show no evidence for enol tautomer formation in either solution or the solid phase even though complete tautomerism would generate a fully aromatic benzotrifuran ring system as shown in Figure 2-5c.

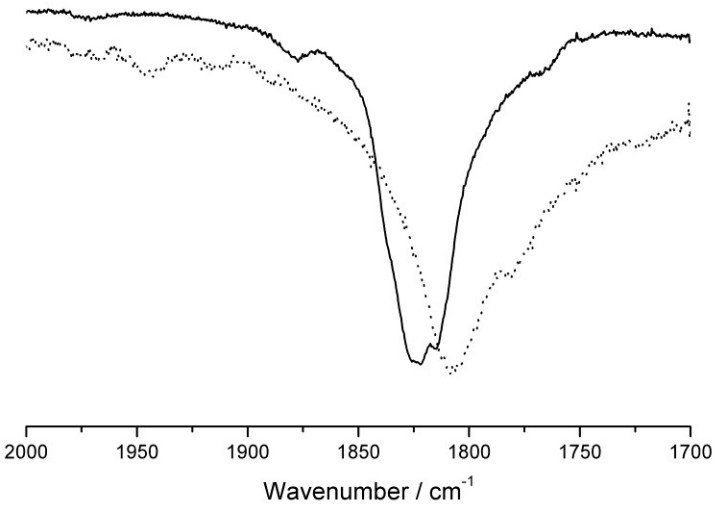

Figure 2-12. The comparison of carbonyl absorptions in IR spectra of **2-1** (dot line) and **2-2** (solid line).

Ring opening of BTF

As discussed before (Figure 2-5a), one important application of BTF is as a key synthetic precursor for C_3-symmetric phloroglucinol derivatives. Upon the attack of different nucleophiles, the lactone rings can be opened to introduce various functional groups on the periphery. This chemistry is illustrated by choosing a series of primary and secondary alkyl amines as nucleophiles as shown in Figure 2-13; the corresponding ring-opened products (**2-13a-d**) were obtained at room temperature in good yields.

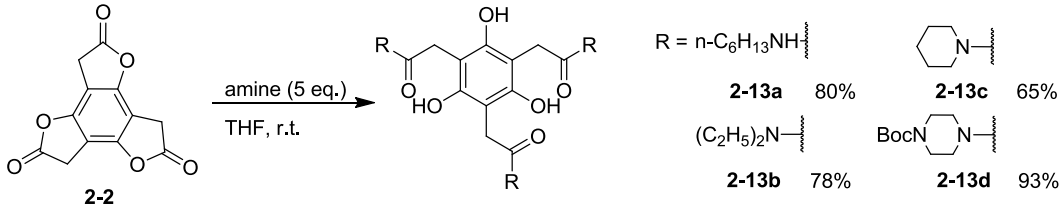

Figure 2-13. Ring opening reactions of BTF with a series of alkyl amines.

However, simply mixing BTF with excess aniline at room temperature nets no reaction due to the poorer nucleophilicity of this species. Upon heating the reaction, multiple ring opening products were obtained and the results are summarized in Table 2-3. According to the results, when the reaction was warmed to 40 °C, only one lactone ring was opened to form dilactone-monoamide species **2-14** and half the starting material was recovered. When the reaction temperature was raised to 50–55 °C, the second lactone ring opened and the reaction formed a mixture of BTF, dilactone **2-14**, and monolactone **2-15**. Ultimately, when the reaction was heated to 70 °C or above, all three lactone rings were opened to form triamide **2-16** (Figure 2-14a).

The set of experiments is important toward understanding how BTF can be used to prepare differentially-substituted phloroglucinol derivatives. BTF is a C_{3h}-symmetric molecule and each lactone ring possesses the same chemical reactivity. It now appears that each lactone opening

affects the reactivity of the remaining lactones, a result consistent with what can be inferred on the basis of IR spectra. One can imagine that the three lactone rings could potentially be opened in a stepwise fashion using different nucleophiles to form C_{2v}- (two different types of arms) or even C_s- (three different types of arms) symmetric phloroglucinol derivatives. One example is shown (Figure 2-14b) that reacts dilactone **2-14** with dodecylamine to form **2-17** in the first C_{2v}-symmetric phloroglucinol derivative synthesis from BTF.

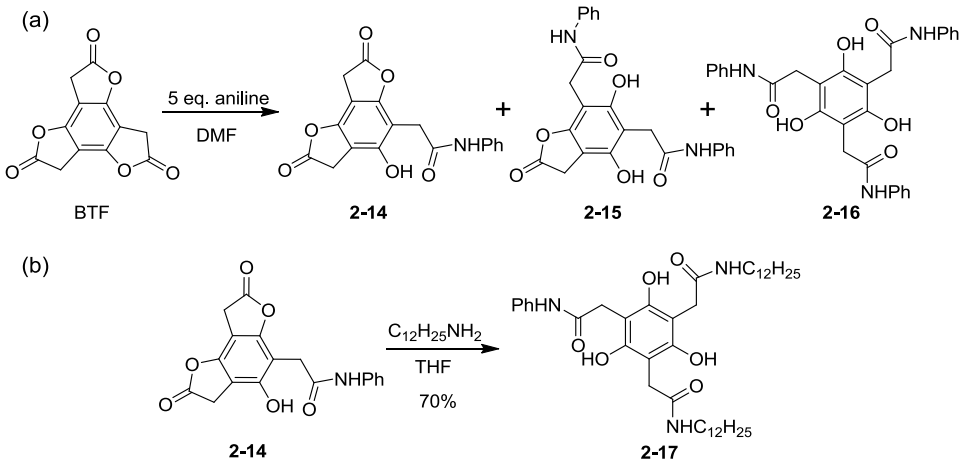

Figure 2-14. (a) The ring-opening of BTF with excess aniline yields multiple products; (b) one example of a C_{2v}-symmetric phloroglucinol derivative prepared from BTF.

Table 2-3. Experimental results for BTF ring opening reactions using excess aniline at different temperatures.

Reaction temperature (°C)	**BTF**	**2-14**	**2-15**	**2-16**
40[a]	50%	50%	trace	0%
50[a]	6%	67%	27%	0%
55[b]	10%	67%	22%	0%
70[a]	0%	0%	0%	quant.

Reaction times: (*a*) 16 hours; (*b*) 3.5 hours.

Ongoing research in the Castellano group is finding that the first lactone ring of BTF can be quite selectively opened when the molecule is treated with a limited amount (1.2 equiv in DMF) of a primary alkyl amine. This new work is showing that sequential opening of the lactone rings of BTF does not have to be limited to poor nucleophiles. In conclusion, symmetry

control of phloroglucinol derivatives is achievable beginning from a simple symmetric BTF precursor, and diverse functionality can likely be introduced to the phloroglucinol platform in this fashion that is relevant to a number of potential applications.

Modification at the α-Carbon of BTF

Inspired by the rich chemical profile of benzofuran-2-one and its derivatives, its C_{3h}-symmetric analogue, BTF **2-2**, could enjoy potential applications as a materials stabilizer, synthetic intermediate, or building block for supramolecular chemistry. Most commercial and reported benzofuranone species feature substituents on their α-carbon positions. The substituents not only improve some physical properties of the lactones (and presumably BTF), such as solubility, but also increase the stability of radical,[118] anion, and even enol species for wider applications in materials and supramolecular chemistry.

Attempts at C-Modification

The most convenient way to generate α-substituted BTF derivatives would be to deprotonate **2-2** under basic conditions, and intercept the intermediate enolate anion with an appropriate electrophile. Unfortunately, after trying various bases (LDA, NaH, Et_3N, etc.) for enolate generation, followed by addition of methyliodide, no alkylated product could be isolated from what were very complicated polar product mixtures. One relevant literature example[83] does indicate that the α-alkylated product of simple benzofuran-2-one quickly reacts with a second equivalent of base and electrophile toward over (C-)alkylation. Other factors, including the high nucleophilic ring opening reactivity of BTF, competitive O-alkylation reactions, oligomerization, etc. make the substitution reaction even worse. Knoevenagel condensations, which would see the lactones react with ketones[119] or aldehydes[120] to functionalize the α-position (as an alkene), also were met with failure (again, presumably due to the lability of the lactone rings under basic conditions).

In most reported cases of α-substituted benzolactone synthesis,[83,113] the substituents have been introduced before lactonization (Figure 2-15a). The synthesis of α-substituted BTF using this approach started from trinitrile compound **2-4**. Methyl groups were installed in good yield via standard S_N2 chemistry to form **2-18a** as a 3:1 mixture of *anti* and *syn* diastereomers. This diastereomeric ratio is predicted by statistics and a full discussion of the result is presented later. Hydrolysis of **2-18a** gives trimethyl substituted triacid **2-19** which, in theory, could be esterified to form the corresponding triester **2-20**. Unfortunately, **2-19** could not be esterified efficiently under a variety of attempted conditions (using different alcohols and acid catalysts) and the reaction yields were consistently low (Figure 2-15b). One possible explanation for the result is that the α-methyl groups increase the steric bulk of triacid **2-19**, impeding the esterification reaction.

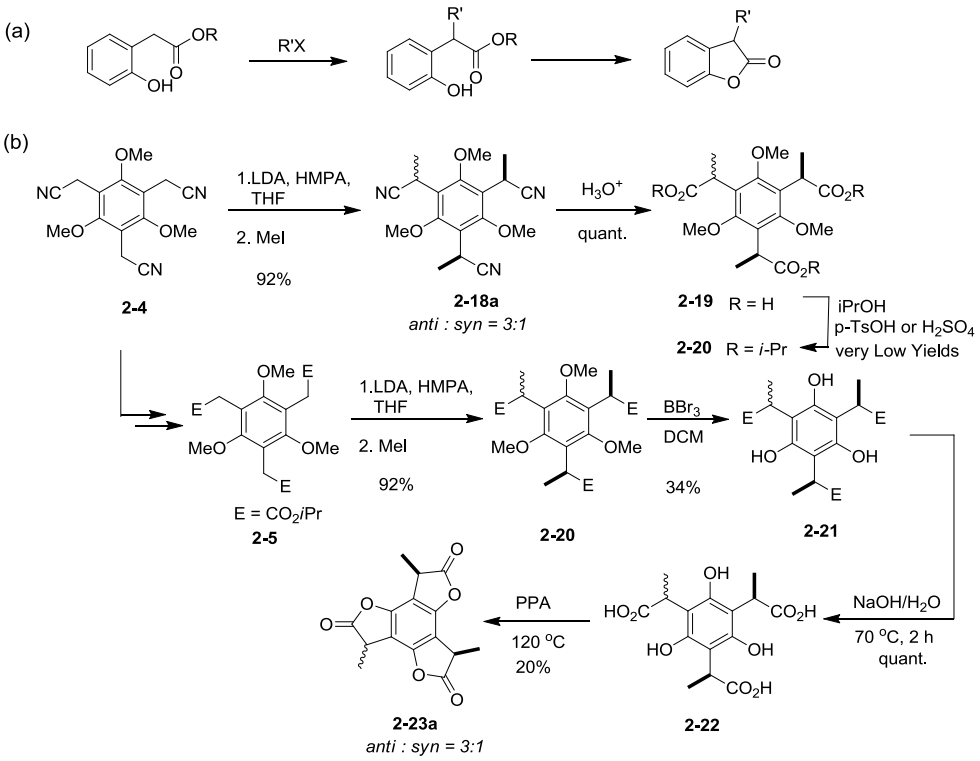

Figure 2-15. (a) A common approach to synthesize α-substituted benzofuranones; (b) synthesis of trimethyl benzotrifuranone (TMBTF) **2-23a**.

To solve the problem, the sequence of reactions was changed and a new synthesis started from triester **2-5**. Methylation using LDA and MeI produced **2-20** in decent yield, and subsequent demethylation, saponification, and lactonization provided the target trimethyl benzotrifuranone (TMBTF) **2-23a** (Figure 2-10b).

Later experiments revealed that a milder base, sodium hydride, could be used in place of LDA to effect the conversion of **2-4** to **2-18a** with no change in the *anti* : *syn* ratio. Using this result, a series of substituted trinitrile compounds **2-18a-d** were synthesized, including some partially alkylated trinitriles (**2-18b, 2-18c**). It was also discovered that treatment of **2-18a-d** with concentrated aqueous HBr (at reflux) resulted in both demethylation and hydrolysis in one pot to yield the corresponding triacid products (without purification). With these in hand, PPA-promoted cyclization then provided desired trilactones **2-23a-d** (Figure 2-16). TMBTF **2-23a** showed much cleaner reactivity in a further α-alkylation reaction compared with BTF **2-2**, and hexamethyl BTF **2-24** was easily obtained by simple treatment with NaH and MeI in a DMF solution.

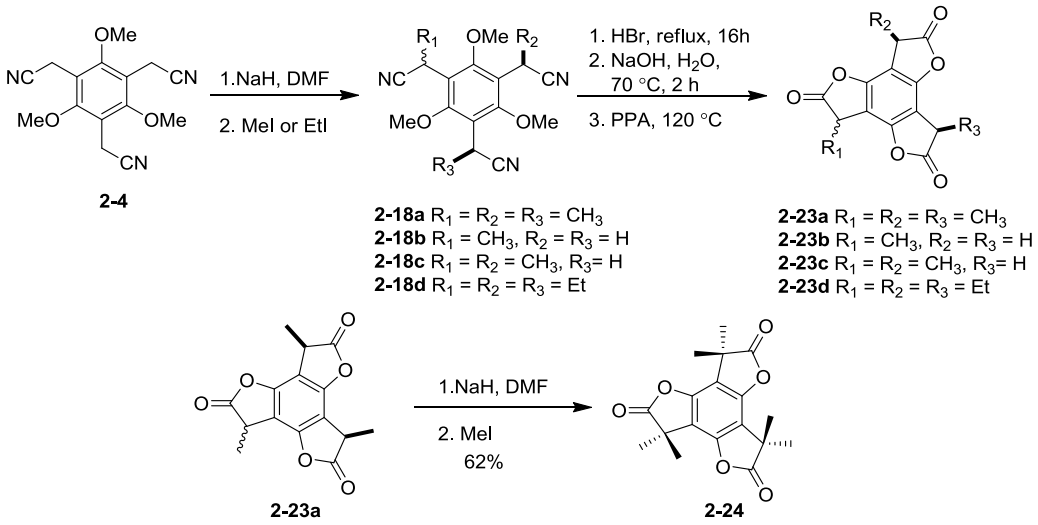

Figure 2-16. Alternative synthetic route to a family of α-substituted BTF derivatives **2-23a–d** and synthesis of hexamethyl BTF **2-24**.

Characterization of TMBTF 2-23a

As predicted, **2-23a** has much better solubility than **2-2** in organic solvents due to its three additional methyl groups. Mentioned above, **2-23a** is formed as a mixture of *syn* and *anti* diastereomers that differ with respect to the orientation of the methyl groups. For the *syn* diastereomer, the substituents point to the same side of central aryl plane, whereas in the *anti* diastereomer only two methyl groups point to a common side. The statistical *syn* : *anti* ratio is 1:3 provided that both diastereomers are similar in energy (Figure 2-17).

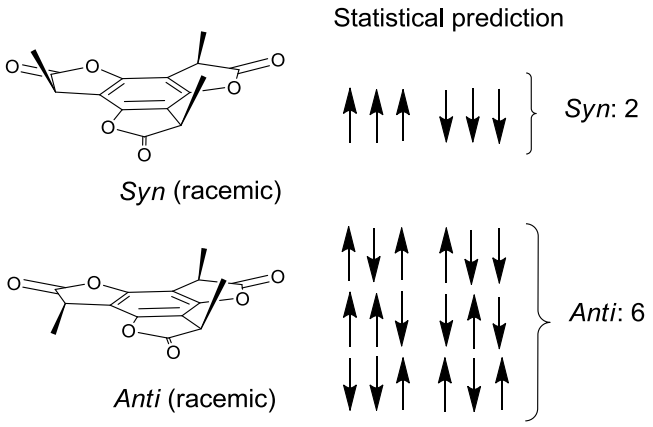

Figure 2-17. Statistical expectation for TMBTF **2-23a** diastereomer formation.

The most useful technique to determine the experimental ratio of the two diastereomers is ^{1}H NMR. The *anti* diastereomer is a C_1-symmetric molecule, so the three methyl groups are each in different chemical environments and should give rise to three equally intense doublets (the methyl protons are coupled to the benzylic proton on the lactones); in comparison, the *syn* diastereomer is a C_3-symmetric molecule and the three methyl groups are chemically equivalent (and only one doublet is expected).

A statistical ratio of the two diastereomers (*syn* : *anti*), combined with the expected peak areas from the above analysis, is expected to produce a maximum of four equal intensity methyl doublets. When the ^{1}H NMR of **2-23a** is taken in deuterated benzene, there are three doublets (*J*

= 7.5 Hz) in the methyl region (1.1–1.2 ppm) with relative areas of 2:1:1 (Figure 2-18a). That the most upfield doublet **a** (1.09 ppm) belongs to the *syn* diastereomer and other two doublets belong to the *anti* diastereomer has come through analysis of the ^{1}H NMR spectrum of *anti*-**2-23a**, obtained as a single crystal. In this case (Figure 2-18b), the intensity of peak **a** significantly decreases, associating this signal to *syn*-**2-23a**. The strongest doublet in both spectra is attributed to coincident signals from methyls **b** and **c** in *anti*-**2-23a** (Figure 2-18) that share very similar chemical environments. Overall, the NMR data proves that the experimental ratio of the two diastereomers is consistent with statistical predictions, and that the two diastereomers are therefore similar thermodynamically.

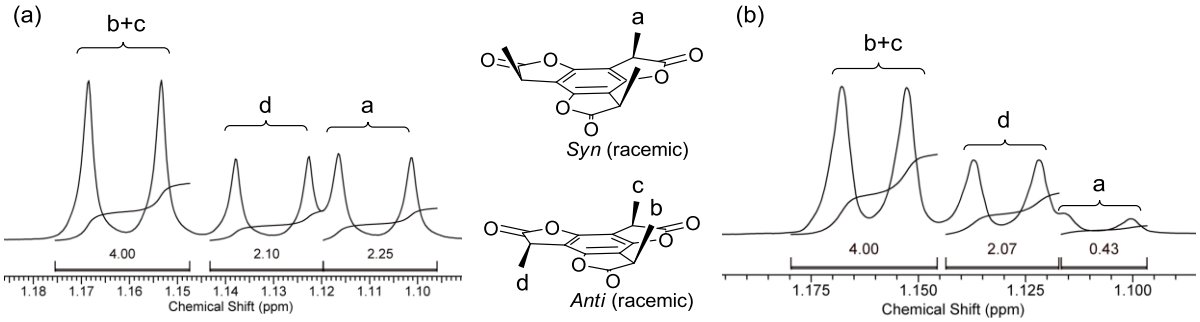

Figure 2-18. The methyl region of the ^{1}H NMR spectra (benzene-d_6) of a (a) diastereomeric mixture of **2-23a** and (b) a single crystal of *anti*-**2-23a**.

Crystallographic Analysis of *syn*-TMBTF.

Colorless single crystals of **2-23a** formed by slow evaporation of the diastereomeric mixture from chloroform solution. X-ray crystal structure analysis indicates that only the *syn* diastereomer crystallizes under these conditions (a single crystal of *anti*-**2-23a** was obtained using a different method, vide infra). In the crystal structure of *syn*-**2-23a** (space group *P21/c*), both enantiomers (*S,S,S* and *R,R,R*) are found in the unit cell and arrayed alternatively. A number

of C−H···O interactions are evident between the two enantiomers where the $C_{(methyl)}$···O and $C_{(CH)}$···O distances are 3.2 Å and 3.3 Å, respectively (Figure 2-19b).

π-π Interactions between the central benzene rings of two adjacent enantiomers also dominate the solid phase packing pattern of *syn*-**2-23a**. Due to this type of interaction and the structural characteristics the diastereomer, the molecules tend to adopt a "back-to-back" packing pattern and form two layers: one π-π stacking layer with an interaction distance of 3.52 Å and one lipophilic layer with a thickness of 4.72 Å (Figure 2-19c).

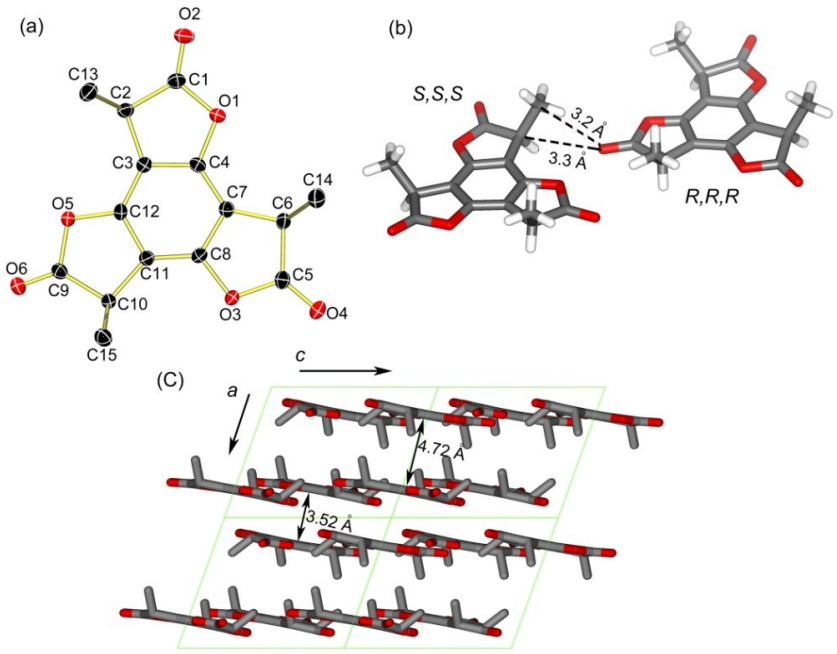

Figure 2-19. X-ray crystal structure of *syn*-**2-23a**: (a) ORTEP plot of the *R,R,R*-enantiomer (thermal ellipsoids shown at the 50% probability level and hydrogen atoms have been removed for clarity); (b) C−H···O interactions found between the *R,R,R* and *S,S,S* enantiomers that define the molecular packing; (c) crystal packing of *syn*-**2-23a** along the *b* axis.

Structurally similar to the *syn* diastereomer of **2-23a**, C_3-symmetric "all-arms-up" platforms (such as persubstituted 1,3,5-triethylbenzene scaffolds[100]) have found applications in molecular recognition, cage molecule formation, and as ligands for metals. Unlike other platforms, the substituted BTF scaffold features a more electron rich central aromatic ring which

could potentially increase its affinity for cationic guests; moreover, easy formation of hexasubstituted BTFs (Figure 2-16) will encourage the exploration of scaffolds with double-sided functionality.

Crystallographic Analysis of *anti* 2-23a.

Colorless single crystals of *anti*-**2-23a** were obtained by slow diffusion of pentane into a concentrated ethyl acetate solution of **2-23a**; the X-ray crystal structure (Figure 2-20) and ^{1}H NMR spectrum (Figure 2-18b) are shown. The crystal is noncentrosymmetric and occupies the orthorhombic space group *Pbca*.

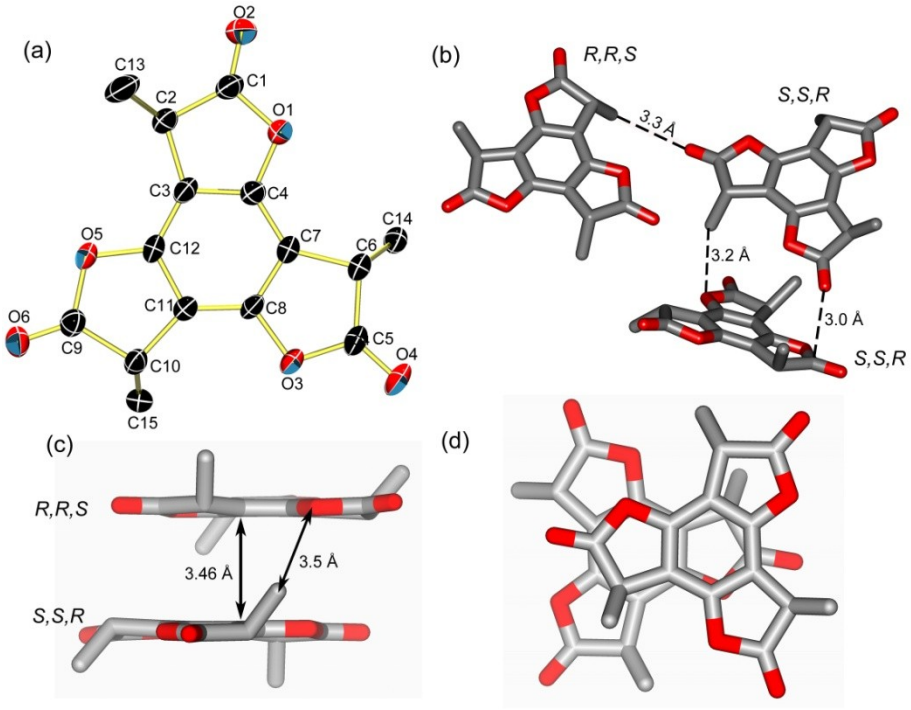

Figure 2-20. X-ray crystal structure of *anti*-**2-23a**. One CH–CH_3 unit (C6–C14) is disordered and has been refined in two parts. The site occupation was refined as 0.85/0.15 for the major and minor parts, respectively, and only the major part is shown: (a) ORTEP plot of *anti*-**2-23a** (thermal ellipsoids shown at the 50% probability level and hydrogen atoms have been removed for clarity); (b) C−H···O and O···C=O interactions between two enantiomers; side view (c) and top view (d) of the π-π stacking interactions between two enantiomers.

There are three chiral centers on *anti*-**2-23a** and its two enantiomers (*R,R,S* and *S,S,R*) are arrayed alternatively in the unit cell. Similar to *syn*-**2-23a**, C−H···O interactions were found in

the crystal with distances of 3.3 Å ($\underline{C}H_3\cdots O(C=O)$) and 3.2 Å ($\underline{C}H_3\cdots O(C-O)$). Additionally, C=O···C=O dipolar interactions were found with an O···C distance of 3.0 Å and an O···C=O angle of 94°, very similar measurements to ones reported for BTF **2-2** (vide supra). Analysis of the π-π stacking interactions between the two enantiomers reveals an intermolecular distance of 3.46 Å (Figure 2-20c), and from the top view of the stacking (Figure 2-20d), one can clearly see that two enantiomers stack in an antiparallel fashion. Each enantiomer has one methyl group pointing toward the counterpart while the remaining two methyl groups point away from the other enantiomer. The methyl groups do not disturb the π-π stacking interactions, instead, they provide some enhancement by C−H···O interactions (distance of $\underline{C}H_3\cdots O(C-O)$ is 3.5 Å).

Interconversion between *syn* and *anti* 2-23a

While the ^{1}H NMR spectra for the single crystals of **2-23a** (in benzene-d_6) show unique peaks for the corresponding diastereomer (in the case of *anti*-**2-23a**, see Figure 2-18b), the ^{1}H NMR spectrum of the mother liquor (from which the crystals were grown) still shows a diastereomeric mixture, identical to the spectrum taken before crystallization. The result suggests interconversion between the two diastereomers under the crystallization conditions; when one diastereomer crystallizes out, the equilibrium is restored through conversion of the enriched diastereomer to its stereoisomer. The enol form of **2-23a** is the only reasonable intermediate through which to achieve this interconversion, despite the lack of evidence for its existence.

If the two diastereomers of **2-23a** interconvert through an enol intermediate as shown in Figure 2-21a, the addition of a deuterium source should result in deuterium incorporation at the benzylic positions of the lactones (Figure 2-21b), a process observable by NMR. The ^{1}H NMR of **2-23a** in DMSO-d_6 is shown in Figure 2-21c. Addition of excess D_2O to the NMR sample solution clearly results in disappearance of the α-CH peak; concomitant decoupling of the methyl

group signal (Figure 2-21c) indicates that the benzylic protons on **2-23a** are completely exchanged. The same deuteration experiments were carried out in acetone and acetonitrile to give similar results. The findings show that the *anti* and *syn* forms of **2-23a** can be rapidly interconverted through the enol form**.** This encourages the design of dynamic hosts from the scaffolds as well as findings ways to lock the enol tautomer to form benzotrifuran derivatives as shown in Figure 2-5c.

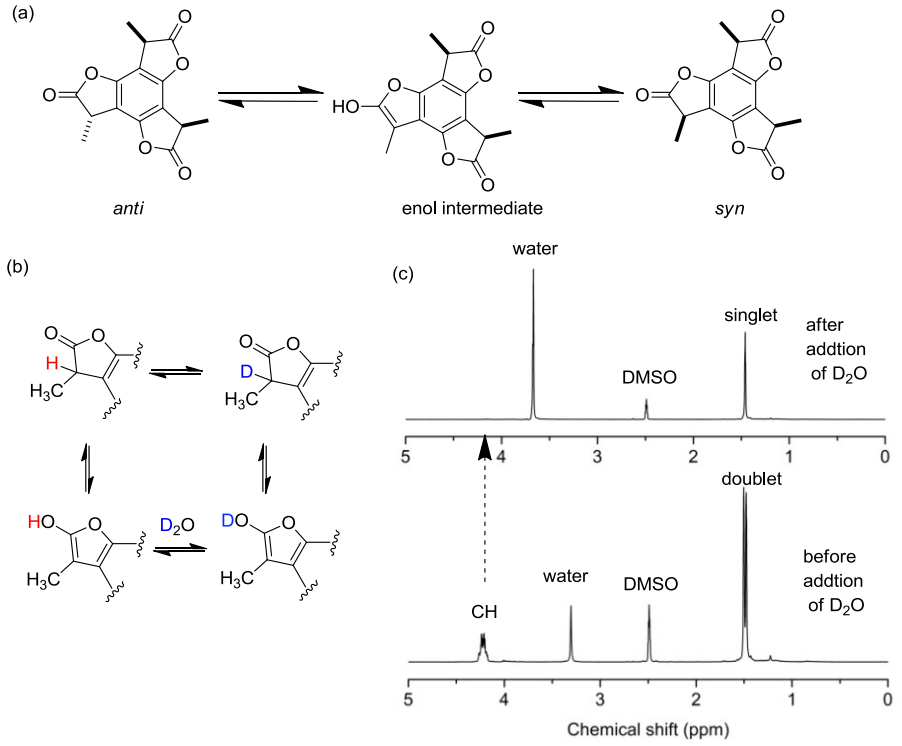

Figure 2-21. Illustration of the (a) equilibrium between the *syn* and *anti* diastereomers of **2-23a** via an intermediate enol; (b) mechanism of H-D exchange and (c) ^{1}H NMR spectra of **2-23a** before and after the addition of D_2O.

Conclusion

A family of benzotrifuranones has been prepared form a commerically available phloroglucinol derivative. BTFs have been characterized by NMR, UV, and IR spectroscopic techniques. An X-ray crystal structure of BTF **2-2** shows that weak C=O···C=O and C–H···O interactions dominate the solid phase packing of **2-2,** resulting in an interesting helical packing

pattern. The ring opening reactivity of **2-2** was also studied, and the experimental results show that the three lactone rings can be opened stepwise by different primary amines, suggesting that symmetry control of phloroglucinol derivatives can be achieved through this approach. Substituted BTF **2-23a** was also studied since its *syn* diastereomer is a very promising scaffold for applications in molecular recognition. X-ray crystal structures of both *syn* and *anti* diastereomers of **2-23a** were obtained and analyzed. The interconversion between the two diastereomers in solution was also studied by NMR experiments and the enol intermediate was suggested to be involved in the mechanism.

Experimental Section

Materials and General Methods

Reagents and solvents were purchased from commercial sources and used without further purification unless otherwise specified. THF, ether, CH_2Cl_2, and DMF were degassed in 20 L drums and passed through two sequential purification columns (activated alumina; molecular sieves for DMF) under a positive argon atmosphere. Thin layer chromatography (TLC) was performed on SiO2-60 F254 aluminum plates with visualization by UV light or staining. Flash column chromatography was performed using Purasil SiO_2-60, 230−400 mesh from Whatman. Melting points (m.p.) were determined on a Mel-temp electrothermal melting point apparatus and are uncorrected. 300 (75) and 500 (125) MHz ^1H (^{13}C) NMR spectra were recorded on Varian Mercury 300 or Gemini 300 or Inova 500 spectrometers. Chemical shifts (δ) are given in parts per million (ppm) relative to TMS and referenced to residual protonated solvent ($CDCl_3$: δ_H 7.27 ppm, δ_C 77.00 ppm; DMSO-d_6: δ_H 2.49 ppm, δ_C 39.50 ppm). Abbreviations used are s (singlet), d (doublet), t (triplet), q (quartet), quin (quintet), hp (heptet), b (broad), and m (multiplet). UV/Vis absorption spectra were obtained using a Cary 100 Bio spectrophotometer and 1 cm quartz cells. ESI-TOF- and DART-TOF-MS spectra were recorded on a Agilent 6210

TOF spectrometer. CI-MS spectra were recorded on a Thermo Trace GC DSQ (single quadrupole) spectrometer. Elemental analyses were performed on a Carlo Erba-1106 instrument.

Synthesis

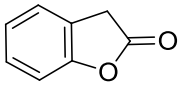

Benzofuran-2(3H)-one (2-1). Benzofuranone **2-1** was synthesized according to a literature procedure:[103] ^{1}H NMR (DMSO-d_6) δ 3.90 (s, 2H), 7.11–7.17 (m, 2H), 7.27–7.37 (m, 2H). ^{13}C NMR (DMSO-d_6) δ 32.6, 110.1, 123.7, 124.3, 124.8, 128.3, 154.1, 174.4.

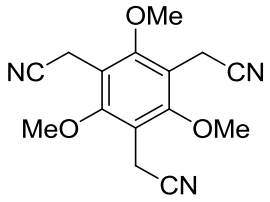

(3,5-Bis-cyanomethyl-2,4,6-trimethoxy-phenyl)-acetonitrile (2-4). To a solution of 1,3,5-tris-bromomethyl-2,4,6- trimethoxybenzene[121] (5.00 g, 11.2 mmol) in CH_3CN (65 mL), was added KCN (3.28 g, 50.4 mmol) and 18-crown-6 (0.74 g, 2.8 mmol), followed by the addition of aqueous KI solution (0.11 g KI in 10 mL water). The resulting solution was stirred at room temperature for 24 hours and then poured into ice-cold water (300 mL). The white precipitate that formed was separated and dried under vacuum to yield **2-4** (2.9 g, 92%) as a white solid: ^{1}H NMR (DMSO-d_6) δ 3.85 (s, 9H), 3.90(s, 6H). ^{13}C NMR (DMSO-d_6) δ 13.0, 62.5, 116.4, 119.0, 158.0.

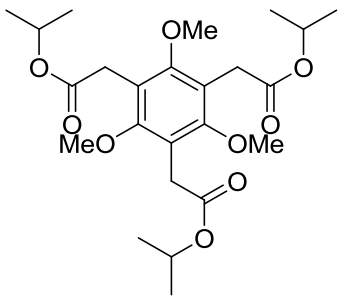

Isopropyl 2,2',2''-(2,4,6-trimethoxybenzene-1,3,5-triyl)triacetate (2-5). To a solution of **2-4** (0.4 g, 1.4 mmol) in ethanol (10 mL) was added a solution of NaOH (5.60 g, 140 mmol) in water (11 mL). The resulting suspension was heated to 100 °C in a sealed 50 mL pressure tube for 12 hours, and then cooled to room temperature. The reaction solution was acidified to pH = 2 with concentrated HCl, extracted with ethyl acetate (50 mL × 2), washed with brine. The collected organic layer was then dried over $MgSO_4$. Removal of the solvent afforded a white solid (0.4 g). The crude material was treated with isopropanol (15 mL) and *p*-TsOH·H_2O (0.50 g, 1.2 mmol) and the resulting mixture was heated to reflux overnight. All volatiles were then removed under reduced pressure and the residue was taken up in EtOAc and washed with dilute NaOH. The organic solution was next dried over $MgSO_4$ and concentrated under reduced pressure. Purification by column chromatography (3:1 hexanes / EtOAc) afforded **2-5** (0.41 g, 75% for two steps) as a colorless solid: ^{1}H NMR ($CDCl_3$): δ = 1.23 (d, J = 6.3 Hz, 18H), 3.63 (s, 6H), 3.72 (s, 9H), 5.05 ppm (m, 3H); ^{13}C NMR ($CDCl_3$) δ 21.7, 30.8, 61.2, 68.0, 118.6, 157.7, 171.5. HRMS (EI) calcd for $C_{24}H_{36}O_9$ (M^+) 468.2359, found 468.2355.

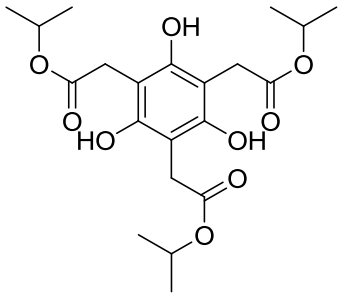

Isopropyl 2,2',2''-(2,4,6-trihydroxybenzene-1,3,5-triyl)triacetate (2-6). To a stirring solution of **2-5** (1.04 g, 2.22 mmol) in dry dichloromethane (60 mL) at –78 °C was added BBr_3 (1.26 mL, 13.3 mmol) and the resulting reaction mixture was allowed to stir for 2 h before warming to room temperature for 20 minutes. It was then quenched with saturated aqueous $NaHCO_3$, poured into a separatory funnel, and extracted with dichloromethane (3 × 50 mL). The

organics were combined, dried over $MgSO_4$, and concentrated under reduced pressure to afford the crude solid. Purification via column chromatography (3:1 hexanes / EtOAc) gave **2-6** (0.68 g, 72%) as a colorless solid: m.p. 163–164 °C; ^{1}H NMR ($CDCl_3$) δ 1.28 (d, J = 6.6 Hz, 18H), 3.75 (s, 6H), 5.03 (m, J = 6.3 Hz, 3H), 8.46 (s, 3H). ^{13}C NMR ($CDCl_3$) δ 21.6, 30.6, 69.9, 103.0, 153.8, 175.3. HRMS (EI) calcd for $C_{21}H_{30}O_9$ (M^+) 426.1890, found 426.1879.

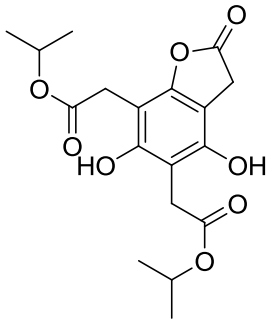

Isopropyl 2,2'-(4,6-dihydroxy-2-oxo-2,3-dihydrobenzofuran-5,7-diyl)diacetate (2-7). During the synthesis and purification of **2-6** as described above, **2-7** (0.16 g, 20%) was isolated by column chromatography (2:1 hexanes / EtOAc) as a white solid: ^{1}H NMR ($CDCl_3$) δ 1.29–1.33 (m, 12H), 3.39 (s,2H), 3.66 (s, 2H), 3.75 (s, 2H), 5.06 (hp, J = 6.3 Hz, 2H), 8.21 (br s, 1H), 8.94 (s, 1H). ^{13}C NMR ($CDCl_3$) δ 21.6, 30.0, 30.8, 31.0, 70.0, 70.5, 97.8, 102.3, 106.2, 151.2, 152.4, 154.9, 174.0, 174.4, 175.2. HRMS (ESI) calcd for $C_{18}H_{22}O_8$ $(M + H)^+$ 367.1387, found 367.1384.

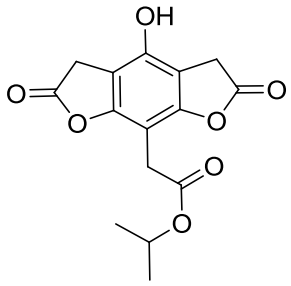

Isopropyl 2-(4-hydroxy-2,6-dioxo-2,3,5,6-tetrahydrobenzofuro[6,5-*b*]furan-8-yl)-acetate (2-8). Tri-ester **2-6** (0.40 g, 0.94 mmol) and TFA (1.80 g, 18.8 mmol) were added to

toluene (20 mL), and the resulting suspension was heated to reflux for 16 h. The reaction solution was cooled to room temperature and a white precipitate formed. The solid was filtered and washed with a small portion of DCM to yield **2-8** (0.16 g, 55%) as an off-white solid. The mother liquor was concentrated and the major product was purified by column chromatography (1:2 hexanes / EtOAc) to yield **2-9** (0.10 g, 35%) as an off-white solid. For **2-8**: ^{1}H NMR (DMSO-d_6) δ 1.19 (d, J = 6.3 Hz, 6H), 3.56 (s, 2H), 3.81 (s, 4H), 4.91 (hp, J = 6.3 Hz, 1H), 10.31 (s, 1H). ^{13}C NMR (DMSO-d_6) δ 21.5, 29.3, 31.3, 68.1, 93.8, 105.1, 148.0, 152.5, 169.1, 174.0. HRMS (CI) calcd for $C_{15}H_{14}O_7$ $(M + H)^+$ 307.0818, found 307.0827.

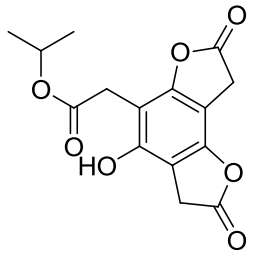

Isopropyl 2-(2-hydroxy-4,5-dioxo-3,4,5,6-tetrahydrobenzofuro[6,5-*b*]furan-8-yl)-acetate (2-9). Compound **2-9** was isolated from the synthesis of **2-8** as described above: ^{1}H NMR ($CDCl_3$) δ 1.31 (d, 6H, J = 6.0 Hz), 3.69 (s, 2H), 3.75 (s, 2H), 3.77 (s, 2H), 5.08 (hp, J = 6.3 Hz), 9.11 (br, 1H). ^{13}C NMR ($CDCl_3$) δ 21.6, 30.5, 31.0, 31.1, 97.6, 100.9, 106.5, 153.5, 172.7, 173.4, 174.1. HRMS (CI) calcd for $C_{15}H_{14}O_7$ $(M + H)^+$ 307.0818, found 307.0827.

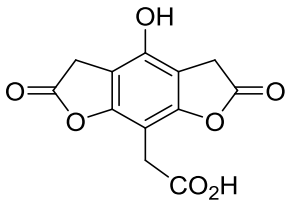

2-(4-Hydroxy-2,6-dioxo-2,3,5,6-tetrahydrobenzofuro[6,5-b]furan-8-yl)acetic acid (2-10). Compound **2-7** (78 mg, 0.25 mmol) was added to toluene (10 mL), followed by the addition

of 5 drops of concentrated HCl. The resulting mixture was heated to reflux for two days and a pink precipitate formed. The solid was filtered, washed with DCM, and dried under vacuum. The material (46 mg, 68%) was identified as **2-10**: ^{1}H NMR (DMSO-d_6) δ 3.50 (s, 2H), 3.81 (s, 4H), 10.27 (s, 1H). ^{13}C NMR (DMSO-d_6) δ 29.1, 31.3, 94.4, 105.0, 147.8, 152.4, 171.0, 174.0.

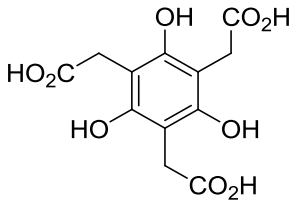

2,2',2''-(2,4,6-Trihydroxybenzene-1,3,5-triyl)triacetic acid (2-11). Tri-ester **2-6** (6.68 g, 1.40 mmol) was dissolved in an aqueous NaOH solution (10.4 g NaOH in 80 mL of water) and the resulting solution was warmed to 70 °C for 2 h. After cooling to room temperature, the solution was acidified to pH = 1 with concentrated HCl and extracted with ethyl acetate (200 mL × 5). The organic layers were combined and dried with anhydrous Na_2SO_4, and the solvent was removed under reduced pressure to afford **2-11** (4.70 g, 99%) as an off-white powdery solid. ^{1}H NMR (DMSO-d_6) δ 3.46 (s, 6H), 8.24 (br s, 3H), 11.94 (br s, 3H). ^{13}C NMR (DMSO-d_6) δ 29.7, 103.0, 153.0, 173.5. HRMS (ESI-TOF) calcd for $C_{12}H_{12}O_9Na$ $(M + Na)^+$ 323.0363, found 323.0374.

Preparation of **2-11** *from* **2-4** *through intermediate* **2-10**:

A solution of **2-4** (13.2 g, 46.3 mmol) in HBr (48%, 150 mL) was heated to reflux overnight. The reaction was then cooled to room temperature, allowing a precipitate to form. The precipitate was filtered, yielding a light brown powder (6.63 g, 54%) identified as **2-10**. The precipitate was then hydrolyzed with NaOH (20.0 g NaOH in 200 mL H_2O) at 70 °C for 3 h. The resultant solution was cooled in an ice bath, acidified with concentrated HCl, and extracted with ethyl acetate (8 × 100 mL). The organics were combined, dried with $MgSO_4$, clarified with activated

carbon, and evaporated in vacuo yielding **2-10** (2.71 g, 19%) as a light brown powder. Subsequently, the eluant from above was diluted with water (200 mL) and extracted with ethyl acetate (10 × 100 mL). The organics were combined, dried with $MgSO_4$ and evaporated in vacuo yielding a brown residue (6.31 g). This residue was then hydrolyzed as above (20.0 g NaOH in 200 mL H_2O for 3 h at 70°C). The hydrolysis solution was then acidified with concentrated HCl and extracted with ethyl acetate (10 × 100 mL). The organics were combined, dried with $MgSO_4$ and evaporated in vacuo yielding **2-11** (3.7 g, 27%) as a light brown solid.

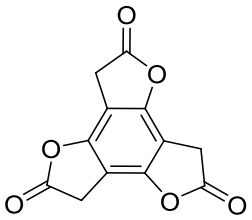

Benzotrifuranone (2-2). Polyphosphoric acid (PPA; 30.0 g) and triacid **2-11** (2.71 g, 9.03 mmol) were mixed and heated to 110 °C with stirring for 16 h. The reaction mixture was cooled to 0 °C in ice bath and ice-cold water (300 mL) was added with stirring. The resultant aqueous solution was then extracted with DCM (4 × 100 mL, emulsion). The organics were combined, washed with water (50 mL) and brine (50 mL), then dried with Na_2SO_4 and evaporated in vacuo to yield **2-2** (1.03 g, 46%) as a tan powder. This product could be further purified by flash column chromatography (1:3 EtOAc/hexanes) and obtained as an off-white powder. ^{1}H NMR ($CDCl_3$) δ 3.81 (s, 6H). ^{13}C NMR ($CDCl_3$) δ 30.2, 101.2, 150.1, 171.8. ^{1}H NMR (DMSO-d_6) δ 4.17 (s, 6H). ^{13}C NMR (DMSO-d_6) δ 30.1, 101.9, 148.8, 173.4. HRMS (CI) calcd for $C_{12}H_6O_6$ $(M + H)^+$ 247.0243, found 247.0229. Anal. Calcd for $C_{12}H_6O_6$: C, 58.55; H, 2.46. Found: C, 58.26; H, 2.34.

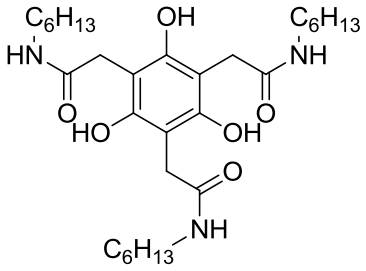

2,2',2''-(2,4,6-Trihydroxybenzene-1,3,5-triyl)tris(N-hexylacetamide) (2-13a) *General BTF ring opening reaction procedure:* To a solution of **2-2** (100 mg, 0.406 mmol) in THF (15 mL) was added hexylamine (410 mg, 4.06 mmol). The resulting solution was stirred overnight and the solvent was evaporated. The residue was taken up in EtOAc (30 mL), washed with 0.1 M HCl, water, and brine sequentially, and dried over Na_2SO_4. The solvent was removed and the residue was purified by flash column chromatography (2/5 EtOAc/hexanes) to yield **2-13a** (179 mg, 80%) as an off-white solid. ^{1}H NMR (300 MHz, $CDCl_3$) δ 0.87 (t, J = 6.57 Hz, 9H), 1.23–1.34 (m, 18H), 1.43–1.58 (m, 6H), 3.21 (q, J = 6.86 Hz, 6H), 3.60 (s, 6H), 6.18 (t, J = 5.84 Hz, 3H), 10.18 (s, 3H); ^{13}C NMR ($CDCl_3$) δ 13.95, 22.49, 26.49, 29.15, 31.37, 40.08, 103.06, 153.82, 174.59. HRMS calcd for $C_{30}H_{51}N_3O_6Na$ $(M + Na)^+$ 614.4140, found 614.4147.

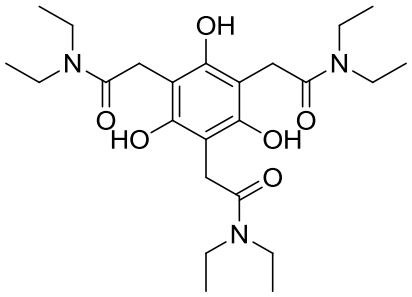

2,2',2''-(2,4,6-Trihydroxybenzene-1,3,5-triyl)tris(N,N-diethylacetamide) (2-13b) Following the general ring opening reaction procedure, **2-2** (80.0 mg, 0.325 mmol) and diethylamine (237 mg, 3.25 mmol) in THF (10 mL) yielded **2-13b** (118 mg, 78%, purified by flash column chromatography with 1/3 EtOAc/hexanes). ^{1}H NMR ($CDCl_3$) δ 1.12 (t, J = 7.18 Hz, 9H), 1.28 (t, J = 7.04 Hz, 9H), 3.37 (q, J = 7.33 Hz, 6H), 3.67 (q, J = 7.33 Hz, 6H), 3.77 (s,

6H) 11.00 (s, 3H); ^{13}C NMR ($CDCl_3$) δ 12.9, 14.6, 28.7, 41.1, 43.4, 102.0, 154.7, 174.3. HRMS (ESI-TOF) calcd for $C_{24}H_{40}N_3O_6$ $(M + H)^+$ 466.2912, found 466.2925.

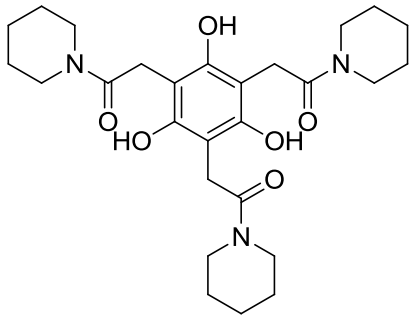

2,2',2''-(2,4,6-Trihydroxybenzene-1,3,5-triyl)tris(1-(piperidin-1-yl)ethanone) (2-13c)

Following the general ring opening reaction procedure, **2-2** (80 mg, 0.32 mmol) and piperidine (272 mg, 3.20 mmol) in acetone (10 mL) yielded **2-13c** (106 mg, 65%, purified by flash column chromatography with 1/3 EtOAc/hexanes). ^{1}H NMR ($CDCl_3$) δ 1.50 – 1.57 (m, 6H) 1.58 – 1.68 (m, 12H), 3.54 (t, J = 5.63 Hz, 6H), 3.79 (s, 6H), 3.83 (t, J = 5.50 Hz, 6H), 10.65 (s, 3H); ^{13}C NMR ($CDCl_3$), δ 24.4, 25.5, 26.5, 28.5, 43.3, 48.3, 102.0, 154.6, 172.8. HRMS (ESI-TOF) calcd for $C_{27}H_{40}N_3O_6$ $(M + H)^+$ 502.2912, found 502.2916.

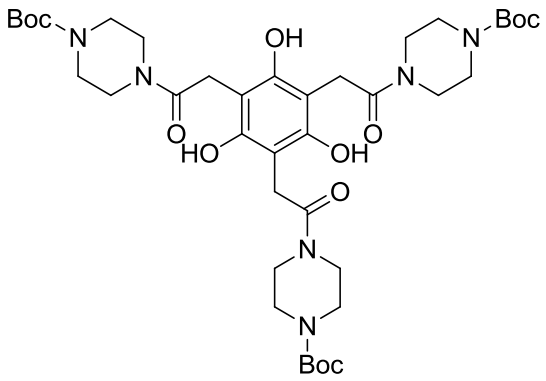

Tri-tert-butyl 4,4',4''-(2,2',2''-(2,4,6-trihydroxybenzene-1,3,5-triyl)tris(acetyl))tris-(piperazine-1-carboxylate) (2-13d) Following the general ring opening reaction procedure, **2-2** (80 mg, 0.32 mmol) and piperidine (300 mg, 1.62 mmol) in THF (10 mL) yielded **2-13c** (240 mg, 93%, purified by flash column chromatography with EtOAc/hexane 2/3).^{1}H NMR ($CDCl_3$) δ

1.44–1.49 (m, 27H), 3.35–3.42 (m, 6H), 3.45 (dd, J = 6.8, 3.4 Hz, 6H), 3.58 (dd, J = 6.8, 3.4 Hz, 6H), 3.78 (s, 6H), 3.84–3.95 (m, 6H), 10.37 (s, 3H); ^{13}C NMR ($CDCl_3$) δ 28.35, 28.58, 41.99, 46.82, 80.31, 101.86, 154.49, 173.28. HRMS (ESI-TOF) calcd for $C_{39}H_{61}N_6O_{12}$ $(M + H)^+$ 805.4342, found 805.4355.

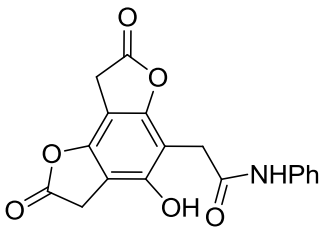

2-(4-Hydroxy-2,7-dioxo-2,3,7,8-tetrahydrobenzo[1,2-b:3,4-b']difuran-5-yl)-N-phenylacetamide (2-14) To a solution of **2-2** (80 mg, 0.32 mmol) in THF (6 mL) was dropwise added an aniline solution (1.63 mL, 1 M in THF). The resulting solution was allowed to stir for 18 h at room temperature and then the reaction was quenched by addition of HCl (1 M). The organic solvent was blown off with nitrogen gas and the residue was taken up in EtOAc. The solution was washed with water and brine sequentially, and dried over Na_2SO_4. After removal of the solvent, the residue was purified by column chromatography (1/2 EtOAc/hexanes) to yield **2-14** (44 mg, 40%) and **2-15** (56 mg, 40%). ^{1}H NMR (DMSO-d_6) δ 3.66 (s, 2H), 3.80 (s, 2H), 3.95 (s, 2H), 7.03 (t, J = 7.41 Hz, 1H), 7.29 (t, J = 7.89 Hz, 2H), 7.59 (d, J = 8.10 Hz, 7H), 10.10 (d, J = 31.85 Hz, 2H); ^{13}C NMR (DMSO-d_6) δ 30.6, 31.1, 31.4, 97.1, 102.6, 104.8, 118.9, 123.0,128.7, 139.2, 147.8, 151.3, 153.7, 168.3,173.9,174.1. HRMS (ESI) calcd for $C_{18}H_{14}NO_6$ $(M + H)^+$ 340.0816, found 340.0813.

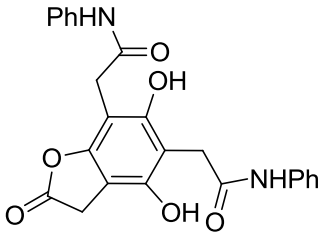

2,2'-(4,6-Dihydroxy-2-oxo-2,3-dihydrobenzofuran-5,7-diyl)bis(N-phenylacetamide) (2-15) Compound **2-15** was isolated from the preparing of compound **2-14**. ^{1}H NMR (DMSO-d_6) δ 3.67 (s, 2H), 3.68 (s., 2H), 3.74 (s, 2H), 7.03 (q, J = 7.6 Hz, 2 H), 7.34 – 7.23 (m, 4H), 7.59 (d, J = 7.9 Hz, 4 H), 9.55 (s, 1 H), 9.70 (s, 1 H), 10.05 (s, 1 H), 10.24 (s, 1H). ^{13}C NMR (DMSO-d_6) δ 31.63, 31.77, 31.92, 98.43, 100.53, 106.69, 119.02, 119.25, 123.00, 123.37, 128.65, 128.70, 138.92, 139.27, 150.45, 152.18, 155.02, 169.69, 170.31, 174.63. HRMS (ESI) calcd for $C_{24}H_{21}N_2O_6(M + H)^+$ 433.1394, found 433.1389.

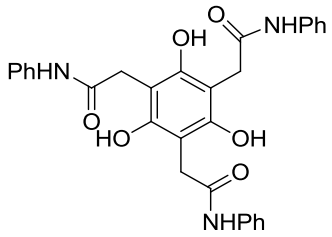

2,2',2''-(2,4,6-trihydroxybenzene-1,3,5-triyl)tris(N-phenylacetamide) (2-16). To the solution of **2-2** (150 mg, 0.610 mmol) in DMF (7 mL) was added aniline (283 mg, 3.00 mmol). The resulting solution was heated to 70 °C for 15h and then cooled to room temperature. The reaction solution was poured into brine (50 mL) and extracted with EtOAc. The combined organic layers were washed with 1 M HCl and water, and then dried over Na_2SO_4. The solvent was removed and the residue was purified by flash column chromatography (1/3 to 1/1 EtOAc/hexanes) to yield **2-16** (247 mg, quant.). ^{1}H NMR (DMSO-d_6) δ 3.71 (s, 6H), 7.05 (t, J = 7.5 Hz, 3H), 7.30 (t, J = 7.8 Hz, 6H), 7.61 (d, J = 7.8 Hz, 6H), 9.32 (s, 3H), 10.21 (s, 3H). ^{13}C NMR (DMSO-d_6) δ 32.4, 103.4, 119.3, 123.4, 128.7, 138.9, 153.6, 171.6.

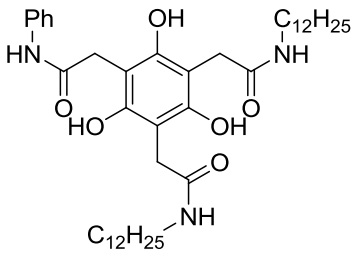

2,2'-(2,4,6-Trihydroxy-5-(2-oxo-2-(phenylamino)ethyl)-1,3-phenylene)bis(N-dodecylacetamide) (**2-17**). To the solution of **2-14** (40 mg, 0.11 mmol) in THF (5 mL) was added dodecylamine (41 mg, 0.22 mmol). The resulting solution was allowed to stir overnight at room temperature and then the solvent was evaporated under reduced pressure. The residue was taken up in EtOAc and the solution was mixed with a small amount of silica gel. After removal of the solvent, the resulting mixture was loaded on a silica gel column for flash column chromatography (1/3 EtOAc/hexanes) to yield **2-17** (46 mg, 70%). ^{1}H NMR ($CDCl_3$) δ 8.06 (6H, t, J = 6.6 Hz), 1.15–1.24 (36H, m), 1.41, (4H, quin, J = 6.6 Hz), 3.11 (4H, q, J =6.7 Hz), 3.55 (s, 4H), 3.71 (s, 2H), 6.37 (t, 2H, J = 5.7 Hz), 7.00–7.06 (m 1H,), 7.18 – 7.24 (m, 2H), 7.40 (m, 2H), 8.27 (s, 1H), 9.70 (s, 2H), 10.26 (s, 1H). ^{13}C NMR ($CDCl_3$) δ 14.11, 22.68, 26.84, 29.20, 29.34, 29.48, 29.55, 29.62, 29.69, 31.90, 32.53, 40.14, 102.77, 103.24, 120.60, 124.96, 128.90, 137.20, 153.74, 154.18, 173.05, 174.61. HRMS (ESI) cald for $C_{48}H_{68}N_3O_6$ (M+H) 710.5103, found 710.5104.

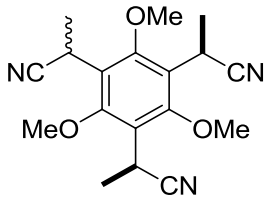

2,2',2''-(2,4,6-Trimethoxybenzene-1,3,5-triyl)tripropanenitrile (2-18a). To the solution of **2-4** (3.38 g, 11.8 mmol) in dry DMF (60 mL) at 0 °C, was slowly added NaH (60% in mineral oil, 1.56 g, 39.1 mmol) in portions. The resulting mixture was allowed to stir for 1 hour at the same temperature, followed by the dropwise addition of MeI (5.52 g, 39.1 mmol). The reaction mixture was gradually warmed to room temperature and stirred overnight, then poured into water (500 mL). Ethyl acetate (150 mL × 3) was used to extract the aqueous solution and the organic layer was separated, washed with water and brine, and dried over $MgSO_4$. The solution was

concentrated under reduced pressure. Flash silica gel column chromatography afforded **2-18a** (3.42 g, 88%; the ratio of *anti* : *syn* diastereomers was 3:1, determined by ^{1}H NMR). ^{1}H NMR ($CDCl_3$, *anti*): δ 1.68 (d, *J* = 7.5 Hz, 6H), 1.71 (d, *J* = 7.2 Hz, 3H), 4.00 (s, 6H), 4.05 (s, 3H), 4.21-4.32 (m, 3H); (*syn*): δ 1.64 (d, *J* = 7.5 Hz, 9H), 4.04 (s, 9H), 4.21-4.32 (m, 3H). ^{13}C NMR ($CDCl_3$, *anti* and *syn*): 18.45, 18.68, 21.48, 21.56, 21.68, 63.47, 63.59, 63.63, 121.71, 121.74, 122.26, 122.60, 122.70, 157.98, 158.01. HRMS (EI) calcd for $C_{18}H_{21}N_3O_3$ (M^+) 327.1583, found 327.1581.

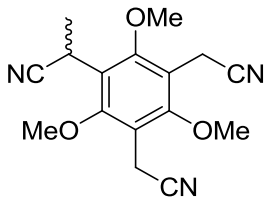

2,2'-(5-(1-Cyanoethyl)-2,4,6-trimethoxy-1,3-phenylene)diacetonitrile (2-18b). Following the procedure for the preparation of **2-18a**, **2-10** (1.50 g, 5.26 mmol), NaH (0.25 g, 6.3 mmol, 60% in mineral oil), MeI (0.82 g, 5.80 mmol) and DMF (25 mL) were used in the reaction. Purification by column chromatography (1/2 to 1/1.5 EtOAc/hexanes) yielded **2-18b** (0.51 g, 43%) as a white solid: ^{1}H NMR ($CDCl_3$): δ 1.64 (d, 3H, *J* = 7.2 Hz), 3.72 (s, 4H), 4.02 (s, 6H), 4.05 (s, 3H), 4.28 (q, 1H, *J* = 7.2 Hz); ^{13}C NMR ($CDCl_3$): δ 13.1, 18.8, 21.4, 62.6, 63.0, 115.9, 117.6, 121.6, 122.4, 158.1, 158.5. HRMS (ESI-TOF) calcd for $C_{16}H_{17}N_3O_3Na$ $(M+Na)^+$ 322.1162, found 322.1170. Another product, **2-18c** (0.39 g, 31%), was also isolated.

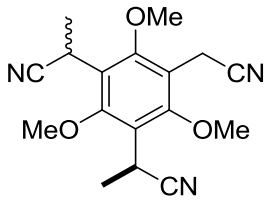

2,2'-(5-(Cyanomethyl)-2,4,6-trimethoxy-1,3-phenylene)dipropanenitrile (2-18c). Compound **2-18c** was isolated during the synthesis of **2-18b** as a white solid (mixture of *syn* and

anti, statistical ratio 1:1): ^{1}H NMR ($CDCl_3$): δ 1.58 (d, 6H, J = 7.5 Hz), 1.61 (d, 6H, J =8.1 Hz), 3.69 (s, 4H), 3.87 (s, 4H), 3.93 (s, 3H), 3.84 (s, 12H), 4.20-4.27 (m, 4H); ^{13}C NMR ($CDCl_3$): δ 13.0, 13.2, 18.4 18.5, 21.2, 62.5, 62.6, 63.3, 117.3, 117.4, 121.4, 121.5, 121.8, 122.0, 156.8, 157.1, 158.0, 158.2. HRMS (ESI-TOF) calcd for $C_{17}H_{19}N_3O_3Na$ $(M+Na)^+$ 336.1319, found 336.1328.

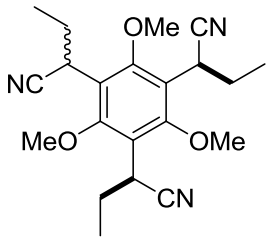

2,2',2''-(2,4,6-Trimethoxybenzene-1,3,5-triyl)tributanenitrile (2-18d). Following the procedure for the preparation of **2-18a**, **2-4** (2.95 g, 10.4 mmol), NaH (0.87 g, 60% in mineral oil, 36.2 mmol), EtI (5.61 g, 36.2 mmol) and DMF (20 mL) were used in the reaction. Purification by column chromatography (1/5 EtOAc/hexanes) yielded **2-18d** (3.08 g, 81%). ^{1}H NMR ($CDCl_3$, *anti*): δ 0.91–1.03 (m, 9H), 1.73–1.78 (m, 3H), 2.15–2.20 (m, 3H), 3.92 (s, 6H), 3.95 (s, 3H), 3.95–4.08 (m, 3H). ^{13}C NMR ($CDCl_3$, *anti*): δ 11.9, 12.1, 25.5, 25.6, 28.8, 28.9, 63.1, 63.2, 120.6, 120.7, 120.8, 121.1, 158.0, 158.2. ^{1}H NMR ($CDCl_3$, *syn*): δ 0.92 (t, 9H, J = 7.5 Hz), 1.78–1.88 (m, 3H), 2.13–2.23 (m, 3H), 3.97 (t, 3H, J = 7.9 Hz), 4.02 (s, 9H); ^{13}C NMR ($CDCl_3$, *anti*): δ 11.9, 26.1, 28.9, 63.5, 121.0, 121.2, 158.4. HRMS (ESI-TOF) calcd for $C_{21}H_{27}N_3O_3Na$ $(M+Na)^+$ 292.1945, found 292.1935.

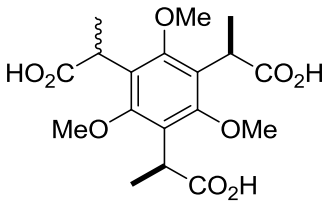

2,2',2''-(2,4,6-Trimethoxybenzene-1,3,5-triyl)tripropanoic acid (2-19). A solution of **2-18a** (1.08 g, 3.30 mmol), NaOH (13.2 g, 330 mmol), EtOH (40 mL), and water (32 mL) was heated to 100 °C in a sealed pressure tube for 12 h. The reaction mixture was then cooled to 10 °C and acidified to pH = 2 with conc. HCl. The solution was then diluted with brine and extracted with EtOAc (2 × 50 mL). The organic layers were combined, dried over $MgSO_4$, decolorized with activated carbon, and concentrated to afford **2-19** (1.20 g, 95%) as a colorless solid: ^{1}H NMR (DMSO-d_6) δ 1.31 (m, 9H), 3.68 (m, 9H), 3.87 (q, J = 6.9 Hz, 3H), 11.95 (s, 3H). ^{13}C NMR (DMSO-d_6) δ 17.0, 35.8, 61.7, 126.3, 155.8, 175.4. HRMS (EI) calcd for $C_{18}H_{24}O_9$ (M) 384.1420, found 384.1423.

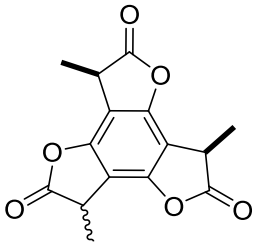

Trimethylbenzotrifuranone (2-23a). The mixture of **2-18a** (2.50 g, 7.64 mmol) and HBr (48% aqueous solution, 50 mL) was heated to reflux for 12 hours and the resulting solution was cooled to room temperature and diluted with water (300 mL). The mixture was extracted with ethyl acetate (100 mL × 3) and the organic layers were combined and dried over Na_2SO_4. The solvent was removed under reduced pressure and the residue was dissolved in NaOH solution (6.00 g NaOH in 30 mL water) and heated to 70 °C for 2 hours. After cooling to the room temperature, the solution was acidified (pH = 1) with concentrated HBr (aq.) and extracted with ethyl acetate (150 mL × 4). The combined organic layers were dried over Na_2SO_4 and concentrated under reduced pressure. The residue was mixed with PPA (15 g) and heated to 110 °C overnight. After cooling to 0 °C in ice bath, the reaction mixture was diluted with ice-cold water (300 mL) and extracted with ethyl acetate (150 mL × 3). The organic layers were

combined and dried over anhydrous Na_2SO_4, and the solvent was removed under reduced pressure. Flash column chromatography (1/6 ethyl acetate/hexanes) afforded **2-23a** (0.46 g, 21%) as a white solid. ^{1}H NMR ($CDCl_3$): δ 1.64 (m, 9H), 3.86 (q, J = 7.2 Hz, 3H). ^{13}C NMR ($CDCl_3$): δ 15.01, 15.03, 36.51, 106.86, 106.91, 106.92, 106.94, 149.00, 176.06, 176.08. HRMS (ESI-TOF) calcd for $C_{15}H_{12}O_6Na$ $(M+Na)^+$ 311.0526, found 311.0523.

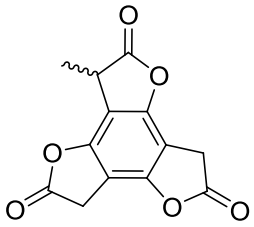

2-Methylbenzotrifuranone (2-23b). Following the same procedure for the preparation of **2-23a**, compound **2-18b** (0.61 g, 2.0 mmol) yielded **2-23b** (0.075 g, 14%) as a sticky solid. ^{1}H NMR ($CDCl_3$): δ 1.66 (d, J = 7.6 Hz,3H), 3.80 (s, 2H), 3.81 (s, 2H) 3.90 (q, J = 7.6 Hz, 1H); HRMS ((-)APCI-TOF) calcd for $C_{13}H_7O_6$ $(M-H)^-$ 259.0248, found 259.0269.

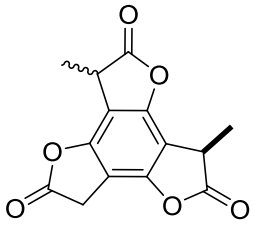

2, 2'-Dimethylbenzotrifuranone (2-23c). Following the same procedure for the preparation of **2-23a**, compound **2-18c** (0.15g, 0.50 mmol) yielded **2-23c** (0.022 g, 17%) as a sticky solid. ^{1}H NMR ($CDCl_3$): δ 1.66 (dd, 3H, J = 3.6, 0.9 Hz), 1.64 (dd, 3H, J = 3.6, 0.9 Hz), 3.79 (s, 2H), 3.88 (m, 2H,); ^{13}C NMR ($CDCl_3$): δ 15.01, 15.06, 29.94, 36.52, 36.69, 36.72, 101.25, 106.84, 106.88, 106.98, 107.01, 148.80, 148.81, 149.15, 150.15, 172.14, 175.89, 175.98, 176.00. HRMS ((-)APCI-TOF) calcd for $C_{14}H_{19}O_6$ $(M-H)^-$ 273.0410, found 273.0405.

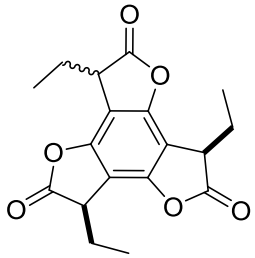

2,2',2''-(2,4,6-Trimethoxybenzene-1,3,5-triyl)tributanenitrile (2-23d). Following the same procedure for the preparation of **2-23a**, compound **2-18d** (2.41 g, 6.53 mmol) yielded **2-23d** (purified by column chromatography; 1/7 EtOAc/hexanes, 0.18 g, 10%) as an off-white solid. ^{1}H NMR ($CDCl_3$): δ 0.94 (m, 9H), 2.17 (m, 6H), 3.90 (dq, 3H, J = 2.3 Hz, 5.6 Hz). ^{13}C NMR ($CDCl_3$): δ 9.96, 10.03, 10.05, 10.11, 23.06, 23.11, 23.18, 23.23, 42.85, 42.87, 42.91, 42.95, 105.05, 105.09, 105.14, 105.15, 149.42, 149.43, 149.46, 149.46, 175.37, 175.39, 175.40, 175.43. HRMS (DIP-CI) calcd for $C_{18}H_{19}O_6$ $(M+H)^+$ 331.1182, found 331.1166.

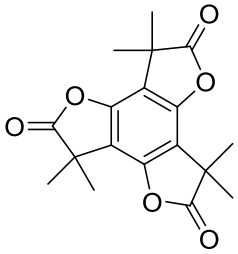

2,2,2',2',2",2"-Hexamethylbenzotrifuranone (2-24). To a stirring solution of **2-23a** (80 mg, 0.28 mmol) and MeI (160 mg, 1.13 mmol) in dry DMF (4 mL) at 0 °C, was added K_2CO_3 (155 mg, 1.12 mmol). The reaction mixture was warmed to room temperature and stirred overnight, and then diluted with saturated NH_4Cl (aq.) solution. The resulting solution was extracted with ethyl acetate (30 mL× 3) and the combined organic layers were washed with water and brine successively. The solution was dried over anhydrous Na_2SO_4 and concentrated under reduced pressure. Flash column chromatography (1/10 EtOAc/hexanes) afforded **2-24** (57 mg, 62%) as a white solid. ^{1}H NMR ($CDCl_3$): δ 1.63 (s, 9H). ^{13}C NMR ($CDCl_3$): δ 24.0, 42.2,

111.8, 147.1, 179.3. HRMS (ESI-TOF) calcd for $C_{18}H_{18}O_6Na$ $(M+Na)^+$ 353.0993, found 353.0996.

X-ray Crystallography

General. Data were collected at 173 K on a Siemens SMART PLATFORM equipped with A CCD area detector and a graphite monochromator utilizing MoK_α radiation (λ = 0.71073 Å). Cell parameters were refined using up to 8192 reflections. A full sphere of data (1850 frames) was collected using the ω-scan method (0.3° frame width). The first 50 frames were re-measured at the end of data collection to monitor instrument and crystal stability (maximum correction on I was < 1 %). Absorption corrections by integration were applied based on measured indexed crystal faces.

The structure was solved by the Direct Methods in *SHELXTL6,* and refined using full-matrix least squares. The non-H atoms were treated anisotropically, whereas the hydrogen atoms were calculated in ideal positions and were riding on their respective carbon atoms.

Compound 2-2. The asymmetric unit consists of two chemically equivalent but crystallographically independent molecules. A total of 325 parameters were refined in the final cycle of refinement using 4097 reflections with $I > 2\sigma(I)$ to yield R_1 and wR_2 of 4.39% and 10.07%, respectively. Refinement was done using F^2.

Compound 2-23a (*anti*). A $CH–CH_3$ unit (C10–C15) is disordered and was refined in two parts. Their site occupation was fixed at 0.85/0.15 for the major and minor parts, respectively. A total of 13268 parameters were refined in the final cycle of refinement using 2078 reflections with $I > 2\sigma(I)$ to yield R_1 and wR_2 of 6.02% and 13.12%, respectively. Refinement was done using F^2.

Compound 2-23a (*syn*). A colorless plate-like specimen of $C_{22}H_{12}O_6$ (approximate dimensions = 0.05 mm x 0.11 mm x 0.25 mm) was used for the X-ray crystallographic analysis. The X-ray intensity data were measured at 100(2) K on a Bruker SMART APEX II system equipped with a graphite monochromator and a Cu Kα fine-focus sealed tube (λ = 1.54178 Å) operated at 1.2 kW power (40 kV, 30 mA). The detector was placed at a distance of 3.975 cm from the crystal.

A total of 2270 frames were collected with a scan width of 0.8° in ω and an exposure time of 30.0 sec/frame. The total data collection time was 21.56 hours. The frames were integrated with the Bruker SAINT software package using a narrow-frame integration algorithm. The integration of the data using a monoclinic unit cell yielded a total of 10909 reflections to a maximum θ angle of 67.85° (0.83 Å resolution), of which 2269 were independent (average redundancy 4.80, completeness = 97.8%, R_{int} = 2.00%, R_{sig} = 1.48%) and 1969 (86.78%) were greater than $2\sigma(F^2)$. The final cell constants of a = 8.3067(2) Å, b = 16.4563(3) Å, c = 9.9877(2) Å, β = 109.7590(10)°, volume = 1284.91(5) $Å^3$, are based upon the refinement of the XYZ-centroids of 6311 reflections above 20 σ(I) with 10.752° < 2θ < 134.217°. Analysis of the data showed negligible decay during data collection. Data were corrected for absorption effects using the multi-scan technique (SADABS). The ratio of minimum to maximum apparent transmission was 0.801. The calculated minimum and maximum transmission coefficients (based on crystal size) are 0.7543 and 0.9475.

The structure was solved and refined using the Bruker SHELXTL (Version 2008.4) Software Package, using the space group P2(1)/c, with Z = 4 for the formula unit, $C_{22}H_{12}O_6$. The final anisotropic full-matrix least-squares refinement on F^2 with 206 variables converged at R1 = 2.92%, for the observed data and wR2 = 7.51% for all data. The goodness-of-fit was 1.037. The

largest peak on the final difference electron density synthesis was 0.221 $e^-/Å^3$ and the largest hole was -0.167 $e^-/Å^3$ with an RMS deviation of 0.035 $e^-/Å^3$. On the basis of the final model, the calculated density was 1.925 g/cm^3 and F(000), 768 e^-.

CHAPTER 3
PREPARATION AND PROPERTIES OF BENZOTRIFURANS FROM BENZOTRIFURANONE PRECURSORS

Introduction to Benzofuran

Discussed in Chapter 2, BTF **2-2** can potentially be utilized as a precursor for the synthesis of benzotrifuran derivatives, discotic heteroaromatic molecules, by trapping the enolates generated from the furanone rings (Figure 2-5c). This application of BTF is attractive because benzofuran itself is an important heteroaromatic molecule in biology and has emerging applications in organic electronic materials research. Regarding the former, the benzofuran substructure is found in a variety of natural products[122-126] and many are attractive for their biological and pharmacological activities. [127,128] One example lies in antidepressant drug (-)-1-(benzofuran-2-yl)-2-propylaminopentane ((-)-BPAP).[129]

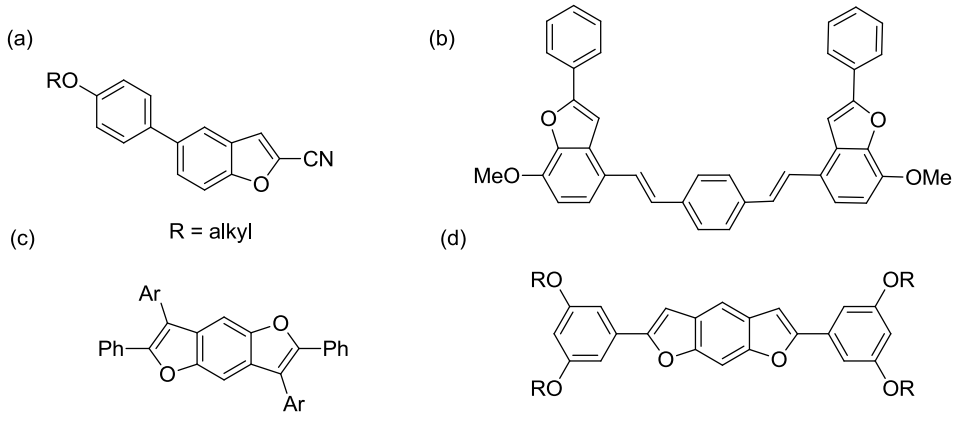

Figure 3-1. Benzofuran containing organic molecules for applications in π-conjugated materials.

In the field of materials science, benzofuran is also a commonly found substructure. Some benzofuran-containing small organic molecules[130] (Figure 3-1a) and polymers[131] have shown liquid-crystalline properties, while some π-conjugated architectures that contain multiple benzofuran moieties (Figure 3-1b) serve as electroluminescent materials with potential applications in organic light-emitting diodes (OLEDs). Likewise, recently reported benzodifuran derivatives[132-134] (Figure 3-1c, d) boast very unique electronic properties and potential

application in organic devices, such as organic field-effect transistors (OFETs), OLEDs, and photovoltaic cells. These and other interesting and useful benzodifuran molecules have encouraged us to investigate C_{3h}-symmetric benzotrifuran derivatives that could possibly be made from BTF and TMBTF.

C_{3h}-symmetric benzotrifuran derivatives have been previously reported[99,135] and the discotic aromatic molecules have been studied in terms of their liquid-crystalline properties.[99] Limiting further investigation of these systems may be that the reported synthetic methods to access them suffer from both low yields and harsh reaction conditions (one example is shown in Figure 3-2). Certainly a more convenient and mild synthesis of the benzotrifuran would facilitate their continued study and the preparation of more highly functionalized derivatives.

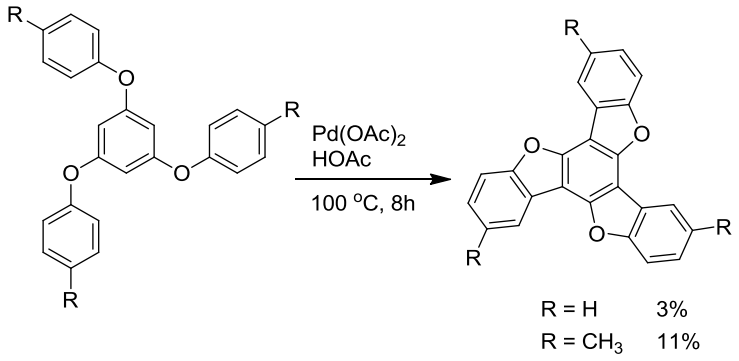

Figure 3-2. An example[135] of synthesis the benzotrifuran derivatives.

Due to the wide-spread applications of benzofuran as a synthetic building block in medicinal chemistry and materials chemistry, the development of novel approaches to benzofurans is of continuing interest. A now classic synthesis of benzofuran was reported as early as 1870 by Perkin,[136] known as the Perkin Rearrangement (coumarin-benzofuran ring contraction), involving the conversion of 3-halocoumarins to benzofuran under basic conditions at high temperature. Most modern synthetic approaches to the benzofuran system are either metal catalyzed or require high reaction temperatures.[137-142] In the context of the benzofuranone

chemistry that was discussed in Chapter 2, benzofuran could be prepared by simply trapping the enolate of benzofuranone. The isotope exchange ^{1}H NMR experiments of TMBTF also support the possibility of preparing benzotrifuran derivatives in this way.

Some reactions have indeed been reported that convert lactones or benzolactones to furans or benzofurans, respectively.[97,143-146] Among the reports, Black[97] and Shaw[146] have demonstrated that the acylation approach can convert benzofuranone to stable 2-*O*-substituted benzofurans (Figure 3-3). The scope of reactants compatible with the reaction as it is reported in the literature is quite limited; only α-substituted benzofuran-2-one enolates and chloroformate electrophiles have been used for furan formation. Extension of this chemistry to the multiple lactone rings of BTF or MTBF could rapidly generate the benzotrifuran system and expose new structures and properties for applications in materials. Requiring testing would be whether the reaction could be extended to non-substituted benzofuranone (e.g., BTF) and simple acid chlorides (as opposed to chloroformates).

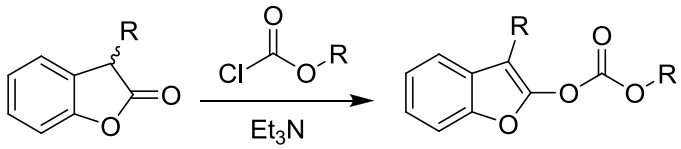

Figure 3-3. Reported reaction for producing benzofruan derivative from benzofuranone.

O-Substituted Benzotrifuran Derivatives

Synthesis

Before attempting the synthesis of benzotrifurans from benzotrifuranones, a model reaction with benzofuran-2-one (**2-1**) and acetyl chloride was optimized (Figure 3-4a). The reaction proceeds very well in the presence of triethylamine in THF at 0 °C and the product **3-1** was obtained in a reasonable yield.

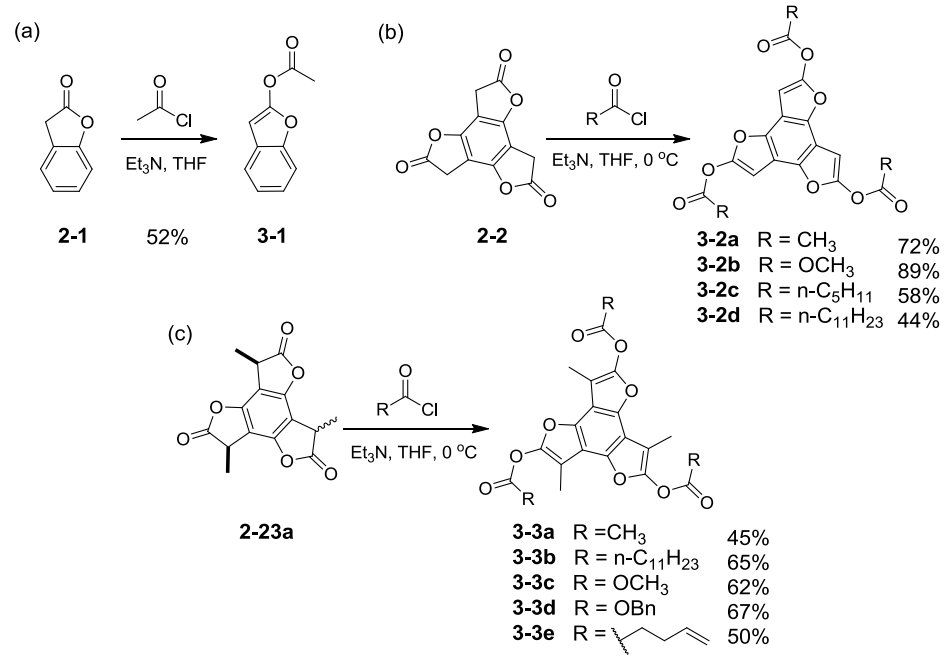

Figure 3-4. Reactions employed for formation of benzotrifuran derivatives: (a) model acylation of benzofuran-2-one; acylation reaction of BTF (b) and MBTF (c) with a variety of chloroformates and acyl chlorides.

Under the same reaction conditions, BTF (**2-2**)and TMBTF (**2-23a**) react with a variety of chloroformates and acyl chlorides to produce a new family of C_{3h}-symmetric benzotrifuran derivatives (**3-2a-d, 3-3a-e**) with various side chains around the periphery (Figure 3-4b, c). This reaction not only generates a family of disk-shaped aromatic molecules conveniently, but also allows various functional groups to be introduced on the periphery of the benzotrifuran core. For example, **3-3e** features a terminal olefin that could potentially be functionalized through cross-metathesis chemistry. The methodology also allows rapid improvement in the solubility of the molecules in non-polar organic solvents via the introduction of long alkyl groups (compare **3-2c**, **3-2d** with **3-2a**) on the benzotrifuran periphery.

Characterization of Benzotrifuran Derivatives

^{1}H and ^{13}CNMR spectra easily confirm the structures of compounds **3-2** and **3-3**; due to the C_{3h} symmetry of these compounds, their NMR spectra are quite simple. In the case of **3-2a**, only

two singlets at 2.41 (CH_3) and 6.60 (CH) ppm are found by ^{1}H NMR; the latter resonance is downfield of the equivalent proton for **3-1** (Figure 3-4a) that appears at δ = 6.34 ppm. The same trend was found in ^{13}C NMR spectra, with the benzofuran carbons (CH) of **3-2a** appearing at δ = 86 ppm, 4ppm downfield of the equivalent carbon for **3-1.** For methyl substituted benzotrifuran derivatives **3-3a-e**, the resonance of the methyl carbons is quite shielded and appears at δ ~ 8 ppm, consistent with the shift reported for a 3-methylbenzofuran derivative[146] and presumably due, in part, to high electron density in the benzofuran ring system.

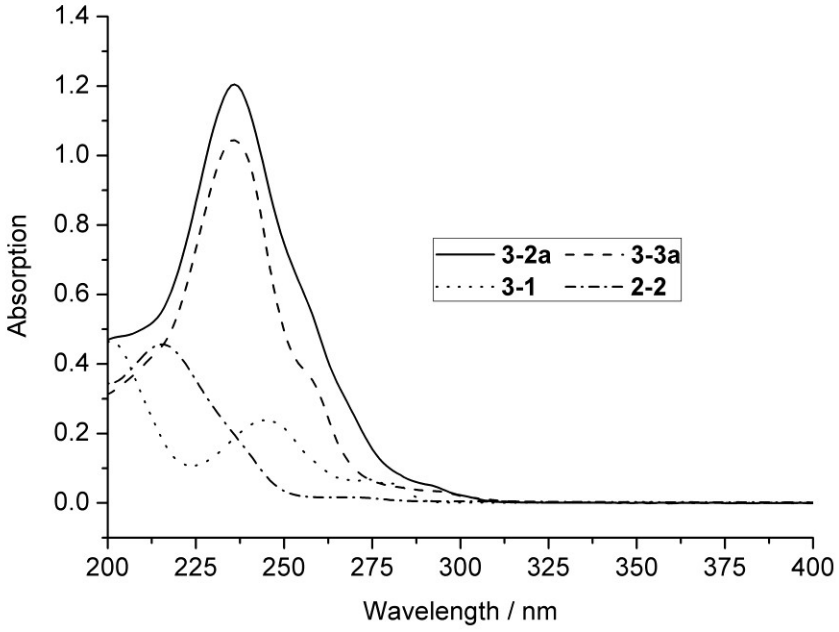

Figure 3-5. UV-Vis spectra of benzotrifuranone **2-2,** benzotrifuran derivatives **3-2a** and **3-3a**, and benzofuran derivative **3-1** (all spectra were recorded in 20 μM CH_3CN solution).

In comparison to the precursor benzotrifuranones **2-2** and **2-23a**, benzotrifuran derivatives **3-2** and **3-3** feature a more extended π-conjugated system, and a narrowed HOMO-LUMO band gap. Theoretically, the major UV absorption bands of **3-2** and **3-3** should red-shift relative to their lactone precursors. The UV-Vis spectra of **3-2a** and **3-2b** were recorded in CH_3CN solution and show that the major absorption band (**3-2a**: λ_{max} = 236 nm; ε = 59600 $M^{-1}cm^{-1}$; **3-3a**: λ_{max} = 236 nm; ε = 51964 $M^{-1}cm^{-1}$) is red-shifted and intensified (~3-fold) relative to BTF **2-2** (Figure

3-5, UV spectrum of **2-23a** is similar to **2-2** and not shown here), consistent with extension of the π-conjugation to include the fused furan ring system. Finally, the extinction coefficient of **3-2** is significantly enhanced (~5-fold) relative to **3-1** (λ_{max} = 245 nm; ε = 12381 $M^{-1}cm^{-1}$ in CH_3CN).

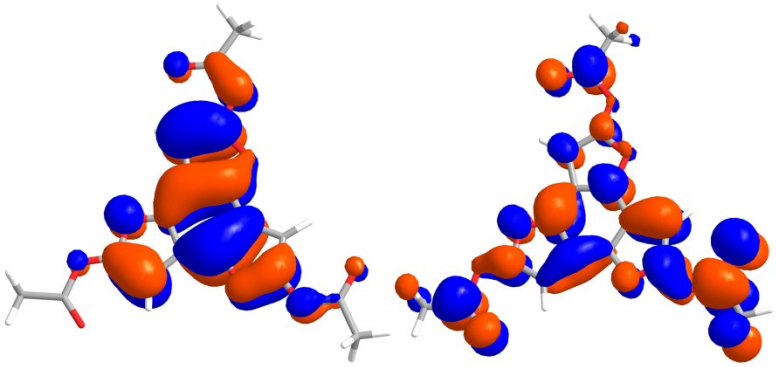

Figure 3-6. HOMO (left) and LUMO (right) plots of benzotrifuran **3-2a** calculated from its RB3LYP/6-311+G* optimized geometry.

Density functional theory (DFT) calculations provide an approach to explore the electronic properties of **3-2a**. The aromaticity of **3-2a** has been probed by calculating its nucleus-independent chemical shifts (NICS), an aromaticity/antiaromaticity criterion introduced by Schleyer[147] in 1996 and widely used to determine and compare aromaticity of cyclic molecules. Simply, NICS is a computational method that calculates the chemical shift of a hypothetical lithium ion placed directly inside the ring. In this method, negative NICS values indicate aromaticity because the ring current inside the aromatic ring deshields the lithium ion, giving negative chemical shifts; on the contrary, positive NICS values indicate antiaromaticity. On the basis of the NICS values (that are large in magnitude and negative), both the central and heterocyclic rings of **3-2a** are aromatic, analogous to simple benzofurans (Table 3-1). The same calculations on **2-2** show, expectedly, essentially nonaromatic peripheral heterocyclic rings. Also accessible from calculations are HOMO and LUMO density plots (Figure 3-6) for the lowest-energy conformation of **3-2a** (bearing C_{3h} symmetry) that confirm delocalization of π-

electron density over the entire benzotrifuran system and a HOMO-LUMO gap (4.77 eV) that is lower than **3-1** (4.99 eV) or recently studied benzodifurans.[148]

Table 3-1. Total NICS values (ppm) calculated for the central and heterocyclic rings of benzofuran, BTF (**2-2**), and **3-2a**.[a]

	central ring		heterocyclic ring	
	NICS(0)	NICS(1)	NICS(0)	NICS(1)
benzofuran	-9.96	-10.98	-10.23	-8.40
	(-9.96)[b]	(-10.99)[b]	(-9.56)[b]	(-8.26)[b]
2-2	-10.32	-8.93	-1.43	-1.90
3-2a	-13.18	-11.28	-10.96	-7.17

[a] NICS values were calculated for the ring centers as defined by the center of mass, NICS(0), and 1 Å above the ring centers, NICS(1). Calculations performed at the RB3LYP/6-311+G* level on RB3LYP/6311+G* minimized structures. [b] Values reported in ref [148].

X-ray Crystal Structure Analysis of 3-3a

A single crystal of **3-3a** was obtained by slow diffusion of pentane into its ethyl acetate solution; the crystal occupies the orthorhombic space group *Pbca*. From the crystal structure of **3-3a**, it is clear that the benzotrifuran core is perfectly planar as predicted for its extended aromatic core. The acetyl groups deviate from the plane of the benzotrifuran ring and give rise to two different conformers (A and B) of **3-3a** in the crystal phase that comprise a dimeric unit. The dimer features π-π stacking interactions (the closest distance between the π surfaces is 3.35 Å) and C−H···O interactions[109] (interatomic distances: $CH_3CO\underline{O}\cdots\underline{C}H_3CO$ ~ 3.46 Å and $C=\underline{O}\cdots\underline{C}H_3C=O$ ~ 3.35 Å) (Figure 3-7b (top)). Additionally, C−H···O interactions between two A conformers from adjacent dimeric units are found with a short distance ($C=\underline{O}\cdots\underline{C}H_3C=O$) of 3.13 Å (Figure 3-7b (bottom)). The packing pattern of **3-3a** (Figure 3-7c) shows that the planar molecules are organized in a 1-D manner. Due to repulsion between the electron-rich benzotrifuran rings and solid-phase packing effects, the stacking fashion is "slipped"[149] instead of cofacial; the distance between the centroids of two stacked benzotrifuran molecules is 4.61 Å (Figure 3-7c).

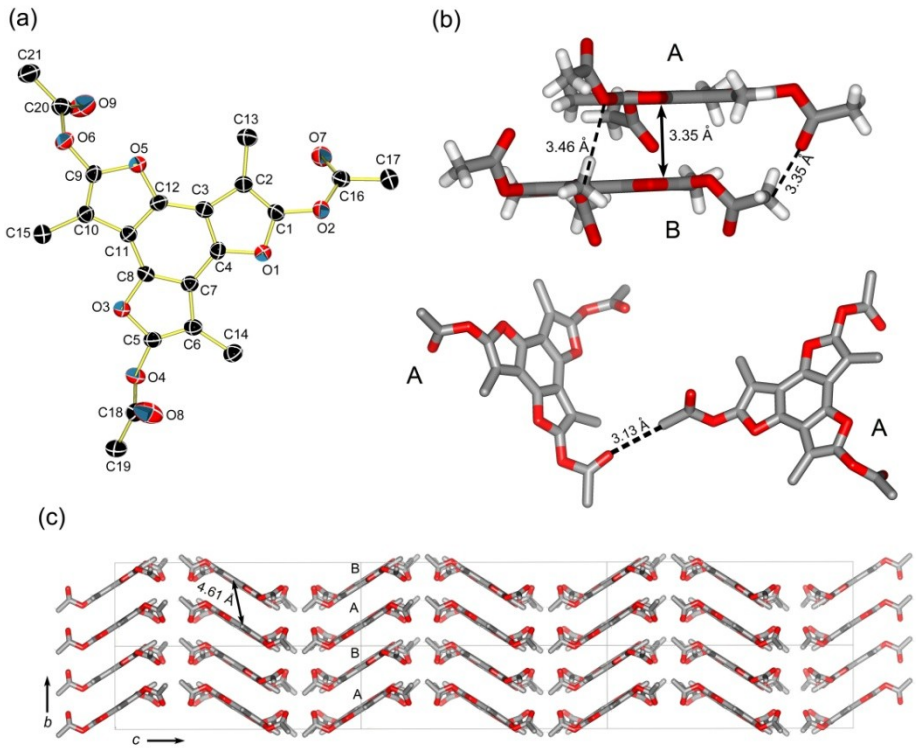

Figure 3-7. X-ray crystal structure **3-3a**: (a) ORTEP plot **3-3a** (B conformer, thermal ellipsoids shown at the 50% probability level and hydrogen atoms have been removed for clarity); (b) top: a dimeric unit formed from both conformers of **3-3a** (A and B) featuring C−H···O and π-π stacking interactions; bottom: C−H···O interaction between adjacent A conformers; (c) crystal packing of **3-3a** along the *a* axis (the distance between the centroids of two stacked molecules is shown).

Preliminary Property Analysis of Functionalized Benzotrifuran

Preliminary functionalization of the periphery of benzotrifuran introduced long alkyl chains through acylation using appropriate acid chlorides. The combination of BTF **2-2** and lauroyl chloride yielded compound **3-2d**, having three undecyl groups attached to the benzotrifuran core. In the same way, undecyl, pentyl, and heptyl groups were introduced to form **3-2c**, **3-2d**, and **3-3b**, respectively (Figure 3-3). We anticipated that the alkyl chains would potentially encourage assembly of the benzotrifuran derivatives through side-chain and π-stacking interactions, where the resulting 1-D assemblies could be useful as functional materials.

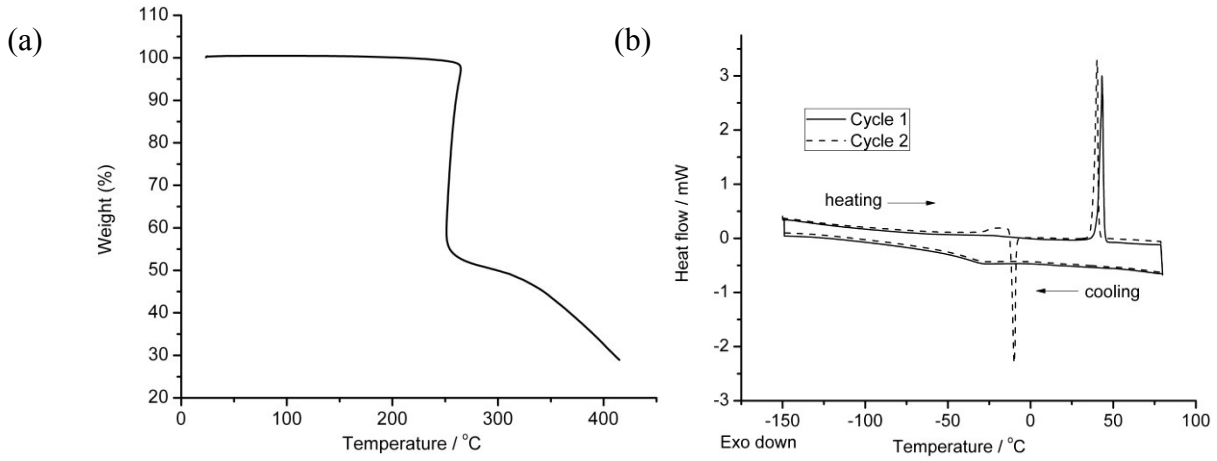

Figure 3-8. Thermal gravimetric analysis (TGA) trace (a) and differential scanning calorimetry (DSC) traces (b) of **3-2d** (the first and second heating–cooling cycles are plotted with solid and dash lines, respectively; heating and cooling rates are 10 °C/min).

Toward diagnosing this behavior, the thermal stability of compound **3-2d** was studied by thermal gravimetric analysis (TGA) and its thermal behavior was evaluated by differential scanning calorimetry (DSC). The TGA data (Figure 3-8a) shows that compound **3-2d** is thermally stable up to 200 °C. The DSC thermogram was recorded at a rate of 10 °C/min between –150 and 80 °C (DSC measurement was carried out one time with pure **3-2d** and has not been repeated for validation). During the first and second heating processes, one endothermic transition is found at ~ 41 °C; no exothermic transition is observed during the first cooling. An exothermic transition is observed during the second heating at ~ –10 °C, so-called cold-crystallization; no additional thermal transitions suggestive of mesophase formation were observed (Figure 3-8b).

To explore the phase behavior further, thermal transitions were investigated using variable-temperature polarized optical microscopy (POM). A phase transition from a crystalline phase to an isotropic phase was observed at 41 °C, consistent with the DSC result; when cooling the compound at the rate of 5 °C/min, well-ordered spherulites nucleated randomly over the whole sample at 24 °C. This crystal growth behavior is atypical for small discotic molecule

systems;[150,151] it is most commonly associated with polymers.[152] High anisotropy and the appearance of a Maltese cross birefringence pattern in the spherulites indicate long-range order. The extinction of light along the polarizer direction implies a radial alignment of 1-D stacked **3-2d** emerging from the center of the spherulites (Figure 3-9a). Lowering the cooling rate to 0.2 °C/min, much thicker and highly birefringent fiber-like crystals formed at 24 °C. This observation suggests that the 1-D stacking structure of **3-2d** is orientated uniaxially along the fiber axis (Figure 3-9b). Interestingly, both types of crystallization occurred during the cooling process at ~ 20 °C and no cold-crystallization was observed through POM.

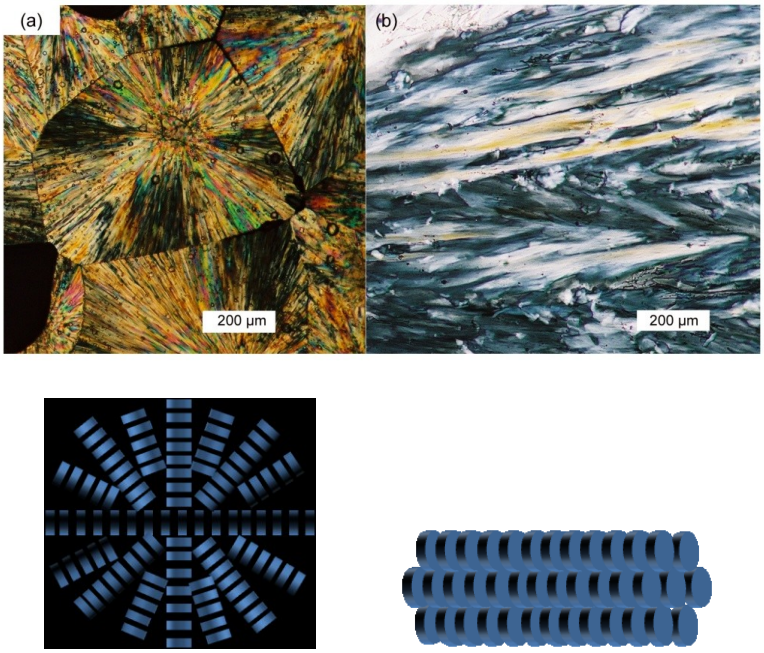

Figure 3-9. POM images of crystals of **3-2d** formed upon cooling the sample from the isotropic melt at rates of (a) 5 °C/min and (b) 0.2 °C/min.

The lack of formation of well-defined mesophases for **3-2d** leave us wondering if the stacked benzotrifurans might not be perfectly columnar as shown in Figure 3-10 (left, middle) due to repulsion between the electron-rich central aromatic rings. However, as an electron rich aromatic molecule, **3-2d** should enjoy enhanced stacking interactions with a complementary

electron poor aromatic system of similar size. The resulting binary material (Figure 3-10 (right)) could additionally display interesting electronic or optical properties through intermolecular charge transfer interactions.[153,154]

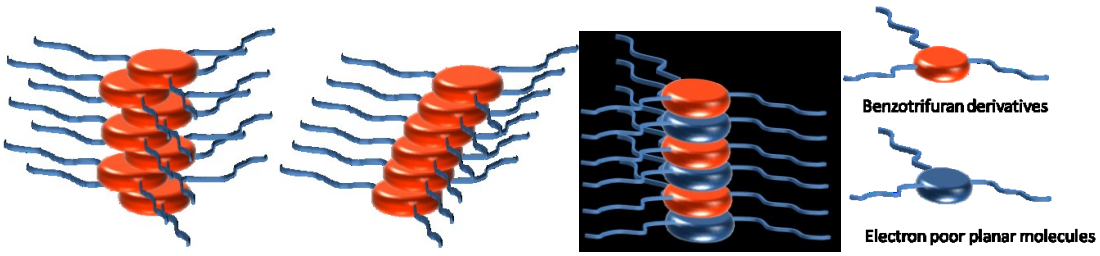

Figure 3-10. Possible stacking patterns of benzotrifuran derivatives with alkyl side chains (left, middle); bi-component mixture stacking pattern of benzotrifurans with complementary electron poor planar molecules (right).

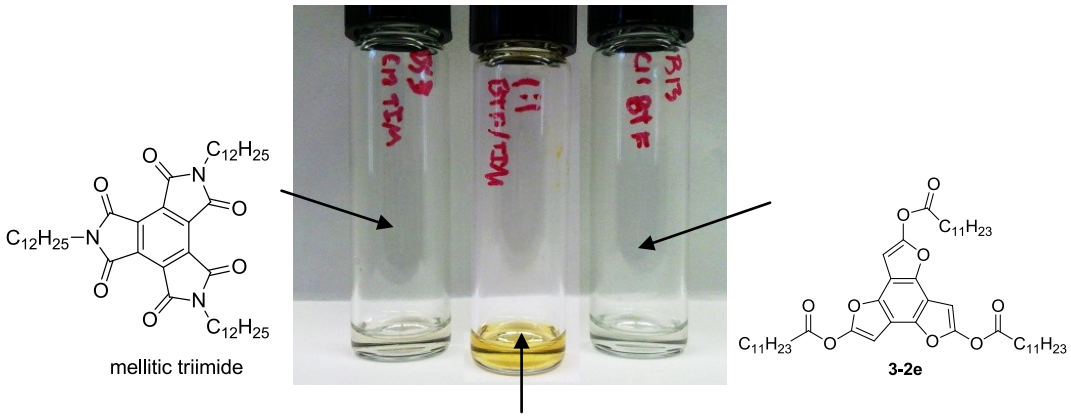

Figure 3-11. Comparison of solutions of **3-2d** (right vial), *N*-dodecyl mellitic triimide (left vial) and concentrated solution of their 1:1 mixture (middle vial). All solutions are 25mM in DCM.

Accordingly, compound **3-2d** was mixed with a D_{3h}-symmetric electron poor planar molecule, an *N*-dodecyl mellitic triimide, made from mellitic acid.[155] When the solutions of two compounds (1:1) (Figure 3-11) are mixed and concentrated, the concentrated mixture solution has an apparent color change from colorless to deep red, associated with a charge-transfer absorption. While the charge transfer interaction may not be the major driving force for self-

assembly, it is a signature of donor and acceptor interactions.[153] Other properties of this type of binary material will be explored further in the future.

Unexpected Introduction of a Donor-π-Acceptor System to Benzofuran

When benzotrifuranone **2-2** was treated with aryl acid chlorides, such as benzoyl chloride, complicated results were found, very different from the reactions with alkyl acid chlorides and chloroformates. Initial results with the C_{3h}-symmetric BTF lead to multiple products of similar polarity making it extremely difficult to isolate products for structural identification.

In order to understand the results of the reactions, a model reaction was carried out with coumaranone **2-1** and benzoyl chloride**.** When **2-1** was treated with benzoyl chloride in the presence of triethylamine, the color of the reaction solution turned deep yellow very quickly. Surprisingly, the major product was not the desired **3-4**, but the unexpected disubstituted product **3-5** (Figure 3-12a). Previously unreported compound **3-5** was isolated as a bright yellow solid. When 1.3 equivalents of benzoyl chloride were used in the reaction, 43% of **3-5** was obtained and only a small amount of **3-4** was isolated; when the amount of benzoyl chloride was increased to 2.2 equivalents, the yield of **3-5** increased to 90% (with only a small amount of **3-4** formed).

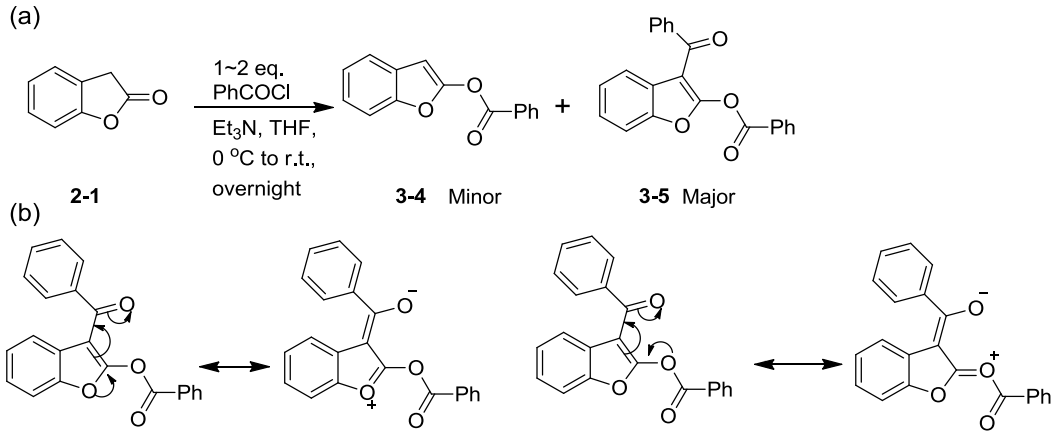

Figure 3-12. Unexpected results from the acylation coumaranone **2-1**, a model compound: (a) formation of **3-5** when treating **2-1** with benzoyl chloride; (b) two possible donor-π-acceptor pathways within compound **3-5**.

Similar reaction results were obtained when 1.0 equivalent of *p*-toluoyl chloride was used in the reaction; although the yield of *O*-acylation product increased to 16%, the major product was still the diacylated benzofuran (Table 3-2). Additionally, none of the starting material (coumaranone) was recovered from the reactions, instead, only a liquid by-product was isolated, the structure of which could not be determined.

Table 3-2. Product distribution obtained upon acylation of coumaranone with aroyl chlorides (ArCOCl).

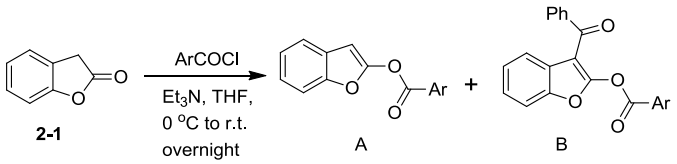

Ar-	**2-1** : ArCOCl	Yield of product A	Yield of product B
C_6H_5-	1 : 1.3	5%	43%
C_6H_5-	1 : 2.2	8%	90%
p-MeC_6H_4-	1 : 1.0	16%	42%

A possible mechanism for the α-acylation reaction is shown in Figure 3-13. The first step of the reaction could be *O*-acylation of **2-1** forming **3-3;** due to the reversibility of the *O*-acylation reaction and the instability of the aryl ester, the acyl group could migrate to the *α*-position of the benzofuranone in the presence of triethylamine (to form intermediate **3-6**). Intermediate **3-6**, a *β*-ketoester, is easily deprotonated to form a stable enolate, and a second *O*-acylation reaction would then yield the major product **3-5**. The existence of product **3-3** even when 2.2 equivalents of benzoyl chloride were used suggests that the first step of the reaction is not *C*-acylation of **2-1.** If irreversible *C*-acylation reaction occurred first, only **3-6** and **3-5** (not **3-3**) should be identified in the product mixture. It seems that competition between *C*-acylation and *O*-acylation in the first step is also not likely, since previous reactions with alkyl acid chloride substrates showed that *O*-acylation is much more favorable under the same reaction conditions (i.e., no *α*-acylation products were isolated previously).

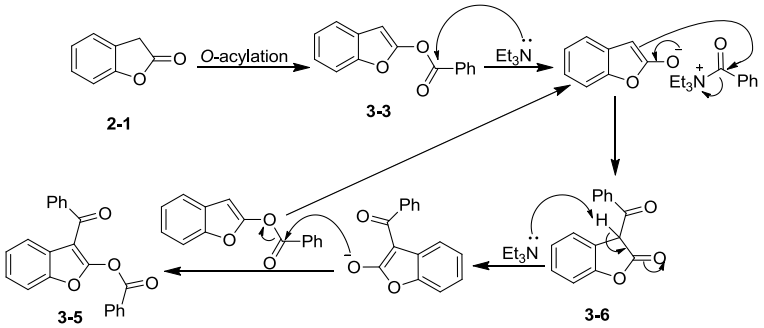

Figure 3-13. Possible mechanism for the formation of **3-5**.

This new disubstituted benzofuran derivative **3-5** features an electron donor (benzofuran oxygen and ester oxygen at α position) and electron acceptor (ketone at β position) on the same furan ring; more interestingly, the introduction of one of the donors and the acceptor is from a one-pot reaction. Two donor-π-acceptor pathways within compound **3-5** are shown in Figure 3-12b in the resonance sense. In comparison with the UV-Vis spectrum of **3-4** (λ_{max} = 209 nm, ε = 21940 cm^{-1} M^{-1}, and λ_{max} = 238 nm, ε = 22420 cm^{-1} M^{-1}) (Figure 3-10), **3-5** has similar absorption in the 200–250 nm region (λ_{max} = 208 nm, ε = 28559 cm^{-1} M^{-1}, and λ_{max} = 238 nm, ε = 27612 cm^{-1} M^{-1}). However, **3-5** also has a broad absorption (λ_{max} = 344 nm, ε = 9830 cm^{-1} M^{-1}) that is red-shifted relative to the major absorption of **3-4** due to its more extended π-conjugated system.

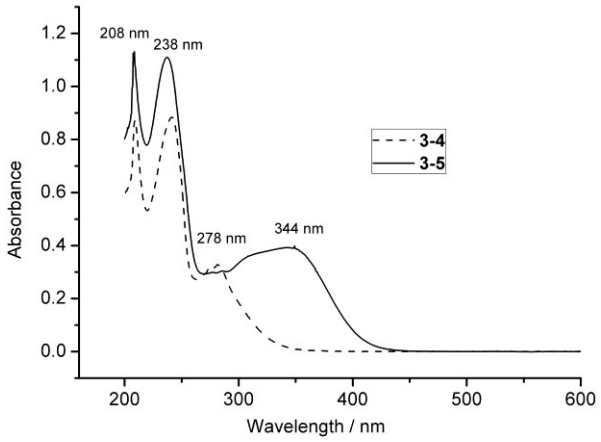

Figure 3-14. UV-Vis spectra of **3-4** (dash line) and **3-5** (solid line) in THF solution (40 μM).

Attempts at C–C Formation

Although various functional groups can be introduced to the benzotrifuran core through the high yielding and simple reaction shown in Figure 3-1, the ester or carbonate linkages are not as robust as simple alkyl side chains; indeed, some of the benzotrifuran derivatives decomposed over months on the bench top at room temperature. Further modification on the benzotrifuran core can be envisioned through C–C bond formation at the α-positions. Wada and coworkers[145] have managed to make the enol trifluoromethanesulfonate (triflate, Tf) from coumaranone and then form C–C bonds to the α-position through cross-coupling with appropriate substituted alkynes.

Before applying such an approach to benzotrifuranone, model reactions were carried out. The reaction reported by Wada[145] was repeated with coumaranone and phenyl acetylene (Figure 3-15a). As originally reported, Tf_2NPh was employed as the triflating reagent in the presence of KHMDS as the base; the enol triflate was then immediately used in a Sonogashira coupling with phenyl acetylene. Different palladium catalysts ($Pd(PPh_3)_2Cl_2$ and $Pd(PPh_3)_4$) were used and both gave modest overall yields (~ 40%) for the two-step reaction (Figure 3-15a), reasonable in comparison with the reported yield (~ 60%).[145] Despite promising results for the model reaction, extension of this chemistry to a dilactone system has thus far been unsuccessful. The formation of the di(enol triflate) has not been confirmed by ^1H NMR and the Sonogashira coupling has not been successful. It is suspected that the di(enol triflate) is quite unstable and the reaction proceeds through a more stable intermediate **3-8**. Through the reaction, desired product **3-10** was isolated in less than 3% yield while the mono-coupled product was obtained in 13% yield (Figure 3-15b).

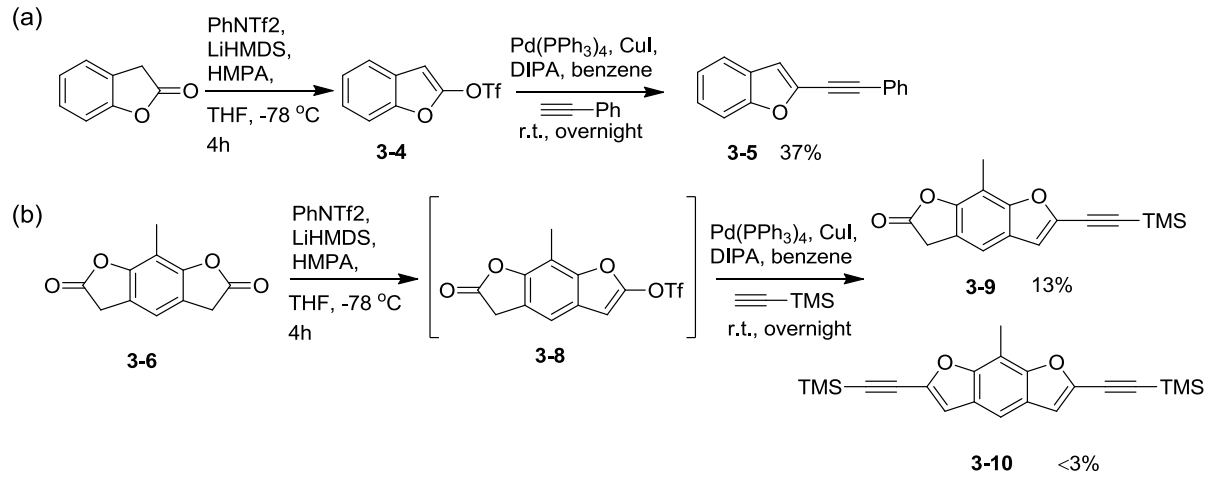

Figure 3-15. (a) Synthesis of α-alkynyl-substituted benzofuran from coumaranone; (b) attempts at C–C formation on benzodifuranone.

Although desired product **3-10**, in theory, can be synthesized from **3-9** by one more triflation and coupling, the low yields of the cross-coupling reactions do not encourage the application of this method to the benzotrifuranone system. In future research, other cross-coupling reactions (such as the Stille reaction[145]) should be considered as an alternative way to form C–C bonds from enol triflate intermediates. Another approach towards substituted benzotrifuran cores could utilize lactone free methods. Larock and coworkers[141] report a convenient method for benzofuran synthesis from *ortho*-alkynyl-methoxybenzene and the reaction works well for substituted benzofuran and benzodifuran synthesis. Known compounds **3-11**[156] and their derivatives could thusly be converted to substituted benzotrifurans **3-12** in one step (Figure 3-16).

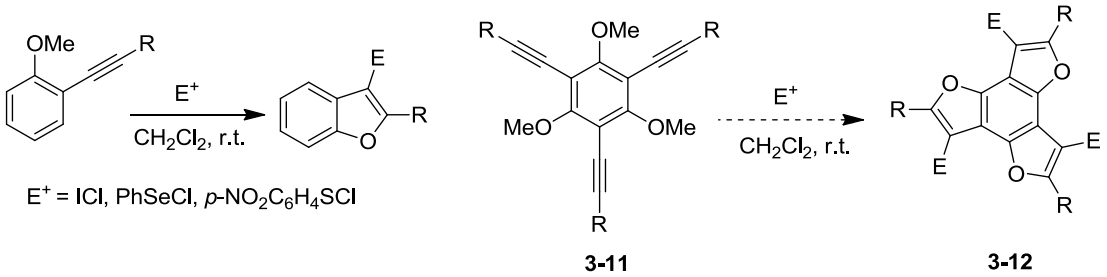

Figure 3-16. Possible approach to substituted benzotrifuran.

Conclusion

A family of benzotrifuran derivatives has been synthesized from BTFs **2-2** and **2-23a** by O-acylation with various acyl chlorides. These new benzotrifuran derivatives feature a C_{3h}-symmetric planar aromatic core and have been characterized by NMR and UV spectroscopic techniques. The X-ray crystal structure shows π-π interactions in the solid phase packing and POM studies indicate a columnar packing motif. Because of the electron-rich property of these benzotrifurans, intermolecular charge transfer was found when mixing them with mellitic triimide, an electron poor planar molecule. These binary donor-acceptor materials have potential applications in materials science and will be a future direction of this research. Although the preliminary attempts at C–C bond formation on benzotrifuran rings with Sonogashira coupling conditions did not succeed, some alternative approaches have been proposed. Additionally, an interesting reaction between coumaranone and aromatic acyl chlorides was found that can introduce electron donors and acceptors on to a benzofuran ring in a one-pot reaction. A reaction mechanism has been proposed and this finding uncovers another direction for this research in the future.

Experimental Section

Characterization Technique

Thermal optical polarized microscopy (TOPM). For all thermal optical polarized microscopy (TOPM) experiments, a Leica DMLP polarized light microscope with a Linkam heating and cooling stage (temperature range of –196 to 350 °C) and a 35 mm automated camera system was used.

Differential scanning calorimetry (DSC) and thermal-gravimetric analysis (TGA). The DSC experiments were performed on a TA Instruments Q1000 equipped with a liquid

nitrogen cooling accessory calibrated using sapphire and high-purity indium metal. All samples were prepared in hermetically sealed pans (1.5–4.0 mg/sample) and were referenced to an empty pan. The scan rate was 10 °C/min. Thermogravimetric analysis (TGA) was performed on a TA Instruments Q5000 IR using the dynamic high-resolution analysis mode and a two point Curie temperature calibration (alumel alloy and high purity nickel); the scan rate was 50 °C/min and N_2 was used as the purge gas.

Synthesis

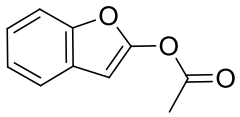

Benzofuran-2-yl acetate (3-1) To a solution of benzofuranone **2-1** (0.50 g, 3.7 mmol) in dry THF (8 mL) at 0 °C, acetyl chloride (0.44 g, 5.6 mmol) was added. The resulting solution was stirred for 30 min, followed by the addition of triethylamine (0.56 g, 5.6 mmol). A precipitate formed immediately and the mixture was allowed to stir for 1 h before warming to room temperature where stirring was continued for 2 h. The reaction mixture was diluted with water (50 mL) and extracted with Et_2O (40 mL × 3). The ethereal layers were combined, washed with water and brine successively, and dried with Na_2SO_4. After removal of the solvent under reduced pressure, flash column chromatography (1/20 ethyl acetate/hexanes) afforded **3-1** (0.34 g, 52%) as a colorless liquid. ^{1}H NMR ($CDCl_3$) δ 2.38 (s, 3H), 6.34 (d, J = 0.9 Hz, 1H), 7.21–7.28 (m, 2H), 7.39–7.42 (m, 1H), 7.50–7.53 (m, 1H). ^{13}C NMR ($CDCl_3$) δ 20.6, 89.2, 110.8, 120.7, 123.2, 123.6, 128.2, 149.2, 153.5, 166.1. HRMS (DART-TOF) calcd for $C_{10}H_{12}NO_3$ $(M+NH_4)^+$ 194.0812, found 194.0812.

2,5,8-Tri[(methoxycarbonyl)oxy]benzo[1,2-*b*:3,4-*b*':5,6-*b*″]trifuran (**3-2b**) General procedure for synthesis of benzotrifuran derivatives: To a solution of **2-2** (75 mg, 0.30 mmol) in

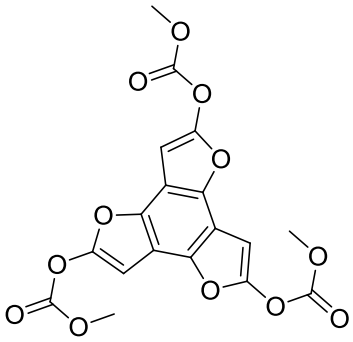

dry THF (8 mL) at 0 °C was added methyl chloroformate (115 mg, 1.22 mmol). The resulting solution was stirred for 30 min, followed by the addition of triethylamine (101 mg, 1.00 mmol). A gray precipitate formed immediately and the mixture was allowed to stir for 1 h before warming to room temperature where stirring was continued for 2 h. The reaction mixture was diluted with water (50 mL) and extracted with Et_2O (40 mL × 3). The ethereal layers were combined, washed with water and brine successively, and dried with Na_2SO_4. After removal of the solvent under reduced pressure, flash column chromatography (1/4 ethyl acetate/hexanes) afforded **4a** (114 mg, 89%) as white, needle-like crystals. ^{1}H NMR ($CDCl_3$) δ 4.00 (s, 9H), 6.61 (s, 3H). ^{13}C NMR ($CDCl_3$) δ 56.4, 86.6, 109.5, 139.5, 151.6, 152.4. HRMS (DART-TOF) calcd for $C_{18}H_{16}NO_{12}$ $(M + NH_4)^+$ 438.0667, found 438.0710. Anal. Calcd for $C_{18}H_{12}O_{12}$: C, 51.44; H, 2.88. Found: C, 51.07; H, 2.86.

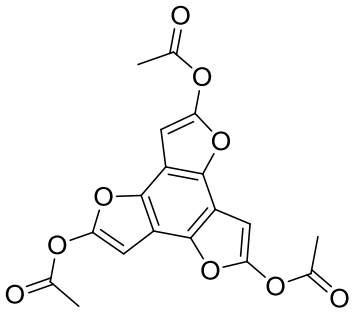

2,5,8-Triacetoxybenzo[1,2-*b*:3,4-*b*':5,6-*b*″]trifuran (**3-2a**) Following the general procedure for the synthesis of benzotrifuran derivatives, **2-2** (80 mg, 0.28 mmol), acetyl chloride (77 mg, 0.98 mmol) and triethylamine (100 mg, 0.980 mmol) generated **3-2a** (114 mg, 89%) as

white crystals, isolated after flash column chromatography (1/3 ethyl acetate/hexanes). ^{1}H NMR ($CDCl_3$): δ 2.40 (s, 9H), 6.60 (s, 3H). ^{13}C NMR ($CDCl_3$): δ 20.6, 86.6, 109.6, 139.1, 152.4, 166.3. HRMS (ESI-TOF) calcd for $C_{18}H_{12}O_9Na$ $(M+Na)^+$ 395.0374, found 395.0391.

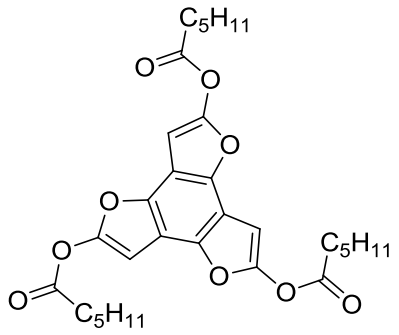

Benzo[1,2-b:3,4-b':5,6-b'']trifuran-2,5,8-triyl trihexanoate(3-2c) Following the general procedure for the synthesis of benzotrifuran derivatives, **2-2** (80.0 mg, 0.325 mmol), triethylamine (134 mg, 1.14 mmol), and hexanoyl chloride (115 mg, 1.14 mmol) yielded **3-2c** (102 mg, 58%) as a colorless, oily solid. ^{1}H NMR ($CDCl_3$) δ 6.60 (s, 3H), 2.65 (t, J = 7.5 Hz, 6H), 1.80 (quin, J = 6.9 Hz, 6H), 1.52–1.30 (m, 12H), 0.95 (t, J = 6.4 Hz, 9H); ^{13}C NMR ($CDCl_3$): δ 13.84, 22.24, 24.23, 31.08, 33.86, 86.49, 109.58, 139.02, 152.52, 169.20. HRMS (ESI-TOF) calcd for $C_{30}H_{36}O_9Na$ $(M+Na)^+$ 563.2252, found 563.2232.

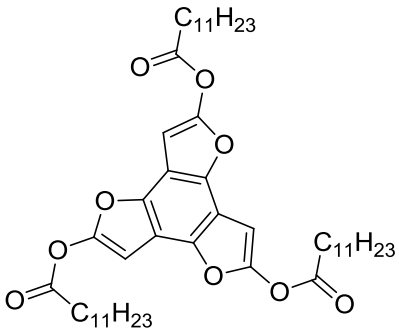

Benzo[1,2-b:3,4-b':5,6-b'']trifuran-2,5,8-triyl tridodecanoate (3-2d) Following the general procedure for the synthesis of benzotrifuran derivatives, **2-2** (70.0 mg, 0.280 mmol), triethylamine (101 mg, 1.00 mmol), and lauroyl chloride (219 mg, 1.00 mmol) yielded **3-2d** (100

mg, 44%) as a colorless, waxy solid. ^{1}H NMR ($CDCl_3$) δ 0.89 (t, J = 6.57 Hz, 10H), 1.24–1.51 (m, 18H), 1.80 (quin, J = 7.30 Hz, 5H), 2.66 (t, J = 7.45 Hz, 7H) 6.60 (s, 1H); ^{13}C NMR ($CDCl_3$): δ 14.12, 22.61, 24.58, 28.97, 29.20, 29.34, 29.41, 29.59, 29.60, 31.91, 33.96, 86.53, 109.60, 139.05, 152.54, 169.24. HRMS (APCI-TOF) calcd for $(M + Na)^+$ $C_{18}H_{12}O_9Na$ 815.5069, found 815.5048.

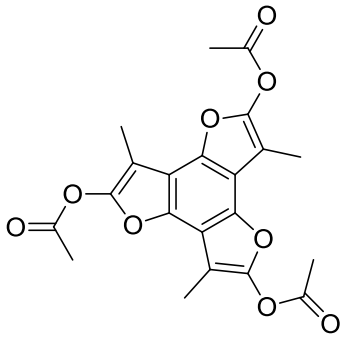

3,6,9-Trimethylbenzo[1,2-b:3,4-b':5,6-b'']trifuran-2,5,8-triyl triacetate (3-3a) **3,6,9-Trimethylbenzo[1,2-b:3,4-b':5,6-b'']trifuran-2,5,8-triyl triacetate (3-3a)** To a solution of **2-23a** (47 mg, 0.16 mmol) in THF (8 mL) at 0 °C was added acetyl chloride (57 mg, 0.72 mmol). The resulting solution was stirred for 30 min, followed by the addition of triethylamine (73 mg, 0.72 mmol). A white precipitate formed immediately and the mixture was gradually warmed to room temperature and stirred overnight. The reaction mixture was diluted with water (50 mL) and extracted with Et_2O (40 mL × 3). Next, the ethereal layers were combined, washed with water and brine successively, and dried with Na_2SO_4. After removal of the solvent under reduced pressure, flash column chromatography (1/4 ethyl acetate/hexanes) afforded **3-3a** (30 mg, 45%) as an off-white solid. ^{1}H NMR ($CDCl_3$): δ 2.32 (s, 9H), 2.40 (s, 9H). ^{13}C NMR ($CDCl_3$): δ 8.1, 20.3, 97.6, 110.9, 140.1, 148.0, 167.5. HRMS (ESI-TOF) calcd for $C_{21}H_{19}O_9$ $(M+H)^+$ 415.1024, found 415.1020.

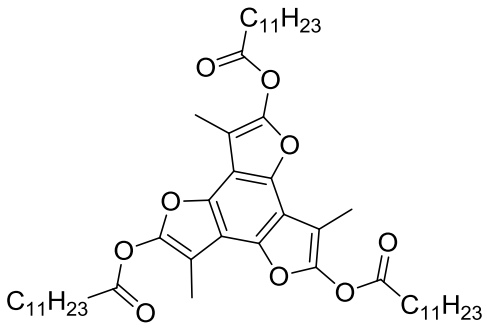

3,6,9-Trimethylbenzo[1,2-b:3,4-b':5,6-b'']trifuran-2,5,8-triyl tridodecanoate (3-3b)

Following the general procedure for the synthesis of benzotrifuran derivatives, **2-23a** (80 mg, 0.280 mmol), triethylamine (101 mg, 1.00 mmol), and lauroyl chloride (219 mg, 1.00 mmol) yielded **3-3b** (152 mg, 65%) as a colorless waxy solid. ^{1}H NMR ($CDCl_3$) δ 2.66 (t, J = 7.5 Hz, 6H), 2.30 (s, 3H), 1.81 (quin, J = 7.3 Hz, 6H), 1.51–1.17 (m, 48H), 0.89 (t, J = 6.4 Hz, 9H); ^{13}C NMR ($CDCl_3$): δ 8.11, 14.10, 22.68, 24.71, 29.01, 29.20, 29.33, 29.44, 29.58, 29.60, 31.90, 33.65, 97.425, 110.95, 140.05, 148.15, 170.49. . HRMS (APCI-TOF) calcd for $C_{51}H_{79}O_9$ $(M+H)^+$ 835.5719, found 835.5702.

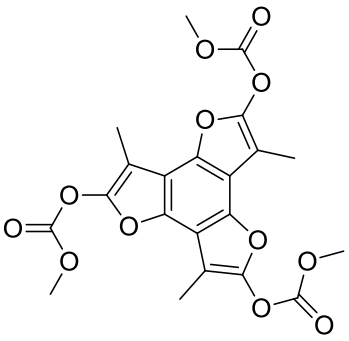

Trimethyl (3,6,9-trimethylbenzo[1,2-b:3,4-b':5,6-b'']trifuran-2,5,8-triyl) tricarbonate (3-3c)

Following the procedure described for the synthesis of **3-3a**, **2-23a** (34 mg, 0.12 mmol) and methyl chloroformate (51 mg, 0.54 mmol) yielded **3-3c** (34 mg, 62%) as a white solid. ^{1}H NMR

($CDCl_3$): δ 2.35 (s, 9H), 5.36 (s, 9H). ^{13}C NMR ($CDCl_3$): δ 7.9, 56.4, 97.6, 110.9, 140.1, 148.2, 152.4. HRMS (ESI-TOF) calcd for $C_{21}H_{19}O_{12}$ $(M+H)^+$ 463.0871, found 463.0868.

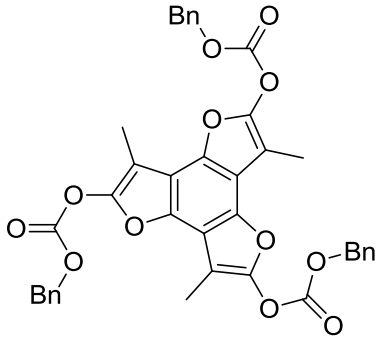

Tribenzyl (3,6,9-trimethylbenzo[1,2-b:3,4-b':5,6-b'']trifuran-2,5,8-triyl) tricarbonate (3-3d)

Following the general procedure for the synthesis of benzotrifuran derivatives, **2-23a** (50 mg, 0.17 mmol) and benzyl chloroformate (134 mg, 0.78 mmol) yielded **3-3d** (80 mg, 67%) as a white solid. ^1H NMR ($CDCl_3$): δ 2.36 (s, 9H), 4.00 (s, 9H), 7,42–7.48 (m, 15H). ^{13}C NMR ($CDCl_3$): δ 7.9, 71.5, 97.6, 110.9,128.6, 128.8, 129.0, 134.0, 140.0, 148.2, 151.8. HRMS (APCI-TOF) calcd for $C_{39}H_{31}O_{12}$ $(M+H)^+$ 691.1810, found 691.1815.

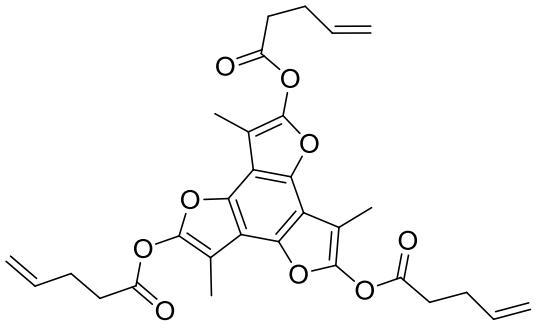

3,6,9-Trimethylbenzo[1,2-b:3,4-b':5,6-b'']trifuran-2,5,8-triyl tris(pent-4-enoate) (3-3e)

Following the general procedure for the synthesis of benzotrifuran derivatives, **2-23a** (100 mg, 0.350 mmol), triethylamine (141 mg, 1.40 mmol), and pent-4-enoyl chloride (166 mg, 1.40 mmol) yielded **3-3e** (90 mg, 50%) as a colorless oil. ^1H NMR ($CDCl_3$) δ 2.30 (s, 9H), 2.57 (q, *J*

= 6.8 Hz, 6H), 2.78 (t, *J* = 7.3 Hz, 6H), 5.13 (ddd, *J* = 10.2, 2.5, 1.2 Hz, 3H), 5.20 (dq, *J* = 17.2, 1.5 Hz, 3H), 5.93 (ddt, *J* = 16.8, 10.2, 6.4 Hz, 3H); ^{13}C NMR ($CDCl_3$): δ 8.08, 28.57, 32.94, 97.52, 110.92, 116.32, 13572, 140.05, 148.00, 169.71. HRMS (ESI-TOF) calcd for $C_{30}H_{31}O_9$ $(M+H)^+$ 535.1963, found 535.1941.

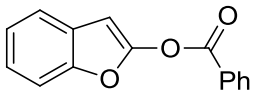

Benzofuran-2-yl benzoate (3-4) To a solution of coumaranone (300 mg, 2.24 mmol) in THF (20 mL) was added benzoyl chloride (405 mg, 2.90 mmol) and the resulting solution was cooled to 0 °C. Triethylamine (293 mg, 2.90 mmol) was added and the reaction solution was allowed to warm to room temperature and stir overnight. The solution was diluted with water (100 mL) and extracted with EtOAc. The organic layer was washed with water and brine, and then dried over Na_2SO_4. The solvent was removed under reduced pressure and the residue was purified by flash column chromatography (DCM/hexanes 1:2) to yield **3-4** (15 mg, 3%) as a colorless solid and **3-5** (327 mg, 43%) as a yellow solid. ^{1}H NMR ($CDCl_3$) δ 6.50 (d, *J* = 0.6 Hz, 1H), 8.25–8.20 (m, 8H), 7.58–7.50 (m, 4H), 7.46–7.41 (m, 1H), 7.28–7.23 (m, 9H); ^{13}C NMR ($CDCl_3$) δ 89.4, 110.8, 120.8, 123.3, 123.6, 127.8, 128.4, 128.8, 130.5, 134.4, 149.3, 153.8, 162.1. HRMS (DART-TOF) calcd for $C_{15}H_{11}O_3$ $(M + H)^+$ 239.0703, found 239.0703.

3-Benzoylbenzofuran-2-yl benzoate (3-5). Compound **3-5** was isolated from the preparation of compound **3-4**. ^{1}H NMR ($CDCl_3$) δ 8.23–8.16 (m, 1H), 7.79–7.71 (m, 1H), 7.64–7.46 (m, 1H), 7.67–7.44 (m, 6H), 7.33–7.23 (m, 1H), 7.13–7.03 (m, 2H), 6.97–6.88 (m, 1H). ^{13}C NMR ($CDCl_3$) δ 110.9, 113.1, 121.3, 121.9, 123.4, 128.6, 128.7, 129.1, 130.3, 130.5, 131.7,

133.6, 133.9, 152.9, 157.3, HRMS (DART-TOF) calcd for $C_{22}H_{15}O_4$ $(M + H)^+$ 3432.0965, found 343.0982.

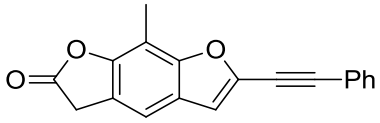

8-Methyl-6-(phenylethynyl)benzo[1,2-b:5,4-b']difuran-2(3H)-one (3-9) A solution of 8-methylbenzofuro[5,6-b]furan-2,6(3H,7H)-dione (100 mg; 0.490 mmol in 5 mL dry THF) was cooled to –78°C, and then 0.70 mL LiHMDS solution (1 M in THF, 0.64 mmol) was added slowly, followed by HMPA (0.13 mL, 0.74 mmol). The mixture was allowed to stir at –78°C for 20 min. A chilled solution (at 0 °C) of $PhNTf_2$ (210 mg, 0.550 mmol in dry 7mL THF) was added to the benzofuranone solution and stirred. The mixture solution was allowed to warm to room temperature for 3 h after which the reaction was quenched with a saturated solution of NH_4Cl and extracted with diethyl ether. The crude material was used without purification in the next step.

The crude product was dissolved in Et_2O (1.5 mL) and then introduced to a dry flask under Ar. Then benzene (5 mL), CuI (13 mg, 0.07 mmol, 0.15 equiv), diisopropylamine (0.270 mL, 1.96 mmol), and trimethylsilyl acetylene (0.14 mL, 0.98 mmol) were added; finally, $Pd(PPh_3)_4$ (60.0 mg, 0.050 mmol) was added and the solution turned black. The resulting mixture was stirred at room temperature overnight. The reaction was quenched with a saturated aqueous solution of NH_4Cl (80 mL), extracted with ether (3 × 30 mL), and the combined ethereal solutions were dried over Na_2SO_4 and concentrated in vacuo. Column chromatography (gradient from pure hexanes to pure EtOAc) recovered dilactone starting material (24 mg, 24%) and yielded **3-9** (18 mg**,** 13%, over two steps) as a beige solid. ^1H NMR ($CDCl_3$): δ 0.31 (s, 3H); 2.48 (s, 3H); 3.83 (s, 2H); 6.92 (s, 1H), 7.25 (s, 1H).

X-ray crystallography

Compound 3-3a. Data were collected at 173 K on a Siemens SMART PLATFORM equipped with A CCD area detector and a graphite monochromator utilizing MoK_α radiation (λ = 0.71073 Å). Cell parameters were refined using up to 8192 reflections. A full sphere of data (1850 frames) was collected using the ω-scan method (0.3° frame width). The first 50 frames were re-measured at the end of data collection to monitor instrument and crystal stability (maximum correction on I was < 1 %). Absorption corrections by integration were applied based on measured indexed crystal faces.

The structure was solved by the Direct Methods in *SHELXTL6,* and refined using full-matrix least squares. The non-H atoms were treated anisotropically, whereas the hydrogen atoms were calculated in ideal positions and were riding on their respective carbon atoms. A total of 277 parameters were refined in the final cycle of refinement using 2425 reflections with $I > 2\sigma(I)$ to yield R_1 and wR_2 of 5.49% and 10.04%, respectively. Refinement was done using F^2.

Computational Details

Using the NWChem suite of programs,[157] we optimized the molecular geometries of **2-2** and **3-2a** by density functional theory (DFT) at the level of RB3LYP/6-311+G*. With the optimized structures, we calculated the UV/Vis spectra using semiempirical molecular orbital theory at the level of Zerner's spectroscopic version of the Intermediate Neglect of Differential Overlap (ZINDO/S),[158,159] which is available in the Hyperchem program.[160] ZINDO/S is parameterized to reproduce UV/Vis spectroscopic transitions when used with the singly excited configuration interaction (CI) method. For our calculations, the weighting factors for sigma-sigma and pi-pi atomic orbital overlap are taken from the default in Hyperchem, which are 1.267 and 0.585, respectively. The highest eight occupied and the lowest eight unoccupied orbitals are

enclosed in the singly excited CI calculations. To explore the aromaticity, we calculated the nucleus-independent chemical shifts (NICS) for selected molecules at the level of RB3LYP/6-311+G* using the Gaussian 03 suite of program.[161] The calculations were performed at the ring center as defined by the center of mass, NICS(0), and 1 Å above the ring centers, NICS(1).

CHAPTER 4
DONOR-σ-ACCEPTOR THROUGH BOND INTERACTION STUDY IN β-AMINO KETONES

Introduction

Discussed in Chapter 1 (Figure 1-2), phloroglucinol is an unusual benzenoid molecule because it can access a fully aromatic "trienol" form and several nonaromatic ketone tautomers. Risch,[162,163] during his habilitation in Germany, reported an ingenious way to capture the triketone by treating substituted phloroglucinols with hexamethylenetetramine (HMTA). The one-step transformation (Figure 4-1) forms an interesting C_{3v}-symmetric molecule, a 1-aza-adamantanetrione, referred to from this point forward as AAT. This chapter explores the donor-σ-acceptor (D-σ-A) hyperconjugative interactions inherent to the AAT molecules with the goal of applying the systems in supramolecular applications.

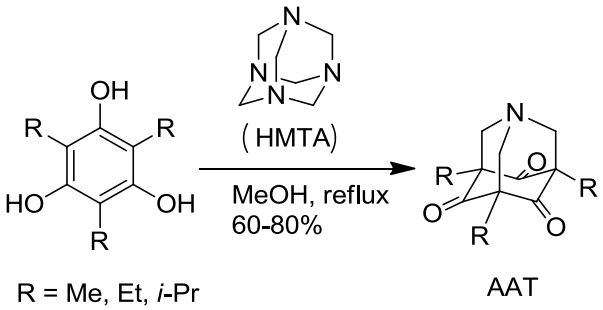

Figure 4-1. Risch's synthesis of 1-aza-adamantanetriones (AATs) from substituted phloroglucinol derivatives.

Donor-σ-Acceptor Interactions

The term "through-bond interaction" (TBI) was first introduced by Hoffmann[164,165] in 1968 to designate the intramolecular interaction between functional groups via intervening σ-bonds. Such "hyperconjugative" interactions were proven to be very sensitive to the geometry of the interacting donor and acceptor orbitals with respect to their intervening σ-bridging bonds.[166] Theoretical studies[164,165,167,168] have shown that interaction between the orbitals is maximized for an all-trans, coplanar arrangement of bonds (and lone pairs) along the σ-framework.

For donor-σ-acceptor systems, in which a strong electron donor (D) and an strong acceptor (A) are connected by three or more bridging σ-bonds, an intramolecular charge transfer (CT) [169-174] absorption and emission can arise due to the interaction between the two groups. The efficiency of CT is dependent on the orientation of D and A, consistent with the theoretical predictions. Verhoeven and coworkers[172,173] have used the spectroscopic signature to prove the stereoelectronic requirements for D-σ-A interactions in cyclic ring systems. Tricyclic D (nitrogen)-σ-A (1-cyano-1-carbethoxyethylene) molecule **4-a** (Figure 4-2) has a rigid structure, thus permanently fixing the nitrogen lone pair into an equatorial orientation (with respect to the six-membered ring (anti-parallel to central C–C σ bond)), and a strong CT absorption is observed. Flexible piperidone **4-b** (Figure 4-2) does not display a similar CT absorption although it possesses the same D and A components. The best explanation for the absence of the CT absorption is that the nitrogen lone pair occupies an axial position in **4-b** (with the methyl group preferentially adopting a more stable equatorial orientation); this conformation is not suitable for optimized TBI in the molecule.

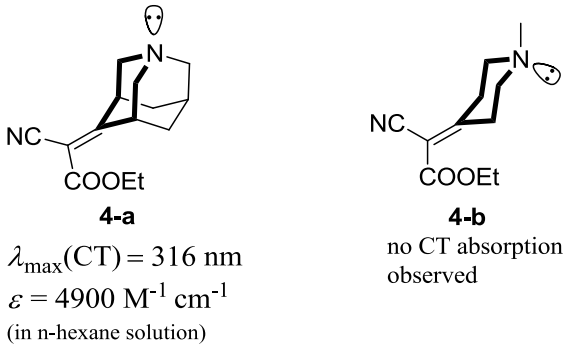

Figure 4-2. Model compounds used[172,173] to illustrate the conformational requirements for D-σ-A TBI.

The β-aminoketone fragment has also emerged as a good framework for studying D-σ-A TBI; it features an electron donor (amino group) and an electron acceptor (carbonyl group) connected by three σ-bonds. As discussed before, donor-acceptor interactions are optimized

when the nitrogen lone pair and carbonyl π system are trans and coplanar with respect to the central C_α–C_β σ-bond (Figure 4-3). The ground and excited state dipoles of molecular systems bearing this fragment are sensitive to the orientation between the electron donor and acceptor. Shown are three cyclic β-aminoketone structures that differ with respect to their conformational freedom along the donor–acceptor pathway. The lone pair of the nitrogen atom in *N*-methylpiperidone and tropinone is not fixed in the optimum position for interaction with the acceptor carbonyl; this configuration is, however, permanently fixed in 1-aza-adamantanone due to its rigid tricyclic structure (Figure 4-3).

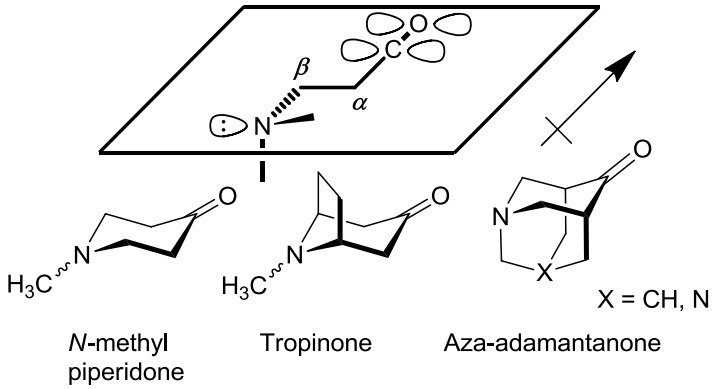

Figure 4-3. Donor-σ-acceptor arrangement in cyclic β-amino ketones.

The AAT core (Figure 4-1) is an interesting C_{3v}-symmetric β-aminoketone species, featuring one electron donor, three electron acceptors, and multiple pathways facilitating TBIs. The net ground state dipole moment of the AAT is related to the through-bond interactions in the molecule and lies along its C_3 axis of symmetry. Molecular dipoles are the basis of useful dipolar interactions that govern self-assembly processes in the fields of supramolecular chemistry and materials science.[175-178] Due to the shape of the AAT core and the direction of its dipole, it is possible that AAT molecules could adopt a head-to-tail self-assembly motif as shown in Figure 4-4.

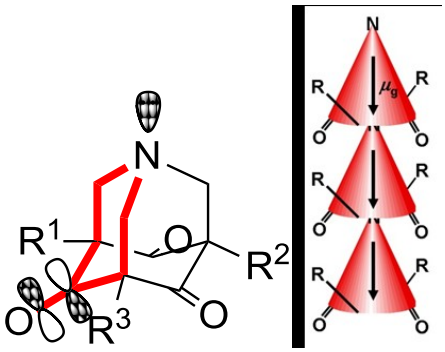

Figure 4-4. A cartoon representation of head-to-tail 1-D self-assembly of AATs as a consequence of dipolar interactions.

AAT synthesis in the Castellano group has focused on introducing functional groups, such as aromatic rings[179] and amides,[180] to the periphery of the AAT core. An interesting macromolecular behavior, organogelation, was discovered for the aryl and aryl-substituted amide AATs in organic solvents such as DMSO and $CHCl_3$. The morphologies of the xerogels have been explored by scanning electron microscopy (SEM) and transmission electron microscopy (TEM) (in the case of compound **4-1** (Ar = Ph), Figure 4-5); in most cases the microscopy images show fibrillar structures consistent with other gelators the assembly of which is generally understood to be 1-D organization of the monomers.[181,182]

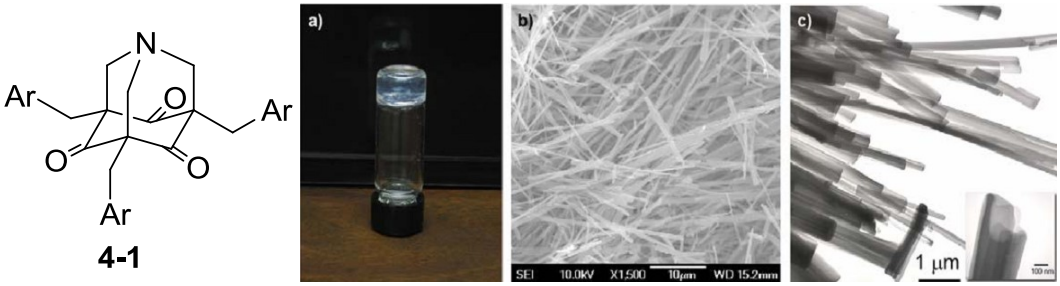

Figure 4-5. Organogels from functionalized AAT **4-1**(Ar = Ph): (a) 0.5 wt % of **4-1** (Ar = Ph) in DMSO after heating and cooling; (b) SEM and (c) TEM images of a xerogel formed from critical point drying of an 0.5 wt % DMSO gel.

DFT-LDA/cc-pVDZ calculations previously identified the lowest energy conformation for self-assembling AATs as the all-arms-up structure shown in Figure 4-6a, a conformation accessible in solution based on NMR experiments (NOEs are observed between hydrogens H^c on

the aromatic ring and H^a on the core; Figure 4-6b). Further molecular dynamics simulations by Sumpter and coworkers[183] revealed the tendency of these donor-σ-acceptor molecule to self-assemble (in the gas phase) in a head-to-tail fashion to create polar columns. The predicted stacked dimer (Figure 4-6c) is stabilized by dipole-dipole interactions and π-π stacking to the tune of ~ 13 kcal/mol (the intercore spacing in the optimized dimer is ~ 5.1 Å). Additionally, computational analysis showed that the electronic structure of an assembly of **4-1** (Ar = Ph) is very different from the monomer alone. Reduction of the HOMO-LUMO energy gap is predicted upon AAT stacking to form a dimer and oligomer; ultimately a band structure develops akin to what is described for π-conjugated molecular system. Formation of molecular wires via the self-assembly of novel non-aromatic architectures is an important development toward organic electronic devices.[183]

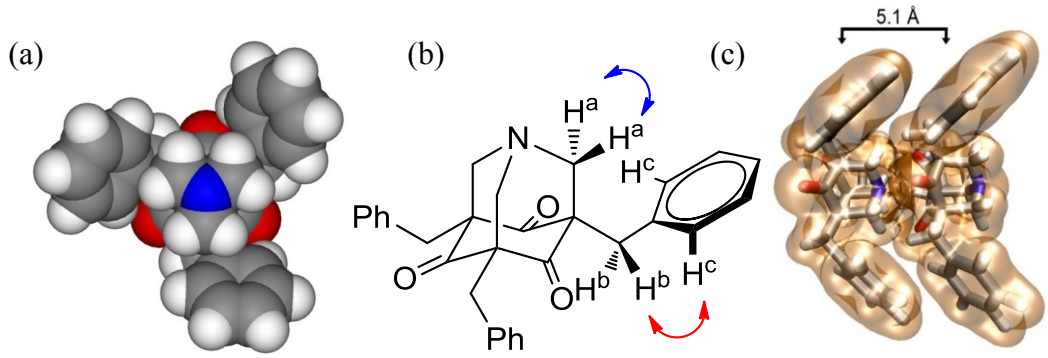

Figure 4-6. (a) Energy-minimized lowest energy "all-arms-up" conformation for **4-1** (Ar = Ph); (b) the NOE contacts identified from a NOESY experiment for **4-1**(Ar = Ph);[179] (c) total charge density isosurface for the gas-phase optimized dimer, obtained from DFT(LDA)/cc-pVDZ calculations.[183]

Limitations of Previous AAT Molecules for TBI Study

Since the self-assembly of AAT molecules has potential applications for new materials development, it is important to understand the consequences of TBI on AAT molecular structure. It is in this way that such interactions could potentially be used to tailor AAT structure and properties for various applications.

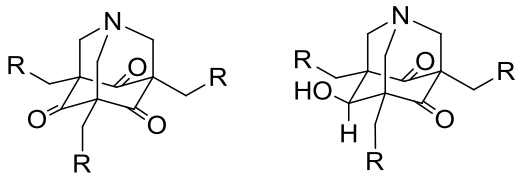

4-1 R = Ar
4-2 R = CONHAr
4-3 R = CO_2-*i*Pr
4-4 R = CH_2CO_2-*i*Pr
4-5 R = n-C_4H_9

4-6 R = CO_2-*i*Pr

Figure 4-7. Structures of the first two generations of AATs **4-1**[179] and **4-2**.[180] Target AAT molecules **4-3**, **4-4**, and **4-5**, and 1-aza-adamantanedione (AAD) molecule **4-6.**

Previously reported[179,180] AAT molecules **4-1** and **4-2** (Figure 4-7) show gelation properties in organic solvents; however, they both suffer from poor solubility in common organic solvents and no propensity to form single crystals suitable for X-ray analysis. These properties prevent reliable studies of TBI in AAT molecules in solution and the solid state. In order to study TBI at the molecular level, new generations of AAT molecules have been prepared bearing ester (**4-3**, **4-4**) and alkyl (**4-5**) (Figure 4-7) groups to improve the solubility of the molecules in organic solvents. In addition, one carbonyl group in **4-3** has been reduced to form 1-aza-adamantanedione (AAD) **4-6**, useful for probing the effect of shutting down TBI pathways.

Synthesis

The synthesis of ester-functionalized AAT **4-3** is quite straightforward. When previously discussed phloroglucinol derivative **2-6** and HMTA are heated to reflux in an appropriate alcoholic solvent (*i*-PrOH), AAT **4-3** forms in 66% yield as a white solid (Figure 4-8). This particular cyclization works best at higher concentrations ($\geq$ 0.1 M). As expected, ester AAT **4-3** is markedly more soluble than the previously synthesized amide derivative **4-2**. The reasonable solubility of **4-3** allowed exploration of carbonyl hydride reductions at low temperature with the goal of isolating and characterizing the corresponding alcohols, and analyzing the structural consequences of the TBIs within a structurally related aza-adamantanone family. Lampkins and

coworkers[184] reported the reduction of AAT **4-3** with diisobutylaluminium hydride (DIBAL-H); three equivalents of DIBAL-H reduced only one ketone carbonyl group of **4-3** to form a mixture of equatorial and axial alcohols. Unfortunately, the two diastereomers were not separable. Another reducing agent, sodium bis(2-methoxyethoxy)aluminum hydride (Red-Al), was used alternatively (by this author) for the reduction reaction. Unlike the DIBAL-H reaction, the AAT starting material was quickly consumed after one equivalent of Red-Al was added to the reaction solution. The reaction was quenched at –78 °C and the major separable product was identified as the equatorial (with respect to the bolded six-membered ring, Figure 4-8) alcohol aza-adamantanedione (AAD) **4-6**; several other more polar products were also obtained but could not be isolated (HRMS suggested that the by-products were di- and tri-alcohols).

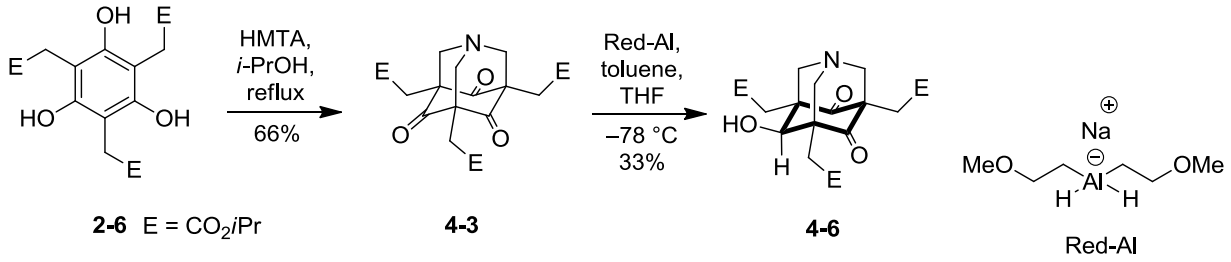

Figure 4-8. Synthesis of ester-functionalized AAT **4-3** and AAD **4-6**.

Ester-functionalized AAT **4-4** has also been prepared (Figure 4-9). The compound is structurally similar to **4-3** and bears one extra methylene spacer between the ester groups and the AAT core. Its preparation begins with previously reported tribromo scaffold **4-7**[179] that is converted to the tripropionic acid **4-10** using a three-step sequence involving alkylation, saponification, and thermally-mediated decarboxylation (78% overall yield for three steps). Subsequent Fischer esterification provides triester species **4-11** in good yield, and a carefully monitored BBr_3-mediated demethylation affords **4-12**. It is worth noting that when the demethylation reaction is quenched above –30 °C, lactone species are formed (similar to the

chemistry shown in Chapter 2, Figure 2-7).[184] The cyclization with HMTA provides AAT **4-4** in 47% yield, again when the reaction is performed in an appropriate alcoholic solvent (i-PrOH). Triester **4-4**, like analogue **4-3**, is again found to be readily soluble in common organic solvents.

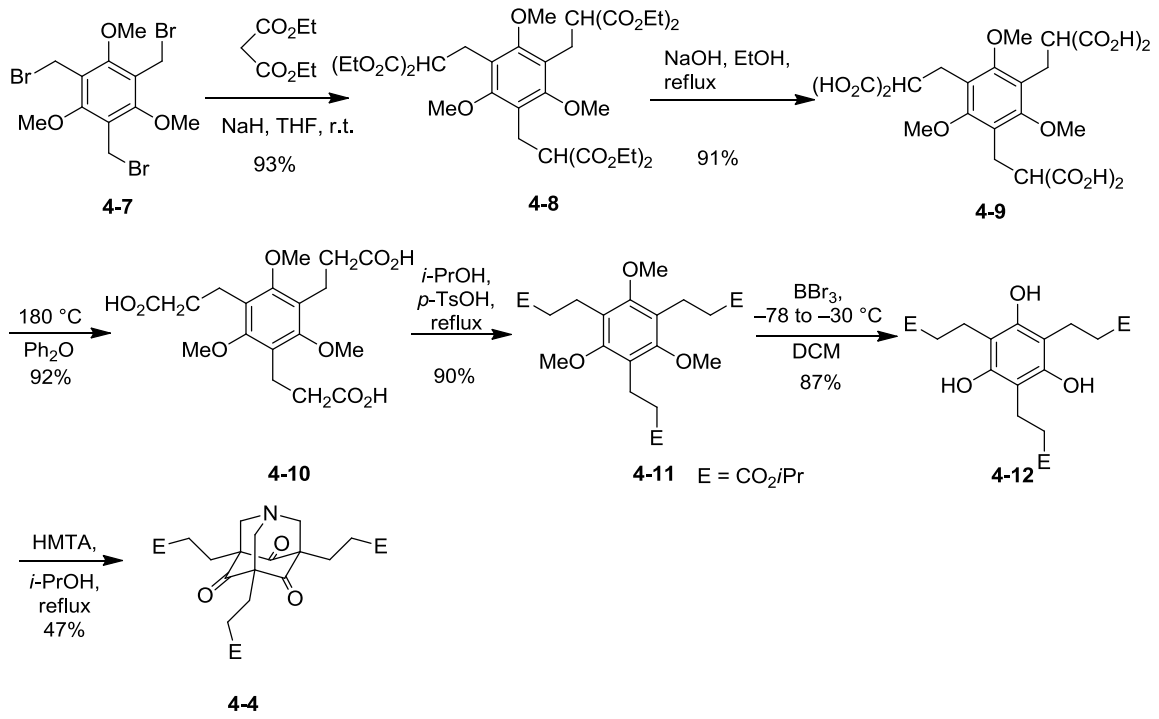

Figure 4-9. Synthesis of ester-functionalized AAT **4-4**.

Tripentyl AAT **4-5** serves as a representative alkyl-substituted AAT species. Its synthesis begins from tribromo scaffold **4-7**; subsequent hydrolysis and oxidation reactions afford intermediate trialdehyde **4-14** in reasonable yield. Three-fold addition of *n*-butyllithium produces the triol **4-15** as a mixture of *anti*,*syn* and *syn*,*syn* isomers; the mixture is then subjected to trimethylsilyl hydride reduction as described for similar compounds by Biali and coworkers[185] to give **4-16**. Demethylation of **4-16** with BBr_3 in DCM produces tripenyl phloroglucinol **4-17**, that is cyclized with HMTA in methanol to provide target molecule **4-5** as a white solid. AAT **4-5** has very good solubility in common organic solvents, and the attached alkyl chains also facilitate its solubility in non-polar solvents such as cyclohexane.

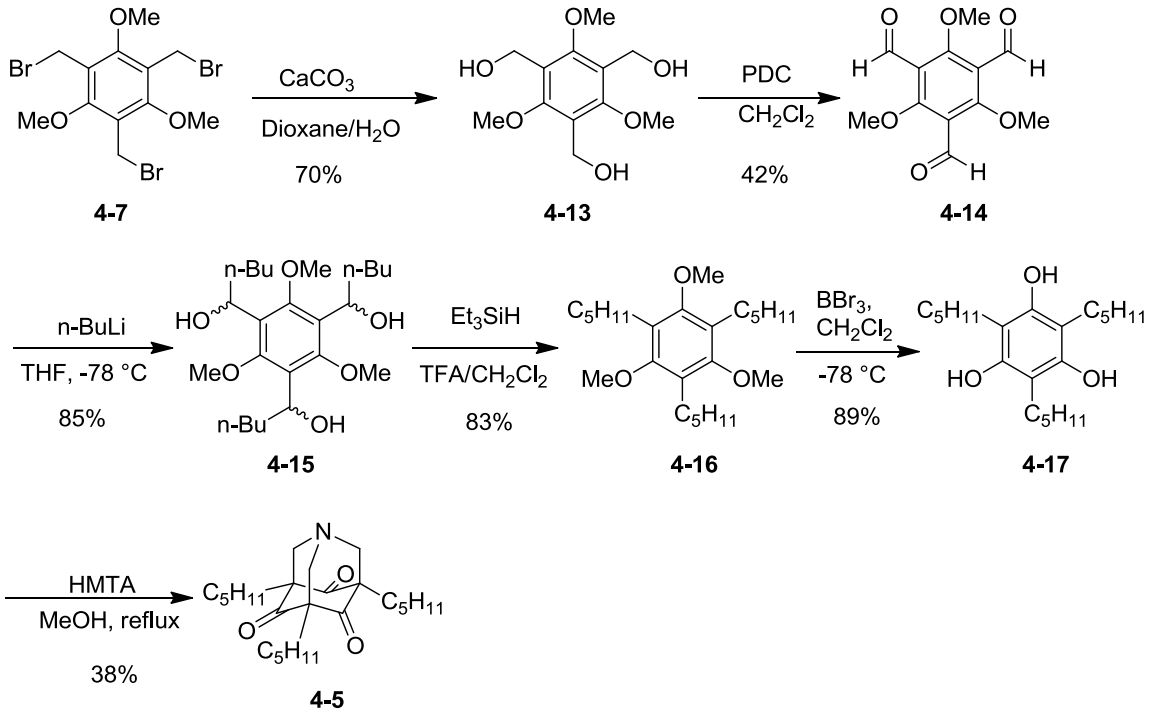

Figure 4-10. Synthesis of alkyl-substituted AAT **4-5**.

Analysis and Discussion of TBIs in AAT and AAD

X-ray Crystal Structure Analysis of AAT 4-3 and AAD 4-6

X-ray crystallography is among the best experimental techniques to reveal the structural consequences (e.g., on bond lengths and angles) of hyperconjugative interactions in donor-σ-acceptor molecules.[174,186,187] Suitable single crystals of ester AAT **4-3** were grown by Lampkins [184] via slow diffusion of pentane to an ethanol solution of **4-3**; this is the first reported crystal structure of an AAT based on a survey of the Cambridge Structural Database (v. 5.28). The asymmetric unit consists of one molecule of **4-3** and two half ethanol molecules, and the structure is disordered with respect to both components. For the AAT, the disorder is localized in the isopropyl side chains, and could be appropriately modeled in the absence of the solvent. The refined monomer structure is shown in Figure 4-11a as an ORTEP plot; additional

crystallographic details (e.g., parameters, bond lengths, and bond angles) are summarized in the next section.

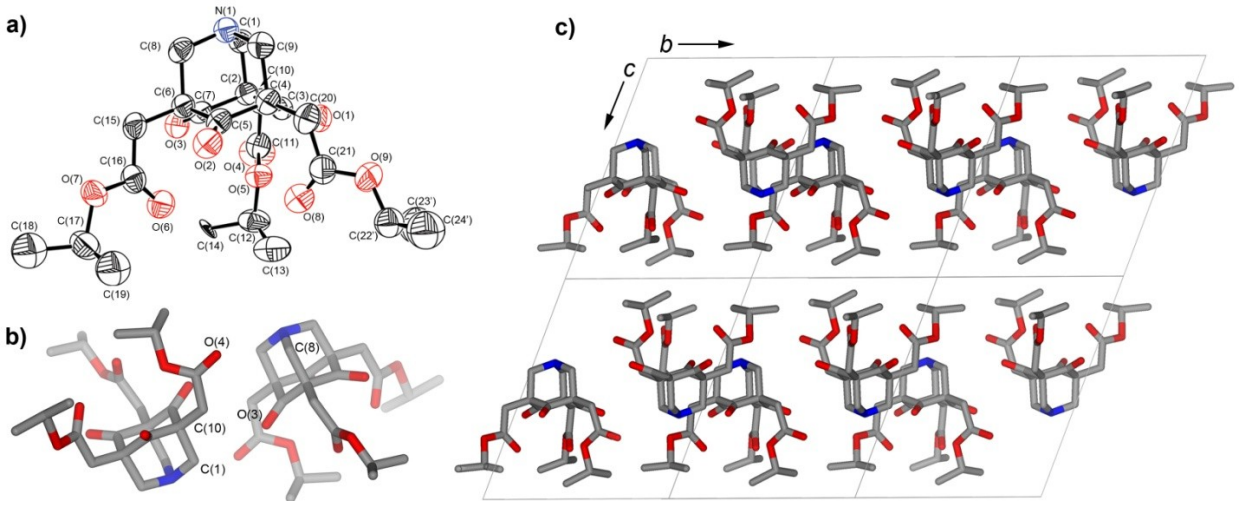

Figure 4-11. The X-ray crystal structure of **4-3**. a) ORTEP plot of monomer structure,where thermal ellipsoids are shown at the 50% probability level (solvent molecules and hydrogen atoms have been removed for clarity). b) Antiparallel alignment of **4-3** within layers that features multiple C–H•••O interactions[109] at the "dimer" interface. c) A packing view (along the *a* axis) showing interaction of the isopropyl side chains at a lipophilic interface.

The packing structure of **4-3** is potentially relevant to the self-assembly of the AATs in solution and worth discussing. Recognizable is an antiparallel alignment of monomers (Figure 4-11c), a consequence presumably of favorable dipolar interactions (the calculated ground state dipole of similar AATs is ~ 4 D);[183] the core-to-core distance is ~ 6.8 Å. Other intermolecular interactions benefit from this arrangement, including multiple C-H···O contacts[109] (C•••O 3.4–3.6 Å) at the interface of the two monomers (e.g. C(10)•••O(3)′, O(4)•••C(8)′). The cores further organize into layers (Figure 4-11d, view along the crystallographic *a* axis), the result of van der Waals interactions between the isopropyl side chains at the discernibly lipophilic interface. The distance between layers in this packing motif is ~ 11.5 Å.

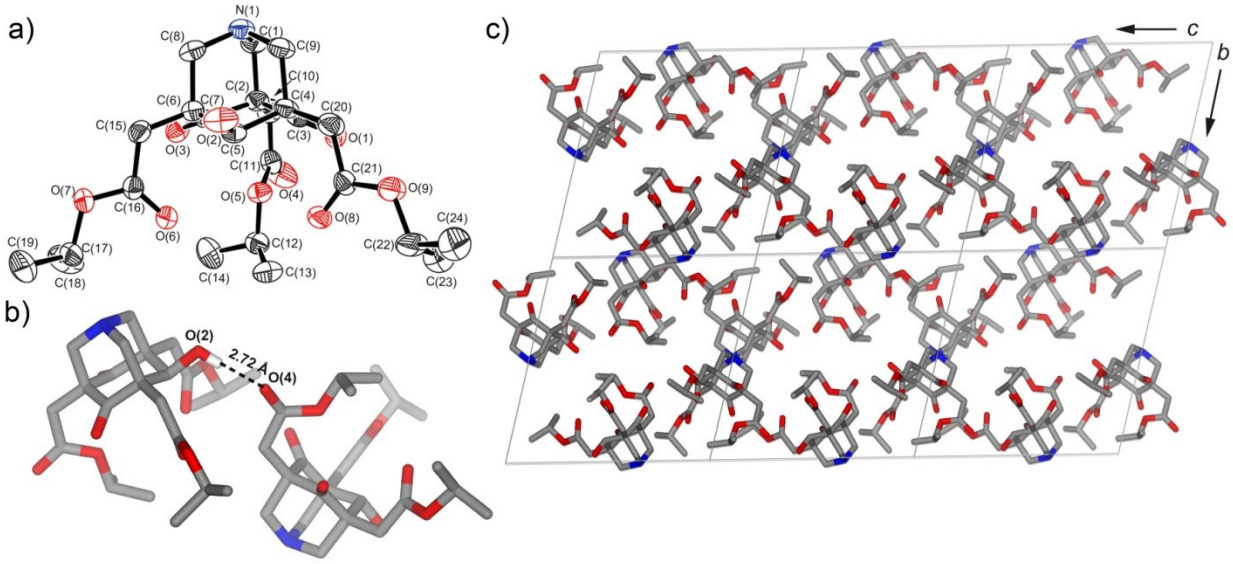

Figure 4-12. The X-ray crystal structure of **4-6**. a) ORTEP plot of monomer structure, where thermal ellipsoids are shown at the 50% probability level (solvent molecules and hydrogen atoms have been removed for clarity). b) Intermolecular hydrogen bonding (indicated by the dashed line) between the alcohol and neighboring ester carbonyl (O(2)•••O(13) = 2.72 Å). c) A packing view (along the *a* axis) showing formation of layers, dominated by side chain interactions

Single crystals of AAD **4-6** could be obtained by evaporating a concentrated methylene chloride solution and the refined monomer structure is shown in Figure 4-12a. The asymmetric unit consists of two molecules of **4-6** (Figure 4-12b), and three of the six isopropyl side chains are disordered (not shown). The alcohol participates in a short hydrogen bond with a neighboring ester carbonyl group (O(2)•••O(13) = 2.72 Å; O(2)–H•••O(13) = 166.7°) in this arrangement. Layers observed by looking along the *a* axis are again dominated by interactions involving the isopropyl side chains (Figure 4-12c).

The ester side chain conformations displayed by the monomers **4-3** and **4-6** in the solid state (Figures 4-11 and 4-12), while certainly influenced by packing of the isopropyl groups, are remarkably similar. The ester C(10)–C(11), C(15)–C(16), and C(20)–C(21) bonds are antiperiplanar to the C_α–C_β bonds (e.g. C(6)–C(8)), and although of "normal" length (average for **4-3** = 1.497 (5) Å; **4-6** = 1.496 (4) Å) (compared with similar isopropyl ester substituents in the

CSD (HEFKOS10 = 1.508 Å; HEFKUY10 = 1.509 Å)), long range TBIs could play a role in stabilizing this conformation. Regardless of the origin, the result for both **4-3** and **4-6** is that three of the ester oxygens are positioned underneath the core with an average O•••O distance of ~ 4.1 Å; whether this space can serve as a binding environment for ions (akin to valinomycin,[188] where O•••O ~ 4.2 Å for the ester carbonyl oxygens) is potentially worth exploring.

Comparative Analysis of Bond Lengths from X-ray Structural Data

Relevant bond lengths and angles for the monomer structures of **4-3** and **4-6** are provided in Table 1 (additional crystallographic data is provided in the Experimental Section); for **4-6**, data for only one of the molecules in the asymmetric unit is provided and discussed since the values for the two are similar. The comparable monomer conformations of **4-3** and **4-6** (Figure 4-11a and Figure 4-12a) indeed encourages this side-by-side comparison. Most striking are the long C_α–C_β bonds (i.e., C(1)–C(2), C(4)–C(9), and C(6)–C(8)) of **4-3**, up to 1.6 Å, that we take a priori as a signature of hyperconjugative interactions. For **4-6**, equivalent elongation is observed only for the C(1)–C(2) bond, the central bond that is flanked by two carbonyl acceptors, highlighting the uniqueness of this arrangement of atoms. Correspondingly, the carbon-carbon bonds for **4-6** that are not within a donor-σ-acceptor framework (e.g., C(4)–C(5), C(5)–C(6)) appear to be of standard length. Further discussion of bond lengths is best done in the context of similarly strained cyclic molecules (below); indeed, the bond angles within **4-3** and **4-6** deviate appreciably from the optimal values (e.g., ∠ C–C–C ≠ 109.5°).

Table 4-1. Selected bond lengths and angles for **4-3** and **4-6**.[a]

Bond	**4-3** [Å]	**4-6** [Å]	Angle	**4-3** [°]	**4-6** [°]
N(1)–C(1)	1.461 (4)	1.442 (4)	C(1)-N(1)-C(8)	110.4 (3)	110.7 (2)
N(1)–C(8)	1.433 (4)	1.463 (4)	C(1)-N(1)-C(9)	110.6 (3)	110.1 (2)
N(1)–C(9)	1.451 (4)	1.456 (4)	C(8)-N(1)-C(9)	111.3 (3)	109.3 (2)
C(1)–C(2)	1.591 (5)	1.591 (4)	N(1)-C(1)-C(2)	111.4 (3)	112.3 (2)

Table 4-1. (continued)

C(4)–C(9)	1.593 (5)	1.560 (4)	N(1)-C(8)-C(6)	111.5 (2)	111.7 (2)
C(6)–C(8)	1.598 (5)	1.565 (3)	N(1)-C(9)-C(4)	111.4 (3)	112.5 (2)
C(2)–C(3)	1.506 (5)	1.520 (4)	C(1)-C(2)-C(3)	103.8 (3)	104.0 (2)
C(3)–C(4)	1.516 (5)	1.505 (4)	C(1)-C(2)-C(7)	103.3 (2)	102.3 (2)
C(4)–C(5)	1.515 (5)	1.543 (4)	C(5)-C(6)-C(8)	103.9 (3)	107.8 (2)
C(5)–C(6)	1.514 (5)	1.540 (4)	C(7)-C(6)-C(8)	103.4 (2)	103.5 (2)
C(6)–C(7)	1.509 (5)	1.508 (4)	C(3)-C(4)-C(9)	103.7 (3)	105.0 (2)
C(2)–C(7)	1.513 (5)	1.517 (4)	C(5)-C(4)-C(9)	103.5 (3)	108.0 (2)
O(1)–C(3)	1.215 (4)	1.213 (3)	C(3)-C(4)-C(5)	111.9 (3)	109.5 (2)
O(2)–C(5)	1.214 (4)	1.426 (3)	C(5)-C(6)-C(7)	112.4 (2)	111.7 (2)
O(3)–C(7)	1.224 (4)	1.214 (3)	C(7)-C(2)-C(3)	112.1 (3)	112.2 (2)
			C(4)-C(5)-C(6)	114.1 (3)	110.3 (2)
			C(6)-C(7)-C(2)	114.4 (3)	113.9 (2)
			C(2)-C(3)-C(4)	114.8 (3)	114.2 (2)
			C(2)-C(3)-O(1)	122.8 (3)	122.1 (3)
			C(4)-C(3)-O(1)	121.5 (3)	123.4 (3)
			C(4)-C(5)-O(2)	122.9 (3)	108.4 (2)
			C(6)-C(5)-O(2)	122.1 (3)	108.5 (2)
			C(6)-C(7)-O(3)	122.8 (3)	123.1 (2)
			C(2)-C(7)-O(3)	122.0 (3)	122.1 (2)

[a] Standard deviations are shown in parentheses.

Again, the comparison of molecules **4-3** and **4-6** to simple structural analogues like *N*-methylpiperidone or tropinone (Figure 4-3) is tempting but would ignore any structural changes associated with ring strain. We have chosen instead to discuss and analyze bond lengths (Figure 4-13 and Table 4-2) and angles (Figure 4-13 and Table 4-3) in the context of related aza- and deaza-adamantane crystal structures. Included in Table 4-2 is the average bond length data for **4-3** and **4-6** alongside data for analogous structures available in the literature (the di-(CSD code KOLSIN[189]) and mono-(OCAYEW[190]) ketones **4-18** and **4-19**, respectively) and a saturated aza-adamantane **4-20** (EJIQUJ[191]). Also shown are average bond lengths for three adamantanediones (DESVIG (**4-21**),[192] LIXFIH (**4-22**),[193] and LIXFUT (**4-23**)[193]), a selected adamantanone

(FITPED (**4-24**)[194]), and variously substituted adamantanes (**AD**). A simplified bond labeling scheme (Figure 4-13) has been adopted to facilitate the comparison; the letters are kept consistent between structures based on the atom bonding sequence. For example, path *a*-*b*-*c*-*d* uniquely describes the donor-σ-acceptor pathway where central bond *b* is flanked by two carbonyl acceptors.

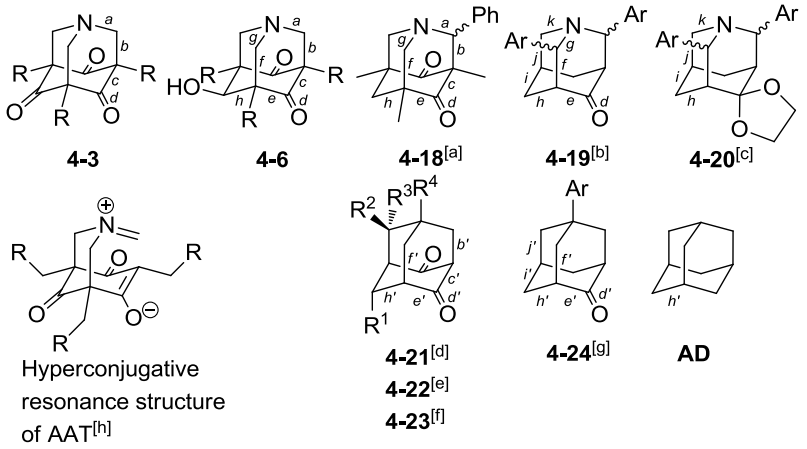

Figure 4-13. Atom labeling scheme for the bond length data presented in Table 4-2. R = CH_2CO_2iPr, R^1–R^4 = various substituents, Ph = phenyl, Ar = *p*-nitrophenyl (**4-19**) or *p*-chlorophenyl (**4-20**), AD = various adamantanes. CSD code and references: [a] KOLSIN[189]; [b] OCAYEW; [190] [c] EJIQUJ;[191] [d] DESVIG;[192] [e] LIXFIH;[193] [f] LIXFUT;[193] [g] FITPED.[194] [h] Hyperconjugative resonance structure of AAT.

The analysis reveals somewhat shortened C–N bonds *a* (1.45 Å) versus *k* (1.48 Å), and a considerably elongated C–C bond *b* (1.59 Å) versus *f* (1.55 Å), *j* (1.53 Å), *f′* (1.54 Å), or *j′* (1.53 Å). There is therefore some hint of the bond length alternation that is a classically predicted consequence of hyperconjugation, visualized, if even crudely, by the resonance structure shown in Figure 4-13. The bond alternation trend does not extend to bonds *c* (1.52 Å versus *e*, *c′*, and *e′* that are all 1.51 Å) or *d* (including *d′*, all C=O bonds are 1.21–1.22 Å). Comparison of bonds *b′*, *f′*, *h′*, and *j′* (1.53–1.55 Å) reveals only a modest sensitivity to inherent structural changes (and strain) within the deaza-adamantanes; this further implicates donor–acceptor effects in the elongation of bond *b*.

Table 4-2. Comparison of average bond lengths[a] [Å] from the X-ray crystal structures of **4-3**, **4-6**, and related tricyclic molecules from Figure 4-13.

Bond[b]	**4-3**[c]	**4-6**[d]	**4-18**[e]	**4-19**[f]	**4-20**[g]	**4-21**[h], **4-22**[i], 4-**23**[j]	**4-24**[k]	AD[l]
a	1.45	1.44	1.46	–	–	–	–	–
b, b′	1.59	1.59	1.59	–	–	1.55	–	–
c, c′	1.51	1.52	1.53	–	–	1.51	–	–
d, d′	1.22	1.21	1.21	1.21	–	1.22	1.21	–
e, e′	–	1.51	1.50	1.51	–	1.50	1.51	–
f, f′	–	1.56	1.54	1.55	–	1.54	1.54	–
g	–	1.46	1.46	1.48	–	–	–	–
h, h′	–	1.54	1.53	1.53	1.53	1.54	1.54	1.54
i, i′	–	–	–	1.54	1.53	–	1.53	–
j, j′	–	–	–	1.53	1.53	–	1.53	–
k	–	–	–	1.47	1.49	–	–	–

[a] The bond lengths for chemically equivalent bonds within each molecule have been averaged. [b] As specified in Figure 4-13. Crystallographic details including CSD codes and references: [c] **4-3**: T = 173 K. [d] **4-6**: T = 173 K. [e] **4-18** (KOLSIN[189]): T = 295 K. [f] **4-19** (OCAYEW[190]): *T* = 293 K. [g] **4-20** (EJIQUJ[191]): T = 291 K. [h] **4-21** (DESVIG[192]): T = 295 K. [i] **4-22** (LIXFIH[193]): *T* = 295 K. [j] **4-23** (LIXFUT[193]): T = 295 K. [k] **4-24** (FITPED[194]): T = 295 K. [l] **AD**: various adamantanes from the CSD.

The bond elongation found for *b* (~ 0.05 Å) is the largest reported for *β*-aminoketones; in work by Verhoeven and coworkers with (admittedly less strained) piperidone and tropinone derivatives (bearing carbonyl groups converted to 1,1-dicyanovinyl functions, better electron acceptors), the C_α–C_β bond elongations are ~ 0.02 Å and taken as fairly definitive evidence for TBIs. Even so, it seems unnecessary, and likely inappropriate,[195] to equate the magnitude of the bond length changes to the "strength" of the TBIs in the molecules; suffice it to say, the consequences of donor–acceptor interactions in these aza-adamantanones are detectable. That pathway *a-b-c-d* emerges as unique (one donor nitrogen communicating with two acceptor carbonyls) is analogous to the "enhanced" through-bond effects noted for the diaza-adamantanones (aza-adamantanone in Figure 4-3, X = N) that feature two donor nitrogens communicating with one acceptor carbonyl.[196]

Comparative Analysis of Bond Angles from X-ray Structural Data

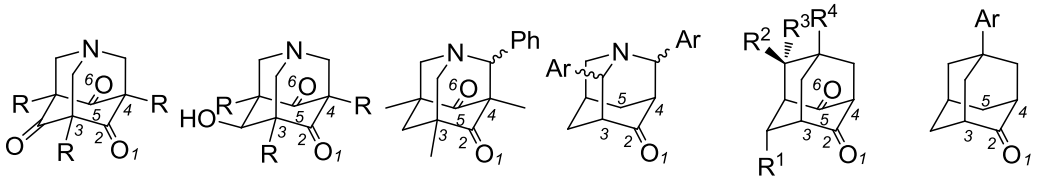

Figure 4-14. Atom labeling scheme for the bond angle data presented in Table 4-3. R = CH_2CO_2iPr, R^1–R^4 = various substituents, Ph = phenyl, Ar = *p*-nitrophenyl (see caption of Figure 4-13 for CSD codes of known structure **4-18**–**4-24**).

Table 4-3. Comparison of average bond angles[a] [°] from the X-ray crystal structures of **4-3**, **4-6**, and related tricyclic molecules from Figure 4-14.

Angle	**4-3**	**4-6**	**4-18**	**4-19**	**4-21**	**4-22, 4-23**	**4-24**
1-2-3		123.4	123.5	124.1	124.9	124.1	123.7
1-2-4	122.3	122.1	121.8	123.2	121.2	122.7	123.9
4-5-6		122.1	121.4	–	121.4	123.1	–
3-2-4	114.4	114.2	114.5	112.7	113.5	112.9	112.3
2-4-5	112.1	112.2	105.8	108.9	105.8	110.5	109.5
$\sum_{CNC}$	332.3	330.1	330.2	329.4	–	–	–

[a] The bond angles for chemically equivalent bonds within each molecule have been averaged.

Comparison of selected bond angles of **4-3** and **4-6** to those of structural analogues (Figure 4-14) is provided in Table 4-3; an arbitrary atom labeling scheme has been adopted for the analysis (Figure 4-14) that should not be confused with the atom labels reported in the crystallographic data files. There are no significant trends that can be identified for the angles that describe the cyclohexane ring that includes atoms 2–5 across the series. The C–C=O angles (e.g. angle 1-2-3) fall within 122–125°, and angle 3-2-4 (C–C(=O)–C) is only slightly larger (~ 1°) for **4-3**, **4-6**, and **4-18** than for the deaza-adamantanones (but certainly larger than **4-20** and **AD**, where it is 109–110°). The greatest variation is found at the bridgehead carbon angle, 2-4-5, although the angle for **4-3** and **4-6** is only 1.7° larger than what is found for deaza-analogues **4-22** and **4-23**. Based on the sum of the bond angles at nitrogen in the aza-adamantane derivatives, structures **4-3** and **4-6** are perhaps slightly flattened, but the sums are not significantly different

from those found for structures **4-18**, **4-19**, or **4-20** ($\sum_{C-N-C}$ = 328° for **4-20**). Without comparing every bond angle for each structure throughout the series, our conclusion is that while **4-3** and **4-6** (and **4-18**) are certainly considerably strained molecules, it is not obvious that their respective bond length changes (in particular elongation of the C_α–C_β bonds) are solely due to this effect.

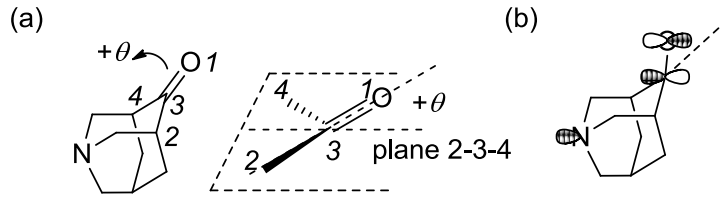

Figure 4-15. (a)Angle θ that quantifies pyramidalization of the carbonyl carbon atoms of **4-3** and **4-6**, calculated as the angle between the carbonyl bond and the mean plane defined by carbon atoms *2*, *3*, and *4*; (b) pyramidalization makes the π-orbitals of the C=O function more parallel with the central C_α–C_β bond.

Further identified from close inspection of the crystal structures of **4-3** and **4-6** is pyramidalization of the carbonyl carbon atoms (labeled 2 in Figure 4-14).[197] Similar distortion has been noted by Verhoeven and coworkers in 1,1-dicyanovinyl-modified piperidone and tropanone derivatives.[174,186,187,198] Figure 4-15a shows one way to report this distortion, namely, as the angle (θ) between the carbonyl vector and the mean plane defined by the three core carbons (*2*, *3*, and *4*). For **4-3**, θ = 8.7° (the average of three carbonyl groups), and for **4-6** θ = 7.3° (average of four carbonyl groups, two from each molecule in the asymmetric unit); the carbonyl group is bent in the axial direction. The largest value reported from Verhoeven's work (recalculated here in the fashion shown in Figure 4-15) is 6.1°. While the pyramidalization could reduce ring strain, that it occurs in such a way ($+\theta$ rather than $-\theta$) to further position the carbonyl π-bond parallel to the C_α–C_β bonds (Figure 4-15b) presumably also optimizes interaction with the nitrogen donor. For **4-21**, that lacks TBIs, θ = –6.7° for one of the two carbonyl groups.

UV-Vis Spectra of AATs and AAD

UV spectroscopy is a routinely used method to diagnose TBIs in β-aminoketones where a new absorption band appears (the lower energy component of a split carbonyl π-π* transition, the so-called σ-coupled transition) to signify communication between the donor and acceptor.[169] The absorption data for AATs and AAD for three solvents is provided in Table 4-4. A new absorption maximum (λ_{max}) is indeed observed in the 260–275 nm window (Figure 4-16). The frequency deviates little neither with solvent polarity—not surprising given the nominal charge-transfer character of these donor-σ-acceptor molecules—nor peripheral substitution. The molar extinction coefficients (ε) are ~ 3,000 M^{-1} cm^{-1} for the AATs **4-3**, **4-4**, and **4-5**; this value decreases commensurately (i.e. by about one third) for AAD **4-6**. An identical trend has been reported in related aza-adamantanones[199] and speaks to the participation of all three acceptor carbonyls to the donor–acceptor system.

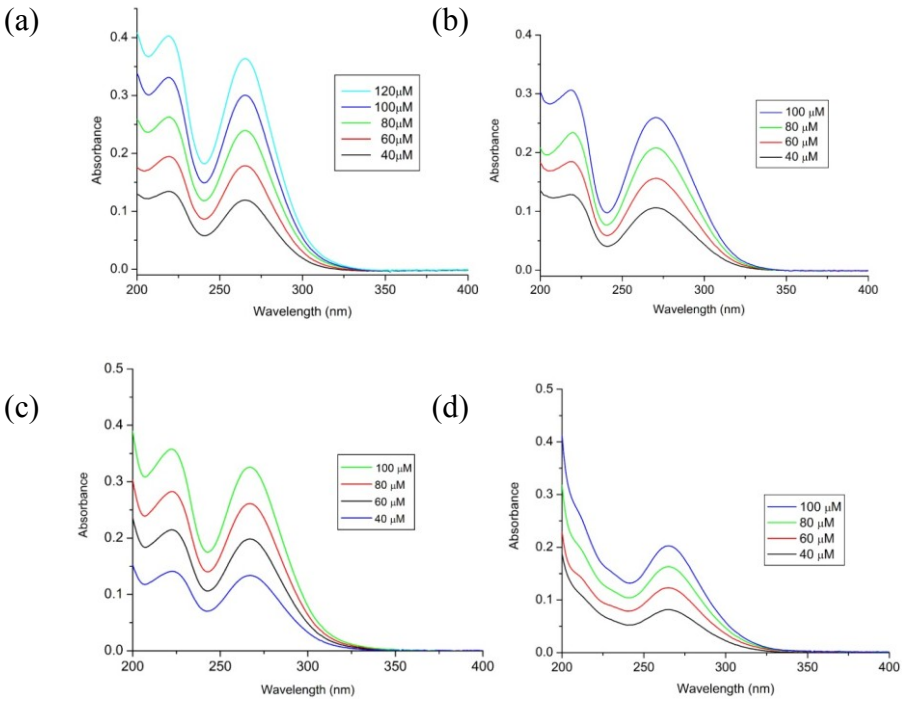

Figure 4-16. UV-Vis spectra of AATs and AAD molecules: **4-3** in ethanol (a) and CH_3CN (b); (c) **4-4** in CH_3CN; (d) **4-6** in CH_3CN.

Interestingly, the σ-coupled transition can be reversibly abolished upon protonation by TFA in acetonitrile (Figure 4-17). Quenching the σ-coupled transition upon addition of TFA is predictable because the origin of the transition, the TBIs, are "turned off" when the electron donor, the lone pair of AAT nitrogen, is not available and cannot interact with the acceptor orbitals.

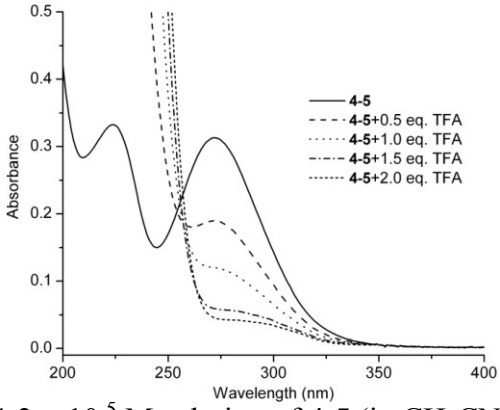

Figure 4-17. Treatment of a 1.2×10^{-5} M solution of **4-5** (in CH_3CN) with TFA results in disappearance of the σ-coupled transition.

Table 4-4. UV absorption data for AATs and AAD in different solvents.

AAT or AAD	λ_{max} [nm]	ε [M^{-1} cm^{-1}]	λ_{max} [nm]	ε [M^{-1} cm^{-1}]	λ_{max} [nm]	ε [M^{-1} cm^{-1}]
	cyclohexane		acetonitrile		ethanol	
4-3	270	2600	263	3230	265	3010
4-4	–	–	265	2040	263	1910
4-5	–	–	267	3270	267	2980
4-6	271	3060	273	2860	275	3270

IR and NMR spectroscopic evidence for TBI

IR and ^{13}C NMR data have seldom been used to report on donor-σ-acceptor interactions and in our estimation interpretation of these data warrants some caution. Notwithstanding the obvious complications of solvation (and experimental conditions in general), differences identified from single point comparison are difficult to attribute to any one particular phenomenon, although this is often done. Additional complication enters when considering IR data for the aza- and deaza-adamantanones bearing two or more ketones in a 1,3-relationship that

display Fermi-type coupling, cooperative stretching of carbonyls in the AAT system (noted before[200] although never comprehensively discussed); we have used the average carbonyl stretch for making a quick comparison. The comparative data, including the data for AATs and AAD, is shown in Table 4-5. Across representative adamantanones (Figure 4-18, two monoketones,[201-203] two diones,[204,205] and one trione[206]) identified from the literature, the carbonyl stretching frequency is relatively invariant (average value ~ 1720 cm^{-1}). A similar consistency is observed for a series of representative aza-adamantanones (including **4-3**–**4-6**),[163,202,203] although the analysis reveals a ~ 5–20 cm^{-1} shift to lower wavenumber for these donor-σ-acceptor molecules. In some previously reported cases the carbonyl stretch has been restored to higher frequency upon protonation or methylation at nitrogen,[203,207] although these experiments have not generally considered structural changes associated with the chemical transformations. The average shift to lower energy is consistent with predictions based on through-bond donor–acceptor interactions that would weaken the carbonyl bond.

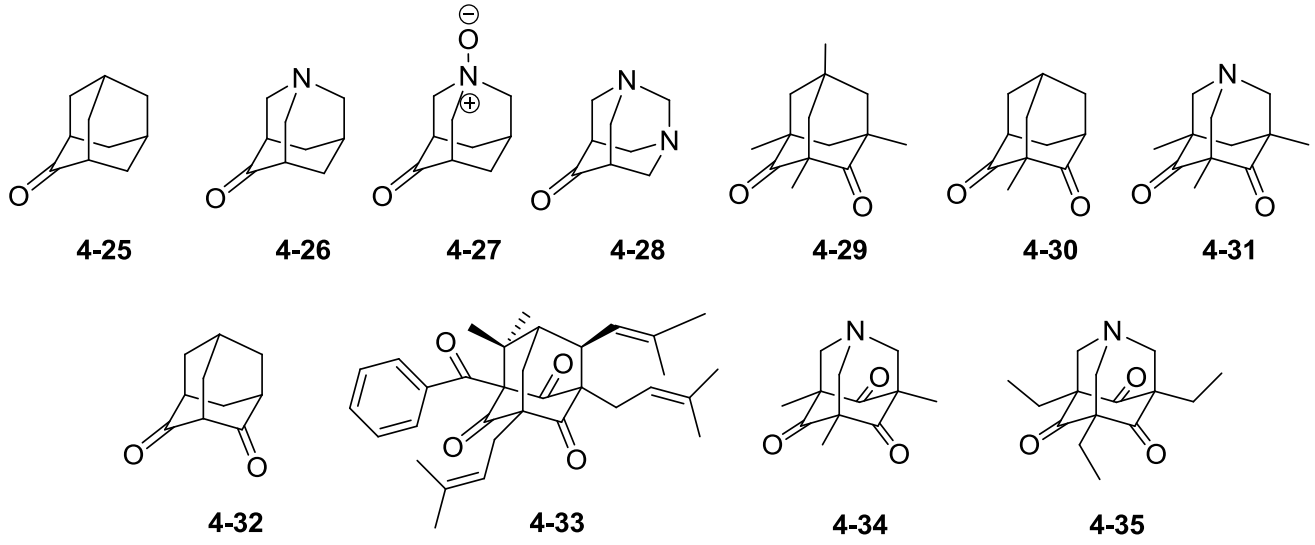

Figure 4-18. Selected molecules for IR and NMR comparison with **4-3**–**4-6**.

Table 4-5. Carbonyl IR frequency [cm^{-1}] for **4-3**–**4-6** and reported molecules shown in Figure 4-18.

4-25[a]	**4-26**[a]	**4-27**[a]	**4-28**[a]	**4-29**[b]	**4-30**[b]	**4-31**[a]	**4-4**[a]	**4-33**[c]	**4-34**[a]	**4-3**[a]	**4-5**[a]	**4-6**[a]
1720[d]	1700[d]	1729[e]	1670[d]	1733, 1704[f]	1738, 1708[g]	1720, 1685[h]	1726, 1697	1742, 1703, 1699, 1685[i]	1736, 1688[j]	1731, 1700	1732, 1693	1733, 1692

[a] KBr. [b] CCl_4 solution. [c] film. [d] Ref. [208]. [e] Ref. [209]. [f] Ref. [210]. [g] Ref. [211]. [h] Ref. [212]. [i] Includes the phenyl ketone stretch: Ref. [213]. [j] Ref. [214].

A similar treatment of the ^{13}C NMR data for adamantanones and aza-adamantanones reveals, for both series, that the carbonyl resonance shifts upfield as the number of carbonyl groups increases (the complete comparative data, including that of **4-3**–**4-6**, is shown in Table 4-6). Such a subtle effect does not emerge from the X-ray crystallography data. For example, $\delta_{C=O}$ shifts from ~ 218 ppm for adamantanones (in $CDCl_3$),[171,201] to ~ 208 ppm for adamantanediones,[215] to ~ 202 ppm for adamantanetriones.[206] The aza-adamantanones (including diones and triones) are on-average upfield shifted (~ 3–5 ppm) from these values. From monoketone, to dione, to trione the values are ~ 214 ppm,[171] 202 ppm (for **4-4**), and 197–200 ppm, respectively. This trend is again consistent with the hyperconjugative interactions depicted in Figure 4-2, but such an analysis remains admittedly oversimplified.

Table 4-6. Carbonyl ^{13}C NMR chemical shift [ppm] in $CDCl_3$ for **4-3**–**4-6** and reported molecules shown in Figure 4-18.

4-25	**4-26**	**4-32**	**4-31**	**4-4**	**4-33**	**4-35**	**4-3**	**4-5**	**4-6**
218.7[a]	214.0[d],[e]	207.6[f]	206.6[g]	201.7	203.3, 202.2, 201.8[h]	200.3[i]	197.2	200.1	200.5
217.9[b]									
217.8[c]									

[a] Ref. [216]. [b] Ref. [217]. [c] Ref. [218]. [d] Ref. [208]. [e] Ref. [218]. [f] Ref. [219]. [g] Ref. [212]. [h] Ref. [213]. [i] Ref. [214].

Conclusion

A combination of experimental techniques and comparative analysis has shown that the through-bond donor–acceptor interactions in appropriately functionalized β-aminoketones can be

particularly assessable. For the 1-aza-adamantanones, molecules whose donor and acceptor orientation is permanently optimized, some of the hallmark consequences of through-bond communication emerge. These include elongation of the central C–C bond in the donor-σ-acceptor pathway (to ~ 1.6 Å), the presence of a new absorption band in the molecules' UV/Vis spectra, and IR/^{13}C NMR spectroscopic shift trends (versus similarly strained molecules that lack either the donor or acceptor groups) consistent with theoretical expectations.

We previously showed that molecules like **4-1** and **4-2** self-assemble in solution and that the emergent macromolecular properties respond to molecular-level changes that also influence the TBIs. The current molecular-level analysis that finds pronounced structural and spectroscopic consequences for traditionally weak effects suggests that D-σ-A motifs have been largely overlooked on the supramolecular scale where similarly modest interactions are often amplified. Left now is to introduce these D-σ-A arrangements into macromolecules, where even the simplest motifs could offer ways to tune bulk properties not available to more traditional weak interactions.

Experimental Section

Synthesis

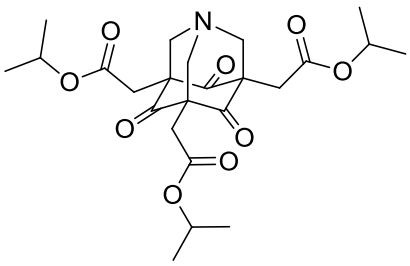

2,5,7-Tris-(2-isopropoxycarbonylmethyl)-1-aza-adamantane-4,6,10-trione (4-3). To a solution of **2-6** (0.820 g, 1.93 mmol) in isopropanol (15 mL) was added HMTA (0.270 g, 1.93 mmol) and the reaction mixture was heated to reflux for 20 h. After cooling to room temperature, all volatiles were removed under reduced pressure. The residue was purified by

column chromatography (3:2 hexanes/EtOAc) to afford **4-3** (0.61 g, 66%) of a colorless solid: m.p. 111–112 °C. ^{1}H NMR ($CDCl_3$) δ 1.22 (d, J = 6.0 Hz, 18H), 2.73 (s, 6H), 3.76 (s, 6H), 4.99 (hp, J = 6.0 Hz, 3H). ^{13}C NMR ($CDCl_3$) δ 21.6, 32.0, 68.2, 70.3, 70.8, 169.0, 197.2. IR (KBr): $\tilde{\nu}$ = 2984, 2924, 2853, 1731, 1700, 1191, 1109, 798 cm^{-1}; UV/Vis (ethanol): λ_{max} (ε) = 265 nm (3010); HRMS (EI) calcd for $C_{24}H_{33}NO_9$ $(M)^+$ 479.2155, found 479.2159.

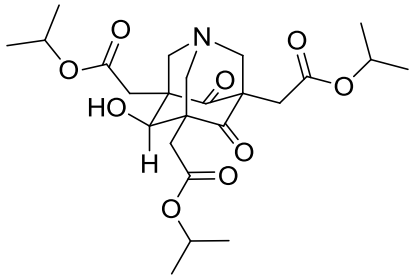

2,5,7-Tris-(2-isopropoxycarbonylmethyl)-10-*exo*-hydroxy-1-aza-adamantane-4,6-dione (4-6). AAT ester **4-3** (0.180 g, 0.376 mmol) was dissolved in dry THF (15 mL) and cooled to –78 °C under a blanket of argon. To this solution was slowly added Red-Al (0.376 mmol, 0.28 mL, 65 wt % in toluene). The solution temperature was maintained at –78 °C until the starting material was consumed (30 min), and then the reaction was quenched with dilute HCl. The resulting mixture was warmed to room temperature and the solvent was removed in vacuo. The residue was redissolved in EtOAc, washed with water and brine, dried over $MgSO_4$, and concentrated in vacuo. Column chromatography (gradient, 2:1 to 1:1 hexanes/EtOAc) afforded **4-6** (60 mg, 33%) as a white solid. m.p. 139–140 °C; ^{1}H NMR ($CDCl_3$) δ = 1.22 (m, 18H), 2.48 (d, J = 15.9 Hz, 2H), 2.56 (d, J = 15.9, 2H), 2.62 (s, 2H), 2.98 (d, J = 12.6 Hz, 2H), 3.54 (s, 2H), 3.53 (s, 1H), 3.80 (d, J = 12.9 Hz, 2H), 4.52 (s, 1H), 4.98 ppm (m, 3H); ^{13}C NMR ($CDCl_3$) δ 21.6, 21.7, 31.7, 34.6, 54.8, 59.2, 68.0, 68.3, 68.7, 69.9, 71.1, 169.7, 170.9, 201.7 ppm; IR (KBr): $\tilde{\nu}$ = 3467, 2981, 2936, 2877, 1726, 1697, 1374, 1195, 1109, 823 cm^{-1}; UV/Vis

(ethanol): λ_{max} (ε) = 263 nm (1910); MS (EI) calcd for $C_{24}H_{35}NO_9$ $(M)^+$: 481.2312, found 481.2298.

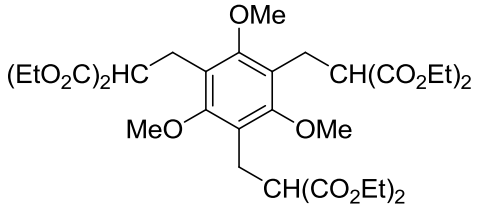

3-[3,5-Di-(2,2-diethoxycarbonylethyl)-2,4,6-trimethoxyphenyl]-2-ethoxycarbonyl-propionic acid ethyl ester (4-8). A suspension of NaH (60% in mineral oil, 0.157 g, 3.92 mmol) and dry THF (15 mL) in a dry flask was cooled to 0 ºC and diethyl malonate (0.591 g, 3.69 mmol) was slowly added. The reaction was allowed to warm to rt and stir for 1 h to facilitate anion formation. Then, **4-7** (0.500 g, 1.12 mmol), dissolved in a small amount of dry THF, was added dropwise to the stirring solution and the resulting solution was stirred for 12 h. The solvent was then removed in vacuo and the remaining oily residue was taken up into water (30 mL) and ether (30 mL) and acidified with 10% aqueous HCl. The organic phase was separated and the aqueous layer was extracted with ether (2 × 20 mL). The combined ethereal layers were dried over $MgSO_4$ and concentrated to dryness to afford a crude colorless oil. Purification by flash chromatography using hexanes/ethyl acetate (2:1) afforded **4-8** (0.712 g, 93%) as a colorless oil: ^{1}H NMR ($CDCl_3$) δ 1.21 (t, 18H, J = 7.2 Hz), 3.20 (d, 6H, J = 7.2 Hz), 3.69 (s, 9H), 3.76 (t, 3H, J = 7.2 Hz), 4.15 (m, 12H). ^{13}C NMR ($CDCl_3$) δ 13.9, 23.9, 51.5, 61.2, 61.2, 121.4, 157.8, 169.4. HRMS (ESI) calcd for $C_{33}H_{48}O_{15}Na$ $(M + Na)^+$ 707.2885, found 707.2856.

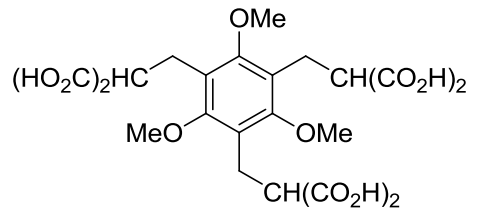

3-[3,5-Di-(2,2-dicarboxyethyl)-2,4,6-trimethoxyphenyl]-2-carboxy-propionic acid (4-9). A mixture of **4-8** (0.300 g, 4.39 mmol), NaOH (0.400 g, 10.0 mmol), and absolute EtOH (10 mL) was heated reflux, open to the atmosphere, for 12 h. After cooling to room temperature., the reaction mixture was diluted with EtOH (5 mL) and allowed to stir for 4 h. Acetonitrile (30 mL) was then added to the mixture until a white solid completely precipitated. This precipitate was isolated by suction filtration and was dissolved in a minimum amount of water (5 mL). The aqueous solution was acidified with 3.5 M HCl and extracted with warm ethyl acetate (3 × 25 mL). The organic extracts were combined, dried over $MgSO_4$, and concentrated to dryness to afford **4-9** (0.206 g, 91%) as a white solid: m.p.182–184 ºC; ^{1}H NMR (DMSO-d_6) δ 3.07 (d, 6H, J = 6.9 Hz), 3.57 (t, 3H, J = 6.9 Hz), 3.61 (s, 9H), 12.64 (s, 3H). ^{13}C NMR (DMSO-d_6) δ 23.6, 51.3, 60.6, 121.4, 157.1, 170.7. HRMS (ESI) calcd for $C_{21}H_{24}O_{15}Na$ $(M + Na)^+$ 539.1007, found 539.1029.

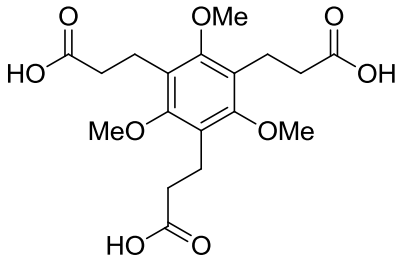

3-[3,5-Di-(2-carboxyethyl)-2,4,6-trimethoxyphenyl]-propionic acid (4-10). A solution of **4-9** (0.155 g, 0.300 mmol) and diphenyl ether (10 mL) was heated to 180 ºC, open to the atmosphere, for 4 h. After cooling to room temperature, it was diluted with chloroform (5 mL) and extracted with 0.5 M NaOH (3 × 15 mL). The aqueous extracts were combined, washed with toluene, acidified to pH = 2 with conc. HCl, and extracted with EtOAc (3 × 30 mL). The organic extracts were combined, dried over $MgSO_4$, and concentrated under reduced pressure to afford **4-**

10 (0.106 g, 92%) as a white solid: m.p. 156–157 ºC; ^{1}H NMR (DMSO-d_6) δ 2.41 (t, 6H, J = 8.7 Hz), 2.76 (t, 6H, J = 8.7 Hz), 3.67 (s, 9H), 12.18 (bs, 3H). ^{13}C NMR (DMSO-d_6) δ 20.0, 34.8, 61.3, 123.5, 156.3, 174.0. HRMS (ESI) calcd for $C_{18}H_{24}O_9Na$ $(M + Na)^+$ 407.1313, found 407.1306.

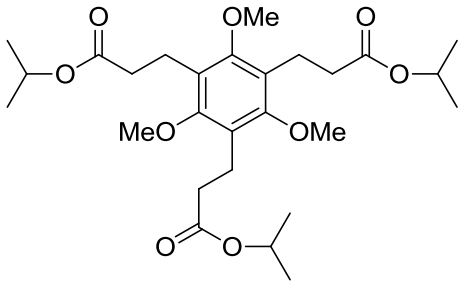

3-[3,5-Bis-(2-isopropoxycarbonyl-ethyl)-2,4,6-trimethoxy-phenyl]-propionic acid isopropyl ester (4-11). To a solution of **4-10** (2.00 g, 5.21 mmol) in isopropanol (50 mL) was added *p*-toluenesulfonic acid monohydrate (2.23 g, 11.7 mmol) and the reaction mixture was heated to reflux for 12 h, under an argon atmosphere. All volatiles were then removed under reduced pressure and the remaining residue was taken up in EtOAc (100 mL) and washed with 0.5 M NaOH (20 mL), water (20 mL), and brine (20 mL). The remaining organic layer was dried over $MgSO_4$, and evaporated in vacuo, and purified by column chromatography (6:1 hexanes/EtOAc) to afford **4-11** (2.38 g, 90%) as a colorless oil: ^{1}H NMR ($CDCl_3$) δ 1.23 (d, J = 6.3 Hz, 18H), 2.54 (t, J = 8.7 Hz, 6H), 2.90 (t, J = 8.7 Hz, 6H), 3.74 (s, 9H), 5.02 (hp, J = 6.3 Hz, 3H). ^{13}C NMR ($CDCl_3$) δ 20.3, 21.9, 34.8, 61.6, 67.5, 123.7, 156.8, 172.9. HRMS (ESI) calcd for $C_{27}H_{42}O_9Na$ $(M + Na)^+$ 533.2721, found 533.2723.

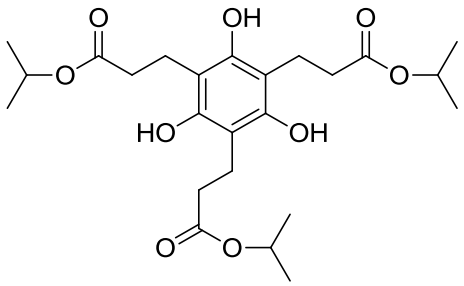

3-[2,4,6-Trihydroxy-3,5-bis-(2-isopropoxycarbonyl-ethyl)-phenyl]-propionic acid isopropyl ester (4-12). To a solution of **4-11** (0.56 g, 1.1 mmol) in dry methylene chloride (25 mL) stirring at –78 ºC was added BBr_3 (0.62 mL, 6.5 mmol). The reaction was allowed to stir, under argon, at that temperature for 2 h before gradually allowing it to warm to –30 ºC, where it was remained for 90 min. The reaction was then quenched via careful addition of sat. aq. $NaHCO_3$ and extracted with methylene chloride (3 × 100 mL). The organic extracts were combined, dried over $MgSO_4$, and evaporated in vacuo to afford a crude oil. This material was then purified via flash chromatography (4:1 hexanes /EtOAc) to afford **4-12** (0.447 g, 87%) as a colorless solid: m.p. 118–120 ºC; ^{1}H NMR ($CDCl_3$) δ 1.21 (d, J = 6.0 Hz, 18H), 2.72 (t, J = 6.0 Hz, 6H), 2.84 (t, J = 6.0 Hz, 6H), 4.99 (hp, J = 6.0 Hz, 3H), 8.27 (s, 3H). ^{13}C NMR ($CDCl_3$) δ 18.4, 21.7, 34.5, 69.0, 108.6, 152.8, 177.3. HRMS (ESI) calcd for $C_{24}H_{36}O_9Na$ $(M + Na)^+$ 491.2252, found 491.2252.

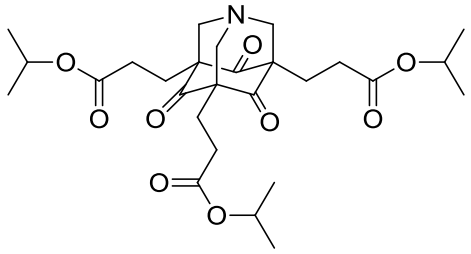

3-[5,7-Bis-(2-isopropoxycarbonyl-ethyl)-4,6,10-trioxo-1-aza-tricyclo[3.3.1.1]dec-3-yl]-propionic acid isopropyl ester (**4-4**). To a solution of **4-12** (0.88 g, 1.9 mmol) in dry isopropanol (10 mL) was added HMTA (0.29 g, 2.0 mmol) and the reaction mixture was heated to reflux for 72 h under argon. The solvent was then removed in vacuo and the residue taken up in EtOAc (50 mL). The organic layer was sequentially washed with 0.5 M NaOH (10 mL), 0.5 M HCl (10 mL), water (10 mL), and brine (10 mL). The remaining organic layer was dried over $MgSO_4$ and evaporated in vacuo to a crude solid which was purified via flash chromatography

(1:1 hexanes/EtOAc; R_f = 0.55) to afford **4-4** (0.47 g, 47%) as a flaky, colorless solid: m.p. 169–170 ºC; ^{1}H NMR ($CDCl_3$) δ 1.22 (d, J = 6.3 Hz, 18H), 2.03 (t, J = 8.4 Hz, 6H), 2.47 (t, J = 8.4 Hz, 6H), 3.39 (s, 6H), 4.99 (hp, J = 6.3 Hz, 3H). ^{13}C NMR ($CDCl_3$) δ 21.8, 22.3, 28.7, 67.7, 71.5, 72.8, 172.8, 200.1. HRMS (EI) calcd for $C_{27}H_{39}NO_9$ $(M)^+$ 521.2625, found 521.2623. UV/Vis (acetonitrile): λ_{max} (ε) = 267 nm (3270 mol^{-1} dm^3 cm^{-1}), (ethanol): λ_{max} (ε) = 267 nm (2980 mol^{-1} dm^3 cm^{-1}); IR (KBr): $\tilde{\nu}$ = 2980, 2924, 2852, 1732, 1693, 1192, 1109, 811 cm^{-1}.

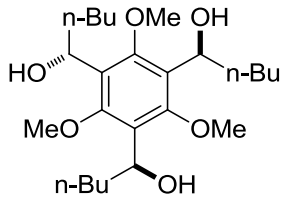

(*anti,syn*)- and **(*syn,syn*)-1,1',1''-(2,4,6-Trimethoxybenzene-1,3,5-triyl)tripentan-1-ol** (*anti,syn*- and *syn,syn*-**4-15**)**.** To a stirring solution of **4-14**[220] (1.13 g, 4.48 mmol, dissolved in 50 mL dry THF) at –78 °C under a blanket of argon, was slowly added a solution of *n*-butyllithium (1.6 M in hexane, 27 mmol). The resulting mixture was maintained at –78 °C for 2 h, and then allowed to gradually warm to room temperature. After being stirred at rt for 0.5 h, the reaction mixture was quenched by dropwise addition of dilute HCl, and extracted with EtOAc. The combined organic extracts were dried over $MgSO_4$, filtered, and concentrated to a crude residue, which was purified via flash column chromatography (1:1 EtOAc/hexanes) to afford *anti,syn*-**4-15** (0.95 g, 50%) as a yellowish oil, and *syn,syn*-**4-15** (0.46 g, 24%) as a yellow oil. *anti,syn*-**4-15**: ^{1}H NMR ($CDCl_3$) δ 0.87 (t, 9H, J = 6.9Hz), 1.14 – 1.48 (m, 12H), 1.76 (m, 3H), 1.96 (m, 3H), 3.20 (br, 3H), 3.86, 3.87 (two singlets, 9H combined), 4.88 (m, 3H). ^{13}C NMR ($CDCl_3$) δ 14.0, 22.5, 28.8, 28.9, 37.7, 38.4, 63.8, 64.0, 68.9, 127.3, 157.2, 157.7. HRMS (CI) calcd for $C_{24}H_{42}O_6Na$ $(M + Na)^+$ 449.2874, found 449.2919. *syn,syn*-**4-15**: ^{1}H NMR ($CDCl_3$) δ 0.89 (t, 9H, J = 6.9 Hz), 1.33 (m, 12H), 1.79 (m, 3H), 1.98 (m, 3H), 3.15 (br, 3H), 3.86, 3.88 (two

singlets, 9H combined), 4.92 (m, 3H). ^{13}C NMR ($CDCl_3$) δ 14.0, 22.6, 29.1, 37.5, 64.1, 68.5, 127.6, 157.4. HRMS (CI) calcd for $C_{24}H_{42}O_6Na$ $(M + Na)^+$ 449.2874, found 449.2919.

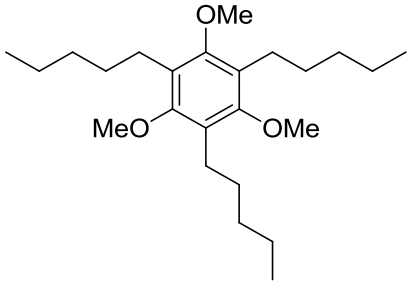

1,3,5-Tripentyl-2,4,6-trimethoxybenzene (4-16). To the solution of compound **4-15** as a mixture of *anti*,*syn* and *syn*,*syn* isomers (1.56 g, 3.66 mmol) in dry CH_2Cl_2 (40 mL), were added trifluoroacetic acid (5.00 g, 43.9 mmol) and triethylsilane (10.2 g, 87.9 mmol) at rt. The resulting solution was allowed to stir at room temperature for 3 days, and then quenched with saturated aqueous $NaHCO_3$. The organic layer was separated, dried over $MgSO_4$, and concentrated under the vacuum. The residue was purified via flash column chromatography (1:30 EtOAc/hexanes) to afford **4-16** (1.15 g, 83%) as a colorless oil: ^1H NMR ($CDCl_3$) δ 0.95 (m, 9H), 1.39 (m, 12H), 1.58 (m, 6H), 2.57 (m, 6H), 3.79 (s, 9H). ^{13}C NMR ($CDCl_3$) δ 14.1, 22.5, 25.1, 30.5, 32.6, 61.4, 125.6, 156.0. HRMS (DIP-CI-MS) calcd for $C_{24}H_{42}O_3$ $(M)^+$ 378.3134, found 378.3124.

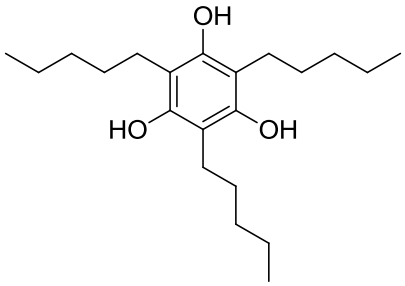

2,4,6-Tripentylbenzene-1,3,5-triol (4-17). To a solution of **4-16** (1.15 g, 3.04 mmol) dissolved in dry CH_2Cl_2 (40 mL) at –78 °C under a blanket of argon, was slowly added BBr_3 (3.05 g, 12.2 mmol). The resulting solution was maintained at –78 °C for 1 h, and then allowed

to gradually warm to room temperature over 3h. The reaction mixture was stirred overnight at rt, then quenched with saturated aqueous $NaHCO_3$, and extracted with CH_2Cl_2. The organic layer was dried over $MgSO_4$, and the solvent was removed in vacuo to provide **4-17** (0.91 g, 89%) as a yellowish oil. ^{1}H NMR ($CDCl_3$) δ 0.91 (t, 9H, J = 6.9 Hz), 1.37 (m, 12H), 1.51 (m 6H), 2.56 (t, 6H, J = 7.8 Hz), 4.64 (s, 3H). ^{13}C NMR ($CDCl_3$) δ14.1, 22.6, 23.7, 29.3, 32.0, 107.0, 150.2. High-resolution mass spectrometry data could not be obtained.

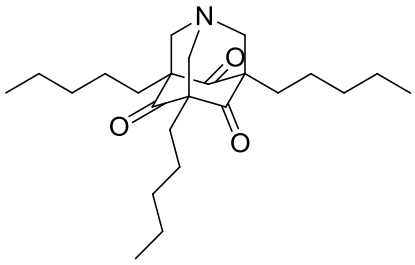

3,5,7-Tripentyl-1-aza-4,6,10-adamantanetrione (4-5). A solution of **4-17** (0.900 g, 2.68 mmol) in methanol (15 mL) was treated with HMTA (0.560 g, 4.02 mmol) and heated to reflux overnight. Some white precipitated formed after the solution was cooled to room temperature. The precipitated solid was collected by filtration and washed with cold methanol to afford **4-5** (0.430 g, 38%) as a white solid. Further purification to remove traces of HMTA is possible by column chromatography (1:1 EtOAc/hexanes): m.p. 181–182 ºC. ^{1}H NMR ($CDCl_3$) δ 0.90 (t, 9H, J = 6.9 Hz), 1.34 (m, 18H), 1.71 (m, 6H), 3.41 (s, 6H). ^{13}C NMR ($CDCl_3$) δ 14.0, 22.4, 23.2, 27.3, 32.7, 71.5, 72.3, 200.5. HRMS (DIP-CI-MS) calcd for $C_{24}H_{40}NO_3$ $(M + H)^+$ 390.3003, found 390.2969. UV/Vis (acetonitrile): λ_{max} (ε) = 273 nm (2860 mol^{-1} dm^3 cm^{-1}), (cyclohexane): λ_{max} (ε) = 271 nm (3060 mol^{-1} dm^3 cm^{-1}), (ethanol): λ_{max} (ε) = 275 nm (3270 mol^{-1} dm^3 cm^{-1}); IR (KBr): $\tilde{\nu}$ = 2950, 2919, 2856, 1733, 1692, 816 cm^{-1}.

X-ray Crystallography

Compound 4-6. Data were collected at 173 K on a Siemens SMART PLATFORM equipped with A CCD area detector and a graphite monochromator utilizing MoK_α radiation (λ

= 0.71073 Å). Cell parameters were refined using up to 8192 reflections. A full sphere of data (1850 frames) was collected using the ω-scan method (0.3° frame width). The first 50 frames were re-measured at the end of data collection to monitor instrument and crystal stability (maximum correction on I was < 1 %). Absorption corrections by integration were applied based on measured indexed crystal faces.

The structure was solved by the Direct Methods in *SHELXTL6,* and refined using full-matrix least squares. The non-H atoms were treated anisotropically, whereas the hydrogen atoms were calculated in ideal positions and were riding on their respective carbon atoms. A total of 628 parameters were refined in the final cycle of refinement using 5600 reflections with $I > 2\sigma(I)$ to yield R_1 and wR_2 of 5.87% and 13.25%, respectively. Refinement was done using F^2.

The toluene molecule were disordered and could not be modeled properly, thus program SQUEEZE, a part of the PLATON package of crystallographic software, was used to calculate the solvent disorder area and remove its contribution to the overall intensity data.

CHAPTER 5
INTRAMOLECULAR H-BONDING IN PHLOROGLUCINOL SCAFFOLDS

Introduction

The hydrogen bond (HB) is one of the most important noncovalent interactions that has been intensively studied and widely utilized in vaious fields of chemistry. In phloroglucinol derivatives, the phloroglucinol core has three phenolic hydroxyl groups that are good H-bond donors for either intra- or intermolecular HBs. Appropriate application of the HBs could impart interesting and useful properties to the phloroglucinol derivatives for use as supramolecular scaffolds. This chapter will discuss seven-membered-ring inramolecular HBs that can be used to control the conformation and shape of phloroglucinol derivatives.

Conformational Control through Intramolecular HBs

Intramolecular H-bonding is a well-known strategy employed by nature to control the conformation of a molecule. The secondary structure of proteins (i.e. the α-helix and β-sheet) features intramolecular HBs, typically between carbonyl oxygen atoms and amide (N-H) hydrogen atoms.[221] Intramolecular HBs have also been used by synthetic chemists. For example, HBs embedded within peptidobiomimetics can control the conformation of biomaterials.[222] Parquette and coworkers[223] have successfully controlled the conformation of dendrimers by using intramolecular HBs (Figure 5-1a). Meijer and coworkers[224] used intramolecular hydrogen bonding to preorganize the conformation of the ureidopyrimidinone monomer for quadruple intermolecular HB formation; the stability of the dimer is greatly enhanced due to this additional stabilizing factor. Similarly, it was reported that 2,6-diaminopurines (DAP)[225] (Figure 5-1b) that feature a preorganized conformation via intramolecular HBs show stable quadruply H-Bonded dimers in solution.

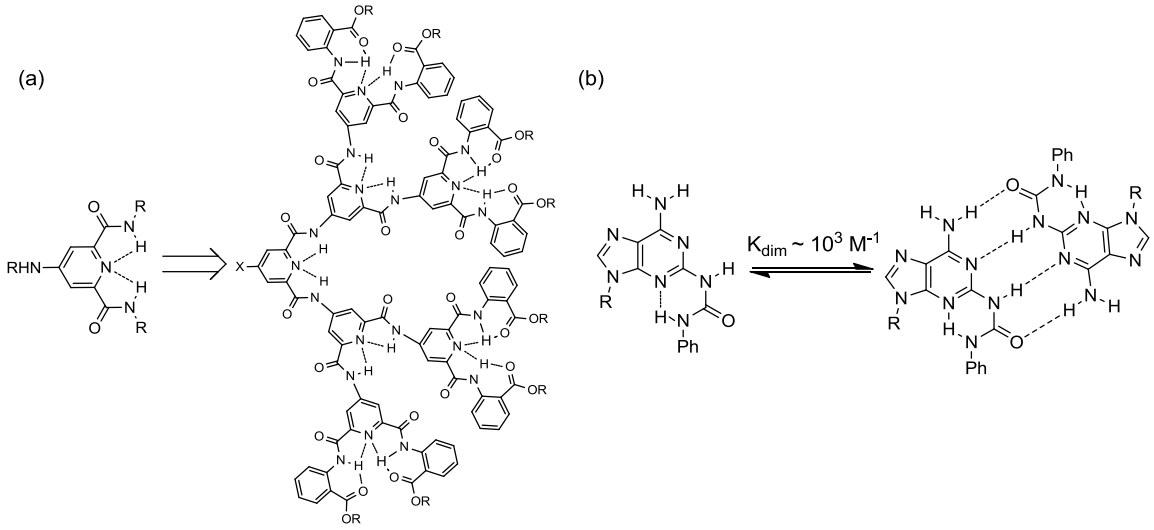

Figure 5-1. (a) Controlled conformation of a dendrimer by intramolecular HBs.[223] (b) Enhanced quadruply H-bonded dimerization of DAPs via a intramolecularly H-bonded, conformation-controlled purine monomer.[225]

Applications of Intramolecular HBs in Supramolecular Chemistry

HBs are among the most useful noncovalent interactions in supramolecular chemistry, and foldamers demonstrate the utility of intramolecular HBs nicely. Foldamers — generally synthetic oligomers that adopt a defined secondary structure stabilized by noncovalent interactions[226] — derive their inspiration from natural self-folding materials (e.g., peptides, nucleic acids, and polysaccharides). Foldamers have potential applications in many areas of supramolecular chemistry, including ion recognition,[227] organogelation,[228] catalysis, etc. One example[228] is shown in Figure 5-2, wherein an arch-shaped foldamer adopts a spring-shaped conformation through multiple intramolecular H-bonds and steric hindrance. Further stacking allows the formation of fibril networks that are capable of immobilizing the organic solvent to form organogels. In another example,[227] oligomers of α-aminoxy acids are reported to form helical structures assisted by intramolecular HBs, and the resultant structures can potentially serve as anion receptors and artificial anion channels.

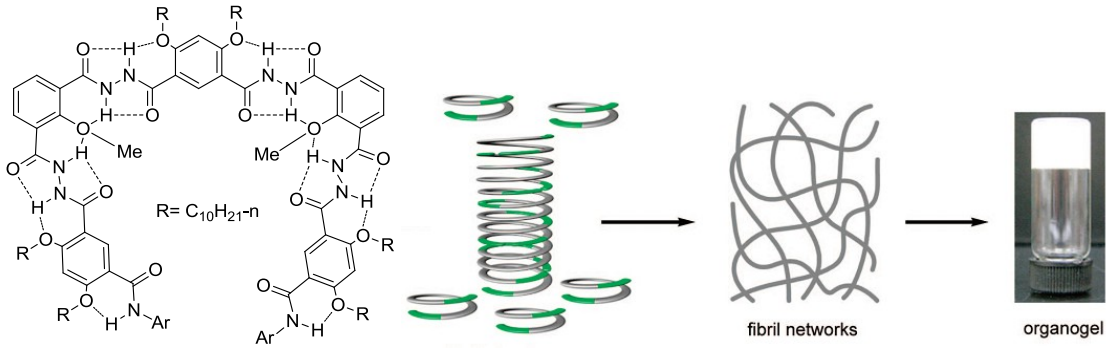

Figure 5-2. Organogel formation from a synthetic foldamer whose oligomer conformation is stabilized by intramolecular H-bonding.[228] Figure reprinted (adapted) with permission from Ref 228. Copyright 2008 American Chemical Society.

Host-guest chemistry is one of the major research areas in the field of supramolecular chemistry. For host molecules, a suitable conformation (i.e. a cavity or a pocket conformation) is critical for recognizing guest molecules; usually intramolecular HBs play important roles for reorganizing the host molecules to adopt an optimal conformation. Calixarenes are one family of extensively studied cavitands that feature multiple intramolecular HBs[229] between their phenolic hydroxyl groups; these interactions help the molecules adopt a cavity-shaped (Figure 5-3a) conformation for molecular recognition.[230]

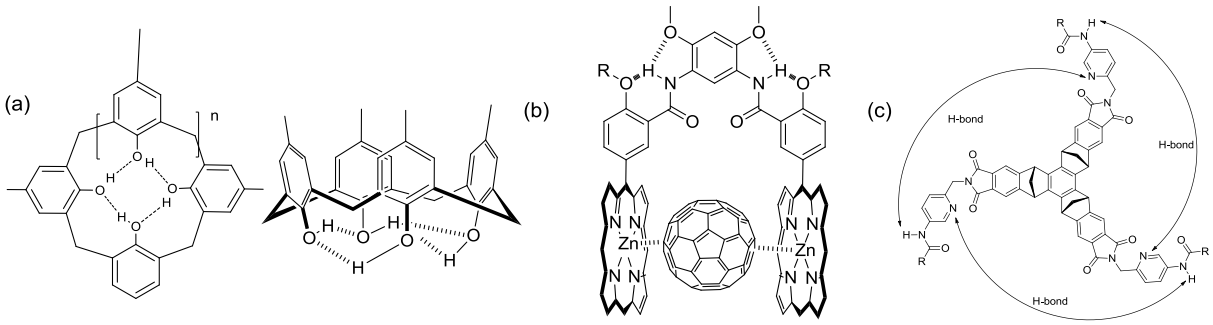

Figure 5-3. Examples of host molecules with preorganized conformations through intramolecular HBs: (a) top (left) and side (right) views of calixarenes; (b) molecular tweezers[225] and (b) molecular baskets[228] featuring intramolecular HBs.

Li and coworkers[231,232] have reported a family of tweezer-shaped molecules that are used to recognize C_{60} and C_{70} molecules. The "tips" of these "tweezers" are zinc-complexed porphyrins that can interact with the guests, and the "root" moiety is driven by intramolecular

HBs to ensure the "tips" are close to "catch" the guests (Figure 5-3b). Recently, Badjić[233,234] reported a C_3-symmetric "molecular basket" that features an aryl ring as the bottom of the "basket", and three side chains that are tethered by three intramolecular HBs between amide NHs and pyridines to form the side walls (Figure 5-3c). Both theoretical[233] and experimental[234] studies have shown that the design creates a good host for small organic molecules.

Conformational control through HBs can also be found in materials science. Valiyaveettil and coworkers[235] reported a series of asymmetrically functionalized amphiphilic conjugated polymers, some of which contain HB donors and acceptors. Intramolecular HBs are employed to promote planarization of the polymer backbone, and to tune the optical properties of the polymers. Significant changes in optical and fluorescence spectra result from the formation or absence of intramolecular HBs, thus indicating the importance of conformational control in tuning the properties of materials (Figure 5-4).

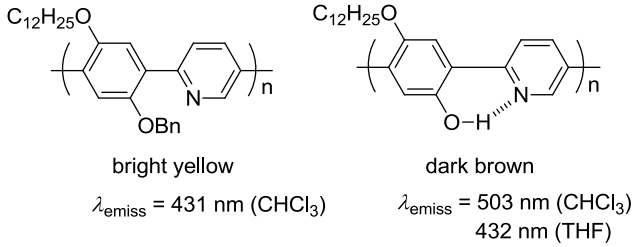

Figure 5-4. Comparison of two conjugated polymers[235] that have different optical properties due to their intramolecular hydrogen bonding capabilities.

Opportunities for the Phloroglucinol Platform

For phloroglucinol, intramolecular HBs between the phenolic OH groups and HB acceptors X (e.g. N, O) in substituents at the 2,4,6-positions (Fig. 5-5) are expected to both control the conformation about the scaffold and create a well-defined shape. A survey of the Cambridge Structural Database (CSD) offers a few examples of such seven-membered ring HBs (Fig. 5-6a, b)[236,237] between phenolic OH groups and appropriate side chains. ^{1}H NMR chemical

shifts for the hydroxyl groups are 10~11 ppm. Seven-membered-HBs involving benzotriazoles (Figure 5-6c) and amides (Figure 5-6d) have only been suggested by published ^{1}H NMR spectra.[238-243] The exploration of these types of H-bonding patterns with respect to the phloroglucinol core could produce new synthetic templates, building blocks for AAT chemistry (described in Chapter 4), precursors for cage molecules, new ligands (for metals), or receptors of neutral or ionic small molecules.

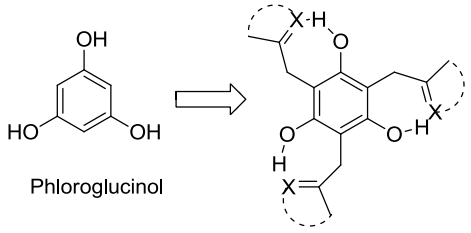

Figure 5-5. Architectural design of intramolecularly H-bonded scaffold molecules based on the phloroglucinol platform.

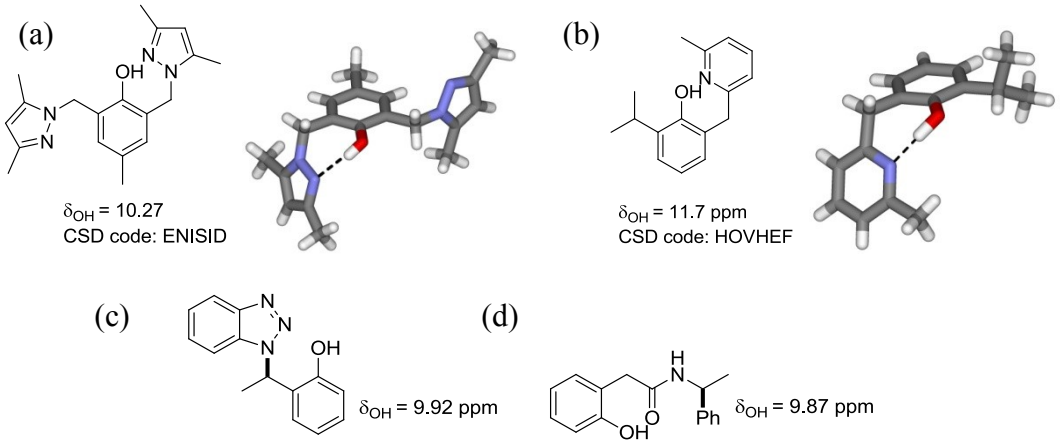

Figure 5-6. Some examples of seven-membered ring intramolecular HBs involving phenol (the shown chemical shifts are measured in $CDCl_3$).

Design and Preliminary Modeling

Initial computations show that one of the two lowest energy conformations of the N-heterocycle- and triamide-substituted phloroglucinol derivatives (Figure 5-7) involves three substituents on the same side of the benzene plane. Three seven-membered ring HBs stabilize

this conformation to form a preorganized cavity that exists as a slightly twisted cup-shape, following what has been shown in Figure 5-7. These types of phloroglucinol derivatives can potentially be used as host molecules for the recognition of guest molecules of suitable size.

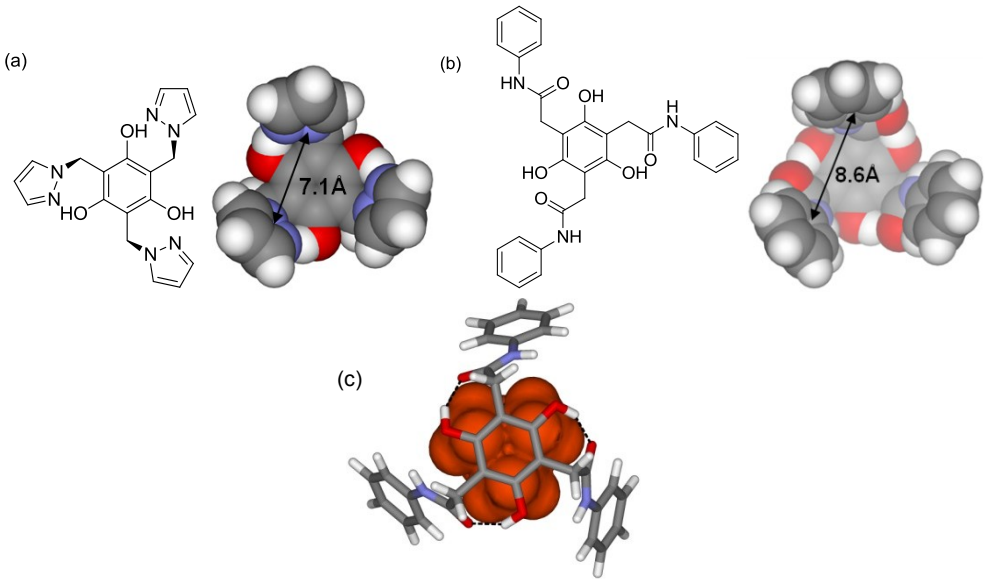

Figure 5-7. (a) Energy-minimized model of a tripyrazole phloroglucinol derivative. (b) Energy-minimized model of a triamide phloroglucinol derivative. (c) Complexation of the trimethylammonium ion by the triamide host. Calculations were performed using MacroModel V. 9.0 and the Amber* force field.

Modeling also elucidates some complexities of the systems, discussed in the context of Figure 5-8. Since HBs are directional, each hydroxyl group on the phloroglucinol has two directional choices to form HBs, and enantiomeric rotational senses develop, *syn* and *syn′* (Figure 5-8). The first challenge is how to control the chiral sense. Secondly, computation (Figure 5-7) shows that the *syn* conformation is not the only lowest energy conformation. The derivatives can also adopt the *anti* conformation, and the two conformations are nearly isoenergetic. Thus, a total of four low-energy conformers (*syn*, *syn′*, *anti*, *anti′*) should exist at equilibrium (Figure 5-8). The methods that can shift the equilibrium to the syn conformer need to be explored as well.

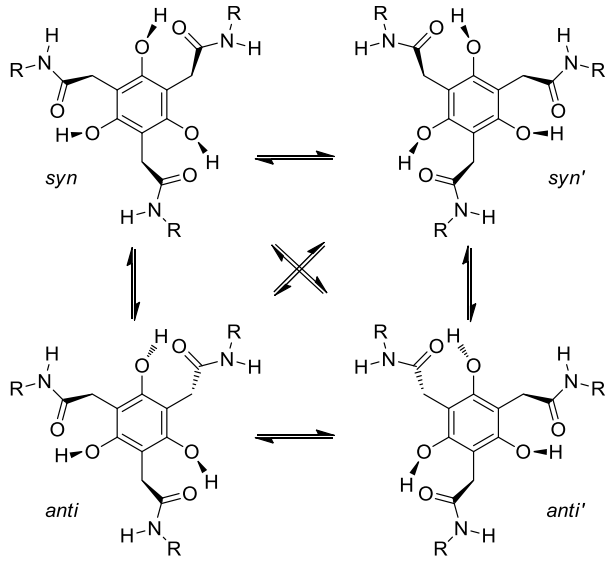

Figure 5-8. An equilibrium should exist between four low-energy conformers of the intramolecularly H-bonded triamide systems.

Synthesis and Characterization

Synthesis and Characterization of Pyrazole-functionalized Phloroglucinol Derivatives

Various pyrazole derivatives could be prepared (Figure 5-9) through three-fold nucleophilic substitution of previously introduced tribromo scaffold **4-7**. Commercially-available nucleophiles included two simple pyrazoles and one indazole and offered the tri-substituted scaffolds **5-1**–**5-3** in moderate yields (the lower yield of **5-3** was due to low regioselectivity of the alkylation reaction). The final step employed BBr_3 at low temperature to deprotect the methyl ether groups, giving final target molecules **5-4**–**5-6** in very good yields.

^{1}H NMR spectra of **5-4**, **5-5**, and **5-6** in $CDCl_3$ showed singlets for the hydroxyl protons that were shifted far downfield (**5-4**: 11.33 ppm; **5-5**: 10.91 ppm; **5-6**: 10.27 ppm) compared to 2,4,6-tripentylphloroglucinol **4-17** (4.67 ppm) and 2,4,6-tribenzylphloroglucinol[179] (~ 4.6 ppm), indicating their participation in H-bonding. The more electron-rich dimethylpyrazole of **5-4** is a better HB acceptor than the pyrazole of **5-5**, and its –OH resonance is shifted ~ 0.4 ppm downfield. A variable concentration ^{1}H NMR experiment was carried out with **5-5** to classify

the H-bonding as either inter- or intramolecular at the concentrations used. The results (Table 5-1) showed little change between 0.4 and 50 mM, indicating that intramolecular H-bonding was predominant in this range.

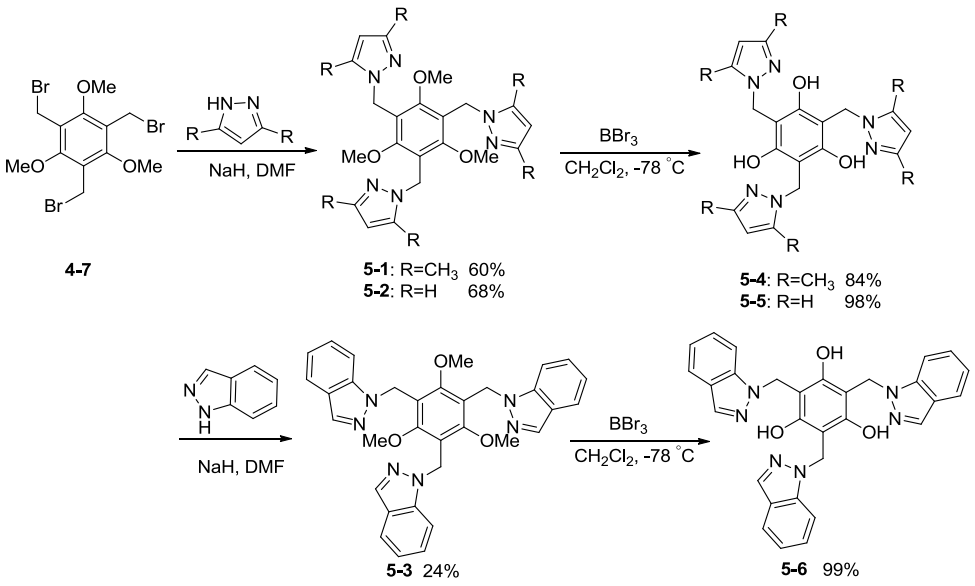

Figure 5-9. The synthesis of pyrazole-functionalized phloroglucinol derivatives.

Table 5-1. Concentration-dependent ^{1}H NMR chemical shift data for **5-5** in $CDCl_3$.

Concentration (mM)	δ_{OH} (ppm)
0.4	10.90
2.0	10.89
10	10.89
50	10.81

X-ray Crystal Structure Analysis of 5-5

In order to further prove intramolecular H-bonding in the pyrazole systems and study its conformational consequences, a single crystal of **5-5** was obtained by slowly diffusing pentane into its chloroform solution (Figure 5-10). X-ray analysis clearly shows intramolecular H-bonding; related parameters are all in accord with similar data reported in the literature[237] (Table 5-2). The conformation that is adopted by **5-5** in the solid phase is one of the two lowest energy conformations, the "*anti*" conformation, as described previously. It is likely that the C_1-

symmetric *anti* and *anti'* conformers can pack more efficiently than the C_3-symmetric *syn* conformer, and in this case, they pack into dimeric units (Figure 5-10b) that are stabilized by π-π interactions (Figure 5-10b, the π-stacking distance is 3.48 Å). In the crystal packing, the *anti* and *anti'* conformers are found to array alternately (Figure 5-10c).

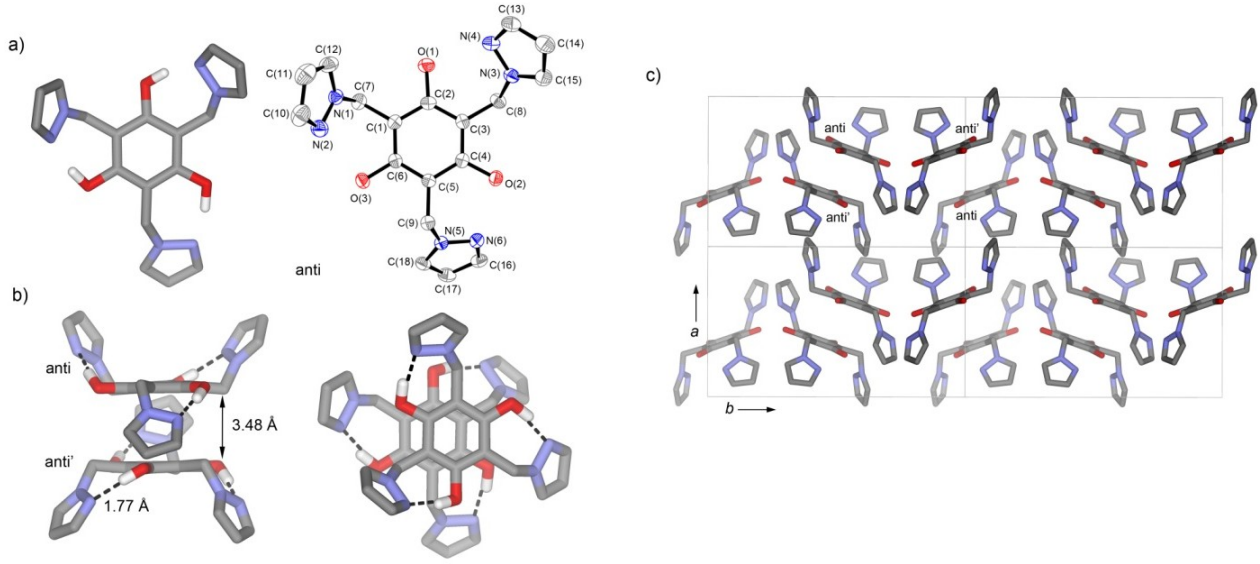

Figure 5-10. X-ray crystal structure **5-5**: (a) monomer and ORTEP plot of **5-5** (*anti* conformer, thermal ellipsoids shown at the 50% probability level and hydrogen atoms have been removed for clarity); (b) the side view (left) and top view (right) of a dimeric unit formed from both conformers of **5-5** (*anti* and *anti'*) featuring intramolecular HBs and π-π stacking interactions; (c) crystal packing of **5-5** along the *c* axis.

Table 5-2. Comparison between the crystallographic data of **5-5** and relevant molecules from the literature (D: HB donor; A: HB acceptor).

Parameter	Lit. data (CSD code)	**5-5**
O…N (Å)	2.7[237](HOVHEF[a])	2.74/2.72/2.69
(O)H…N(Å)	1.7[237](HOVHEF)	1.77/1.77/1.707
∠ DHA (deg)	169[237](HOVHEF)	165.4/165.9/167.3
D-H	0.84[236] (ENISID[b])	0.97/0.99/1.00

[a][b]: the chemical and crystal structures of HOVHEF and ENISID were shown in Figure 5-6.

In solution, there exists a rapid equilibrium between the *syn* and *anti* conformers and a time-averaged ^{1}H NMR spectrum is observed. Given that the *syn* conformer is C_3-symmetric and the *anti* conformer is C_1-symmetric, the benzylic protons of each could potentially be

distinguishable if the equilibrium was slowed down. We attempted a low temperature ^{1}H NMR experiment to this end (Figure 5-11), but even at -50˚C there were no significant changes in the spectra. The energy barrier for interconversion of the two conformers is simply too low to make this analysis possible.

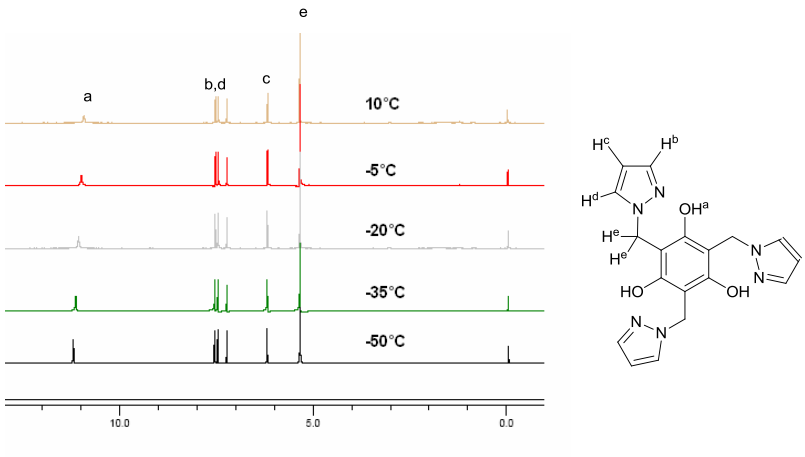

Figure 5-11. ^{1}H NMR spectra of **5-5** in $CDCl_3$ at different temperatures.

Attempted Synthesis of Triazole-functionalized Phloroglucinol Derivatives

Pyrazole-functionalized phloroglucinol derivatives have served a valuable proof-of-principle role in our studies. The idea of controlling conformation by seven-membered ring intramolecular H-bonding has been demonstrated with these phloroglucinol derivatives in solution and solid state. Unfortunately, the synthetic chemistry and commercial sources of symmetrically-substituted pyrazoles are limited. To advance our strategy, we next considered tristriazole phloroglucinol derivatives where we could employ "click chemistry"[244] to both construct the heterocycles and introduce various substituents onto the phloroglucinol periphery (Figure 5-11). Two strategies can be used that involve 1,2,3-triazole formation from the 1,3-dipolar cycloaddition reaction of azides and alkynes with Cu (I) catalysts.[245-252] In the first strategy (Figure 5-11a), the triazide phloroglucinol precursor is treated with an appropriate terminal alkyne. This results in the N(2) of the triazole acting as the HB acceptor. In the second

strategy (Figure 5-11b), a trialkyne phloroglucinol derivative is reacted with an azide. Here, the more Lewis basic triazole nitrogen, N(1), acts as the HB acceptor. Both strategies are suitable to investigate.

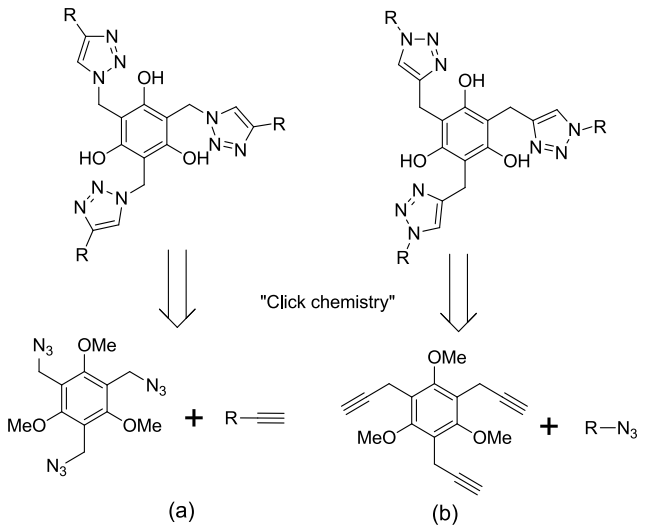

Figure 5-11. Triazole-functionalized phloroglucinol derivatives via "click chemistry".

The syntheses (Figure 5-12) started from the tribromo compound **4-7** which was reacted with sodium azide to introduce the requisite three azido groups. Tri-azide compound **5-7** was obtained in excellent yield. The subsequent 1,3-dipolar cycloaddition reactions, performed with three different alkynes, employed $Cu(Ph_3P)_3Br$ as a catalyst. This stable copper (I) reagent[253] has good catalytic activity, and affords tris-triazole compounds **5-8a-c** in reasonable yields. Unfortunately, the subsequent BBr_3 demethylation step did not work well for **5-8b** and **5-8c**, and very polar product mixtures were obtained that were difficult to purify. We presume that the strongly Lewis acidic BBr_3 coordinates not only with the O of the methoxy groups but also the basic N on the triazole ring, leading to destruction or replacement of the triazole ring by nucleophilic attack. The only pure target molecule isolated from this synthetic route was **5-9**; its insolubility in dichloromethane and precipitation during the reaction likely prevented

decomposition of the triazole rings. Unfortunately, the insolubility of **5-9** in less polar solvents prevents its H-bonding study through routine ^{1}H NMR experiments.

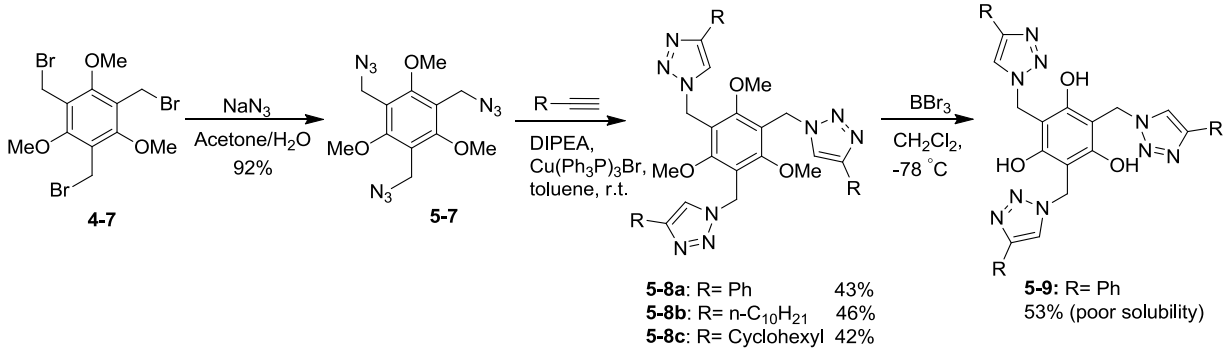

Figure 5-12. The first "click chemistry" approach to triazole-functionalized phloroglucinol derivatives.

In order to make the connection between the phloroglucinol core and triazole "arms" robust enough to survive the BBr_3 reaction, a regioisomeric family was considered (Figure 5-11b). These molecules feature C–C bonds as connections between the benzylic positions and the triazole rings. The structural change also allows the more basic nitrogen atom of the heterocycle to serve as the HB acceptor.

Synthesis began with reaction of TMS-protected acetylene with **4-7** in the presence of base and CuI to afford **5-10** in reasonable yield (Figure 5-13). Silver nitrate and potassium cyanide were used to remove the TMS-protecting groups[254] to afford trialkyne **5-11**. This reagent was adopted for removal of the TMS groups rather than TBAF due to reports of allene formation with the latter.[255] Under the same click chemistry conditions, compound **5-11** was reacted with benzyl azide and *n*-heptyl azide to form **5-12a** and **5-12b**, respectively**.** Unfortunately, discouraging results were obtained in the final demethylation reactions. A very polar mixture was obtained which was hard to purify in each case. The isolation of intermediates, elucidation of mechanistic details, and reaction optimization will be important tasks for the future.

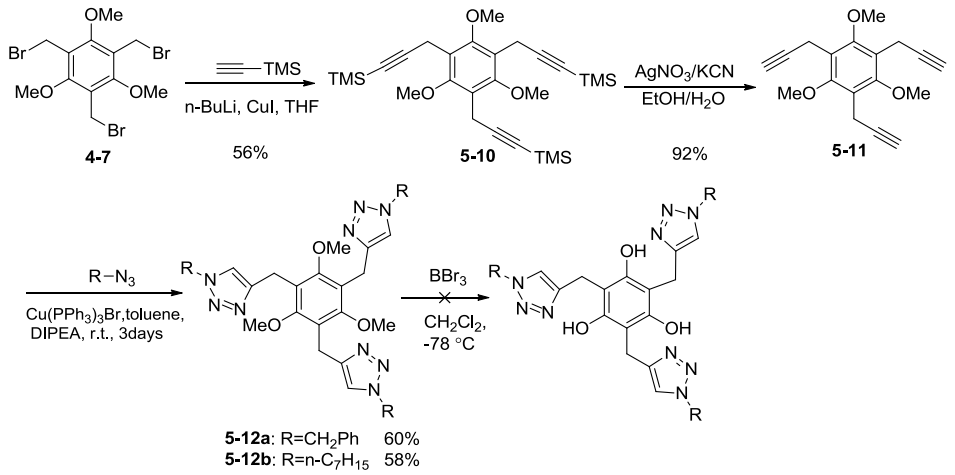

Figure 5-13. The attempted synthesis of C–C linked triazole-functionalized phloroglucinol derivatives.

Syntheses of Triamide-functionalized Phloroglucinol Derivatives

Similar to the basic nitrogen atoms of pyrazole and triazole rings, carbonyl oxygens can also be used as intramolecular HB acceptors. Inspired by the computational results described earlier (Figure 5-7), a family of triamide-functionalized phloroglucinol derivatives was prepared.

Two approaches to triamide-functionalized phloroglucinol derivatives were entertained. One began from compound **2-4** (Figure 5-14), which was hydrolyzed to form triacid **5-13** in near quantitative yield. Conversion to acid chloride **5-14** followed by treatment with different amines gave triamides **5-15a**–**b**, all subsequently deprotected with BBr_3 to afford target molecules **5-16a**–**b** in good yields. An alternative approach to phloroglucinol triamides involves BTF as described in Chapter 2 (Figures 2-13 and 2-14). A variety of amines were used to open the lactone rings of BTF to form symmetrically-substituted **2-13a**–**d** and **2-16**; differentially functionalized phloroglucinol **2-17** was also obtained from BTF as discussed in Chapter 2 (Figure 2-14).

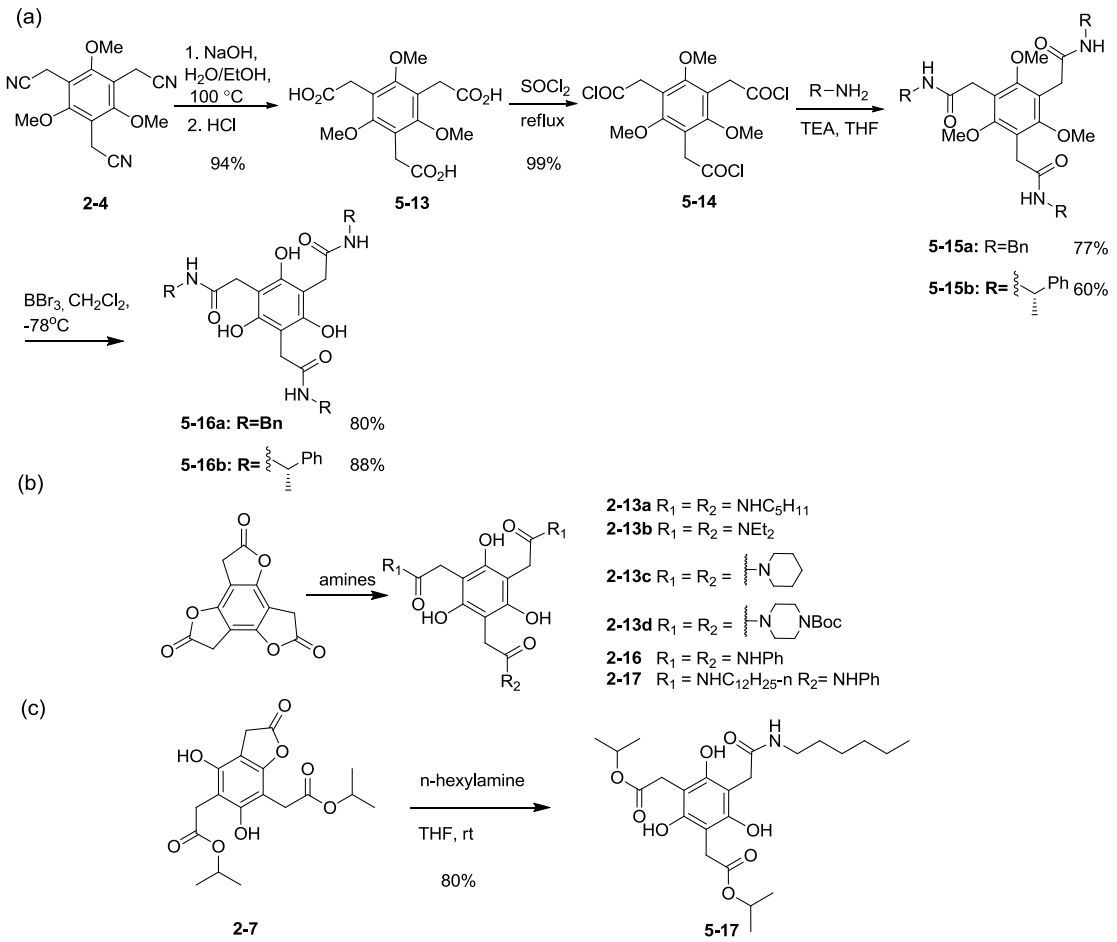

Figure 5-14. Synthesis of amide functionalized phloroglucinol derivatives via (a) a traditional approach and (b) the BTF approach (the detailed reaction conditions for the BTF approach are provided in Figures 2-13 and 2-14).

The phloroglucinol OH chemical shifts for the triamide derivatives have been summarized in Table 5-3; the significantly deshielded resonances are good evidence for HBs. Notably, the two chemically distinct hydroxyl groups within **2-17** and **5-17** give rise to two sets of signals in each case. For **2-17**, the chemical shifts of the OHs that are positioned between the hexyl and phenyl amides appear at 9.88 ppm, upfield relative to trialkylamide species **5-16a** (10.29 ppm) but downfield relative to triphenylamide **2-16** (9.76 ppm). Similar results are found for **5-17** where the chemical shift of the OHs adjacent to both an ester and an amide group (9.41 ppm) lies between the shift observed for trialkylamide **5-16a** (10.29 ppm) and triester **2-6** (8.46 ppm, not

shown in Table 5-3, see Chapter 2, Figure 2-7a). The results indicate that the intramolecular HBs are dynamic at room temperature since the chemical shifts recorded reflect the averaged chemical environment for the phenolic OHs.

Table 5-3. ^{1}H NMR chemical shift data[a] for amide-functionalized phloroglucinol derivatives.

Compounds	δ_{OH} (ppm)
5-16a	10.29
5-16b	10.06
2-13a	10.18
2-13b	11.00
2-13c	10.65
2-13d	10.37
2-16	9.76
2-17	10.26 (1H), 9.88 (2H)
5-17	9.41 (2H), 8.61 (1H)

[a] Spectra recorded at 1.0 ~ 5.0 mM in $CDCl_3$.

X-ray Crystal Structure Analysis of 5-16b

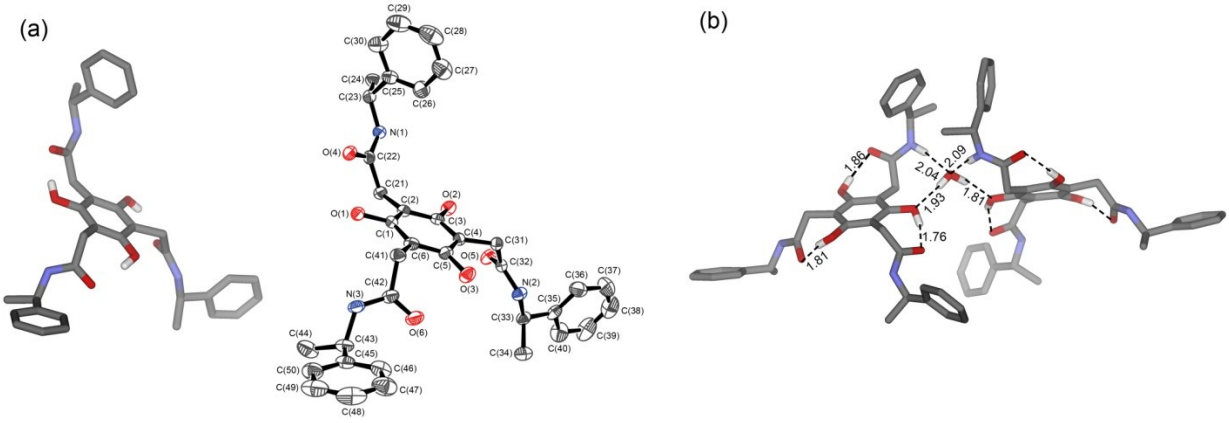

Figure 5-15. The X-ray crystal structure of **5-16b**: (a) monomer and ORTEP plot of **5-16b** (*anti* conformer, thermal ellipsoids shown at the 50% probability level and hydrogen atoms have been removed for clarity except for the phloroglucinol hydroxyls); (b) a dimeric unit (including two **5-16b** and one water molecule) found in the crystal. HBs (dashed lines) and distances (Å) between HB acceptors and donors are indicated.

A single crystal of **5-16b** was obtained by slow evaporation of its ethyl acetate solution. In the crystal structure (Figure 5-15), the expected HBs are found between the amide carbonyls and the phenolic hydroxyls. Additionally, the molecules of **5-16b** are organized into water-bridged dimers in the crystal unit cell (Figure 5-15b), an interesting assembly wherein all of the H-

bonding sites of water are perfectly satisfied. Also interesting, only the *anti'* conformer is observed in the crystal structure. The result contrasts with the crystal structure of compound **5-5** wherein both the *anti* and *anti'* forms were found. For **5-16b**, its peripheral stereogenic centers remotely control the chiral sense of phloroglucinol H-bonding at the core.

Conclusion

We have synthesized two families of phloroglucinol derivatives that feature seven-membered-ring intramolecular HBs. The intramolecular HBs have been studied in the solution and solid phase via ^{1}H NMR and X-ray crystallography, respectively. Although the popular "click chemistry" approach has been shown unsuitable for generating diverse heteroaromatic-substituted phloroglucinol derivatives, the BTF strategy introduced in Chapter 2 is a promising alternative. Phloroglucinol rings that subscribe to the H-bonding recipe discussed do have discrete conformations in solution that make them attractive for applications in supramolecular chemistry.

Experimental Section

Synthesis

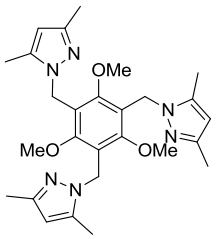

2,4,6-Tris-(3,5-dimethyl-pyrazol-ylmethyl)-1,3,5-trimethoxybenzene (5-1). General procedure for *N*-heterocycle alkylation. To a suspension of NaH (60% in mineral oil, 0.470 g, 11.7 mmol) and dry DMF (40 mL) in a dry flask was added 3,5-dimethylpyrazole (1.06 g, 11.1 mmol), after which the reaction was heated to 50 °C for 1 hour. After cooling to room

temperature, **4-7** (1.50 g, 3.36 mmol) was dissolved in a small amount of dry DMF and slowly added to the stirring solution. Upon completion of addition, the reaction was warmed to 50 °C for 12 hours. After cooling to room temperature, the reaction was carefully quenched, poured into water (40 mL), and extracted with ethyl acetate (3 × 50mL). The organic layers were combined, dried over $MgSO_4$ and concentrated to a crude oil. Flash chromatography using ethyl acetate/hexanes (2:1) afforded **5-1** (1.0 g, 60%) as a white solid: ^{1}H NMR ($CDCl_3$) δ 2.15 (s, 9H), 2.24 (s, 9H), 3.47 (s, 9H), 5.12 (s, 6H), 5.76 (s, 3H). ^{13}C NMR ($CDCl_3$) δ 11.7, 14.0, 43.0, 62.9, 105.8, 122.5, 141.0, 147.7, 160.9.

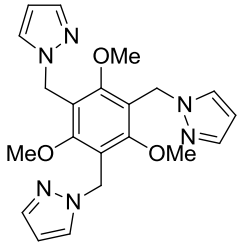

2,4,6-Tris-pyrazol-1-ylmethyl-1,3,5-trimethoxybenzene (5-2). Compound **5-2** was prepared from pyrazole (0.53 g, 7.4 mmol) and **4-7** (1.0 g, 2.2 mmol) according to the general procedure for *N*-heterocycle alkylation above. Flash chromatography (EtOAc/hexanes 1/5) afforded **5-2** (0.62 g, 68%) as a white solid: ^{1}H NMR ($CDCl_3$) δ 3.57 (s, 9H), 5.34 (s, 6H), 6.20 (m, 6H), 7.44 (m, 6H). ^{13}C NMR ($CDCl_3$) δ 45.4, 62.4, 105.4, 120.5, 129.2, 138.8, 160.2.

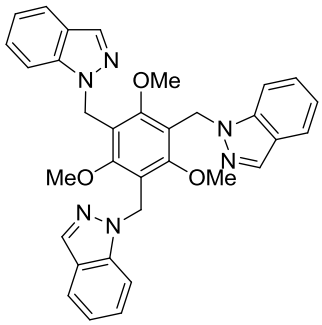

1,1',1''-((2,4,6-Trimethoxybenzene-1,3,5-triyl)tris(methylene))tris(1H-indazole) (5-3)

Compound **5-3** was prepared from indazole (0.96 g, 7.8 mmol) and **4-7** (1.0 g, 2.2 mmol)

according to the general procedure for *N*-heterocycle alkylation above. Flash chromatography (EtOAc/hexanes 1/1) afforded **5-2** (0.30 g, 24%) as a white solid. ^{1}H NMR ($CDCl_3$) δ 3.54 (s, 9H), 5.66 (s, 6H), 7.22 (t, *J* = 7.59 Hz, 3H), 7.40 (t, *J* = 7.67 Hz, 3H), 7.56 (d, *J* = 8.47 Hz, 3H), 7.80 (d, *J* = 8.03 Hz, 3H), 8.08 (sk, 3H). ^{13}C NMR ($CDCl_3$) δ 42.7, 62.3, 109.5, 120.3, 120.4, 120.8, 123.9, 126.1, 132.7, 139.5, 160.3. HRMS (ESI-TOF) calcd for $C_{36}H_{34}N_9O_3$ $(M + H)^+$ 559.2452, found 559.2409.

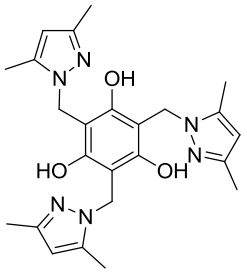

2,4,6-Tris-(3,5-dimethyl-pyrazol-ylmethyl)-benzene-1,3,5-triol (5-4). General demethylation procedure: To a solution of **5-1** (0.50 g, 1.01 mmol) and dry methylene chloride (10 mL) at –78 °C in a dry flask equipped with a stirrer was added BBr_3 (3.56 g, 14.2 mmol). After 1 hour the reaction was allowed to gradually warm to room temperature and stirred overnight. After cooling to 0 °C, the reaction was quenched by dropwise addition of cold saturated aqueous $NaHCO_3$ until gas evolution ceased. The reaction mixture was then poured into saturated aqueous $NaHCO_3$ and extracted with methylene chloride (3 × 30 mL). The organic layers were combined, washed with brine, dried over $MgSO_4$, and concentrated under the reduced pressure to afford **5-4** (0.38 g, 84%) as a white solid: ^{1}H NMR ($CDCl_3$) δ 2.16 (s, 9H), 2.38 (s, 9H), 5.20 (s, 3H), 5.70 (s, 3H), 11.33 (s, 3H). ^{13}C NMR ($CDCl_3$) δ 10.8, 13.17, 41.81, 104.6, 105.9, 139.5, 146.7, 156.0.

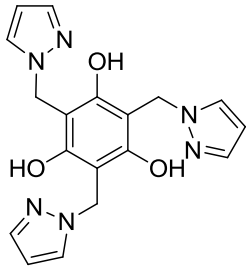

2,4,6-Tris-pyrazol-1-ylmethyl-benzene-1,3,5-triol (5-5). The demethylation of **5-4** was performed on a scale of 1.66 mmol, according to the general demethylation procedure above to afford **5-5** (0.60 g, 98%) as a white solid: ^{1}H NMR ($CDCl_3$) δ 5.39 (s, 6H), 6.21 (t, J = 2.1 Hz, 3H), 7.49 (d, J = 2.1Hz, 3H), 7.56 (d, J = 2.1Hz, 3H), 10.91 (s, 3H). ^{13}C NMR ($CDCl_3$) δ 45.2, 105.2, 105.9, 129.8, 138.5, 155.9.

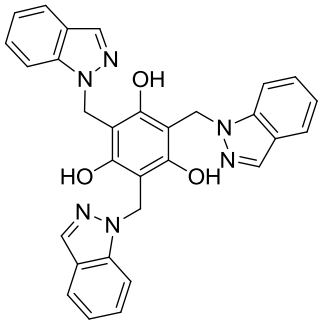

2,4,6-Tris((1H-indazol-1-yl)methyl)benzene-1,3,5-triol (5-6) Following the general demethylation procedure, compound **5-6** was prepared from **5-3** (0.30 g, 0.54 mmol) to afford 0.28 g (99%) of product. ^{1}H NMR ($CDCl_3$) δ 5.64 (s, 6H), 7.14 (ddd, J = 0.8 Hz, 6.9 Hz, 8.2 Hz), 7.46 (ddd, J = 1.1 Hz, 6.9 Hz, 8.5 Hz), 7.68 (dd, J = 0.9 Hz, 8.6 Hz), 7.99 (d, J = 1.0 Hz). ^{13}C NMR ($CDCl_3$) δ 41.7, 105.8, 110.1, 116.3, 121.0, 123.1, 127.1, 132.3, 139.0, 155.7. HRMS (APCI-TOF) calcd for $C_{30}H_{25}N_6O_3$ $(M + H)^+$ 517.1983, found 517.1964.

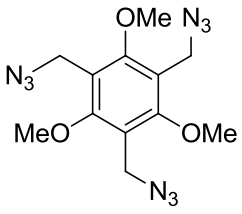

1,3,5-Tris-azidomethyl-2,4,6-trimethoxy-benzene (5-7). To a solution of **4-7** (2.00g, 4.48 mmol) in acetone (50 mL) at reflux was added NaN_3 (1.28 g, 19.7 mmol). To the resulting suspension, water (40 mL) was slowly added over 15 minutes and the solution was allowed to stir at 55 °C overnight. After cooling to room temperature, the reaction mixture was poured in ice water (100 mL) and the cold solution was extracted with ether (200 mL × 2). The ethereal extracts were combined, dried over $MgSO_4$, and evaporated in vacuo to afford **5-7** (1.36 g, 92%) as a colorless, viscous oil: ^{1}H NMR ($CDCl_3$) δ 3.93 (s, 9H), 4.46 (s, 6H). ^{13}C NMR ($CDCl_3$) δ 44.4, 63.5, 120.0, 160.5.

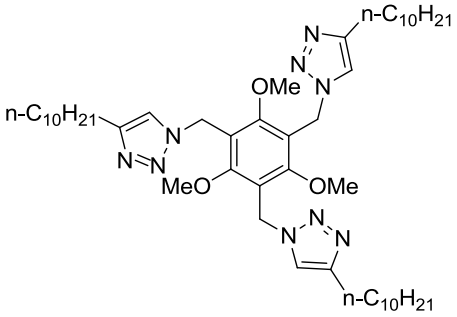

1-(3,5-Bis((4-decyl-1H-1,2,3-triazol-1-yl)methyl)-2,4,6-trimethoxybenzyl)-4-decyl-1H-1,2,3-triazole (5-8b). *Preparation of the catalyst, $Cu(PPh_3)_3Br$*: In an Erlenmeyer flask equipped with a Teflon stir bar, methanol (40 mL) was heated to boiling and triphenylphosphine (2.5 g, 9.5 mmol) was slowly added to the stirring methanol. After the complete dissolution of triphenylphosphine, $CuBr_2$ (0.50 g, 2.2 mmol) was added as a solid, in portions. Upon addition of the $CuBr_2$, a white precipitate was formed. After complete addition, the contents were stirred for 10 minutes and the flask was allowed to cool to ambient temperature. The reaction mixture was then filtered and the white residue was washed repeatedly with ethanol and then with diethyl ether. The resultant white solid was dried under vacuum to give a solid product (2.0 g, 97%).

To the solution of **5-7** (0.70 g, 2.1 mmol) and 1-dodecyne (1.15 g, 6.93 mmol) in toluene (30 mL), the $Cu(PPh_3)_3Br$ (0.68 g, 0.74 mmol) was added followed by DIPEA (2.5 g, 19 mmol)

that was added dropwise. The resulting mixture was allowed to stir for 48 hours and concentrated in vacuo to form a green solution. Flash chromatography using ethyl acetate/hexanes (1:1) afforded **5-8b** (0.80 g, 46%) as a white solid: ^{1}H NMR ($CDCl_3$) δ 0.88 (m, 9H), 1.28 (m, 42H), 1.62 (m, 6H), 2.66 (t, 3H, J = 7.5 Hz), 3.69 (s, 9H), 5.52 (s, 6H), 7.32 (s, 3H). ^{13}C NMR ($CDCl_3$) δ 14.1, 22.6, 25.7, 31.9, 43.5, 63.0, 120.0, 120.8, 148.7, 160.5. HRMS ((-) ESI) calcd for $C_{48}H_{81}N_9O_3Cl$ $(M + Cl)^-$ 866.6145, found 866.6113.

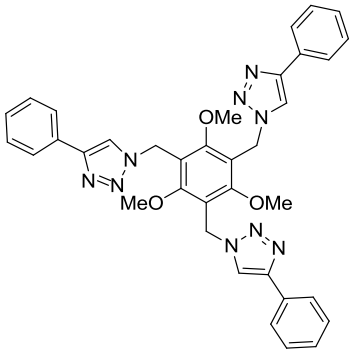

1-(2,4,6-Trimethoxy-3,5-bis((4-phenyl-1H-1,2,3-triazol-1-yl)methyl)benzyl)-4-phenyl-1H-1,2,3-triazole (5-8a). To a solution of **5-7** (0.430 g, 1.29 mmol) and phenyl acetylene (0.400 g, 3.87 mmol) in CH_2Cl_2 (30 mL) was added $Cu(PPh_3)_3Br$ (0.36 g, 0.39 mmol), followed by DIPEA (1.50 g, 11.6 mmol) that was added dropwise. The resulting mixture was allowed to stir overnight. A white precipitate appeared and was filtered off to yield a white solid (0.18 g). The filtrate was concentrated under reduced pressure at 50 °C and redissolved in CH_2Cl_2 for flash chromatography using ethyl acetate/hexanes (3:2) to afford **5-8a** as a white solid (0.18 g). The combined portions of the product yielded 0.36 g (42%). ^{1}H NMR (DMSO-d_6) δ 3.79 (s, 9H), 5.64 (s, 6H), 7.30–7.40 (m, 9H), 7.81 (d, 6H, J = 8.4 Hz), 8.46 (s, 3H). ^{13}C NMR (DMSO-d_6) δ 43.62, 62.49, 119.61, 121.56, 125.10, 127.79, 128.78, 130.58, 146.12, 159.93. HRMS (EI) calcd for $C_{36}H_{33}N_9O_3$ $(M+ H)^+$ 640.2785, found 640.2775.

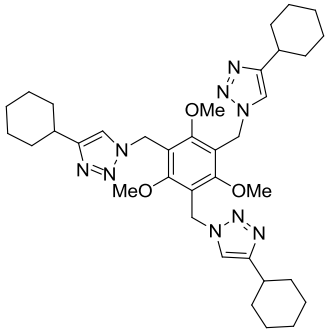

1-(3,5-Bis((4-cyclohexyl-1H-1,2,3-triazol-1-yl)methyl)-2,4,6-trimethoxybenzyl)-4-cyclohexyl-1H-1,2,3-triazole (5-8c). To a solution of **5-7** (0.67 g, 2.0 mmol) and ethynylcyclohexane (0.65 g, 6.0 mmol) in CH_2Cl_2 (30 mL) was added $Cu(PPh_3)_3Br$ (0.56 g, 0.60 mmol). DIPEA (2.30 g, 18 mmol) was subsequently added dropwise. The resulting solution was allowed to stir for 48 hours. The reaction solution was then washed with 1.0 M HCl (50 mL × 2), water (50 mL), and brine (50 mL). The organic layer was dried over $MgSO_4$ and concentrated. Flash chromatography using ethyl acetate/hexanes (from 3:2 to 3:1) afforded **5-8c** (0.53 g, 42%) as a white solid: ^{1}H NMR ($CDCl_3$) δ 1.26–1.41 (m, 15H), 1.69–1.78 (m, 9H), 2.03 (m, 6H), 2.72 (b, 3H), 3.70 (s, 9H), 7.31 (s, 3H). ^{13}C NMR ($CDCl_3$) δ 26.0, 26.1, 33.0, 35.3, 43.5, 63.0, 119.6, 120.0, 153.9, 160.5. HRMS (ESI) calcd for $C_{36}H_{52}N_9O_3$ $(M+H)^+$ 658.4188, found 658.4213.

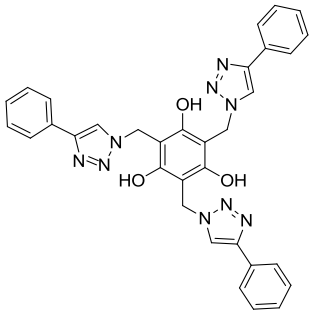

2,4,6-Tris((4-phenyl-1H-1,2,3-triazol-1-yl)methyl)-phloroglucinol (5-9). To a suspension of **5-8a** (0.12g, 0.19 mmol) in dry methylene chloride (70 mL) at –78 °C was added BBr_3 (0.25 mL, 2.6 mmol). The resulting mixture was allowed to stir for 1 hour and warmed to room temperature with stirring overnight. The reaction mixture was cooled to 0 °C and treated

with saturated $NaHCO_3$ solution (dropwise) to quench the reaction. The resulting mixture was extracted with CH_2Cl_2 (30 mL ×3), and the organic layers were combined and washed with water (30 mL), brine (30 mL), and dried over $MgSO_4$. The organic solvent was evaporated and dried under vacuum to yield **5-9** (0.06 g, 53%) as a slightly yellow solid. ^{1}H NMR (d_6-DMSO) δ 5.64 (s, 6H), 7.29 ~ 7.40 (m, 9H), 7.83 (d, 6H, J = 6.6Hz), 8.24 (s, 3H), 9.71 (s, 3H). ^{13}C NMR (DMSO-d_6) δ 43.4, 103.4, 120.6, 125.0, 127.6, 128.7, 130.8, 145.6, 156.9. HRMS (ESI) calcd for $C_{66}H_{54}N_{18}O_6Na$ $(2M+Na)^+$ 1217.4366, found 1217.4370.

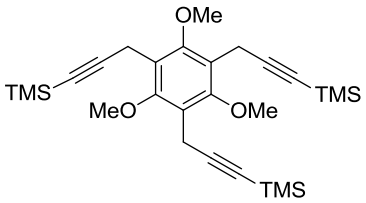

1,3,5-Trimethoxy-2,4,6-tris(3-(trimethylsilyl)prop-2-ynyl)benzene(5-10). THF (50 mL) was cooled to –78 °C and then treated with ethynyltrimethylsilane (6.91 g, 70.5 mmol). *n*-BuLi (28.2 mL, 2.5 M solution in hexane) was added dropwise. The resulting mixture was stirred for 30 min after which CuI (1.34 g, 7.05 mmol) was quickly added. After an additional 30 min of stirring at –78°C, a solution of **4-7** (3.50 g, 7.83 mmol) in THF (15 mL) was added dropwise. The resulting reaction mixture was warmed to room temperature and stirred for 48 hours. The reaction was quenched with saturated aqueous NH_4Cl (25 mL) and the mixture was poured into a saturated NH_4Cl solution (40 mL). The organic material was extracted with diethyl ether (3 × 100 mL). The ethereal layer was washed with water and brine, decolorized with activated charcoal, and dried over $MgSO_4$. The solution was concentrated and the product was obtained by recrystallization. The mother liquor was purified by flash chromatography (1:2 CH_2Cl_2/hexanes) to acquire more product. The combined portions of product yielded 2.2 g (56%) of **5-10**. ^{1}H NMR ($CDCl_3$) δ 0.13 (s, 27H), 3.61 (s, 6H), 4.04 (s, 9H). ^{13}C NMR ($CDCl_3$) δ –0.03, 15.35,

62.67, 84.21, 106.42, 121.13, 156.82. HRMS (ESI) calcd for $C_{27}H_{42}O_3Si_3Na$ $(M + Na)^+$ 521.2334, found 521.2339.

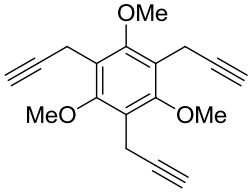

1,3,5-Trimethoxy-2,4,6-tri(prop-2-ynyl)benzene (5-11). $AgNO_3$ (0.61 g, 3.6 mmol) was dissolved in an aqueous ethanol solution (7.2 mL ethanol/16.8 mL H_2O). Compound **5-10** (0.4 g, 0.8 mmol) was dissolved in ethanol (18 mL) and the resulting solution was added dropwise; a white precipitate formed. The reaction mixture was stirred overnight at room temperature in the dark. KCN (0.62 g, 9.6 mmol) was dissolved in water (3 mL) and the resulting solution was added to the reaction mixture. After an additional 1 hour of stirring, the solution was poured into diethyl ether (250 mL) and then washed with water and brine. The ethereal layer was dried over $MgSO_4$ and the solvent was removed under reduced pressure to yield **5-11** (0.21 g, 94%). ^1H NMR ($CDCl_3$) δ 2.04 (t, J = 2.7 Hz, 3H), 3.58 (d, J = 2.7 Hz, 6H), 4.03 (s, 9H). ^{13}C NMR ($CDCl_3$) δ 13.90, 62.47, 68.20, 83.47, 120.97, 156.78. HRMS (EI) calcd for $C_{18}H_{19}O_3$ $(M+ H)^+$ 283.1329, found 283.1334

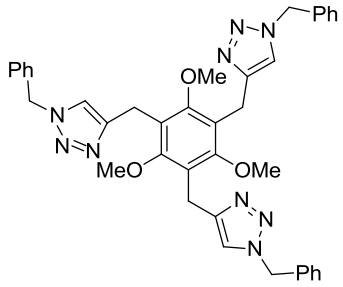

4-(3,5-Bis((1-benzyl-1H-1,2,3-triazol-4-yl)methyl)-2,4,6-trimethoxybenzyl)-1-benzyl-1H-1,2,3-triazole (5-12a). To a solution of **5-11** (0.25 g, 0.88 mmol) in CH_2Cl_2 (15 mL) was dropwise added a solution of benzyl azide (0.46 g, 3.5 mmol) in CH_2Cl_2 (5 mL). To the resulting

solution were added $Cu(PPh_3)_3Br$ (0.24 g, 0.26 mmol) and DIPEA (1.02 g, 7.92 mmol). The reaction mixture was stirred for 48 hours at room temperature. The reaction solution was then diluted with CH_2Cl_2 (20 mL) and quenched with HCl. The organic layer was separated, washed with water and brine, and dried over $MgSO_4$. After concentration in vacuo, the product was separated by flash column chromatography (first EtOAc/hexane 1/3 to remove impurities, then neat EtOAc to isolate the product) to yield **5-12a** (0.38 g, 63%). ^{1}H NMR ($CDCl_3$) δ 3.61 (s, 9H), 4.07 (s, 6H), 5.44 (s, 6H), 7.20–7.36 (m, 18H). ^{13}C NMR ($CDCl_3$) δ 21.51, 53.85, 61.66, 121.79, 122.63, 127.67, 128.41, 128.88, 135.05, 147.68, 157.04. HRMS (EI) calcd for $C_{39}H_{40}N_9O_3$ $(M+H)^+$ 682.3249, found 682.3242.

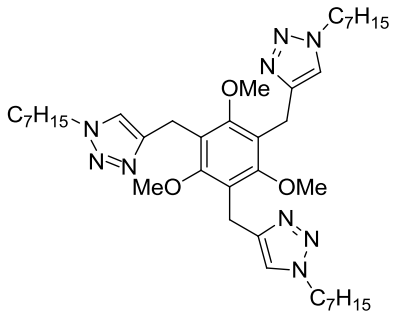

4,4',4''-((2,4,6-Trimethoxybenzene-1,3,5-triyl)tris(methylene))tris(1-heptyl-1H-1,2,3-triazole) (5-12b). Following the same procedure for the preparation of **5-12a**, **5-11** (0.25 g, 0.88 mmol), heptyl azide (0.49 g, 3.5 mmol), $Cu(PPh_3)_3Br$ (0.24 g, 0.26 mmol), and DIPEA (1.02 g, 7.92 mmol) yielded **5-12b** (0.36 g, 58%) as a colorless solid. ^{1}H NMR ($CDCl_3$) δ 0.83 (t, J = 6.6 Hz, 9H), 1.15–1.35 (m, 24H), 1.95–1.71 (m, 6H), 3.63 (s, 9H), 4.05 (s, 6H), 4.21 (t, J = 7.3 Hz, 6H) 7.27 (s, 3H). ^{13}C NMR ($CDCl_3$) δ 13.9, 21.4, 22.4, 26.3, 28.5, 30.2, 31.4, 50.1, 61.6, 121.5, 122.7, 147.0, 156.9.

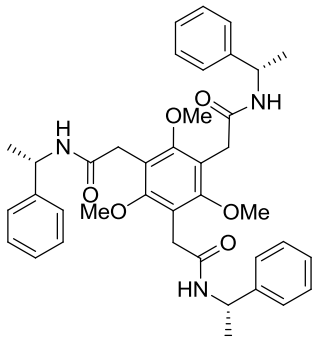

***N*-((S)-1-Phenylethyl)2-(2,4,6-trimethoxy-3,5-bis-(S)-1-methyl-benzylcarbamoylmethyl-phenyl)-acetamide (5-15b).** A solution of **5-13**[180] (0.620 g, 1.83 mmol) and thionyl chloride (35 mL) was heated to reflux for 2 hours. After cooling, the solvent was removed in vacuo. The remaining crude brown oil (**5-14**) was dissolved in dry THF (10 mL) and slowly added to a solution of (S)-1-phenylethanamine (0.73 g, 6.04 mmol), TEA (1.85 g, 18.3 mmol), and dry THF (10 mL) in a dry round bottom flask. The resulting solution was allowed to stir overnight. The reaction mixture was then diluted with methylene chloride (120 mL), washed with 10% aq. HCl (60 mL), water (60 mL), brine (60 mL), dried over $MgSO_4$, and evaporated in vacuo. Flash chromatography using methylene chloride/methanol (10:1) afforded **5-15b** (0.70 g, 60%) as a white solid: ^{1}H NMR (DMSO-d_6) δ 1.36 (d, J = 6.6 Hz, 9H), 3.43 (d, J = 4.8 Hz, 6H), 3.51 (s, 9H), 4.93 (m, 3H), 7.29 (m, 15H), 8.44 (d, J = 8.1 Hz, 3H). ^{13}C NMR (DMSO-d_6) δ 21.77, 32.80, 48.83, 61.08, 119.74, 126.01, 127.15, 128.49, 143.23, 157.67, 169.80. HRMS (FAB) calcd. for $C_{39}H_{45}N_3O_6Na$ $(M+Na)^+$ 674.3206, found 674.3214.

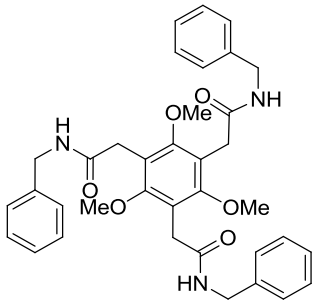

***N*-Benzyl-2-(2,4,6-trimethoxy-3,5-bis-benzylcarbamoylmethyl-phenyl)-acetamide (5-15a).** This compound was synthesized from **5-13** (0.500 g, 1.46 mmol) according to the preparation described for **5-15b** to afford **5-15a** as an off-white solid (0.70 g, 77%): ^{1}H NMR ($CDCl_3$) δ 3.63 (s, 6H), 3.77 (s, 9H), 4.35 (d, J = 6 Hz, 6H), 6.29 (t, J = 6 Hz, 3H), 7.18–7.36 (m, 15H). ^{13}C NMR($CDCl_3$): δ 32.8, 43.5, 61.9, 119.9,127.4, 128.5, 138.3, 157.6,170.5.

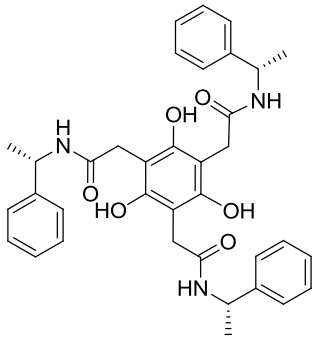

N-((S)-1-Phenylethyl)2-(2,4,6-trihydroxy-3,5-bis-((S)-1-methyl-benzylcarbamoylmethyl)-phenyl)-acetamide (5-16b). The demethylation of **5-15b** was performed on a scale of 0.40 g (0.61 mmol) according to the general demethylation procedure above to afford **5-16b** (0.33 g, 88%) as a white solid: ^{1}H NMR ($CDCl_3$) δ 1.47 (d, 9H, J = 6.9Hz), 3.60 (dd, J = 14.1Hz, 6H), 5.00 (m, 3H), 6.41 (b, 3H), 7.29 (m, 15H), 10.06 (s, 3H). ^{13}C NMR ($CDCl_3$) δ 21.85, 32.56, 49.50, 102.98, 125.97, 127.47, 128.72, 142.40, 153.92, 173.89. HRMS (CI) calcd for $C_{36}H_{40}N_3O_6$ $(M + H)^+$ 610.2917, found 610.2924.

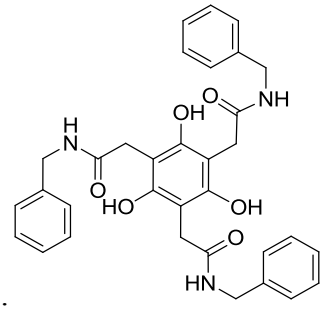

N-Benzyl-2-(2,4,6-trihydroxy-3,5-bis-benzylcarbamoylmethyl-phenyl)-acetamide (5-16a). This compound was synthesized from **5-15a** (0.20 g, 0.33 mmol) according to the general demethylation procedure above to afford **5-16a** (0.15 g, 80%) as an off-white solid: ^{1}H NMR (DMSO-d_6) δ 3.55 (s, 3H), 4.26 (d, J = 5.4 Hz, 6H), 7.23-7.32 (m, 15H), 8.85 (t, J = 5.4 Hz, 3H), 10.29 (s, 3H). ^{13}C NMR (DMSO-d_6) δ 31.3, 42.4, 102.9, 126.8, 127.3, 128.3, 138.7, 153.8, 173.4.

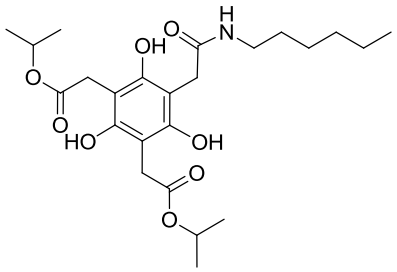

Diisopropyl 2,2'-(5-(2-(hexylamino)-2-oxoethyl)-2,4,6-trihydroxy-1,3-phenylene)diacetate (5-17) To a solution of **2-7** (100 mg, 0.273 mmol) in THF (10 mL) was added hexylamine (30.0 mg, 0.300 mmol). The resulting solution was allowed to stir overnight and then diluted with water and extracted with EtOAc. The organic layer was washed with HCl (0.1 M), water, and brine, sequentially. After removal of the solvent, **5-17** (102 mg, 80%) was isolated as an off-white solid. ^{1}H NMR ($CDCl_3$) δ 0.85–0.89 (m, 3H), 1.24–1.30 (m, 18H), 1.50 (m, 2H), 3.22 (q, J = 7.2 Hz, 2H), 3.60 (s, 2H), 3.76 (s, 4H), 5.02 (quint. J = 6.3 Hz, 2H), 6.00 (t, 1H), 8.62 (s, 1H), 9.41 (s, 1H). ^{13}C NMR ($CDCl_3$) δ 13.9, 21.6, 22.5, 26.4, 29.2, 30.6, 31.4, 32.6, 40.0, 69.9, 102.5, 153.7, 154.0, 174.3, 175.7. HRMS (ESI) calcd for $C_{24}H_{38}NO_8$ $(M + H)^+$ 468.2591, found 468.2602.

X-ray Crystallography

General. Data were collected at 173 K on a Siemens SMART PLATFORM equipped with A CCD area detector and a graphite monochromator utilizing MoK_α radiation (λ = 0.71073

Å). Cell parameters were refined using up to 8192 reflections. A full sphere of data (1850 frames) was collected using the ω-scan method (0.3° frame width). The first 50 frames were re-measured at the end of data collection to monitor instrument and crystal stability (maximum correction on I was < 1 %). Absorption corrections by integration were applied based on measured indexed crystal faces.

The structure was solved by the Direct Methods in *SHELXTL6,* and refined using full-matrix least squares. The non-H atoms were treated anisotropically, whereas the hydrogen atoms were calculated in ideal positions and were riding on their respective carbon atoms.

Compound 5-5. Each hydroxyl proton is involved in an intramolecular H bond. A total of 257 parameters were refined in the final cycle of refinement using 3670 reflections with $I > 2\sigma(I)$ to yield R_1 and wR_2 of 3.71% and 8.97%, respectively. Refinement was done using F^2.

Compound 5-16b. The asymmetric unit consists of two molecules linked together by a water molecule through H bonding. A total of 876 parameters were refined in the final cycle of refinement using 40011 reflections with $I > 2\sigma(I)$ to yield R_1 and wR_2 of 6.16% and 13.08%, respectively. Refinement was done using F^2.

APPENDIX A
SYNTHESIS OF AN ACE2 ACTIVATOR AS AN ANTI-HYPERTENSION DRUG CANDIDATE

Bioactivity and Synthesis of "XNT" as an ACE2 Activator

Angiotensin-converting enzyme 2 (ACE2) has been identified as a new drug target for the treatment of hypertension. Activation of ACE2 can convert more angiotensin I to angiotesin 1-9, therefore lowering the production of angiotensin II which causes high blood pressure. Our collaborators have found one xanthenone derivative, XNT, to be a very powerful ACE2 activator and potential antihypertensive (Figure A-1).[256] Although it is a known compound, the reported synthesis (Figure A-2) has considerable practical flaws that precluded the large-scale synthesis required for biological testing.

(a) (b)

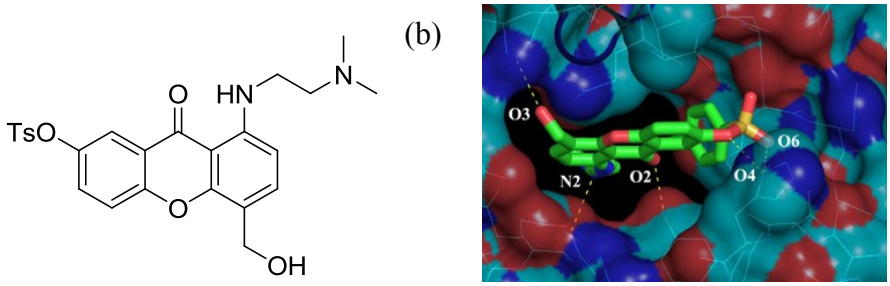

Figure A-1. (a) The chemical structure of XNT and (b) molecular docking model of ACE2 with its small-molecule activator (XNT).

The published synthetic route[257] to XNT is shown in Figure A-2(a). One of the major problems is at the second step in the synthesis. When fusing the xanthone ring by a dehydration reaction with PPA, the poor regioselectivity of the precursor causes a loss of half of the material and an extremely difficult separation of two regioisomers. The last step that introduces the hydroxymethyl group onto the xanthone core also has a regioselectivity problem and the reaction suffers from a low yield (30%) and long reaction time (3 days). For the rest of the synthesis, almost every step needs column chromatography for purification which is not convenient for scaling up the synthesis.

An improved synthetic route to XNT was designed that solved the regioselectivity problem described above by beginning with 2-chloro-4-iodo-toluene as a starting material; the pendant methyl group could be converted to the required hydroxymethyl group later in the synthesis (Scheme 5). Although the new route is one step longer than the original one, the overall yield increased from less than 2% to 14%, in part also because most of the intermediates could be purified now by recrystallization. This approach has produced gram quantities of XNT that has been used in further testing of the drug and subsequent publications.[258]

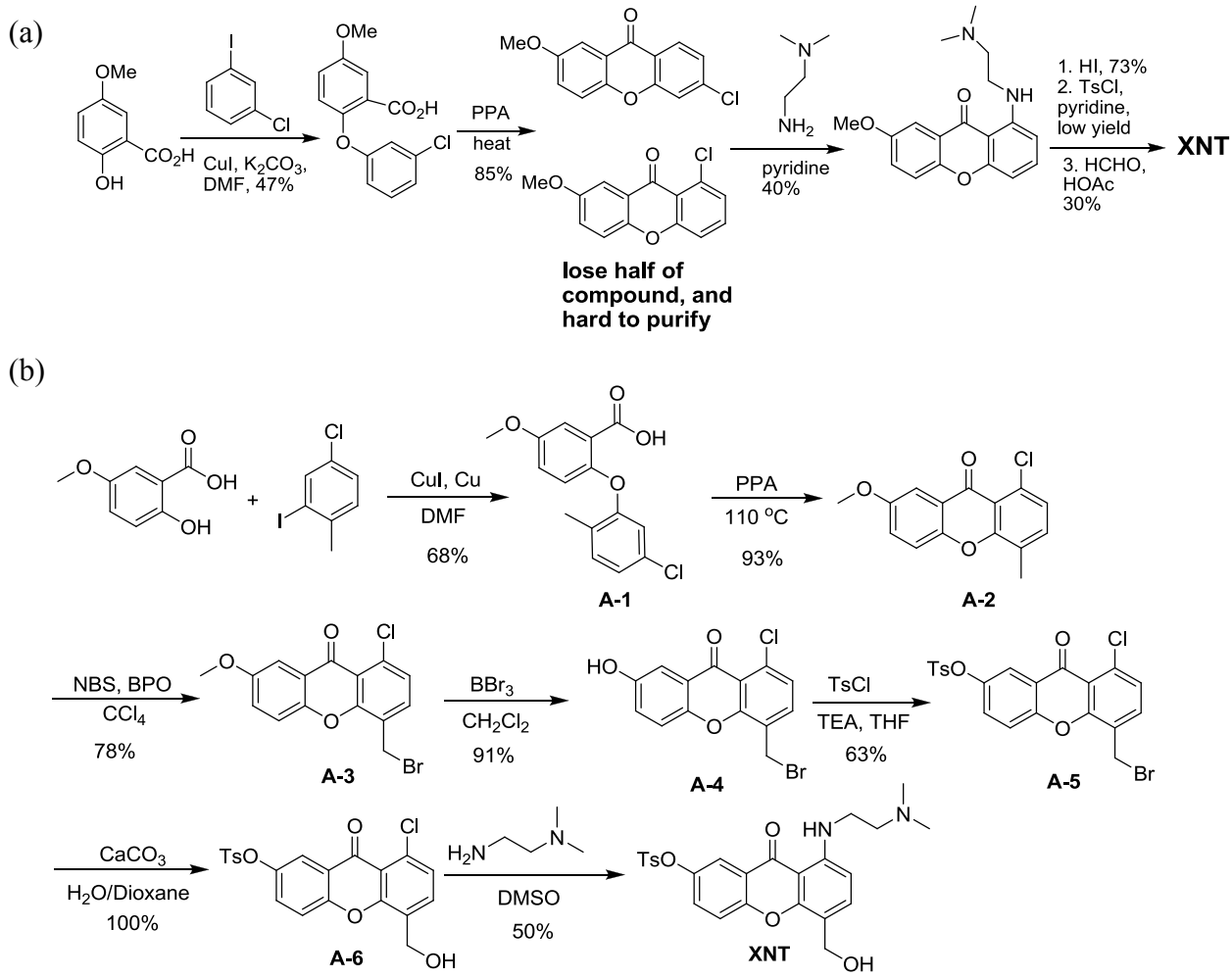

Figure A-2. Different synthetic routes of XNT molecule: (a) reported route and (b) redesigned route.

Experimental Section

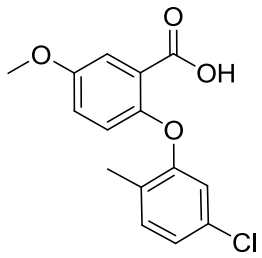

2-(2-Chloro-5-iodophenoxy)-5-methoxybenzoic acid (A-1). 2-(2-Chloro-5-iodophenoxy)-5-methoxybenzoic acid (A-1). A suspension of 5-methoxysalicylic acid (15 g, 90 mmol) and anhydrous K_2CO_3 (24.6 g, 180 mmol) in dry DMF (300 mL) was heated to 120 ºC for 10 min. 4-Chloro-2-iodo-1-toluene (15 mL, 108 mmol) was added dropwise, followed by the addition of Cu (0.3 g, 4.5 mmol) and freshly prepared CuI (0.84 g, 4.5 mmol). The resulting mixture was heated to reflux under argon for 48 hours. The reaction mixture was cooled to room temperature and the insoluble material was removed by suction filtration. The filtrate was concentrated to yield a gummy residue which was then dissolved in water. The resulting aqueous solution was acidified (pH = 2) with 2 M HCl, and extracted with EtOAc. The organic layer was washed with water and brine, decolorized with activated charcoal, dried with $MgSO_4$, and concentrated under reduced pressure. The resulting residue was recrystallized from hexanes/EtOAc to give **A-1** (17.71 g, 68%) as off-white, needle-like crystals: ^{1}H NMR ($CDCl_3$) δ 2.25 (s, 3H), 3.87 (s, 3H), 6.76 (d, J = 9.3 Hz, 1H), 6.85 (d, J = 2.7 Hz, 1H), 7.05-7.12 (m, 2H), 7.21 (d, J = 8.4 Hz, 1H), 7.68 (d, J = 3 Hz, 1H). HRMS (APCI-TOF) calcd. for $C_{15}H_{14}ClO_4$ (M+H) 293.0575, found 293.0578.

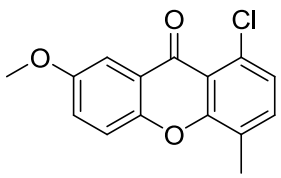

1-Chloro-7-methoxy-4-methyl-9H-xanthen-9-one (A-2). To polyphosphoric acid (115% as H_3PO_4 equivalent, 50.0 g) preheated to 120 ºC was added **A-1** (6.60 g, 22.5 mmol). The solution was stirred at 110–120 ºC for 6 hours, after which it was poured into water (400 mL). After dissolving the yellow gum, the resulting suspension was neutralized with 10% NaOH and then extracted with CH_2Cl_2 (3 × 150 mL). The combined organic layers were washed with water, brine, dried with $MgSO_4$, and the removal of the solvent under reduced pressure gave **A-2** (5.74 g, 93%) as a white solid: ^{1}H NMR ($CDCl_3$) δ 2.51 (s, 3H), 3.92 (s, 3H), 7.25–7.34 (m, 2H), 7.40–7.45 (m 2H), 7.69 (d, J = 3.3 Hz, 1H); ^{13}C NMR δ 16.0, 55.9, 106.0, 117.9, 118.9, 122.6, 124.7, 126.1, 126.5, 131.5, 134.4, 149.7, 155.8, 156.2, 176.2. HRMS (APCI-TOF) calcd. for $C_{15}H_{12}ClO_3$ (M+H) 275.0469, found 275.0470.

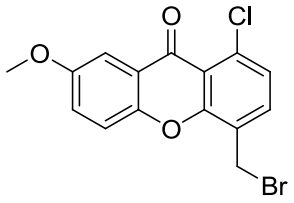

4-(Bromomethyl)-1-chloro-7-methoxy-9H-xanthen-9-one (A-3). To CCl_4 (200 mL) was added **A-2** (5.00 g, 18.2 mmol), *N*-bromosuccinimide (4.00 g, 21.8 mmol), and benzoylperoxide (200 mg); the resulting solution was heated to reflux overnight. When cooling the reaction solution to room temperature, crystals formed that were filtered off by the suction filtration. The crystals were dissolved in CH_2Cl_2, washed with water and brine, dried with $MgSO_4$, and the removal of the solvent in vacuo gave pure **A-3**. The filtrate of the first filtration was concentrated under reduced pressure, and the residue was dissolved in CH_2Cl_2 and washed with water and brine. After removal of the solvent in vacuo, the resulting solid was recrystallized to give **A-3**. The two batches of product were combined to give **A-3** (5.00 g, 78%) as a white solid: ^{1}H NMR ($CDCl_3$) δ 3.93 (s, 3H), 4.78 (s, 2H), 7.34-7.38 (m, 2H), 7.50 (d, J = 9 Hz, 1H), 7.63 (d, J = 8.2

Hz, 1H), 7.7 (d, J = 3 Hz, 1H); HRMS (ESI-TOF) calcd. for $C_{15}H_{11}BrClO_3$ (M+H) 354.9553, found 354.9572.

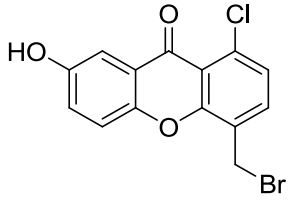

4-(Bromomethyl)-1-chloro-7-hydroxy-9H-xanthen-9-one (A-4). The solution of **A-3** (4.20 g, 11.8 mmol) in CH_2Cl_2 (400 mL) was cooled to –78 ºC and treated with BBr_3 (29.8 g, 118 mmol). The resulting mixture was stirred at –78 ºC for 2 hours and warmed to room temperature with stirring for 3 hours. The reaction was quenched by the addition of a few mLs of $NaHCO_3$ (aq., saturated); the resulting mixture was poured into cold $NaHCO_3$ (aq., saturated) and extracted with EtOAc. The organic layer was separated, dried with anhydrous Na_2SO_4, and then the solvent was removed in vacuo to give **A-4** (3.68 g, 91%) as an off-white solid: ^{1}H NMR (DMSO-d_6) δ 4.96 (s, 2H), 7.32 (dd, J = 3.0 and 9.0 Hz, 1H), 7.41-7.46 (m, 2H), 7.70 (d, J = 9.0 Hz, 1H), 7.90 (d, J = 8.1 Hz, 1H); ^{13}C NMR δ 27.5, 108.7, 117.4, 119.1, 122.2, 124,5, 126.3, 126.5, 133.0, 135.2, 147.6, 154.3, 154.7, 174.3. HRMS (ESI-TOF) calcd. for $C_{14}H_9BrClO_3$ (M+H) 340.9396, found 340.9382.

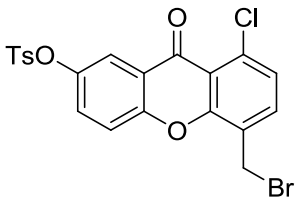

5-(Bromomethyl)-8-chloro-9-oxo-9H-xanthen-2-yl 4-methylbenzenesulfonate (A-5). To the solution of **A-4** (3.60 g, 10.5 mmol) in dry THF (100 mL) was added TsCl (3.02 g, 15.9 mmol) and triethylamine (7.3 mL, 52.5 mmol). The resulting solution was heated to reflux for 3 hours (monitored by TLC until all starting material disappeared), and then cooled to room

temperature. The solvent was removed in vacuo and the residue was taken up in CH_2Cl_2 and washed with water and brine, and dried with $MgSO_4$. The solution was concentrated in vacuo and purified by column chromatography (2:1 CH_2Cl_2/hexanes) to afford **A-5** (3.30 g, 63%) as a white solid: ^{1}H NMR ($CDCl_3$) δ 2.46 (s, 3H), 4.87 (s, 2H), 7.33–7.40 (m, 3H), 7.50–7.59 (m, 2H), 7.67–7.75 (m, 4H); ^{13}C NMR δ 21.7, 39.8, 118.3, 119.4, 119.7, 122.7, 125.7, 127.1, 128.4, 129.9, 130.0, 131.8, 134.8, 135.1, 145.9, 146.0, 152.7, 154.9, 174.4. HRMS (APCI-TOF) calcd. for $C_{21}H_{15}BrClO_5S$ (M+H) 494.9486, found 494.9492.

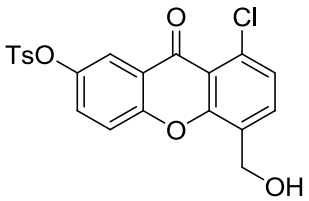

8-Chloro-5-(hydroxymethyl)-9-oxo-9H-xanthen-2-yl 4-methylbenzenesulfonate (A-6). To the solution of **A-5** (1.50 g, 3.03 mmol) in 1,4-dioxane (100 mL) was added water (100 mL) and $CaCO_3$ (1.52 g, 15.2 mmol), and then the resulting suspension was heated to reflux overnight. The cooled reaction mixture was neutralized with 1 M HCl (to pH = 5) and then extracted with EtOAc; the organic layer was dried with anhydrous Na_2SO_4, followed by the removal of solvent to give **A-6** (1.31 g, quantitative) as a white solid: ^{1}H NMR (DMSO-*d6*) δ 2.42 (s, 3H), 4.80 (d, *J* = 6.0 Hz, 2H), 5.51 (t, *J* = 6 Hz, 1H), 7.46- 7.51 (m, 4H), 7.67-7.84 (m, 5H); ^{13}C NMR δ 21.1, 57.1, 116.8, 118.4, 120.3, 122.1, 126.6, 128.2, 129.4, 130.2, 130.4, 130.8, 131.2, 132,4, 144.9, 146.0, 152.5, 153.8, 173.9. HRMS (ESI-TOF) calcd. for $C_{21}H_{16}ClO_6S$ (M+H) 4301.0351, found 431.0339.

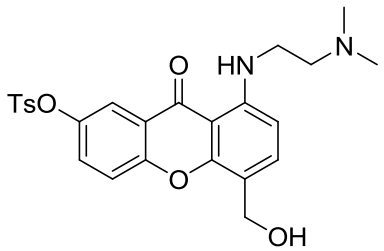

8-(2-(Dimethylamino)ethylamino)-5-(hydroxymethyl)-9-oxo-9H-xanthen-2-yl 4-methylbenzenesulfonate (XNT). To the solution of **A-6** (1.20 g, 2.78 mmol) in DMSO (10 mL) was added *N*,*N*-dimethylethane-1,2-diamine (4.5 mL, 42 mmol), and the resulting solution was heated to reflux (bath temperature 150 ºC) for 3 hours. The solution was cooled to room temperature, poured into water (300 mL), and extracted with CH_2Cl_2. The organic layer was washed with brine, dried over anhydrous $NaSO_4$, and concentrated under reduced pressure. The residue was purified by column chromatography (15:1 CH_2Cl_2/methanol) to afford **XNT** (0.66 g, 50%) as a yellow solid: ^{1}H NMR ($CDCl_3$) δ 2.34 (s, 6H), 2.46 (s, 3H), 2.65 (t, *J* = 6.6 Hz, 2H), 3.34 (q, *J* = 6.6 Hz, 2H), 4.82 (s, 2H), 6.42 (d, *J* = 9 Hz, 1H), 7.31–7.40 (m, 4H), 7.52 (d, *J* = 9 Hz, 1H), 7.72 (d, *J* = 8.1 Hz, 2H), 7.79 (d, *J* = 2.7 Hz, 1H), 9.51 (t, *J* = 4.8 Hz, 1H); ^{13}C NMR δ 21.7, 45.7, 45.3, 57.6, 59.9, 103.7, 106.1, 113.5, 118.8, 119.3, 122.5, 128.5, 128.6, 129.9, 131.9, 136.8, 145.3, 145.7, 151.3, 153.2, 155.2, 178.4. Anal. Calcd for $C_{25}H2_6N_2O_6S$: C, 62.23; H, 5.43; N, 5.81 Found: C, 61.93; H, 5.41; N, 5.71.

APPENDIX B
NMR SPECTRA

2-7 ^{1}H NMR ($CDCl_3$)

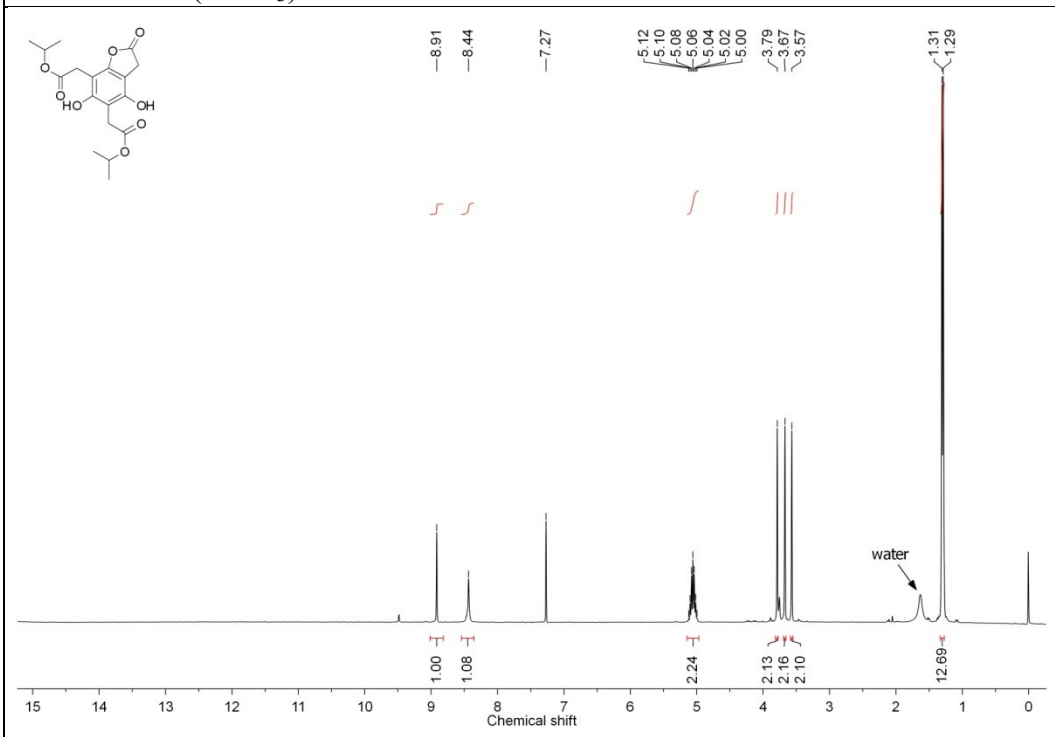

2-8 ^{1}H NMR (DMSO-d_6)

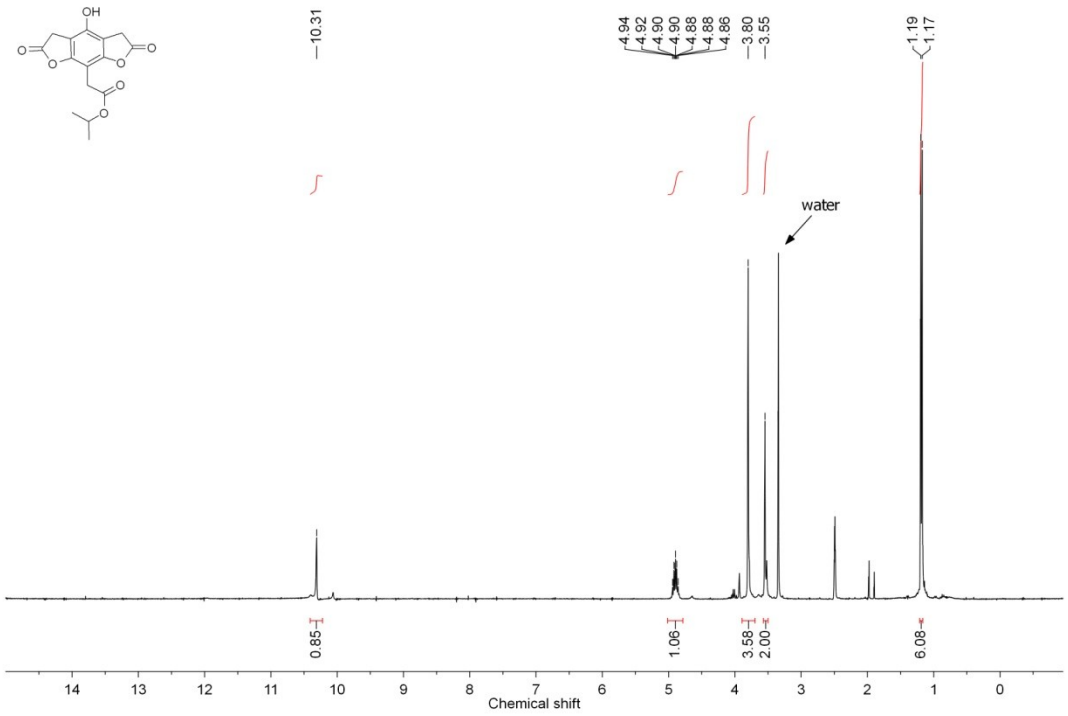

2-9 ^{1}H NMR ($CDCl_3$)

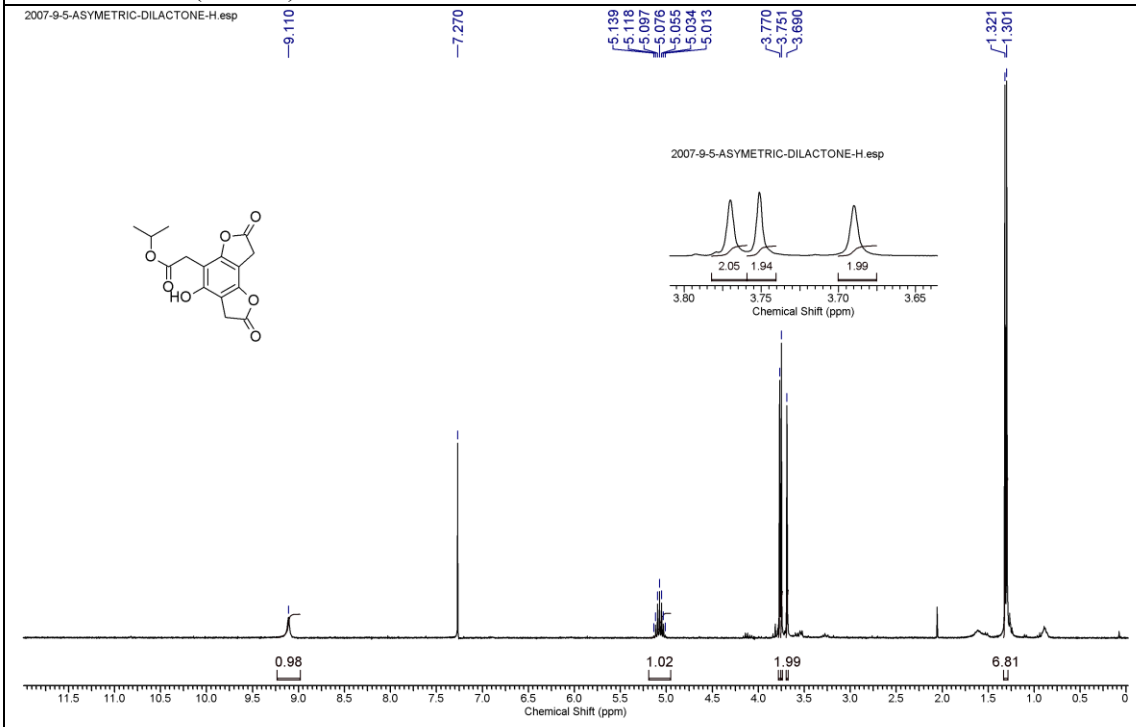

2-10 ^{1}H NMR (DMSO-d_6)

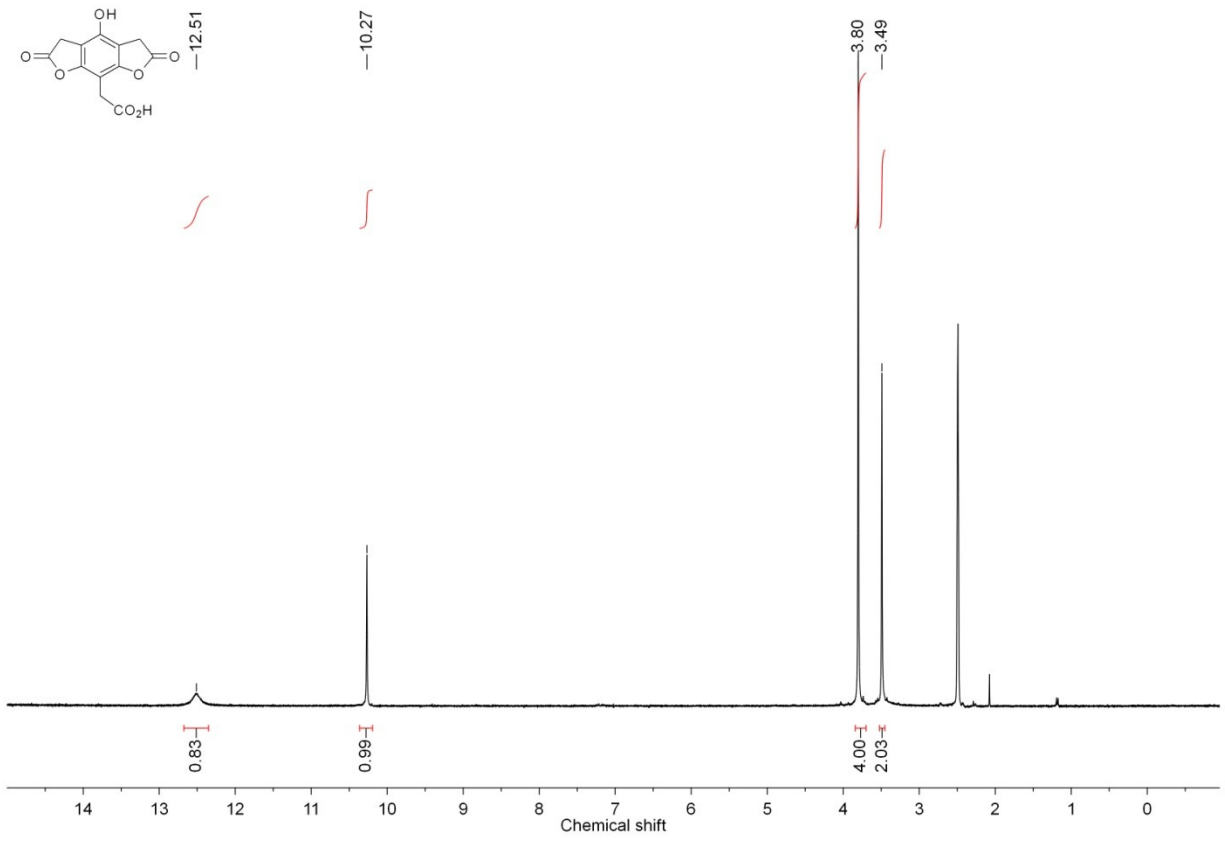

2-13a ^{1}H NMR ($CDCl_3$)

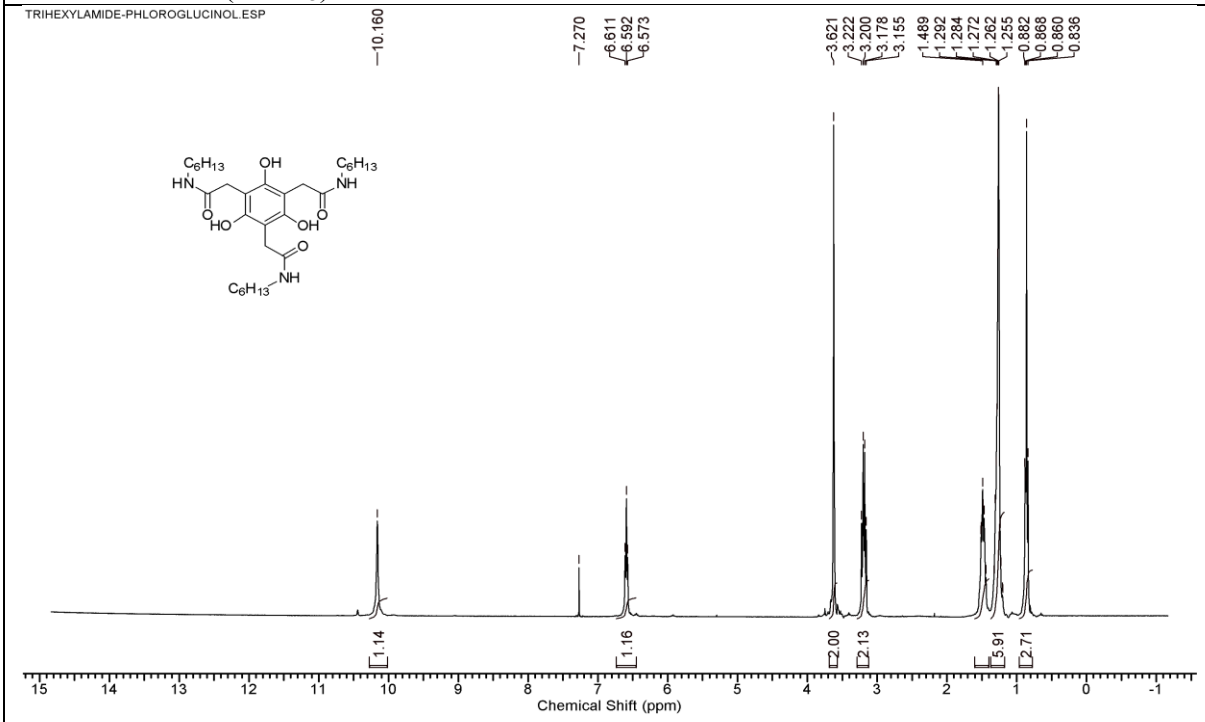

2-13b ^{1}H NMR ($CDCl_3$)

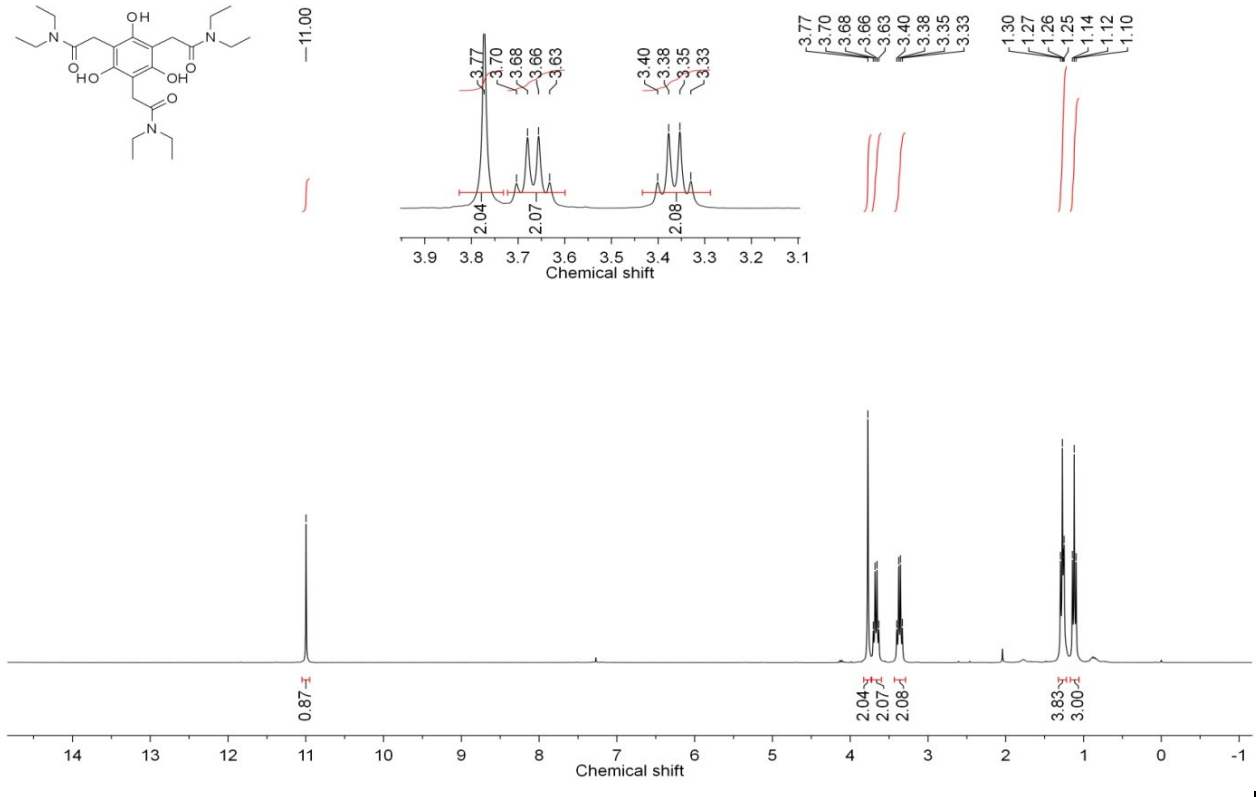

2-13c ^{1}H NMR ($CDCl_3$)

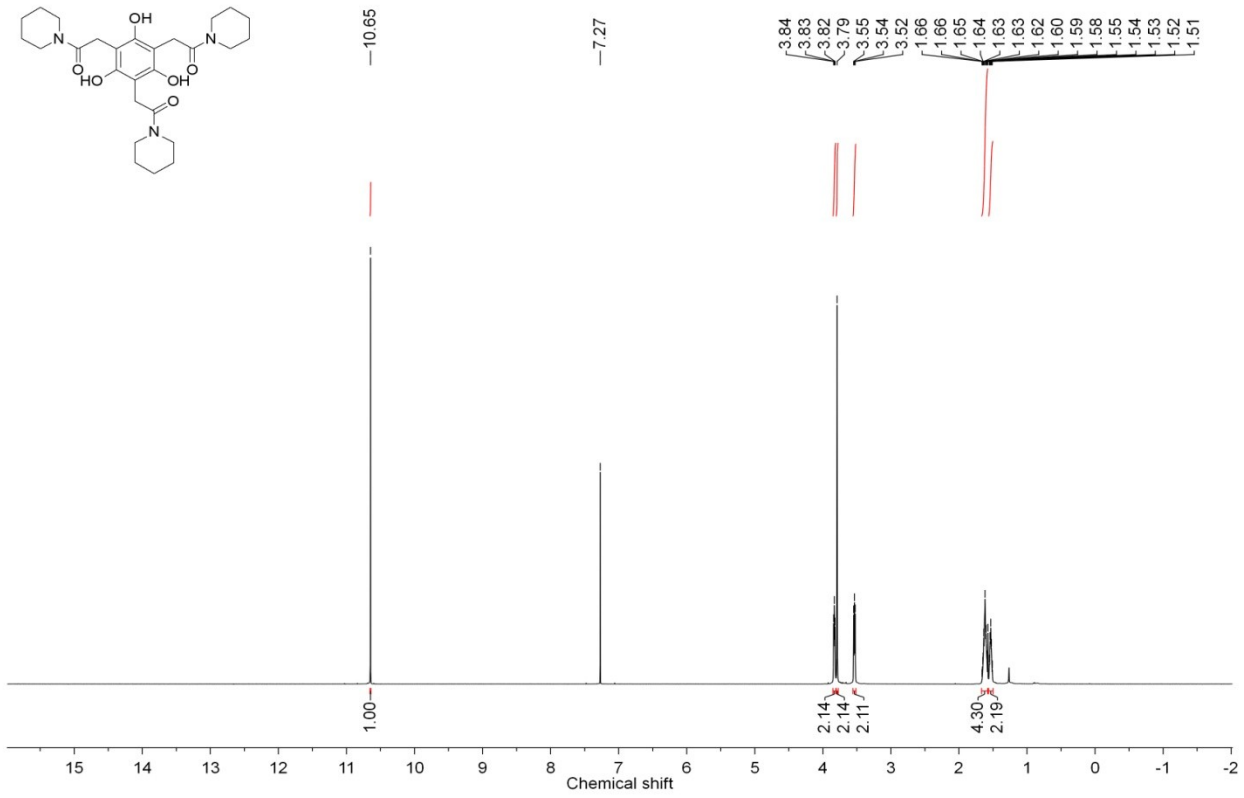

2-13d ^{1}H NMR ($CDCl_3$)

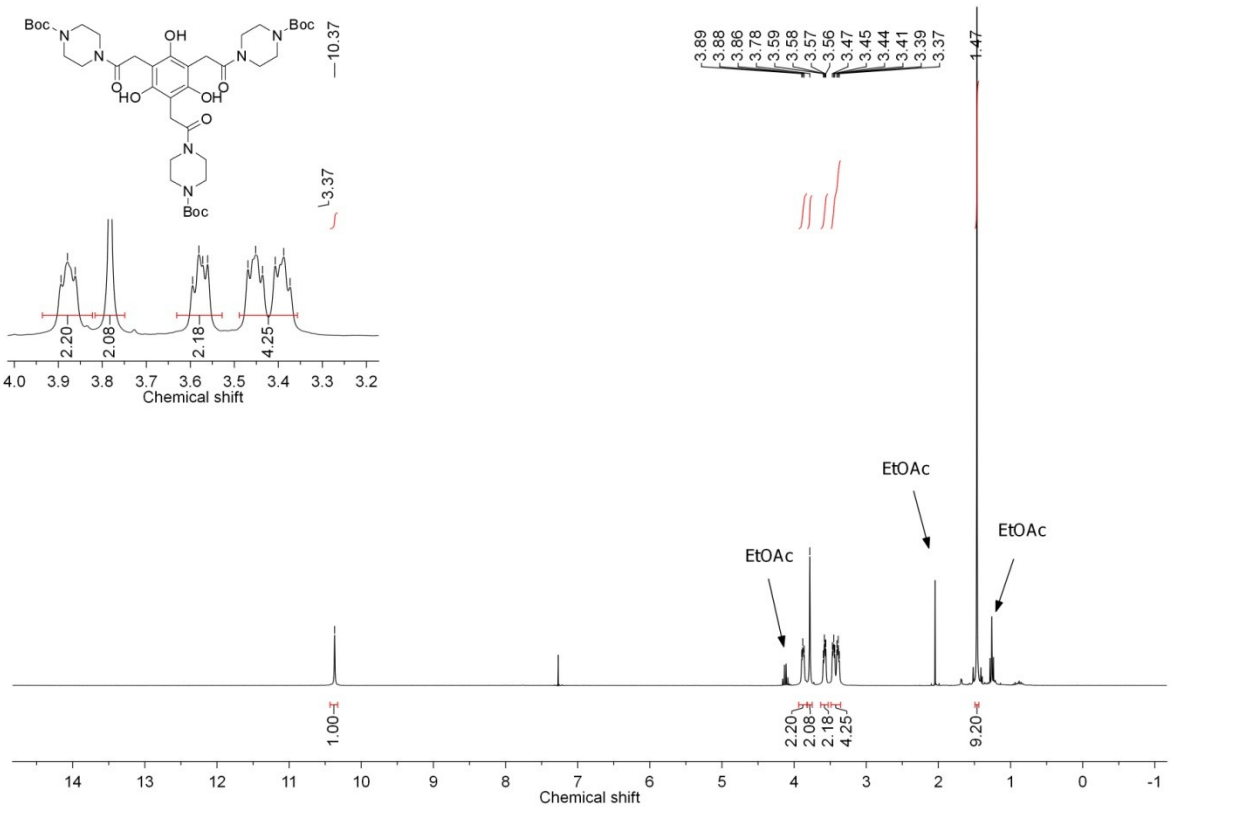

2-14 ^{1}H NMR (DMSO-d_6)

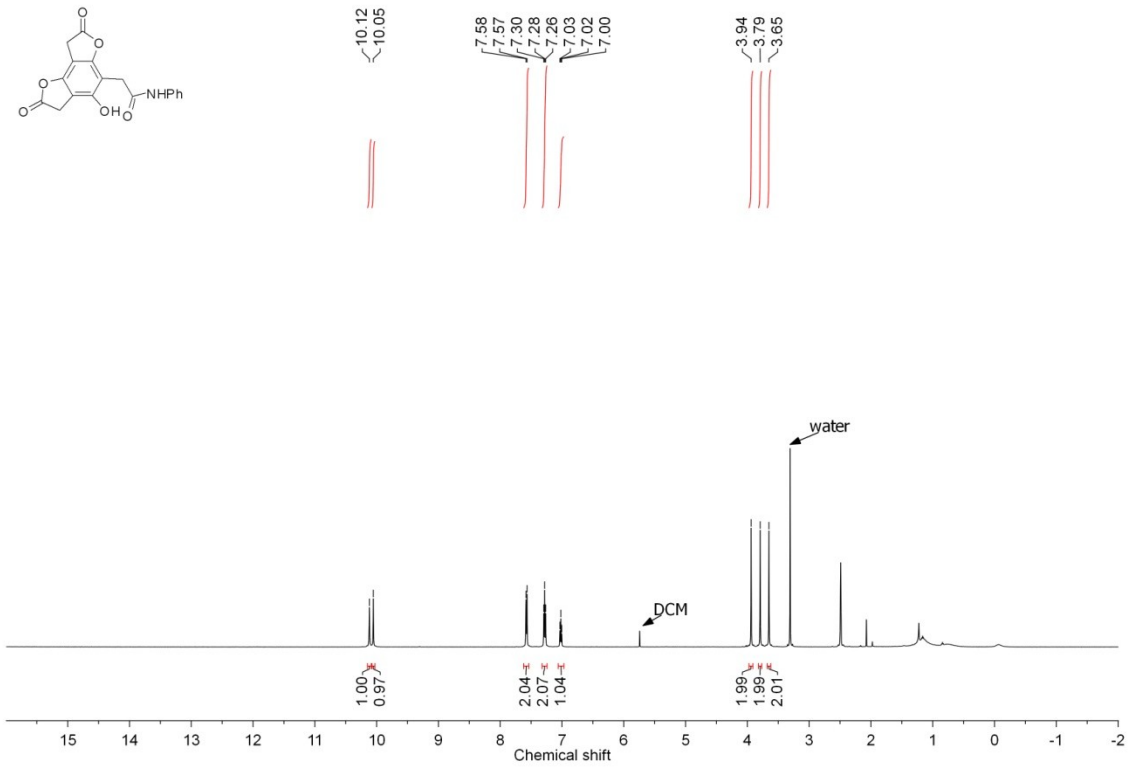

2-15 ^{1}H NMR (DMSO-d_6)

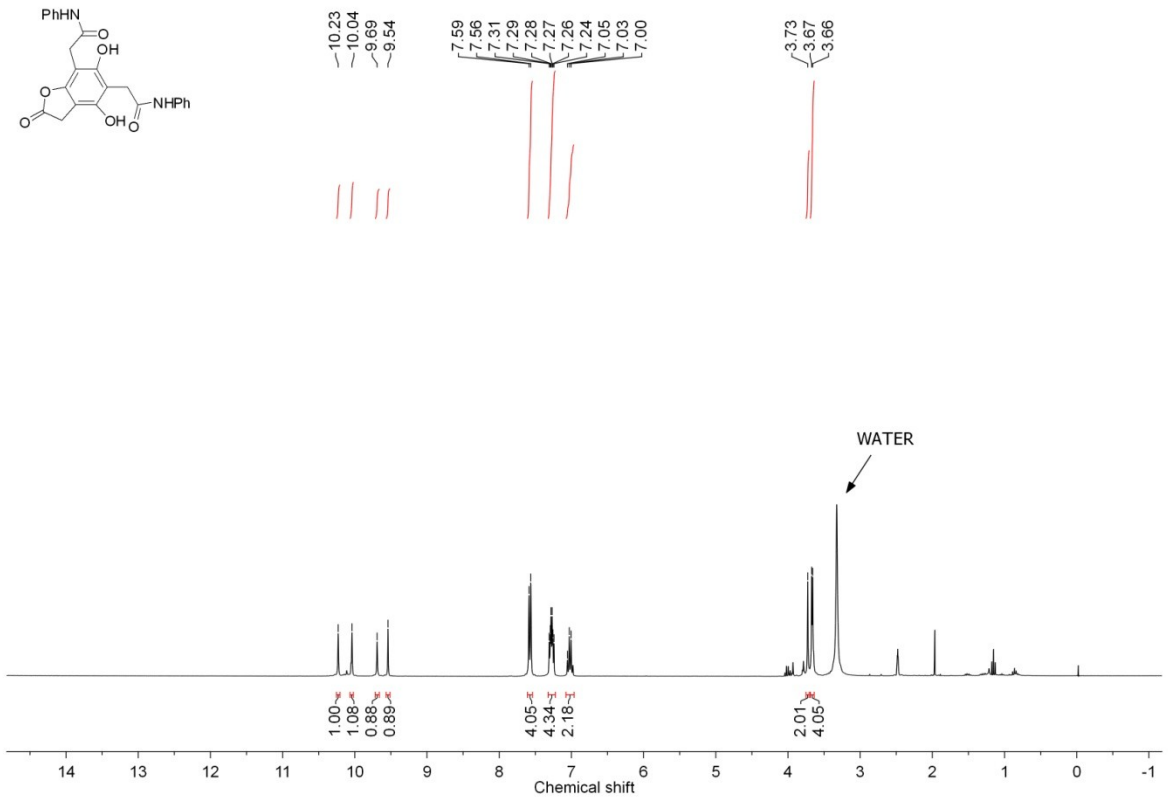

2-17 ^{1}H NMR (DMSO-d_6)

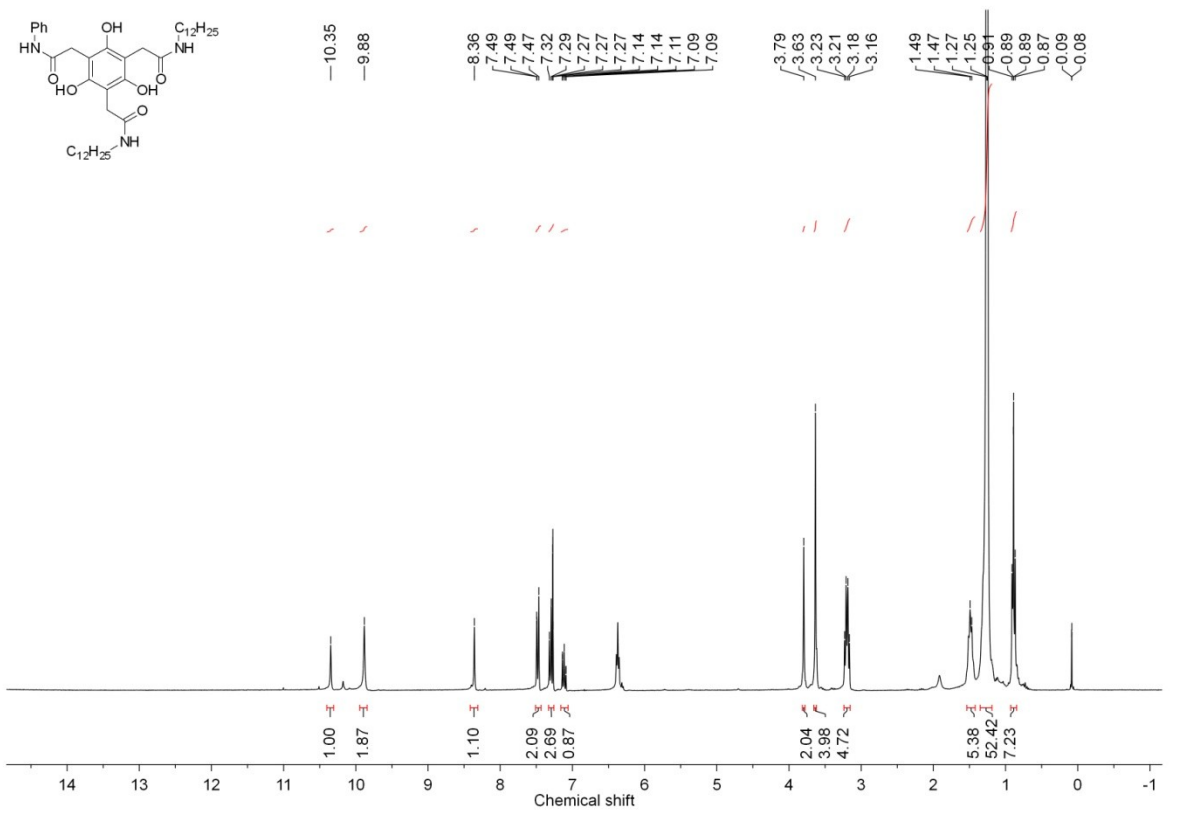

2-18a ^{1}H NMR ($CDCl_3$)

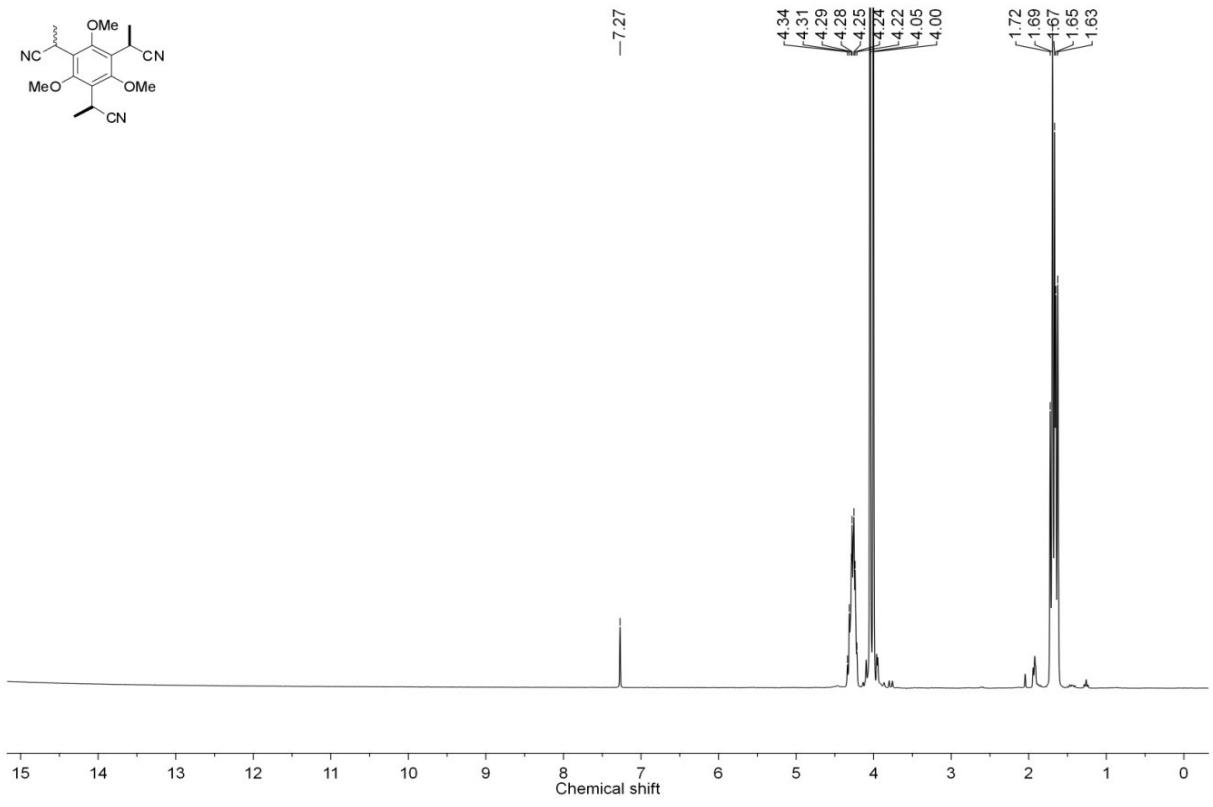

2-18b ^{1}H NMR ($CDCl_3$)

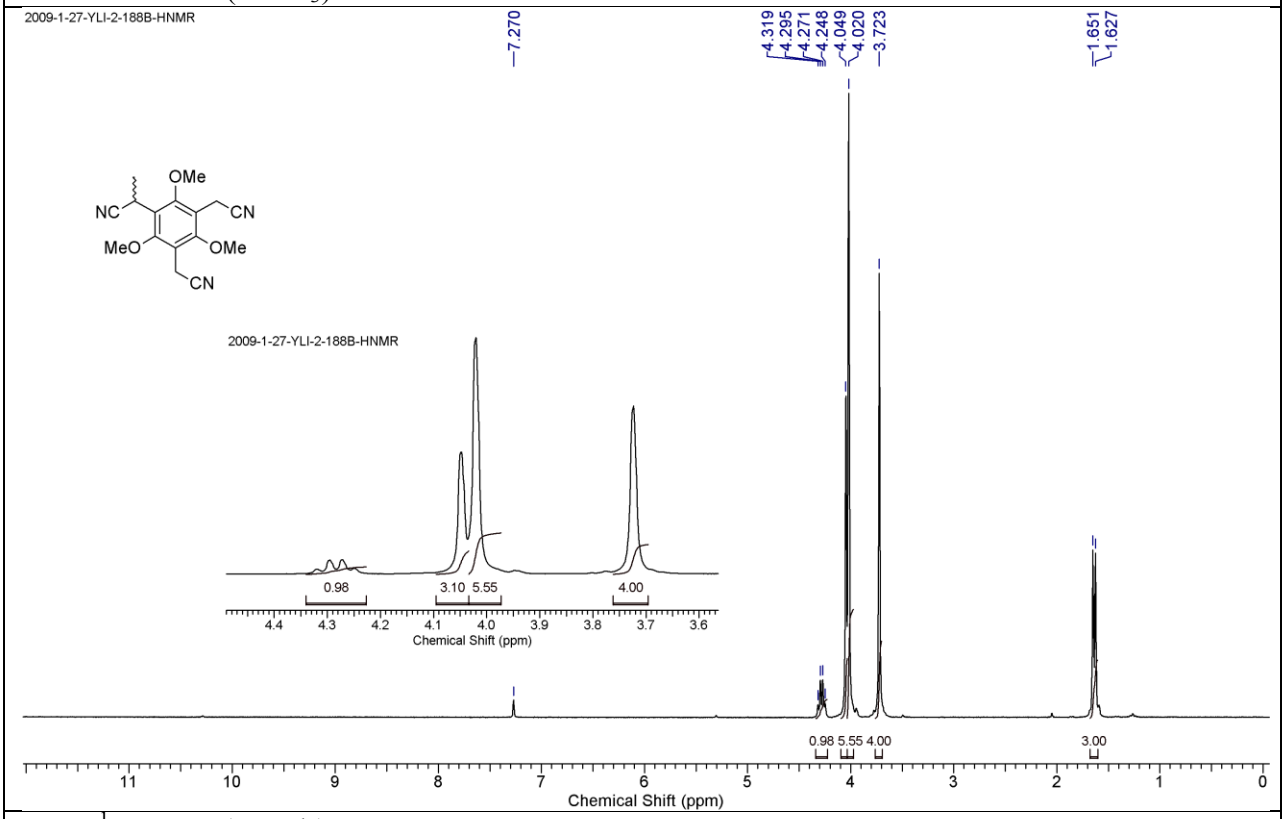

2-18c ^{1}H NMR ($CDCl_3$)

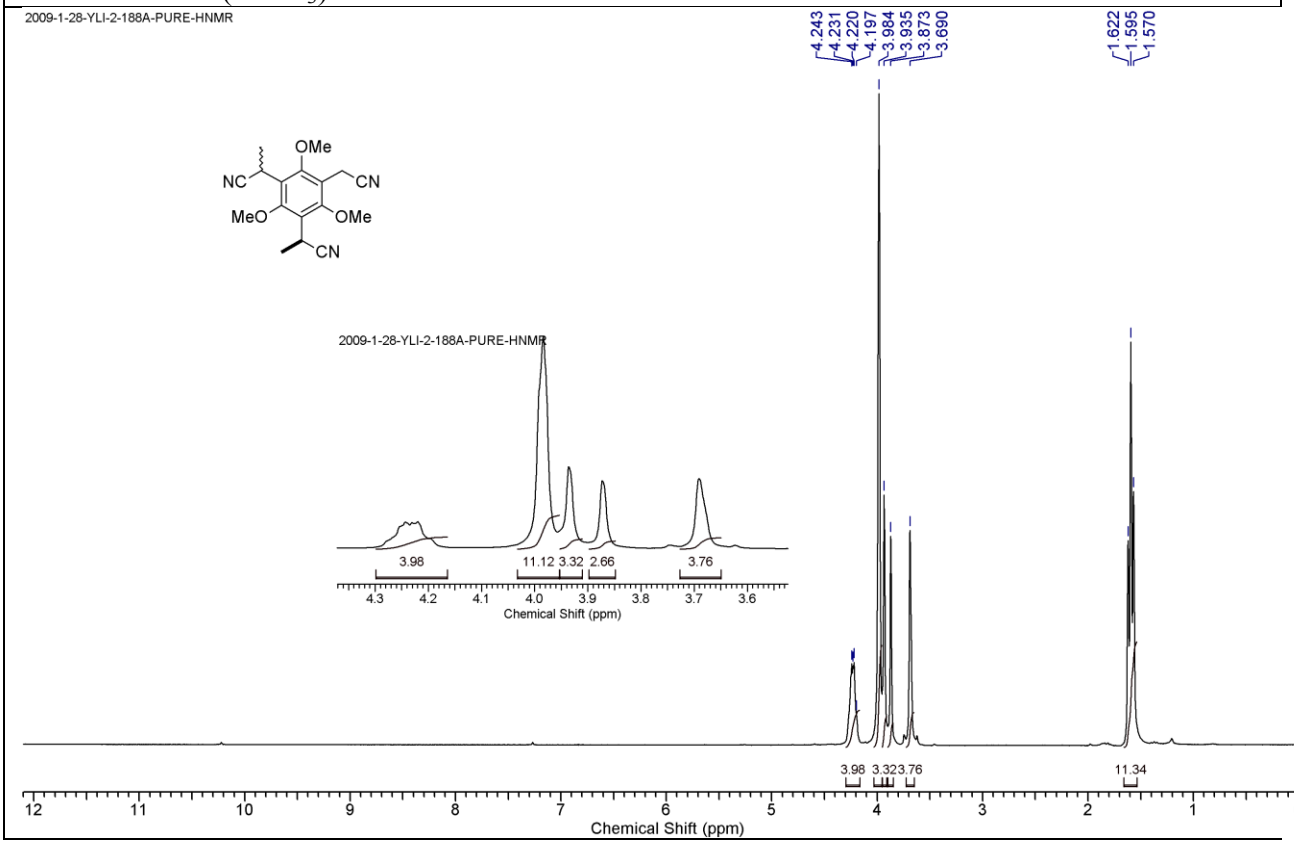

2-18d(*syn*) ^{1}H NMR ($CDCl_3$)

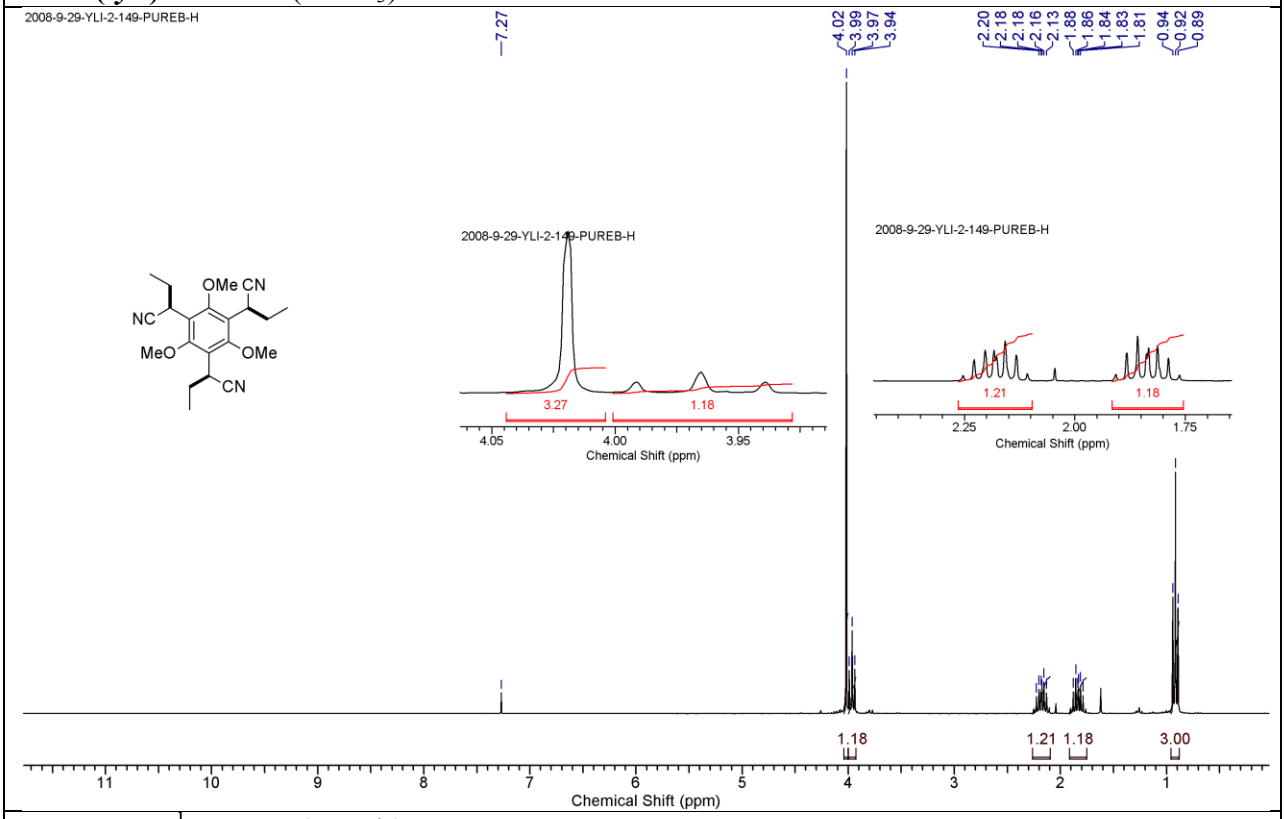

2-18d(*anti*) ^{1}H NMR ($CDCl_3$)

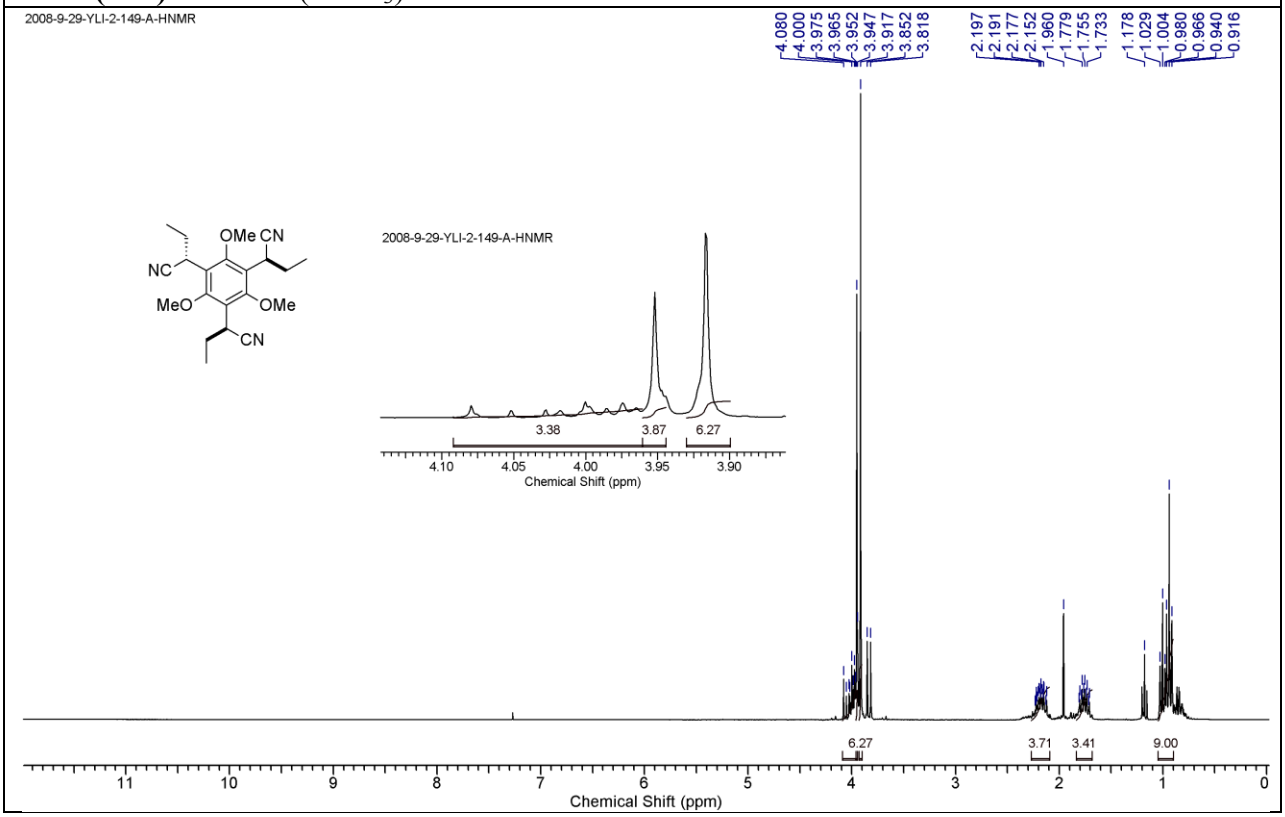

2-23a ^{1}HNMR ($CDCl_3$)

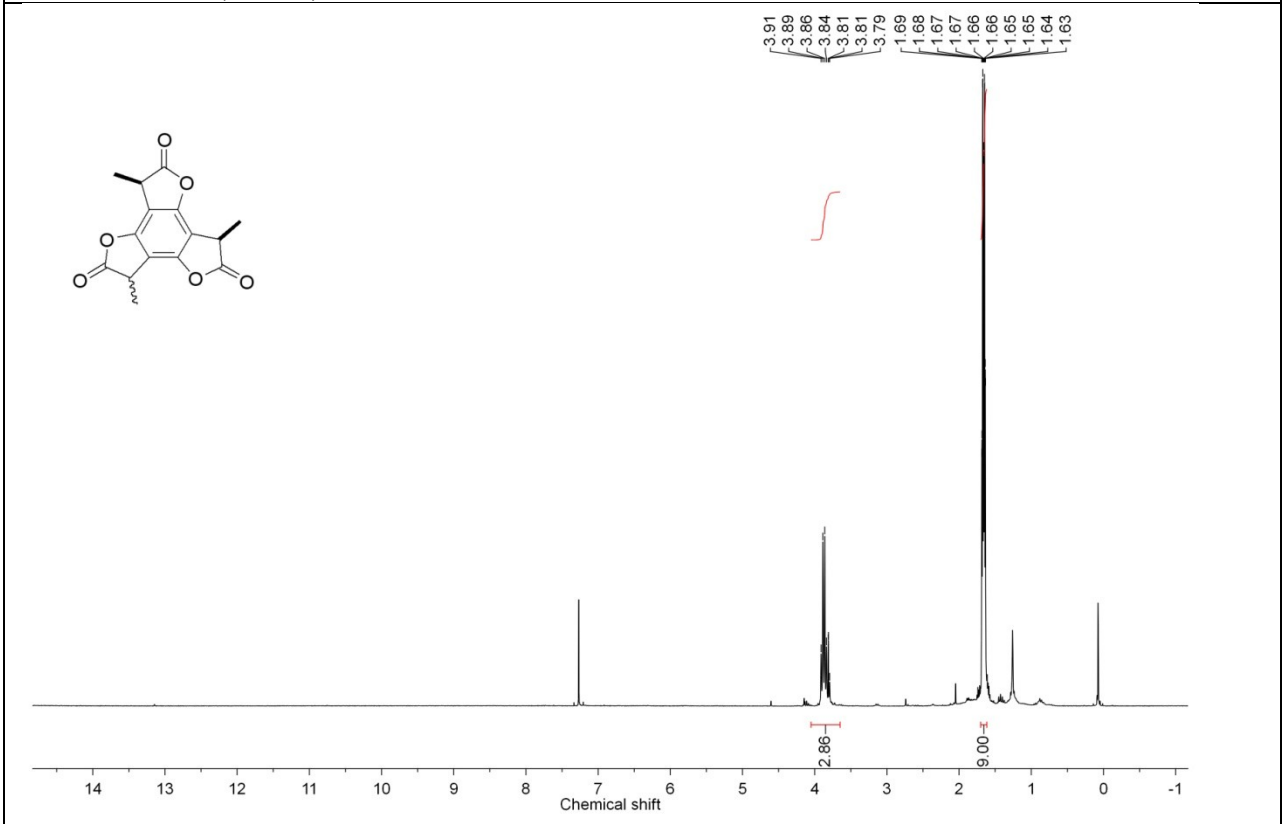

2-23a ^{1}HNMR (bezene-d_6)

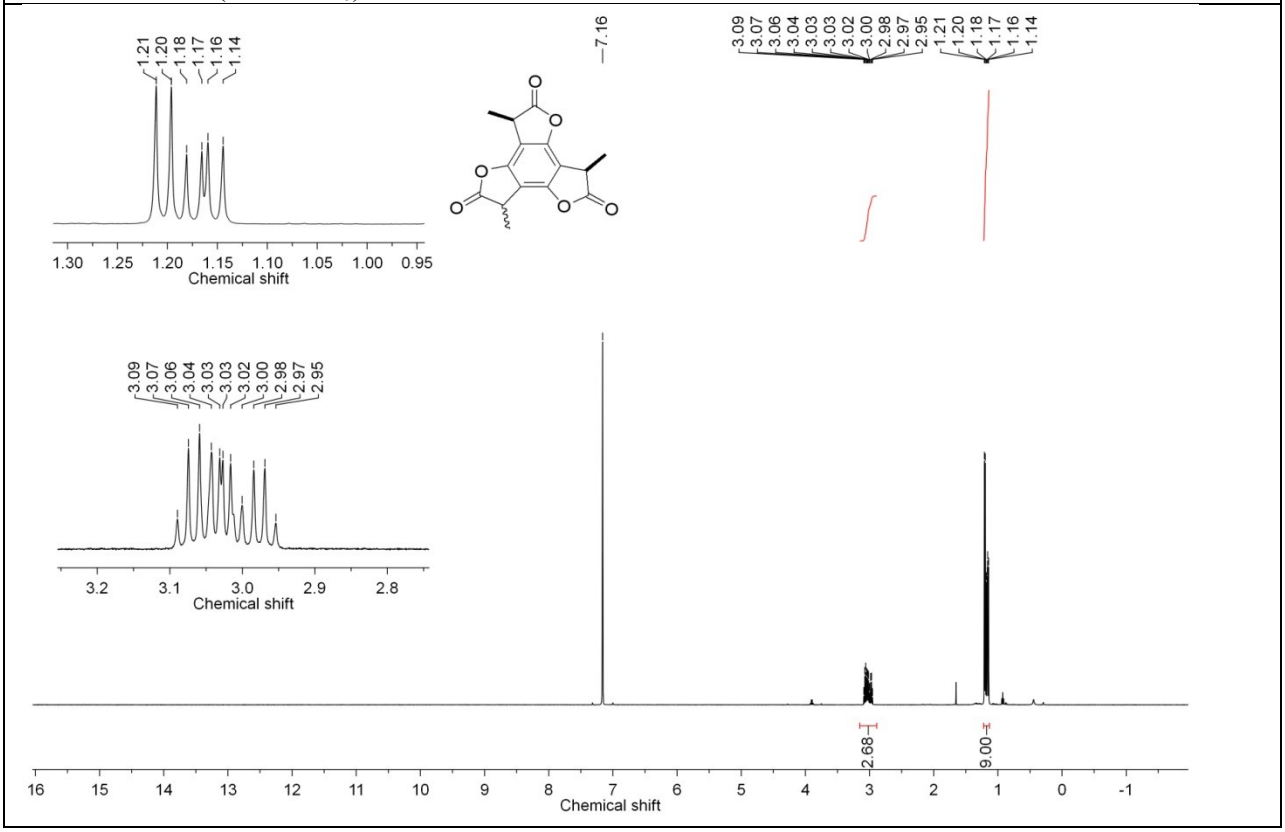

2-23b ^{1}HNMR ($CDCl_3$)

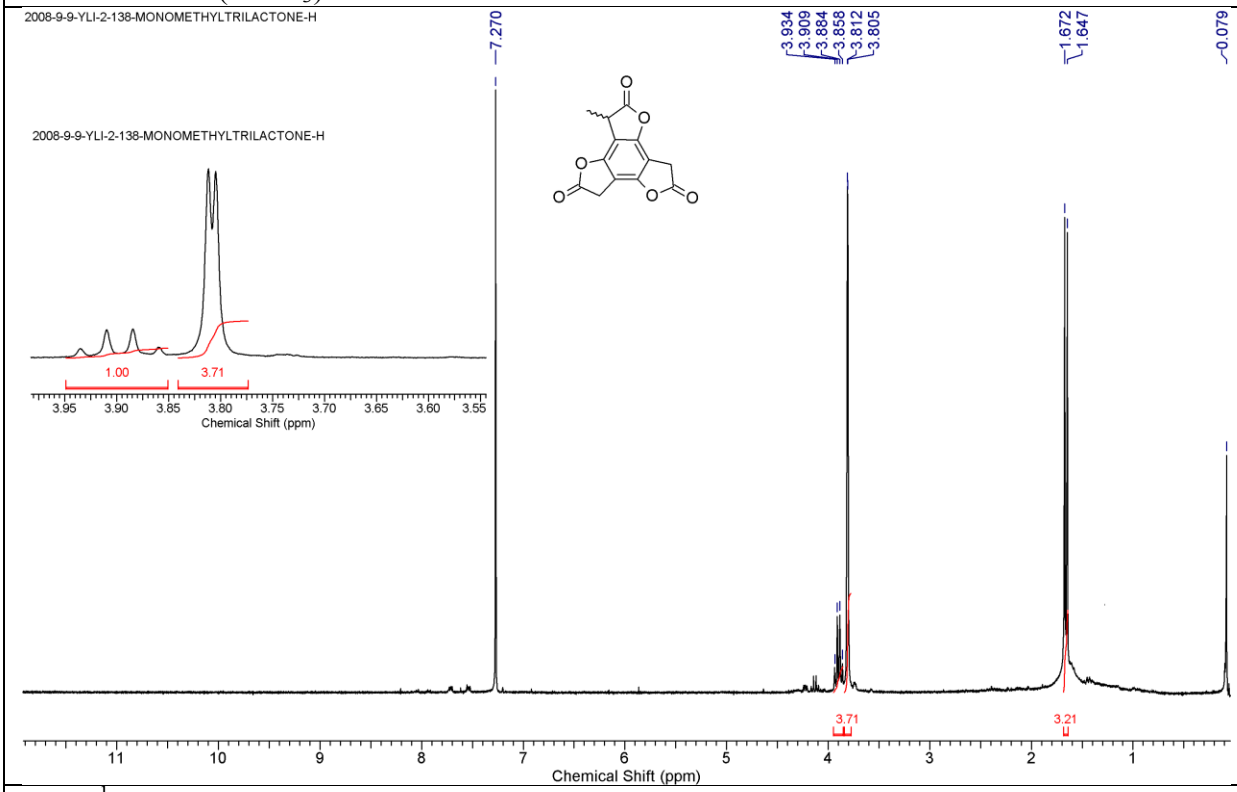

2-23c ^{1}HNMR

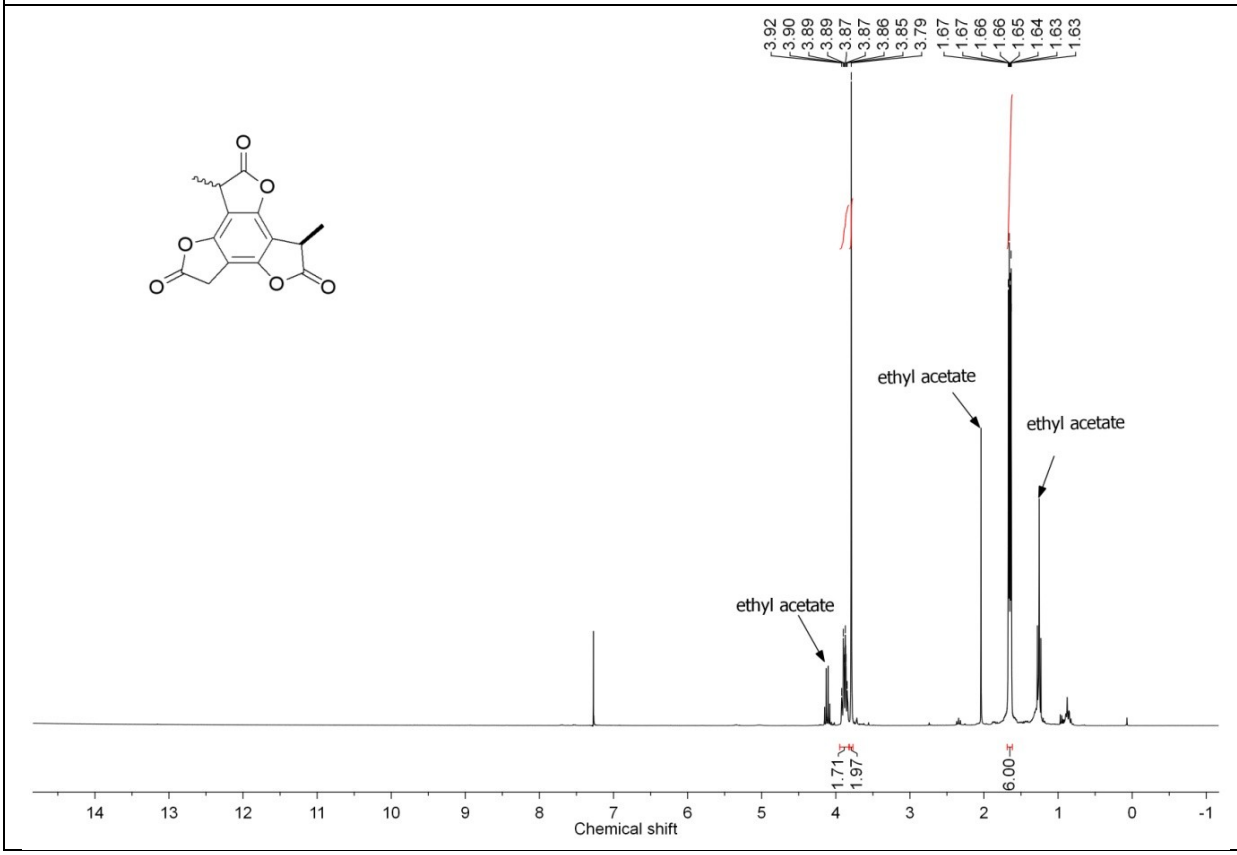

2-23d ^{1}HNMR ($CDCl_3$)

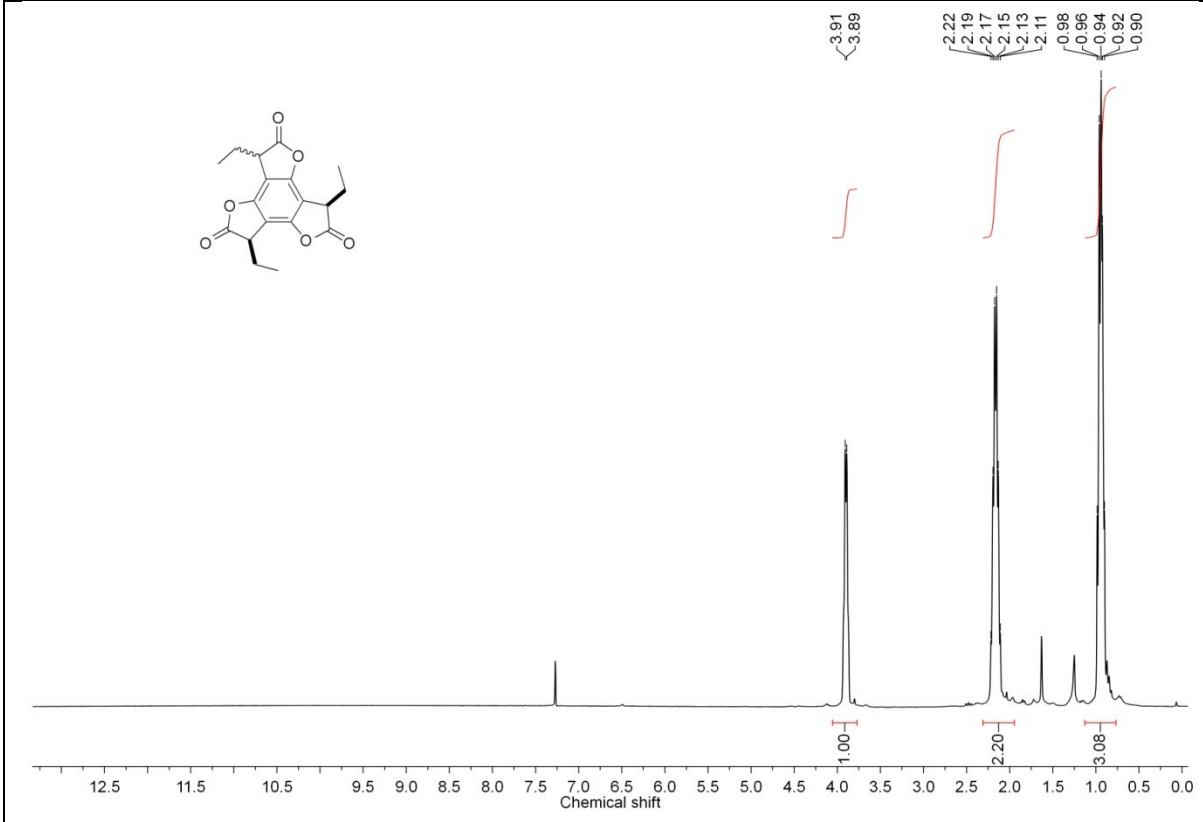

2-24 ^{1}H NMR ($CDCl_3$)

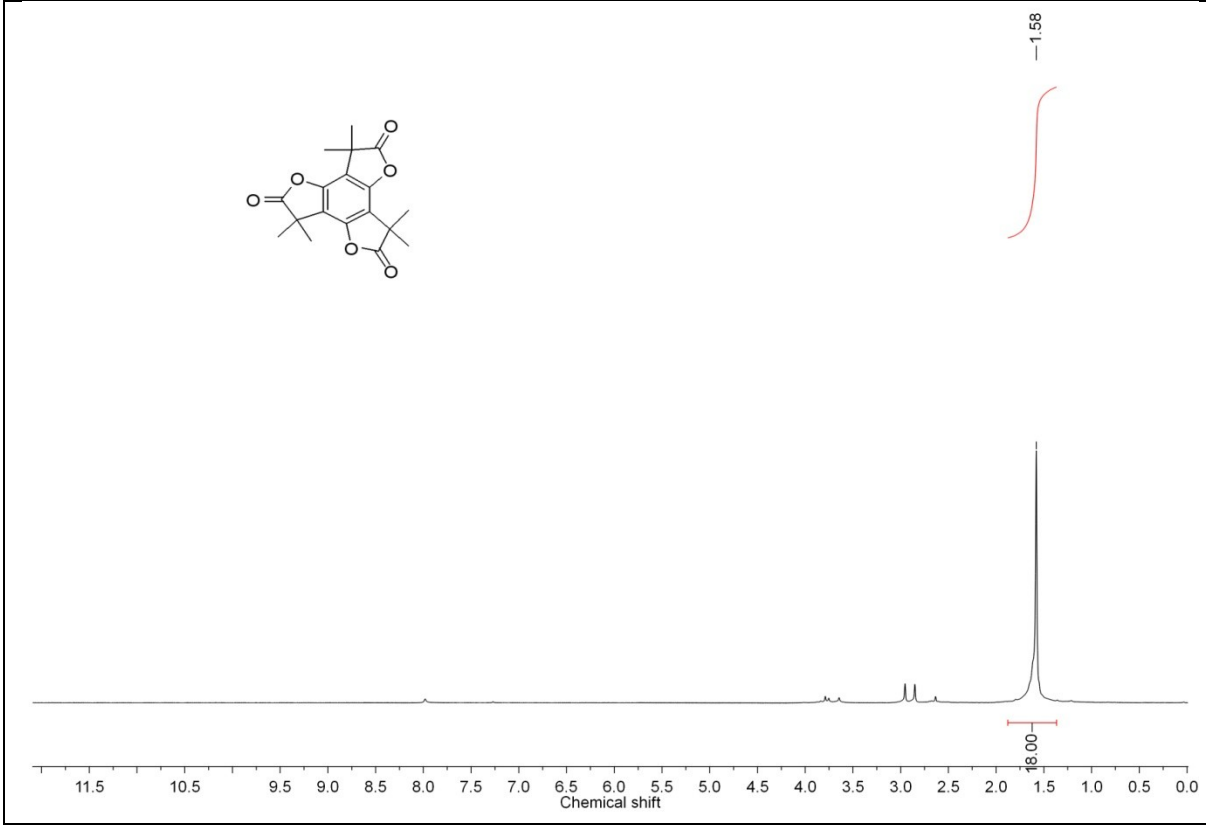

3-2c ^{1}H NMR ($CDCl_3$)

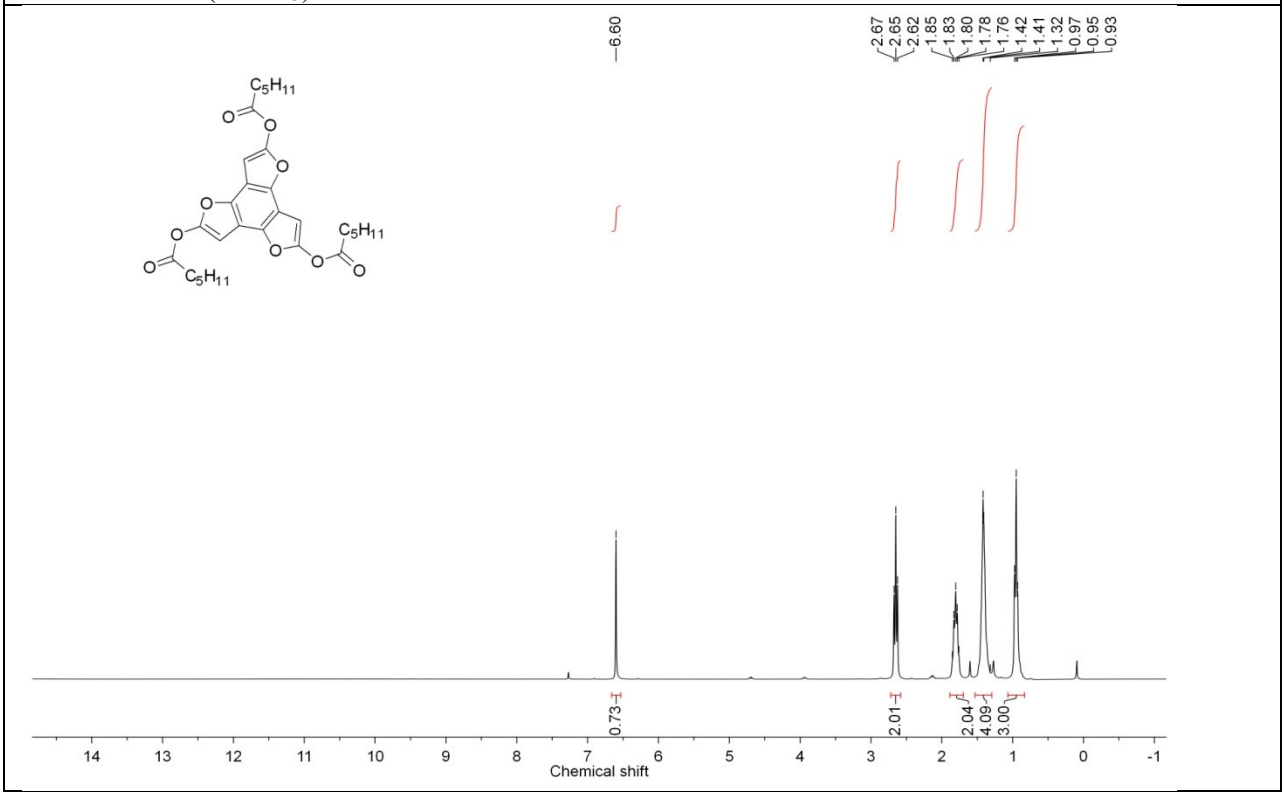

3-2d ^{1}H NMR ($CDCl_3$)

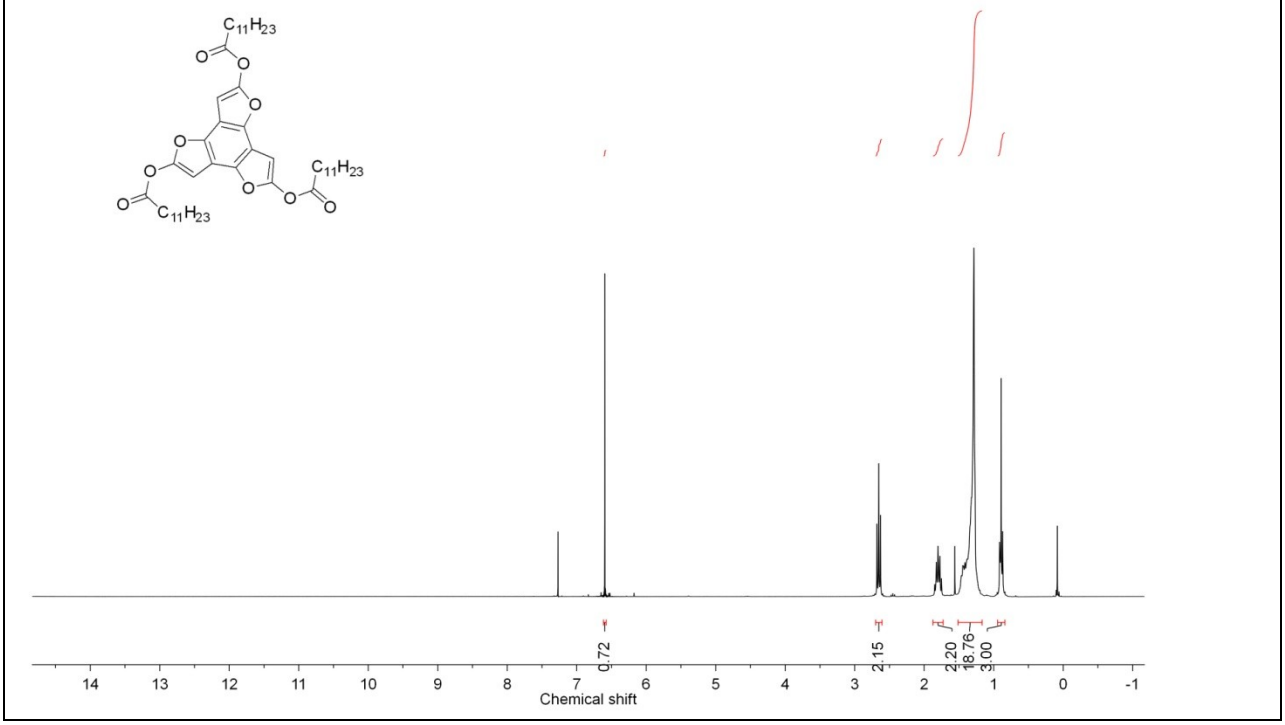

3-3a ^{1}H NMR ($CDCl_3$)

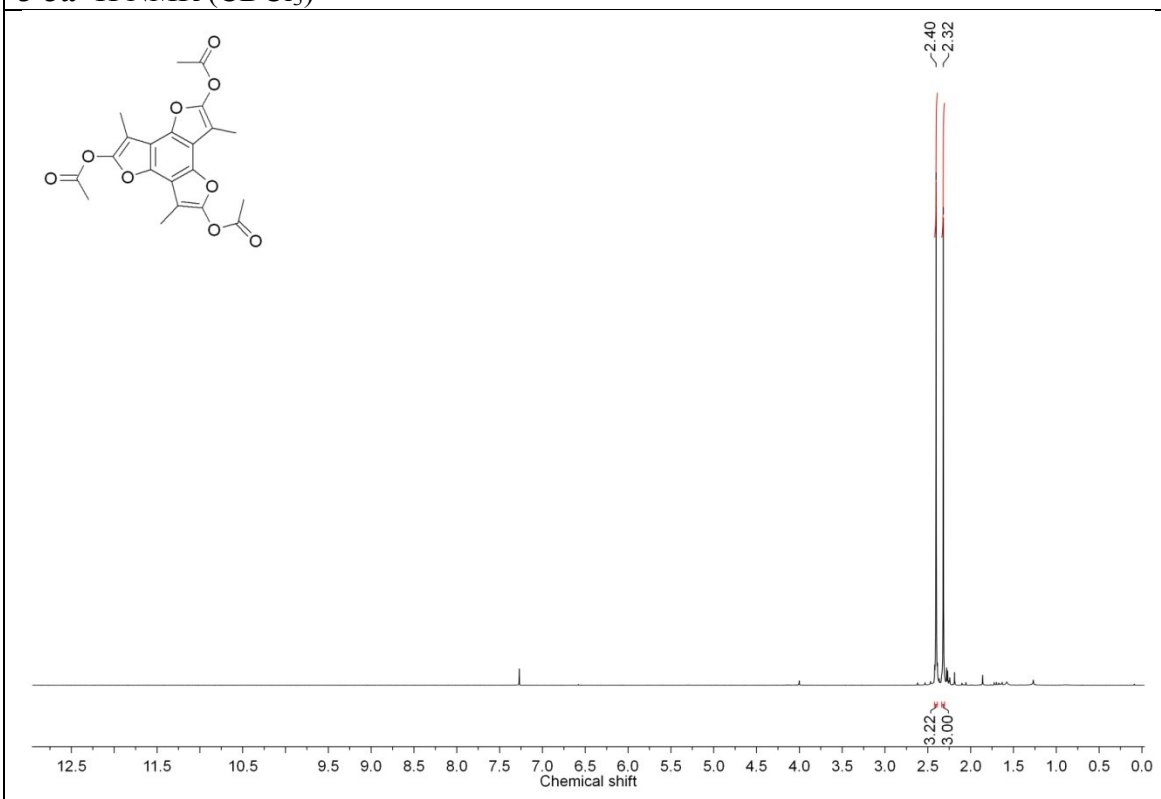

3-3b ^{1}H NMR ($CDCl_3$)

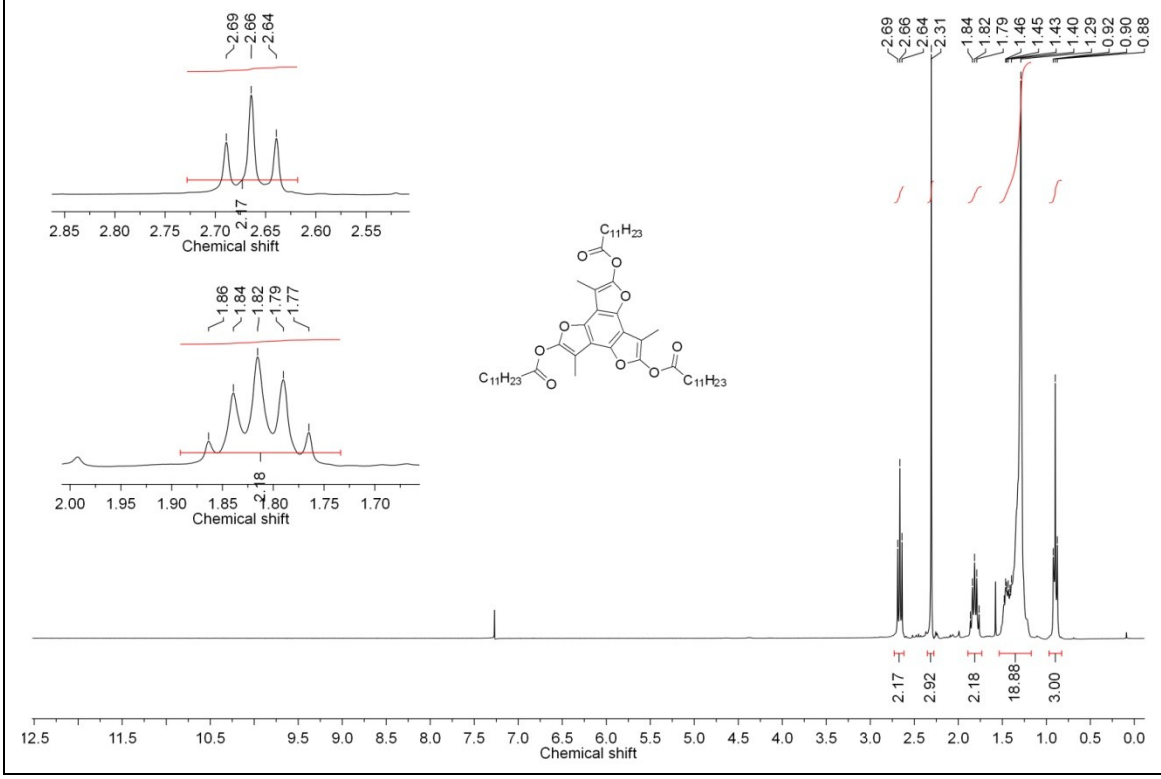

3-3c ^{1}H NMR ($CDCl_3$)

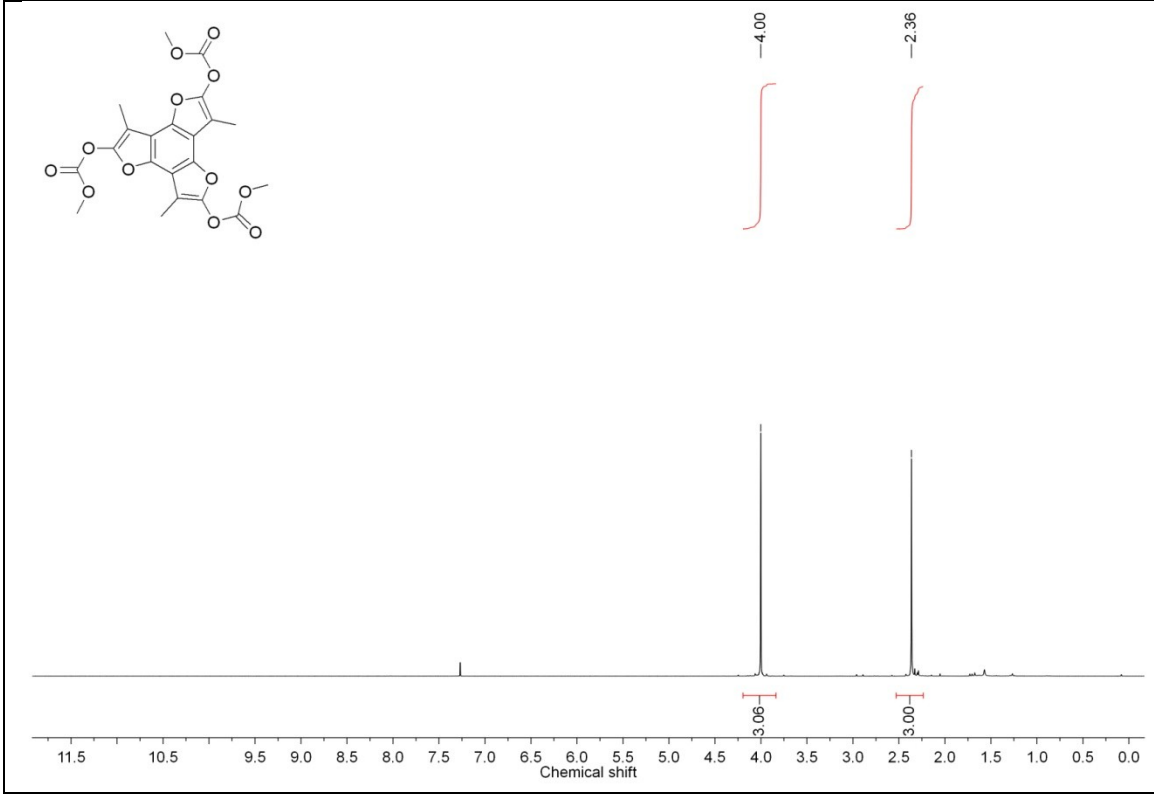

3-3d ^{1}H NMR ($CDCl_3$)

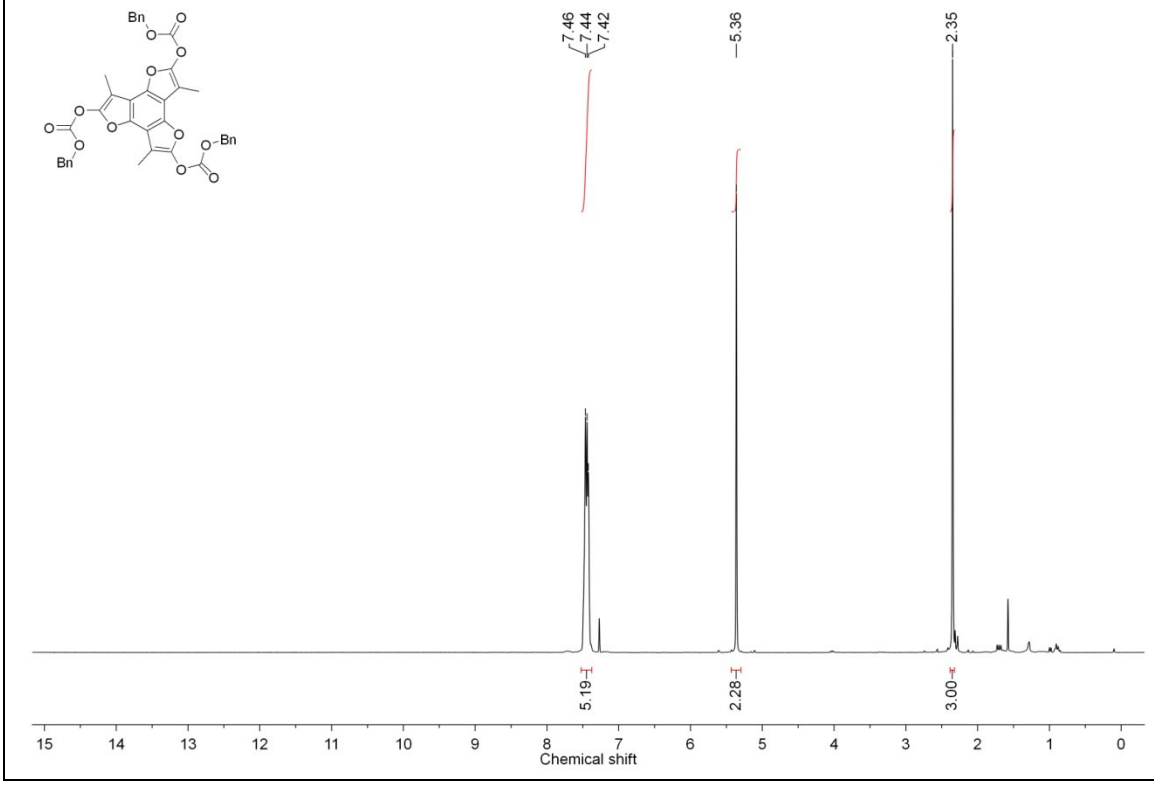

3-3e ^{1}H NMR ($CDCl_3$)

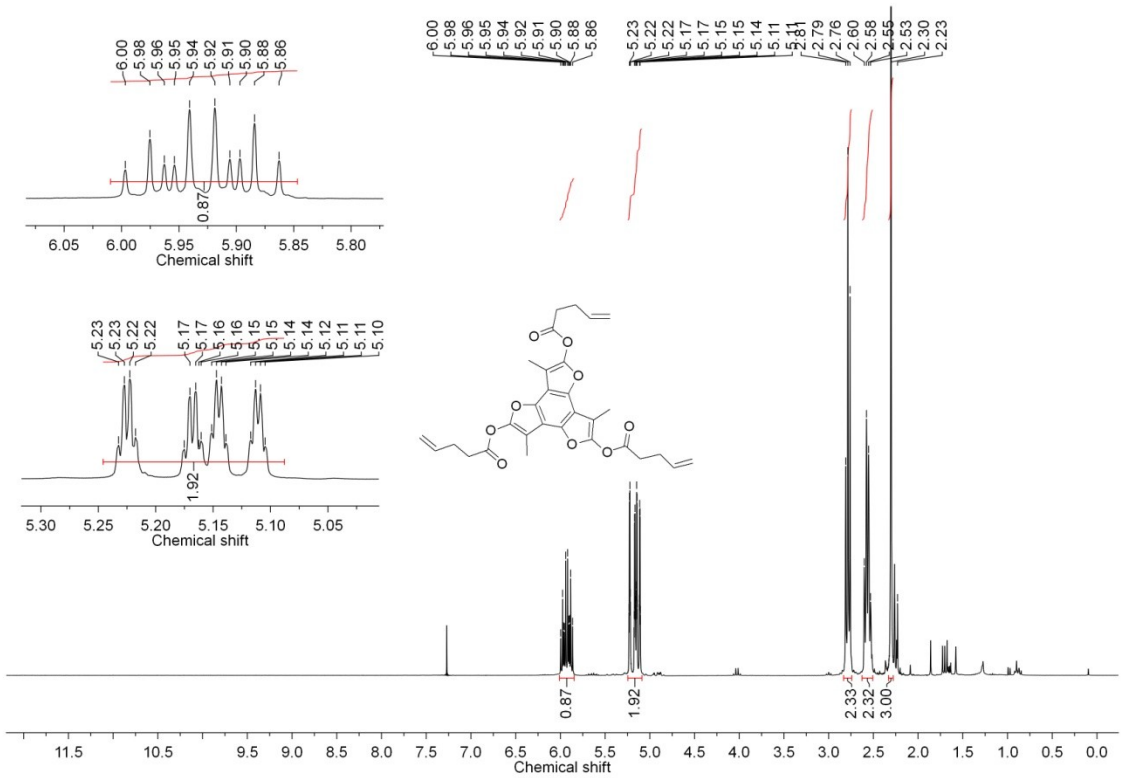

3-4 ^{1}H NMR ($CDCl_3$)

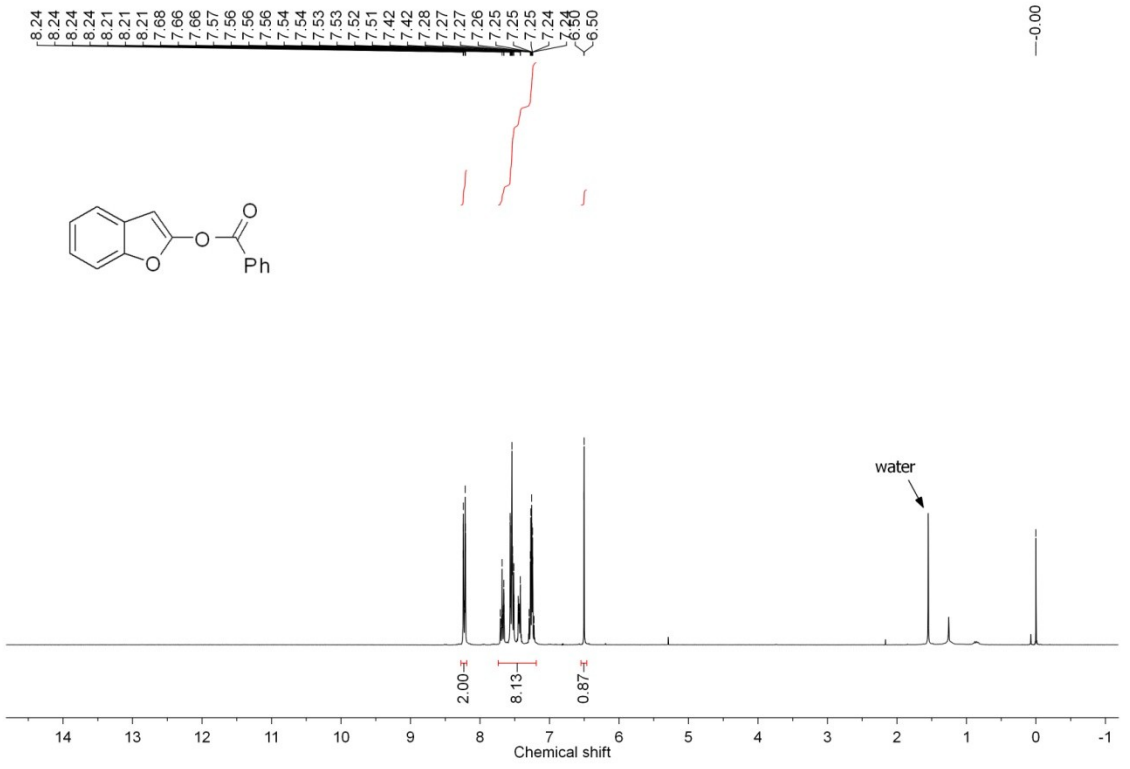

3-5 ^{1}H NMR ($CDCl_3$)

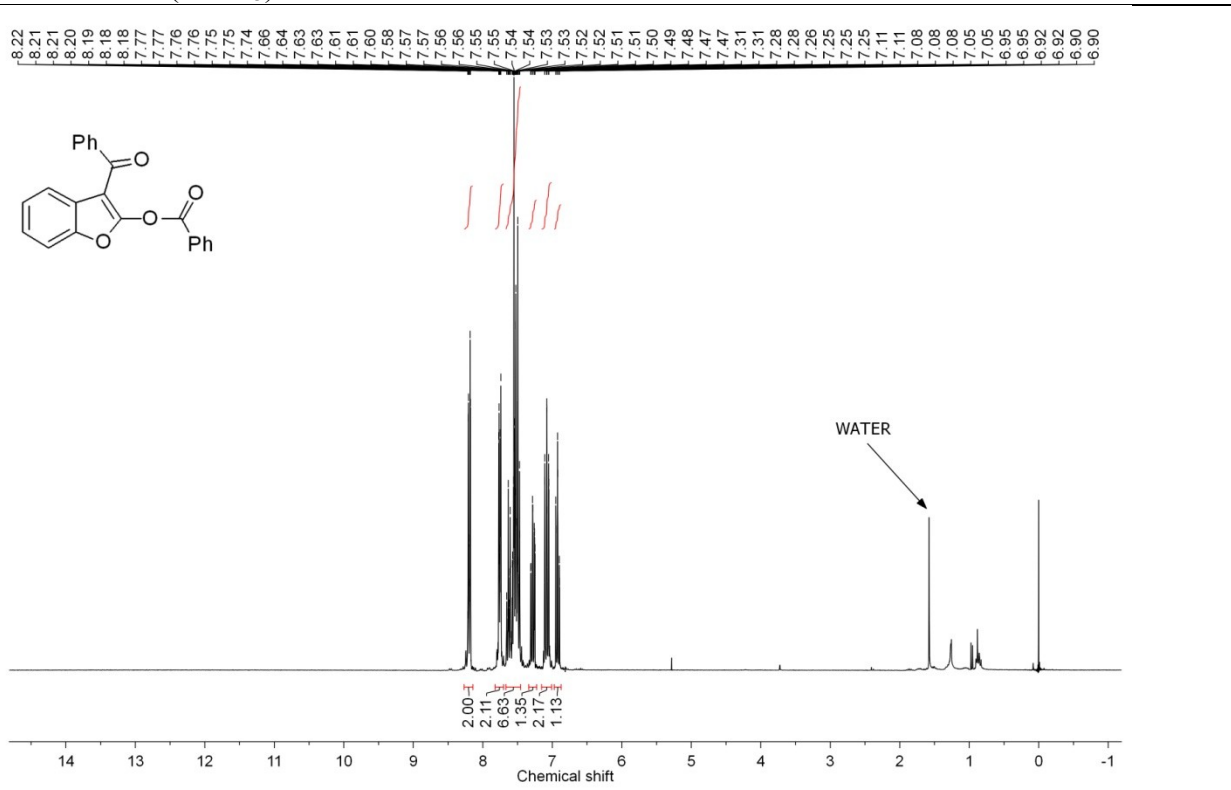

5-3 ^{1}H NMR ($CDCl_3$)

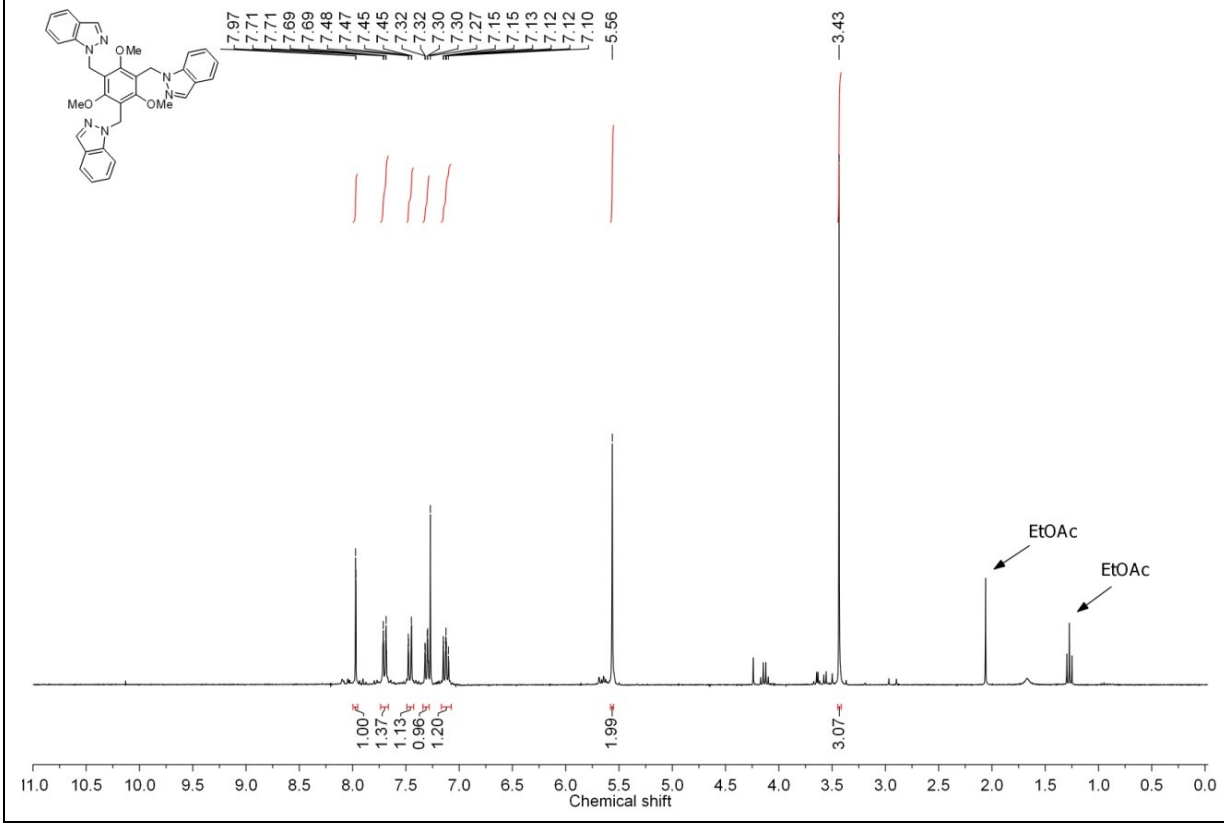

5-5 ^{1}H NMR ($CDCl_3$)

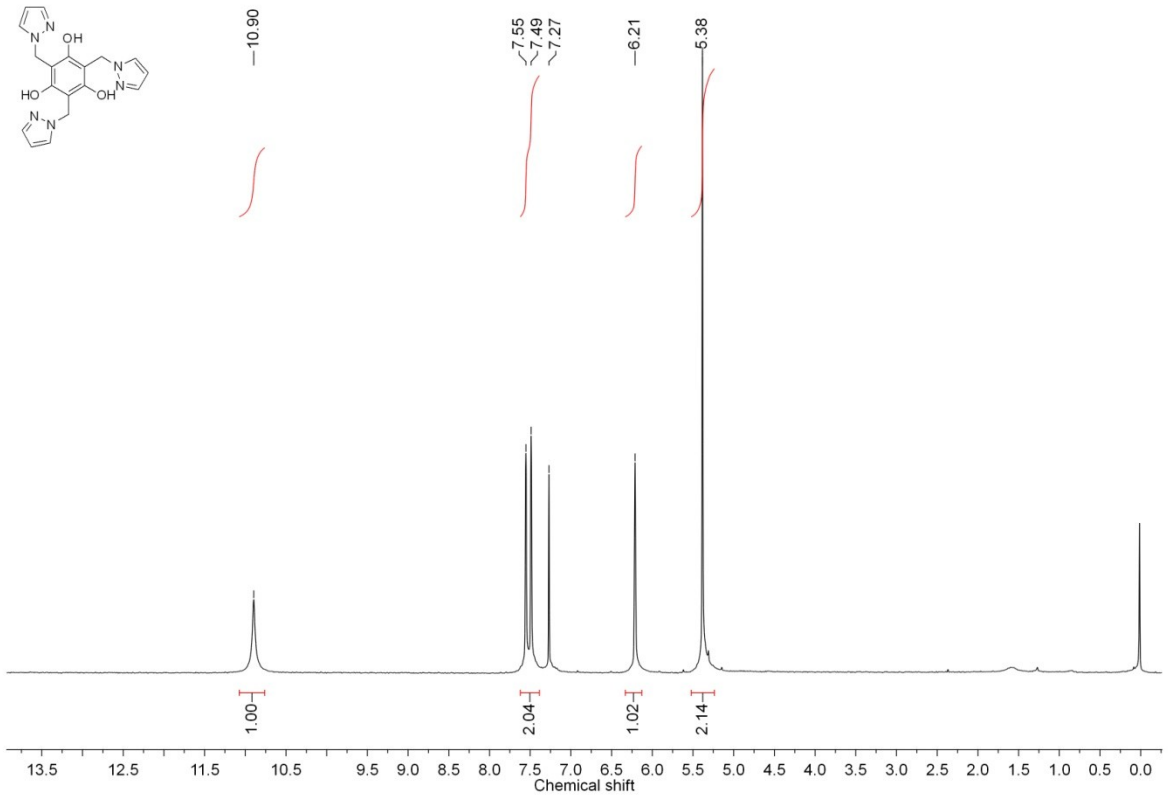

5-6 ^{1}H NMR ($CDCl_3$)

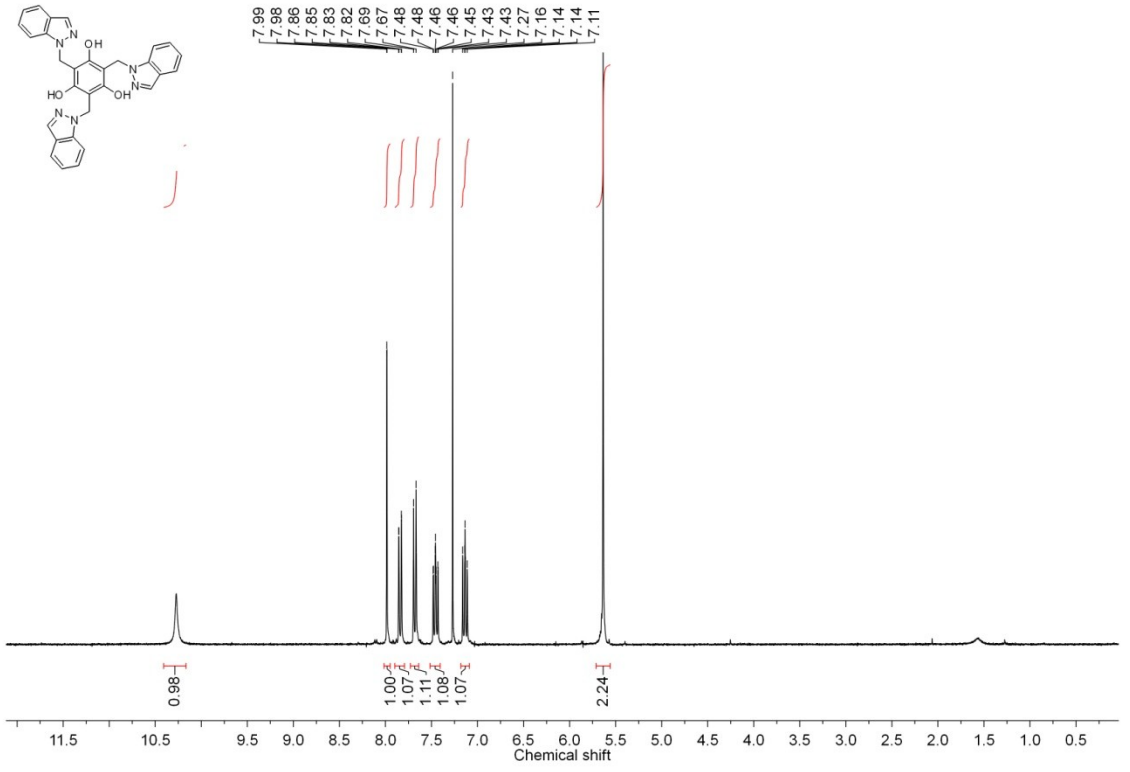

5-7 ^{1}H NMR ($CDCl_3$)

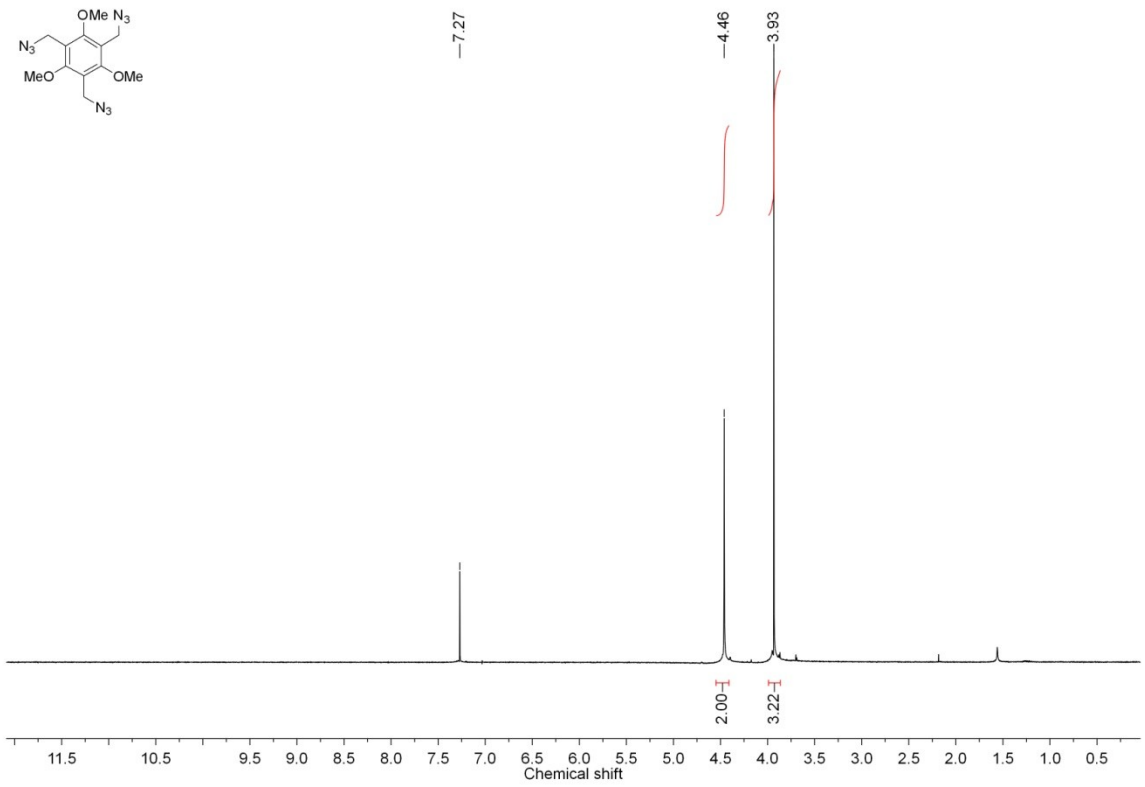

5-8a ^{1}H NMR (DMSO-d_6)

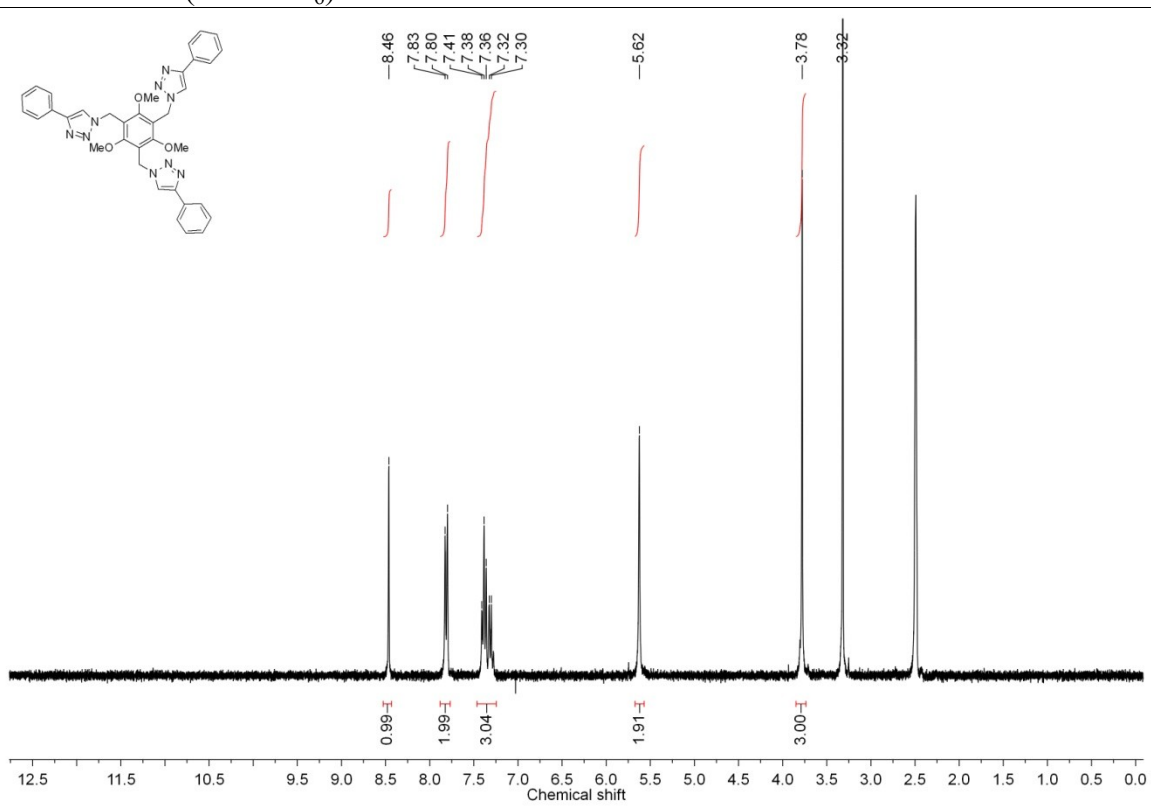

5-8b ^{1}H NMR ($CDCl_3$)

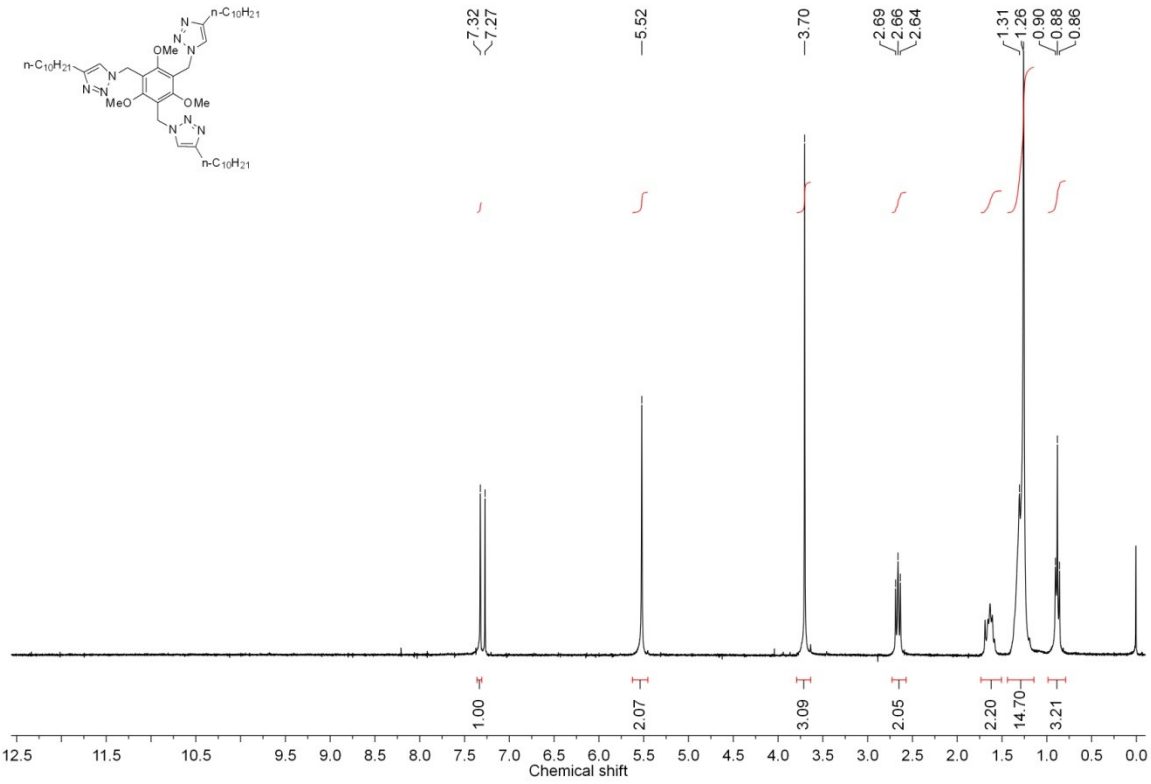

5-8c^{1}H NMR ($CDCl_3$)

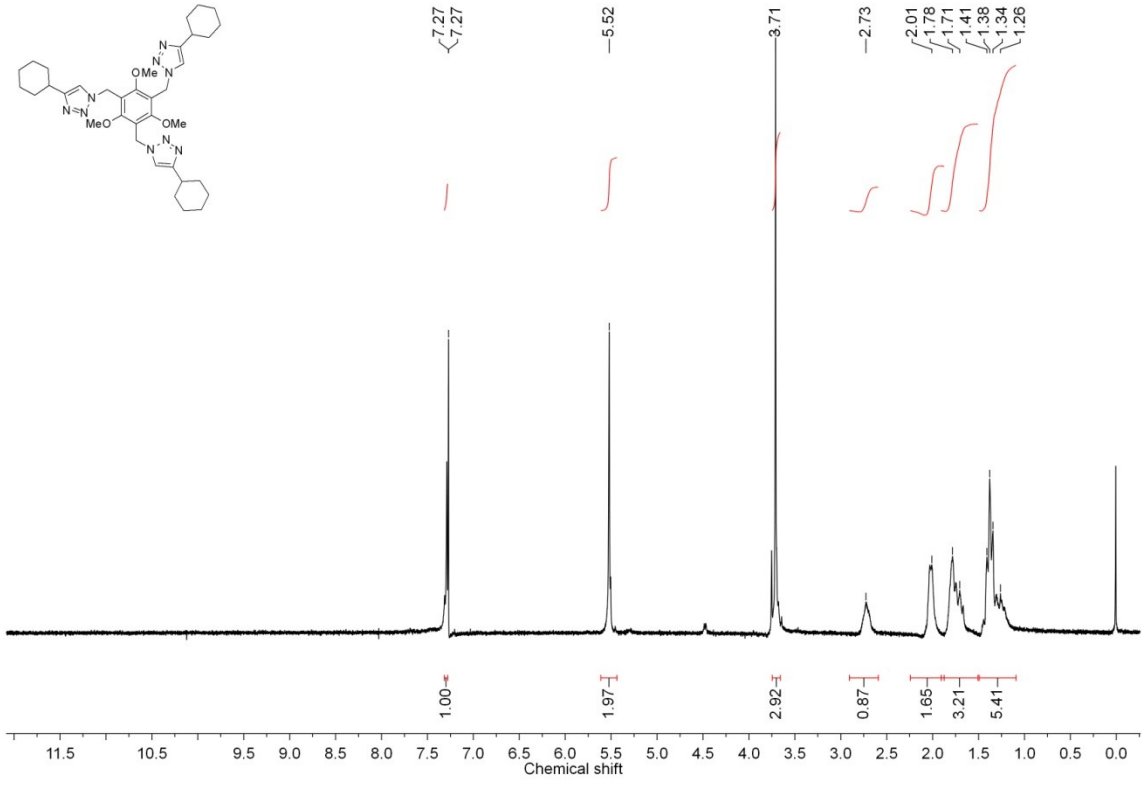

5-9 ^{1}H NMR (DMSO-d_6)

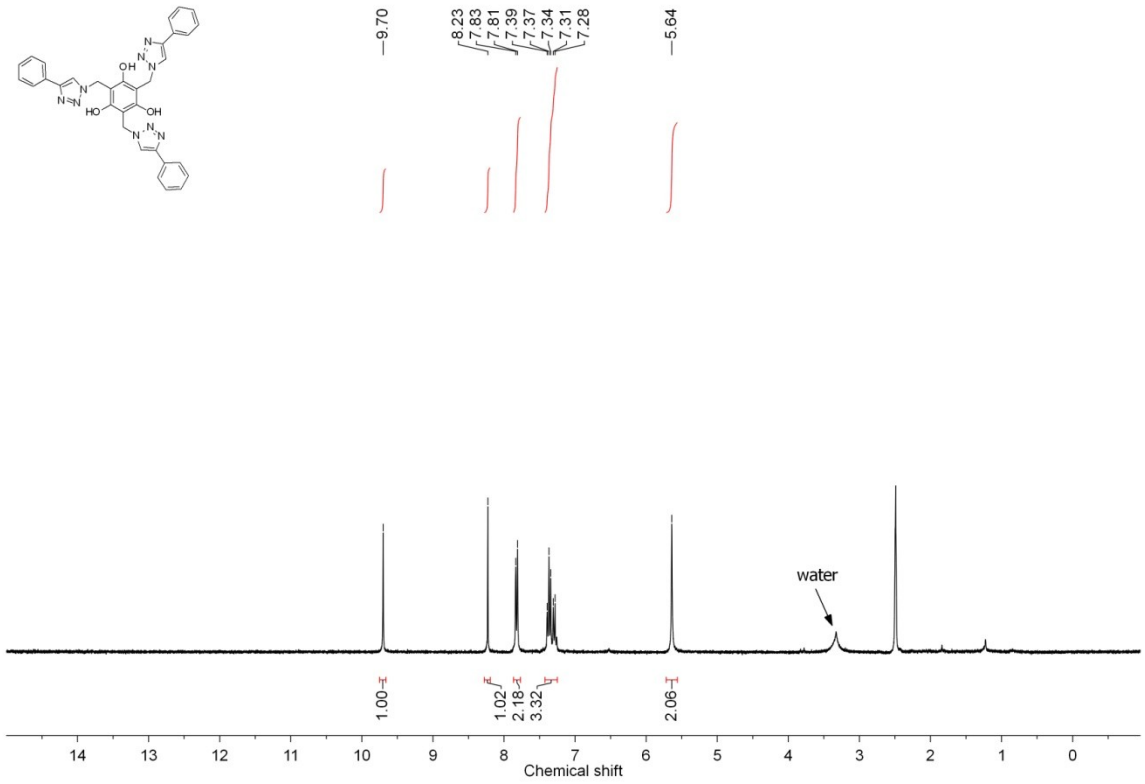

5-12a ^{1}H NMR ($CDCl_3$)

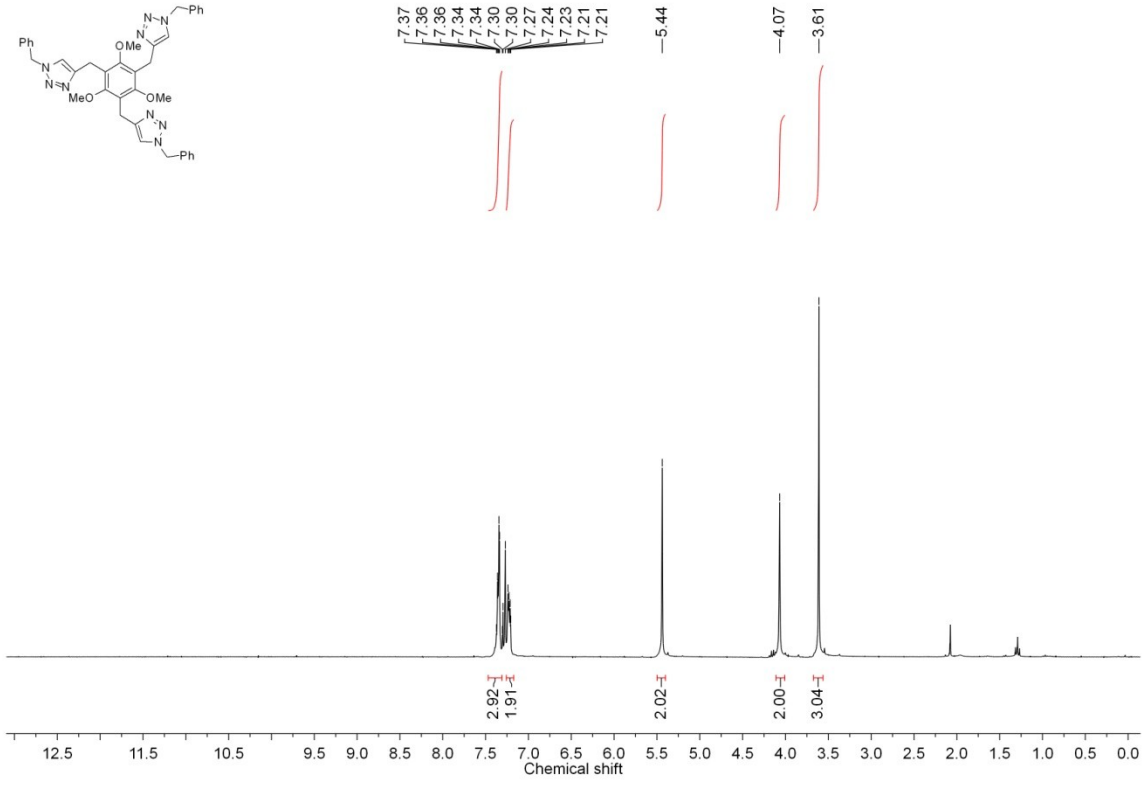

5-12b ^{1}H NMR ($CDCl_3$)

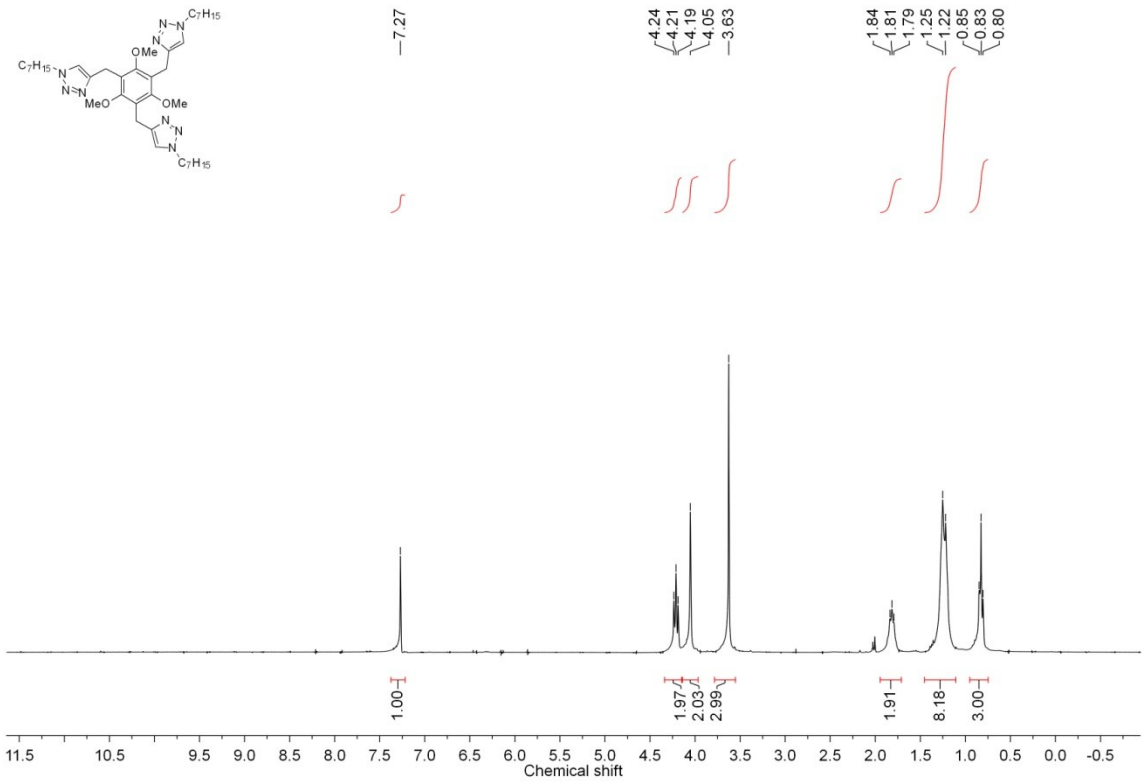

5-15b ^{1}H NMR ($CDCl_3$)

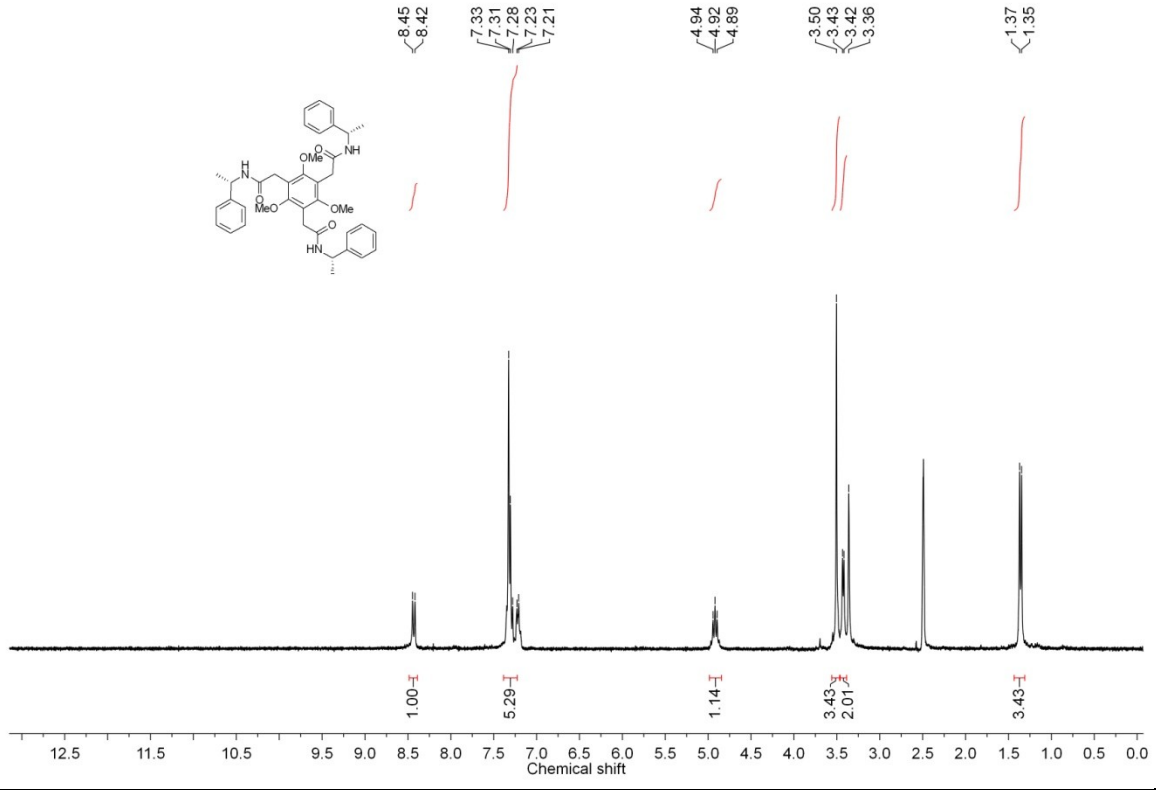

5-16b ^{1}H NMR ($CDCl_3$)

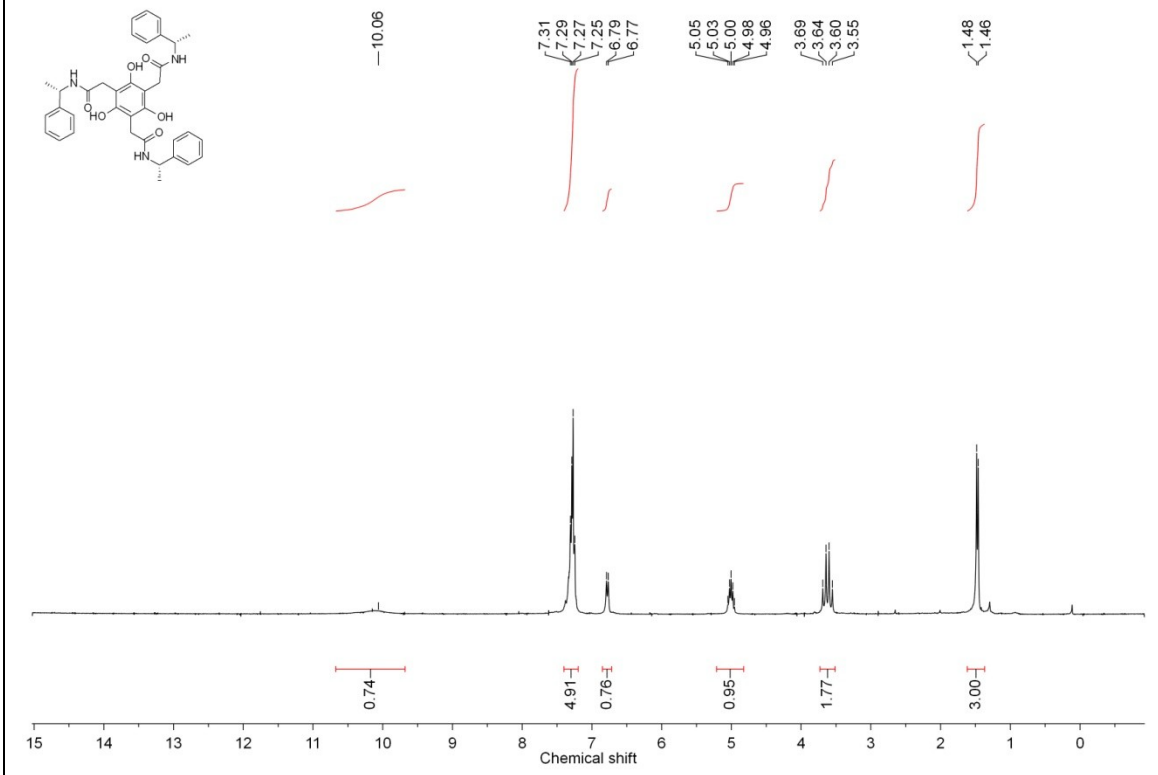

5-17 ^{1}H NMR ($CDCl_3$)

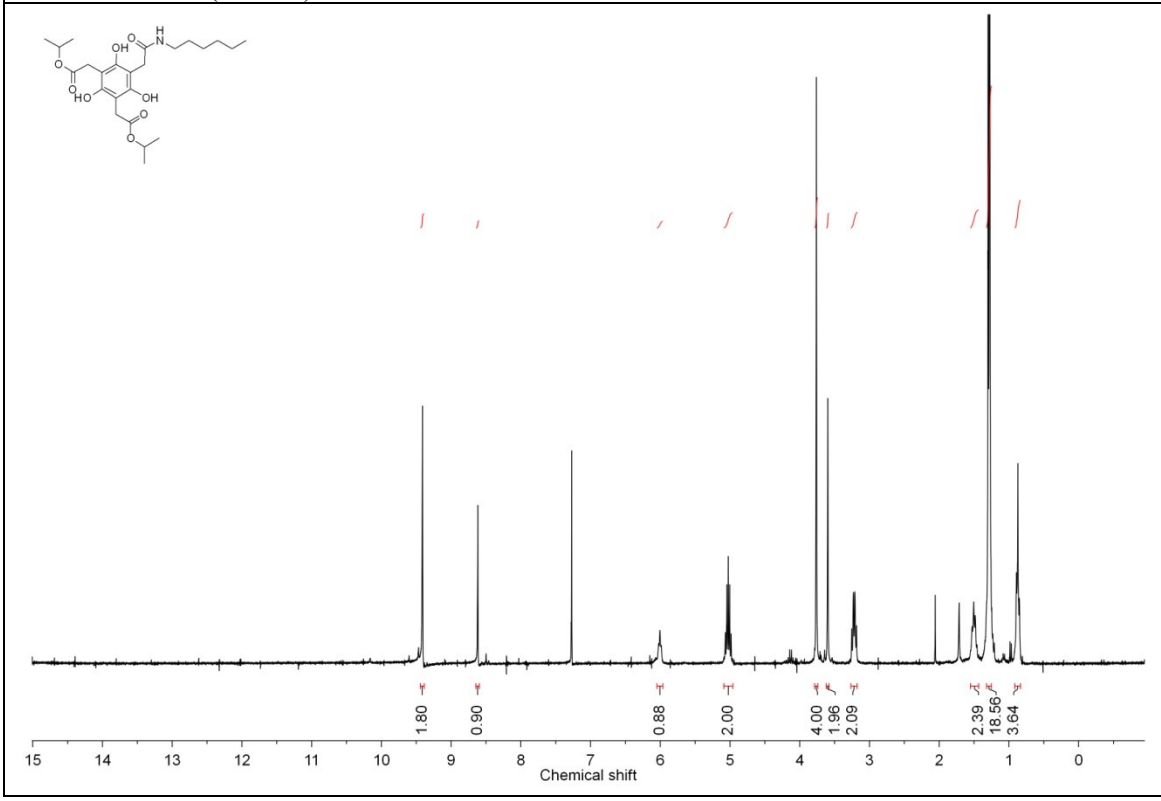

LIST OF REFERENCES

(1) Steed, J. W.; Atwood, J. L. *Supramolecular Chemistry*; John Wiley & Sons, Ltd, 2000.

(2) Nguyen, S. B. T.; Gin, D. L.; Hupp, J. T.; Zhang, X. *Proc. Natl. Acad. Sci.* **2001**, *98*, 11849.

(3) Asselberghs, I.; Hennrich, G.; Clays, K. *J. Phys. Chem. A* **2006**, *110*, 6271.

(4) Katz, H. E.; Huang, J. *Annu. Rev. Mater. Res.* **2009**, *39*, 71.

(5) Mazik, M.; Hartmann, A. *J. Org. Chem.* **2008**, *73*, 7444.

(6) Hennrich, G.; Anslyn, E. V. *Chem. Eur. J.* **2002**, *8*, 2219.

(7) Hsu, H.-F.; Lin, M.-C.; Lin, W.-C.; Lai, Y.-H.; Lin, S.-Y. *Chem. Mater.* **2003**, *15*, 2115.

(8) In *Encyclopedia of Chemical Technology*; Fouth ed.; HoweGrant, M., Ed.; John Wiley & Sons; Vol. 19, p 792.

(9) Achkar, J.; Xian, M.; Zhao, H.; Frost, J. W. *J. Am. Chem. Soc.* **2005**, *127*, 5332.

(10) Baeyer, A. *Ber. Dtsch. Chem. Ges.* **1886**, *19*, 159.

(11) Mandix, K.; Colding, A.; Elming, K.; Sunesen, L.; Shim, I. *Int. J. Quantum Chem.* **1993**, *46*, 159.

(12) Wang, D.; Hildenbrand, K.; Leitich, J.; Schuchmann, H.-P.; Sonntag, C. v. *Z. Naturforsch* **1993**, *48b*, 478.

(13) Lohrie, M.; Knoche, W. *J. Am. Chem. Soc.* **1993**, *115*, 919.

(14) Hu, Y.-c.; Wu, X.-f.; Gao, S.; Shi-shan Yu; Liu, Y.; Jing Qu; Li, J.; Liu, Y.-b. *Org. Lett.* **2006**, *8*, 2269.

(15) Urgaonkar, S.; Pierre, H. S. L.; Meir, I.; Lund, H.; RayChaudhuri, D.; Shaw, J. T. *Org. Lett.* **2005**, *7*, 5609.

(16) Maloney, D. J.; Deng, J.-Z.; Starck, S. R.; Gao, Z.; Hecht, S. M. *J. Am. Chem. Soc.* **2005**, *127*, 4140.

(17) Maloney, D. J.; Chen, S.; Hecht, S. M. *Org. Lett.* **2006**, *8*, 1925.

(18) Wang, Y.; Tan, W.; Li, W. Z.; Li, Y. *J. Nat. Prod.* **2001**, *64*, 196.

(19) Kostova, I. *Curr. HIV Res.* **2006**, *4*, 347.

(20) Nakagawa-Goto, K.; Bastow, K. F.; Chen, T.-H.; Morris-Natschke, S. L.; Lee, K.-H. *J. Med. Chem.* **2008**, *51*, 3297.

(21) Delmulle, L.; Bellahcene, A.; Dhooge, W.; Comhaire, F.; Roelens, F.; Huvaere, K.; Heyerick, A.; Castronovo, V.; Keukeleire, D. D. *Phytomedicine* **2006**, *13*, 732.

(22) Bharate, S. B.; Khan, S. I.; Yunus, N. A. M.; Chauthe, S. K.; Jacob, M. R.; Tekwani, B. L.; Khan, I. A.; Singh, I. P. *Bioorg. Med. Chem.* **2007**, *15*, 87.

(23) Kabir, M. S.; Engelbrecht, K.; Polanowski, R.; Krueger, S. M.; Ignasiak, R.; Rott, M.; Schwan, W. R.; Stemper, M. E.; Reed, K. D.; Sherman, D.; Cook, J. M.; Monte, A. *Bioorg. Med. Chem. Lett.* **2008**, *18*, 5745.

(24) Lee, H. B.; Kim, J. C.; Lee, S. M. *Arch. Pharm. Res.* **2009**, *32*, 655.

(25) Klink, J. W. v.; Larsen, L.; Perry, N. B.; Weavers, R. T.; Cook, G. M.; Bremer, P. J.; MacKenzie, A. D.; Kirikae, T. *Bioorg. Med. Chem.* **2005**, *13*, 6651.

(26) Collings, P. J.; Hird, M. *Introduction to Liquid Cystals Chemistry and Physics*; Taylor & Francis Ltd., 1997.

(27) Yelamaggad, C. V.; Achalkumar, A. S.; Rao, D. S. S.; Prasad, S. K. *J. Am. Chem. Soc.* **2004**, *126*, 6506.

(28) Yelamaggad, C. V.; Achalkumar, A. S.; Rao, D. S. S.; Prasad, S. K. *J. Org. Chem.* **2007**, *72*, 8308.

(29) Yelamaggad, C. V.; Achalkumar, A. S.; Rao, D. S. S.; Prasad, S. K. *J. Org. Chem.* **2009**, *74*, 3168.

(30) Lehmann, M.; Jahr, M. *Chem. Mater.* **2008**, *20*, 5453.

(31) Lehmann, M.; Gearba, R. I.; Koch, M. H. J.; Ivanov, D. A. *Chem. Mater.* **2004**, *16*, 374.

(32) Lehmann, M.; Jahr, M.; Grozema, F. C.; Abellon, R. D.; Siebbeles, L. D. A.; ller, M. M. *Adv. Mater.* **2008**, *20*, 4414.

(33) Lehmann, M.; Jahr, M.; Donnio, B.; Graf, R.; Gemming, S.; Popov, I. *Chem. Eur. J.* **2008**, *14*, 3562.

(34) Lehmann, M.; Jahr, M.; Gutmann, J. *J. Mater. Chem.* **2008**, *18*, 2995.

(35) Castella, M.; Lopez-Calahorra, F.; Velasco, D. *Liq. Cryst.* **2002**, *29*, 559.

(36) Nithyanandhan, J.; Jayaraman, N.; Davis, R.; Das, S. *Chem. Eur. J.* **2004**, *10*, 689.

(37) Chang, J. Y. *Chem. Mater.* **2000**, *12*, 1076.

(38) Yao, D.-S.; Zhang, B.-Y.; Zhang, W.-W.; Tian, M. *J. Mol. Struct.* **2008**, *881*, 83.

(39) Bushey, M. L.; Hwang, A.; Stephens, P. W.; Nuckolls, C. *J. Am. Chem. Soc.* **2001**, *123*, 8157.

(40) Bushey, M. L.; Hwang, A.; Stephens, P. W.; Nuckolls, C. *Angew. Chem., Int. Ed.* **2002**, *41*, 2828.

(41) Vintiloiu, A.; Leroux, J.-C. *J. Controlled Release* **2008**, *125*, 179.

(42) Sangeetha, N. M.; Maitra, U. *Chem. Soc. Rev.* **2005**, *34*, 821.

(43) Yamanaka, M.; Fujii, H. *J. Org. Chem.* **2009**, *74*, 5390.

(44) Yamanaka, M.; Nakagawa, T.; Aoyama, R.; Nakamura, T. *Tetrahedron* **2008**, *64*, 11558.

(45) Westcott, A.; Sumby, C. J.; Walshaw, R. D.; Hardie, M. J. *New J. Chem.* **2009**, *33*, 902.

(46) Marder, S. R.; Beratan, N. N.; Cheng, L.-T. *Science* **1991**, *252*, 103.

(47) Lee, Y.-K.; Jeon, S.-J.; Cho, M. *J. Am. Chem. Soc.* **1998**, *120*, 10921

(48) Wolff, J. J.; Siegler, F.; Matschiner, R.; Wortmann, R. *Angew. Chem., Int. Ed.* **2000**, *39*, 1436.

(49) Cho, B. R.; Chajara, K.; Oh, H. J.; Son, K. H.; Jeon, S.-J. *Org. Lett.* **2002**, *4*, 1703.

(50) Hennrich, G.; Asselberghs, I.; Clays, K.; Persoons, A. *J. Org. Chem.* **2004**, *69*, 5077.

(51) Hennrich, G.; Cavero, E.; Barbera, J.; Gómez-Lor, B.; Hanes, R. E.; Talarico, M.; Golemme, A.; Serrano, J. L. *Chem. Mater.* **2007**, *19*, 6068.

(52) Hennrich, G.; Omenat, A.; Asselberghs, I.; Foerier, S.; Clays, K.; Verbiest, T.; Serrano, J. L. *Angew. Chem., Int. Ed.* **2006**, *45*, 4203.

(53) Xie, J.; Hu, L.; Shi, W.; Deng, X.; Cao, Z.; Shen, Q. *J. Polym. Sci., Part B: Polym. Phys.* **2008**, *46*, 1140.

(54) Wang, D.; Zhang, S.; Zhang, Y.; Wang, H.; Mu, J.; Wang, G.; Jiang, Z. *Dyes Pigm.* **2008**, *79*, 217.

(55) Hong, J.-I.; Namgoong, S. K.; Bernardi, A.; Still, W. C. *J. Am. Chem. Soc.* **1991**, *113*, 5111.

(56) Na, J. E.; Lee, K. Y.; Seo, J.; Kim, J. N. *Tetrahedron Lett.* **2005**, *46*, 4505.

(57) Glaser, T.; Heidemeier, M.; Krickemeyer, E.; Bogge, H.; Stammler, A.; Frohlich, R.; Bill, E.; Schnack, J. *Inorg. Chem.* **2009**, *48*, 607.

(58) Glaser, T.; Heidemeier, M.; Strautmann, J. B. H.; Hartmut, B.; Stammler, A.; Krickemeyer, E.; Huenerbein, R.; Grimme, S.; Brothe, E.; Bill, E. *Chem. Eur. J.* **2007**, *13*, 9191.

(59) Martin, T.; Obst, U.; Rebek, J., Jr *Science* **1998**, *281*, 1842.

(60) Heinz, T.; Rudkevich, D. M.; Rebek, J., Jr *Nature* **1998**, *394*, 764.

(61) Turner, J. L.; Wooley, K. L. *Nano Lett.* **2004**, *4*, 683.

(62) Fiedler, D.; Leung, D. H.; Bergman, R. G.; Raymond, K. N. *Acc. Chem. Res.* **2005**, *38*, 351.

(63) Rostovtsev, V. V.; Green, L. G.; Fokin, V. V.; Sharpless, K. B. *Angew. Chem., Int. Ed.* **2002**, *41*, 2596.

(64) Morales-Sanfrutos, J.; Mariano Ortega-Munoz; Lopez-Jaramillo, J.; Fernando Hernandez-Mateo, a.; Santoyo-Gonzalez, F. *J. Org. Chem.* **2008**, *73*, 7772.

(65) Kim, J.; Young Kook Kim; Nokyoung Park; Hahn, J. H.; Ahn, K. H. *J. Org. Chem.* **2005**, *70*, 7087.

(66) Ferrini, S.; Fusi, S.; Giorgi, G.; Ponticelli, F. *Eur. J. Org. Chem.* **2008**, 5407.

(67) Sauer, M.; Yeung, C.; Chong, J. H.; Patrick, B. O.; MacLachlan, M. J. *J. Org. Chem.* **2006**, *71*, 775.

(68) Lu, J.; Lei, S. B.; Zeng, Q. D.; Kang, S. Z.; Wang, C.; Wan, L. J.; Bai, C. L. *J. Phys. Chem. B* **2004**, *108*, 5161.

(69) Huang, F.; Slebodnick, C.; Mahan, E. J.; Gibson, H. W. *Tetrahedron* **2007**, *63*, 2875.

(70) Deng, L.; Wang, L.; Yu, H.; Wang, J.; Dong, X.; Jianhua Li; Tan, Q.; Huo, J. *J. Appl. Polym. Sci.* **2008**, *107*, 1539.

(71) Riddle, J. A.; Bollinger, J. C.; Lee, D. *Angew. Chem., Int. Ed.* **2005**, *4*, 6689.

(72) Dalcanale, E.; Ungaro, R. *Supramolecular Science: Where It Is and Where It Is Going*; Kluwer Academic Publishers: Boston, 1999.

(73) Hübner, G. M.; Nachtsheim, G.; Li, Q. Y.; Seel, C.; Vögtle, F. *Angew. Chem., Int. Ed.* **2000**, *39*, 1269.

(74) Younes, A. H.; Ghaddar, T. H. *Inorg. Chem.* **2008**, *47*, 3408.

(75) Jean-Francois Eckert; Declan Byrne; Nicoud, J.-F.; Oswald, L.; Nierengarten, J.-F.; Numata, M.; Ikeda, A.; Shinkai, S.; Armaroli, N. *New J. Chem.* **2000**, *24*, 749.

(76) Fujimoto, Y.; Ubukata, T.; Yokoyama, Y. *Chem. Commun.* **2008**, 5755.

(77) Percec, V.; Cho, W.-D.; Mosier, P. E.; Ungar, G.; Yeardley, D. J. P. *J. Am. Chem. Soc.* **1998**, *120*, 11061.

(78) Chow, H.-F.; Chan, I. Y.-K.; Mak, C. C.; Ng, M.-K. *Tetrahedron* **1996**, *52*, 4277.

(79) Nierengarten, J.-F.; Eckert, J.-F.; Yannick, R.; Carreon, M. d. P.; Gallani, J.-L.; Guillon, D. *J. Am. Chem. Soc.* **2001**, *123*, 9743.

(80) Lehmann, M.; Jahr, M. *Org. Lett.* **2006**, *8*, 721.

(81) Pereira, A.; Vottero, E.; Roberge, M.; Mauk, A. G.; Andersen, R. J. *J. Nat. Prod.* **2006**, *69*, 1469.

(82) Kwon, Y.-J.; Sohn, M.-J.; Zheng, C.-J.; Kim, W.-G. *Org. Lett.* **2007**, *9*, 2449.

(83) Harrowven, D. C.; Lucas, M. C.; Howes, P. D. *Tetrahedron* **2001**, *57*, 791.

(84) Venkateswarlu, S.; Panchagnula, G. K.; Guraiah, M. B.; Subbaraju, G. V. *Tetrahedron* **2006**, *62*, 9855.

(85) Kresge, A. J. *Chem. Soc. Rev.* **1996**, *25*, 275.

(86) Bordwell, F. G.; Fried, H. E. *J. Org. Chem.* **1991**, *56*, 4218.

(87) Capon, B.; Kwok, F.-C. *Tetrahedron Lett.* **1986**, *27*, 3275.

(88) Aliaga, C.; Stuart, D. R.; Aspee, A.; Scaiano, J. C. *Org. Lett.* **2005**, *7*, 3665.

(89) Capon, B.; Kwok, F.-C. *J. Am. Chem. Soc.* **1989**, *111*, 5346.

(90) Kresge, A. J.; Meng, Q. *J. Am. Chem. Soc.* **2002**, *124*, 9189.

(91) Wiberg, K. B.; Waldron, R. F. *J. Am. Chem. Soc.* **1991**, *113*, 7697.

(92) Izbicka, E.; Bolen, D. W. *J. Am. Chem. Soc.* **1978**, *100*, 7625.

(93) Borst, M. L. G.; Ehlers, A. W.; Lammertsma, K. *J. Org. Chem.* **2005**, *70*, 8110.

(94) Magnus, P.; Venable, J. D.; Shen, L.; Lynch, V. *Tetrahedron Lett.* **2005**, *46*, 707.

(95) Frenette, M.; MacLean, P. D.; Barclay, L. R. C.; Scaiano, J. C. *J. Am. Chem. Soc.* **2007**, *128*, 16432.

(96) Nesvadba, P.; Attinger-Sorato, C., U.K. Patent 2257140.

(97) Black, T. H.; Arrivo, S. M.; Schumm, J. S.; Knobeloch, J. M. *J. Org. Chem.* **1987**, *52*, 5425.

(98) Hantzsch, A. *Chem. Ber.* **1886**, *19*, 2934.

(99) Destrade, C.; Tinh, N. H.; Gasparoux, H. *Liq. Cryst.* **1987**, *2*, 229.

(100) Hennrich, G.; Anslyn, E. V. *Chem. Eur. J.* **2002**, *8*, 2218.

(101) Kita, Y.; Akai, S.; Yamamoto, M.; Taniguchi, M.; Tamura, Y. *Synthesis* **1989**, *4*, 334.

(102) Munoz-Muniz, O.; Juaristi, E. *J. Org. Chem.* **2003**, *68*, 3781.

(103) El-Sayrafi, S.; Rayyan, S. *Molecules* **2001**, *6*, 279.

(104) Lampkins, A. J. Ph. D. Dissertation, **2006**.

(105) Lampkins, A. J.; Abdul-Rahim, O.; Li, H. F.; Castellano, R. K. *Org. Lett.* **2005**, *7*, 4471.

(106) Lampkins, A. J.; Abdul-Rahim, O.; Li, H.; Castellano, R. K. *Org. Lett.* **2005**, *7*, 4471.

(107) Bocelli, G.; Grenier-Loustalot, M.-F. *J. Mol. Struct.* **1982**, *82*, 301.

(108) Paulini, R.; Muller, K.; Diederich, F. *Angew. Chem., Int. Ed.* **2005**, *44*, 1788.

(109) Castellano, R. K. *Curr. Org. Chem.* **2004**, *8*, 845.

(110) Burgi, H. B.; Dunitz, J. D.; Shefter, E. *Acta Crystallogr., Sect. B* **1974**, *30*, 1517.

(111) Azumaya, I.; Uchida, D.; Kato, T.; Yokoyama, A.; Tanatani, A.; Takayanagi, H.; Yokozawa, T. *Angew. Chem., Int. Ed.* **2004**, *43*, 1360.

(112) Nalwa, H. S.; Miyata, S. *Nonlinear Optics of Organic Molecules and Polymers*; CRC Press, Inc.: Boca Raton, 1997.

(113) Oude-Alink, B. A. M.; Chan, A. W. K.; Gutsche, C. D. *J. Org. Chem.* **1973**, *38*, 1993.

(114) Crews, P.; Rodriguez, J.; Jaspars, M. *Organic Structure Analysis*; Oxford University Press: New York, 1998.

(115) Iida, M.; Araki, T.; Teranishi, K.; Tani, H. *Macromolecules* **1977**, *10*, 275.

(116) Hall, H. K.; Zbinden, R. *J. Am. Chem. Soc.* **1958**, *80*, 6428.

(117) Hooshyar, H.; Rahemi, H.; Dilmagani, K. A.; Tayyari, S. F. *J. Theor. Comput. Chem.* **2007**, *6*, 459.

(118) Focsaneanu, K.-S.; Scaiano, J. C. *Helv. Chim. Acta* **2006**, *89*, 2473.

(119) Trost, B. M.; Cramer, N.; Silverman, S. M. *J. Am. Chem. Soc.* **2007**, *129*, 12396.

(120) Ryabukhin, S. V.; Plaskon, A. S.; Volochnyuk, D. M.; Pipko, S. E.; Shivanyuk, A. N.; Tolmachev, A. A. *J. Comb. Chem.* **2007**, *9*, 1073.

(121) Li, H.; Homan, E. A.; Lampkins, A. J.; Ghiviriga, I.; Castellano, R. K. *Org. Lett.* **2005**, *7*, 443.

(122) Song, K.-S.; Raskin, I. *J. Nat. Prod.* **2002**, *65*, 76.

(123) Su, B.-N.; Cuender, M.; Hawthorne, M. E.; Kardono, L. B. S.; Riswan, S.; Fong, H. H. S.; Mehta, R. G.; Pezzuto, J. M.; Kinghorn, A. D. *J. Nat. Prod.* **2002**, *65*, 163.

(124) Dat, N. T.; Jin, X.; Lee, K.; Hong, Y.-S.; Kim, Y. H.; Lee, J. J. *J. Nat. Prod.* **2009**, *72*, 39.

(125) Pauletti, P. M.; Araujo, A. R.; Claudia, M.; Young, M.; Giesbrecht, A. M.; Bolzani, V. d. S. *Phytochemistry* **2000**, *55*, 597.

(126) Franke, K.; Porzel, A.; Masaoud, M.; Adam, G.; Schmidt, J. *Phytochemistry* **2001**, *56*, 611.

(127) Greve, H.; Meis, S.; Kassack, M. U.; Kehraus, S.; Anja Krick; Wright, A. D.; Konig, G. M. *J. Med. Chem.* **2007**, *50*, 5600.

(128) Hughes, C. C.; Trauner, D. *Angew. Chem., Int. Ed.* **2002**, *41*, 1569.

(129) http://en.wikipedia.org/wiki/Benzofuranylpropylaminopentane.

(130) Friedman, M. R.; Toyne, K. J.; Goodby, J. W.; Hird, M. *J. Mater. Chem.* **2001**, *11*, 2759.

(131) Pokladko, M.; Sanetra, J.; Gondek, E.; Bogdal, D.; Niziol, J.; Kityk, I. V. *Mol. Cryst. Liq. Cryst.* **2008**, *484*, 335.

(132) Tsuji, H.; Mitsui, C.; Ilies, L.; Sato, Y.; Nakamura, E. *J. Am. Chem. Soc.* **2007**, *129*, 11902.

(133) Hayashi, N.; Saito, Y.; Higuchi, H.; Suzuki, K. *J. Phys. Chem. A* **2009**, *113*, 5342.

(134) Shukla, R.; Wadumethrige, S. H.; Lindeman, S. V.; Rathore, R. *Org. Lett.* **2008**, *10*, 3587.

(135) Bergman, J.; Egestad, B. *Tetrahedron Lett.* **1978**, *34*, 3143.

(136) Perkin, W. H. *J. Chem. Soc.* **1870**, *23*, 368.

(137) Willis, M. C.; Taylor, D.; Gillmore, A. T. *Org. Lett.* **2004**, *6*, 4755.

(138) Otterlo, W. A. L. v.; Morgans, G. L.; Madeley, L. G.; Samuel Kuzvidza; Moleele, S. S.; Thornton, N.; Koning, C. B. d. *Tetrahedron* **2005**, *61*, 7746.

(139) Takeda, N.; Miyata, O.; Naito, T. *Eur. J. Org. Chem.* **2007**, 1491.

(140) Lu, B.; Wang, B.; Zhang, Y.; Ma, D. *J. Org. Chem.* **2007**, *72*, 5337.

(141) Yue, D.; Yao, T.; Larock, R. C. *J. Org. Chem.* **2005**, *70*, 10292.

(142) Chen, C.-y.; Dormer, P. G. *J. Org. Chem.* **2005**, *70*, 6964.

(143) Oisaki, K.; Suto, Y.; Kanai, M.; Shibasaki, M. *J. Am. Chem. Soc.* **2003**, *125*.

(144) Wada, A.; Mizuguchi, Y.; Shinmen, M.; Ito, M.; Nakagawa, K.; Okano, T. *Lett. Drug Des. Discovery* **2006**, *3*, 118.

(145) Wada, A.; Shinmen, M.; Uenishi, J. i.; Ito, M. *Lett. Org. Chem.* **2006**, *3*, 817.

(146) Shaw, S. A.; Aleman, P.; Christy, J.; Kampf, J. W.; Va, P.; Vedejs, E. *J. Am. Chem. Soc.* **2006**, *128*, 925.

(147) Schleyer, P. v. R.; Maerker, C.; Dransfeld, A.; Jiao, H.; Hommes, N. J. R. v. E. *J. Am. Chem. Soc.* **1996**, *118*, 6317.

(148) Chen, Z.; Wannere, C. S.; Corminboeuf, C.; Puchta, R.; Schleyer, P. v. R. *Chem. Rev.* **2005**, *105*, 3842.

(149) Hutchison, G. R.; Ratner, M. A.; Marks, T. J. *J. Am. Chem. Soc.* **2005**, *127*, 16866.

(150) Pisula, W.; Kastler, M.; Wasserfallen, D.; Pakula, T.; Mullen, K. *J. Am. Chem. Soc.* **2004**, *126*, 8074.

(151) Pisula, W.; Dierschke, F.; Mullen, K. *J. Mater. Chem.* **2006**, *16*, 4058.

(152) Hutter, J. L.; Bechhoefer, J. *J. Cryst. Growth* **2000**, *217*, 332.

(153) Park, L. Y.; Hamilton, D. G.; McGehee, E. A.; McMenimen, K. A. *J. Am. Chem. Soc.* **2003**, *125*, 10586.

(154) Okabe, A.; Fukushima, T.; Ariga, K.; Aida, T. *Angew. Chem., Int. Ed.* **2002**, *41*, 3414.

(155) McMenimen, K. A.; Hamilton, D. G. *J. Am. Chem. Soc.* **2001**, *123*, 6453.

(156) Hennrich, G. *Tetrahedron* **2004**, *60*, 9871.

(157) E. Apra, T. L. Windus, T. P. Straatsma, E. J. Bylaska, W. de Jong, S. Hirata, M. Valiev, M. T. Hackler, L. Pollack, K. Kowalski, R. J. Harrison, M. Dupuis, D. M. A. Smith, J. Nieplocha, V. Tipparaju, M. Krishnan, A. A. Auer, E. Brown, G. I. Cisneros, G. Fann, H. Fruchtl, J. Garza, K. Hirao, R. Kendall, J. A. Nichols, K. Tsemekhman, K. Wolinski, J. Anchell, D. Bernholdt, P. Borowski, T. Clark, D. Clerc, H. Dachsel, M. Deegan, K. Dyall, D. Elwood, E. Glendening, M. Gutowski, A. Hess, J. Jaffe, B. Johnson, J. Ju, R. Kobayashi, R. Kutteh, Z. Lin, R. Littlefield, X. Long, B. Meng, T. Nakajima, S. Niu, M. Rosing, G. Sandrone, M. Stave, H. Taylor, G. Thomas, J. van Lenthe, A. Wong, Z. Zhang, "NWChem, A Computational Chemistry Package for Parallel Computers, Version 4.7" (2005), Pacific Northwest National Laboratory, Richland, Washington 99352-0999, USA.

(158) Bacon, A. D.; Zerner, M. C. *Theor. Chim. Acta* **1979**, *53*, 21.

(159) Ridley, J. E.; Zerner, M. C. *Theor. Chim. Acta* **1976**, *42*, 223.

(160) *HyperChem (TM) Professional 8.0.6*, Hypercube , Inc., 1115 NW 4th Street, Gainesville, Florida 32608, USA.

(161) M. J. Frisch, G. W. Trucks, H. B. Schlegel, G. E. Scuseria, M. A. Robb, J. R. Cheeseman, J. A. Montgomery, Jr., T. Vreven, K. N. Kudin, J. C. Burant, J. M. Millam, S. S. Iyengar, J. Tomasi, V. Barone, B. Mennucci, M. Cossi, G. Scalmani, N. Rega, G. A. Petersson, H. Nakatsuji, M. Hada, M. Ehara, K. Toyota, R. Fukuda, J. Hasegawa, M. Ishida, T. Nakajima, Y. Honda, O. Kitao, H. Nakai, M. Klene, X. Li, J. E. Knox, H. P. Hratchian, J. B. Cross, V. Bakken, C. Adamo, J. Jaramillo, R. Gomperts, R. E. Stratmann, O. Yazyev, A. J. Austin, R. Cammi, C. Pomelli, J. Ochterski, P. Y. Ayala, K. Morokuma, G. A. Voth, P. Salvador, J. J. Dannenberg, V. G. Zakrzewski, S. Dapprich, A. D. Daniels, M. C. Strain, O. Farkas, D. K. Malick, A. D. Rabuck, K. Raghavachari, J. B. Foresman, J. V. Ortiz, Q. Cui, A. G. Baboul, S. Clifford, J. Cioslowski, B. B. Stefanov, G. Liu, A. Liashenko, P. Piskorz, I. Komaromi, R. L. Martin, D. J. Fox, T. Keith, M. A. Al-Laham, C. Y. Peng, A. Nanayakkara, M. Challacombe, P. M. W. Gill, B. G. Johnson, W. Chen, M. W. Wong, C. Gonzalez and J. A. Pople, GAUSSIAN 03 (Revision B.04), Gaussian, Inc., Wallingford, CT, 2004.

(162) Risch, N. *J. Chem. Soc., Chem. Commun.* **1983**, 532.

(163) Risch, N. *Chem. Ber.* **1985**, *118*, 4073.

(164) Hoffmann, R.; Imanura, A.; Hehre, W. J. *J. Am. Chem. Soc.* **1968**, *90*, 1499.

(165) Hoffmann, R. *Acc. Chem. Res.* **1971**, *4*, 1.

(166) Dewar, M. J. S.; Wasson, J. S. *J. Am. Chem. Soc.* **1970**, *92*, 3506.

(167) Paddon-Row, M. N. *Acc. Chem. Res.* **1982**, *15*, 245.

(168) Gleiter, R. *Angew. Chem., Int. Ed.* **1974**, *13*, 697.

(169) Cookson, R. C.; Henstock, J.; Hudec, J. *J. Am. Chem. Soc.* **1966**, *88*, 1060.

(170) Hudec, J. *J. Chem. Soc., Chem. Comm.* **1970**, 829.

(171) Dekkers, A. W. J.; Verhoeven, J. W.; Speckamp, W. N. *Tetrahedron* **1973**, *29*, 1691.

(172) Pasman, P.; Rob, F.; Verhoeven, J. W. *J. Am. Chem. Soc.* **1982**, *104*, 5127.

(173) Pasman, P.; Verhoeven, J. W.; Deboer, T. J. *Tetrahedron Lett.* **1977**, 207.

(174) Krijnen, B.; Beverloo, H. B.; Verhoeven, J. W.; Reiss, C. A.; Goubitz, K.; Heijdenrijk, D. *J. Am. Chem. Soc.* **1989**, *111*, 4433.

(175) Frattarelli, D.; Schiavo, M.; Facchetti, A.; Ratner, M. A.; Marks, T. J. *J. Am. Chem. Soc.* **2009**, *131*, 12595.

(176) Zhang, F.; Wang, C. C. *J. Phys. Chem. C* **2008**, *112*, 15151.

(177) Jordan, B. J.; Ofir, Y.; Patra, D.; Caldwell, S. T.; Kennedy, A.; Joubanian, S.; Rabani, G.; Cooke, G.; Rotello, V. M. *Small* **2008**, *4*, 2074.

(178) Wei, Y. H.; Tong, W. J.; Zimmt, M. B. *J. Am. Chem. Soc.* **2008**, *130*, 3399.

(179) Li, H.; Homan, E. A.; Lampkins, A. J.; Ghiviriga, I.; Castellano, R. K. *Org. Lett.* **2005**, *7*, 443.

(180) Lampkins, A. J.; Abdul-Rahim, O.; Li, H.; Castellano, R. K. *Org. Lett.* **2005**, *7*, 4471.

(181) Terech, P.; Weiss, R. G. *Chem. Rev.* **1997**, *97*, 3133.

(182) Estroff, L. A.; Hamilton, A. D. *Chem. Rev.* **2004**, *104*, 1201.

(183) Sumpter, B. G.; Li, H.; Vincent Meunier; Castellano, R. K. *J. Phys. Chem. C* **2007**, *111*, 18912.

(184) Lampkins, A. J. *Ph.D. Dissertation* **2006**.

(185) Simaan, S.; Siegel, J. S.; Biali, S. E. *J. Org. Chem.* **2003**, 3699.

(186) Ridder, D. J. A. D.; Goubitz, K.; Schenk, H.; Krijnen, B.; Verhoeven, J. W. *Helv. Chim. Acta* **2003**, *86*, 799.

(187) Ridder, D. J. A. D.; Goubitz, K.; Schenk, H.; Krijnen, B.; Verhoeven, J. W. *Helv. Chim. Acta* **2003**, *86*, 812.

(188) Degelaen, J. P.; Pham, P.; Blout, E. R. *J. Am. Chem. Soc.* **1984**, *106*, 4882.

(189) Risch, N.; Langhals, M.; Mikosch, W.; Bögge, H.; Müller, A. *J. Am. Chem. Soc.* **1991**, *113*, 9411.

(190) Jiménez-Cruz, F.; Cetina-Rosado, R.; Hernández-Ortega, S.; Toscano, R. A.; Ríos-Olivares, H. *Acta Crystallogr., Sect. C: Cryst. Struct. Commun.* **2001**, *57*, 868.

(191) Jiménez-Cruz, F.; Ríos-Olivares, H.; Hernández-Ortega, S.; Cervantes-Nevarez, A. *J. Mol. Struct.* **2003**, *655*, 23.

(192) Hickmott, P. W.; Ahmed, M. G.; Ahmed, S. A.; Wood, S.; Kapon, M. *J. Chem. Soc., Perkin Trans. 1* **1985**, 2559.

(193) Ahmed, M. G.; Moeiz, S. M. I.; Ahmed, S. A.; Kiuchi, F.; Tsuda, Y.; Sampson, P. *J. Chem. Res. (S)* **1999**, 316.

(194) Tafeenko, V. A.; Prozorovskii, A. E.; Kovalev, V. V.; Knyazeva, I. V. *J. Struct. Chem.* **1987**, *28*, 155.

(195) Baldridge, K. K.; Battersby, T. R.; VernonClark, R.; Siegel, J. S. *J. Am. Chem. Soc.* **1997**, *119,*, 7048.

(196) Sasaki, T.; Eguchi, S.; Kiriyama, T.; Sakito, Y. *J. Org. Chem.* **1973**, *38*, 1648.

(197) Gleiter, R.; Stohrer, W. D.; Hoffmann, R. *Helv. Chim. Acta* **1972**, *55*, 893.

(198) Brouwer, A. M.; Krijene, B. *J. Org. Chem.* **1995**, *60*, 32.

(199) Kardel, D.; Knoche, W.; Risch, N. *J. Chem. Soc., Perkin Trans. 2* **1993**, 1455.

(200) Risch, N. *Chem. Ber.* **1985**, *118*, 4849.

(201) Lightner, D. A.; Bouman, T. D.; Wijekoon, W. M. D.; Hansen, A. E. *J. Am. Chem. Soc.* **1984**, *106*, 934.

(202) Senda, Y.; Morita, M.; Itoh, H. *J. Chem. Soc., Perkin Trans. 2* **1996**, 221.

(203) Hahn, J. M.; Noble, W. J. l. *J. Am. Chem. Soc.* **1992**, *114*, 1916.

(204) Lenoir, D.; Mison, P.; Hyson, E.; Schleyer, P. v. R.; Saunders, M.; Vogel, P.; Telkowski, L. A. *J. Am. Chem. Soc.* **1974**, *96*, 2157.

(205) R. K. Murray, J.; Goff, D. L.; Ford, T. M. *J. Org. Chem.* **1977**, *42*, 3870.

(206) Henry, G. E.; Jacobs, H.; Carrington, C. M. S.; McLean, S.; Reynolds, W. F. *Tetrahedron Lett.* **1996**, *37*, 8663.

(207) Sasaki, T.; Eguchi, S.; Kiriyama, T.; Sakito, Y. *J. Org. Chem.* **1973**, *38*, 1648.

(208) Senda, Y.; Morita, M.; Itoh, H. *J. Chem. Soc., Perkin Trans. 2* **1996**, 221.

(209) Hahn, J. M.; Le Noble, W. J. *J. Am. Chem. Soc.* **1992**, *114*, 1916.

(210) Lenoir, D.; Mison, P.; Hyson, E.; Schleyer, P. v. R.; Saunders, M.; Vogel, P.; Telkowski, L. A. *J. Am. Chem. Soc.* **1974**, *96*, 2157.

(211) Murray, R. K., Jr.; Goff, D. L.; Ford, T. M. *J. Org. Chem.* **1977**, *42*, 3870.

(212) Risch, N.; Billerbeck, U.; Krieger, E. *Chem. Ber.* **1992**, *125*, 459.

(213) Henry, G. E.; Jacobs, H.; Carrington, C. M. S.; McLean, S.; Reynolds, W. F. *Tetrahedron Lett.* **1996**, *37*, 8663.

(214) Risch, N. *Chem. Ber.* **1985**, *118*, 4849.

(215) Duddeck, H.; Wiskamp, V.; Rosenblum, D. *J. Org. Chem.* **1981**, *46*, 5332.

(216) Grill, J. M.; Ogle, J. W.; Miller, S. A. *J. Org. Chem.* **2006**, *71*, 9291.

(217) Lightner, D. A.; Bouman, T. D.; Donald Wijekoon, W. M.; Hansen, A. E. *J. Am. Chem. Soc.* **1984**, *106*, 934.

(218) Dekkers, A. W. J.; Verhoeven, J. W.; Speckamp, W. N. *Tetrahedron* **1973**, *29*, 1691.

(219) Duddeck, H.; Wiskamp, V.; Rosenblum, D. *J. Org. Chem.* **1981**, *46*, 5332.

(220) Domagalska, B. W.; Syper, L.; Wilk, K. A. *Tetrahedron* **2004**, *60*, 1931.

(221) Wade, L. G. *Organic chemistry*; 5th ed.; Pearson Education: Upper Saddle River, N.J., 2003.

(222) Giannis, A.; Kolter, T. *Angew. Chem. Int. Ed.* **1993**, *32*, 1244.

(223) Huang, B. H.; Parquette, J. R. *J. Am. Chem. Soc.* **2001**, *123*, 2689.

(224) Beijer, F. H.; Sijbesma, R. P.; Kooijman, H.; Spek, A. L.; Meijer, E. W. *J. Am. Chem. Soc.* **1998**, *120*, 6761.

(225) Martin, A. M.; Butler, R. S.; Ghiviriga, I.; Giessert, R. E.; Abboud, K. A.; Castellano, R. K. *Chem. Commun.* **2006**, 4413.

(226) Gellman, S. H. *Acc. Chem. Res.* **1998**, *31*, 173.

(227) Li, X.; Wu, Y. D.; Yang, D. *Acc. Chem. Res.* **2008**, *41*, 1428.

(228) Cai, W.; Wang, G. T.; Du, P.; Wang, R. X.; Jiang, X. K.; Li, Z. T. *J. Am. Chem. Soc.* **2008**, *130*, 13450.

(229) Rudkevich, D. M.; Hilmersson, G.; Rebek, J. *J. Am. Chem. Soc.* **1997**, *119*, 9911.

(230) Renslo, A. R.; Tucci, F. C.; Rudkevich, D. M.; Rebek, J. *J. Am. Chem. Soc.* **2000**, *122*, 4573.

(231) Wu, J.; Fang, F.; Lu, W. Y.; Hou, J. L.; Li, C.; Wu, Z. Q.; Jiang, X. K.; Li, Z. T.; Yu, Y. H. *J. Org. Chem.* **2007**, *72*, 2897.

(232) Wu, Z. Q.; Shao, X. B.; Li, C.; Hou, J. L.; Wang, K.; Jiang, X. K.; Li, Z. T. *J. Am. Chem. Soc.* **2005**, *127*, 17460.

(233) Wang, B. Y.; Bao, X. G.; Stojanovic, S.; Hadad, C. M.; Badjic, J. D. *Org. Lett.* **2008**, *10*, 5361.

(234) Wang, B. Y.; Rieth, S.; Badjic, J. D. *J. Am. Chem. Soc.* **2009**, *131*, 7250.

(235) Vetrichelvan, M.; Valiyaveettil, S. *Chem. Eur. J.* **2005**, *11*, 5889.

(236) Yin, C.; Huo, F.; Gao, F.; Guo, J.; Yang, P. *Acta Cryst.* **2003**, *E59*, o1740.

(237) Lindvall, M. K.; Rissanen, K.; Hakala, J. M. L.; Kosinen, A. M. P. *Tetrahedron Lett.* **1999**, *40*, 7427.

(238) Ogata, M.; Matsumoto, H.; Takahashi, K.; Shimizu, S.; Kida, S.; Ueda, M. *J. Med. Chem.* **1984**, *27*, 1142.

(239) Chen, C.; Chang, W.; Sheu, S.; Lee, G.; Ho, T.; Lin, Y.; Wang, Y. *J. Chem. Soc. Dalton Trans.* **1991**, 1569.

(240) Katritzky, A. R.; Zhang, Z.; Lang, H.; Lan, X. *J. Org. Chem.* **1994**, *59*, 7209.

(241) Higgs, T. C.; Carrano, C. J. *Eur. J. Org. Chem.* **2002**, 3632.

(242) Melgar-Fernandez, R.; Gonzalez-Olvera, R.; Juaristi, E. *Tetrahedron* **2003**, *61*, 4329.

(243) Pettigrew, J. D.; Bexrud, J. A.; Freeman, R. P.; Wilson, P. D. *Heterocycles* **2004**, *62*, 445.

(244) Kolb, H. C.; Finn, M. G.; Sharpless, K. B. *Angew. Chem. Int. Ed.* **2001**, *40*, 2004.

(245) Tornoe, C. W.; Christensen, C.; Meldal, M. *J. Org. Chem.* **2002**, *67*, 3057.

(246) Katritzky, A. R.; Singh, S. K. *J. Org. Chem.* **2002**, *67*, 9077.

(247) Rostovtsev, V. V.; Green, L. G.; Fokin, V. V.; Sharpless, K. B. *Angew. Chem. Int. Ed.* **2002**, *41*, 2596.

(248) Perez-Balderas, F.; Ortega-Munoz, M.; Morale-Sanfrutos, J.; Hernandez-Mateo, F.; Calvo-Flores, F. G.; Calvo-Asin, J. A.; Isac-Garcia, J.; Santoyo-Gonzalez, F. *Org. Lett.* **2003**, *5*, 1951.

(249) Chan, T. R.; Hilgraf, R.; Sharpless, K. B.; Fokin, V. V. *Org. Lett.* **2004**, *6*, 2853.

(250) Sivakumar, K.; Xie, F.; Cash, B. M.; Long, S.; Barnhill, H. N.; Wang, Q. *Org. Lett.* **2004**, *6*, 4603.

(251) Zhou, Z.; Fahrni, C. J. *J. Am. Chem. Soc.* **2004**, *126*, 8862.

(252) Orgueira, H. A.; Fokas, D.; Isome, Y.; Chan, P. C.-M.; Baldino, C. M. *Tetrahedron Lett.* **2005**, *46*, 2911.

(253) Gujadhur, R.; Venkataraman, D.; Kintigh, J. T. *Tetrahedron Lett.* **2001**, *42*, 4791.

(254) Gopalsamuthiram, V.; Wulff, W. D. *J. Am. Chem. Soc.* **2004**, *126*, 13936.

(255) Jung, M. E.; Hagenah, J. A. *J. Org. Chem.* **1987**, *52*, 1889.

(256) Prada, J. A. H.; Ferreira, A. J.; Katovich, M. J.; Shenoy, V.; Qi, Y. F.; Santos, R. A. S.; Castellano, R. K.; Lampkins, A. J.; Gubala, V.; Ostrov, D. A.; Raizada, M. K. *Hypertension* **2008**, *51*, 1312.

(257) Archer, S.; Zayed, A. H.; Rej, R.; Rugino, T. A. *J. Med. Chem.* **1983**, *26*, 1240.

(258) Fraga-Silva; Ferreira, R. A.; A. J.; Sorg, B. S.; Wankhede, M. M.; deDeugd, C.; Y., J. J.; Baker, M. B.; Li, Y.; Castellano, R. K.; Katovich, M. J.; Raizada, M. K. *Molecular Medicine*, accepted.

BIOGRAPHICAL SKETCH

Yan Li was born in Beijing, China, 1978. When he was four months old, he moved with his parents to Jinan city, the capital of Shandong Province, and grew up in that beautiful city. He received his bachelor degree in chemistry from Shandong University in 2001. After graduation, he decided to stay in Shandong University for his graduate study and research under the guidance of Prof. Jianwu Wang and he received his master degree in organic chemistry in 2004. In August, 2004, he came to the University of Florida and joined Prof. Ronald K. Castellano's research group to pursue his Ph.D. research in organic and supramolecular chemistry. He received his Ph.D. degree in May, 2010.